Advances in Science, Technology & Innovation
IEREK Interdisciplinary Series for Sustainable Development

Narasimman Sundararajan · Mehdi Eshagh · Hakim Saibi
Mustapha Meghraoui · Mansour Al-Garni · Bernard Giroux *Editors*

On Significant Applications of Geophysical Methods

Proceedings of the 1st Springer Conference of the Arabian Journal of Geosciences (CAJG-1), Tunisia 2018

IEREK RESEARCH & KNOWLEDGE ENRICHMENT

Springer

Advances in Science, Technology & Innovation

IEREK Interdisciplinary Series for Sustainable Development

Advances in Science, Technology & Innovation (ASTI) is a series of peer-reviewed books based on the best studies on emerging research that redefines existing disciplinary boundaries in science, technology and innovation (STI) in order to develop integrated concepts for sustainable development. The series is mainly based on the best research papers from various IEREK and other international conferences, and is intended to promote the creation and development of viable solutions for a sustainable future and a positive societal transformation with the help of integrated and innovative science-based approaches. Offering interdisciplinary coverage, the series presents innovative approaches and highlights how they can best support both the economic and sustainable development for the welfare of all societies. In particular, the series includes conceptual and empirical contributions from different interrelated fields of science, technology and innovation that focus on providing practical solutions to ensure food, water and energy security. It also presents new case studies offering concrete examples of how to resolve sustainable urbanization and environmental issues. The series is addressed to professionals in research and teaching, consultancies and industry, and government and international organizations. Published in collaboration with IEREK, the ASTI series will acquaint readers with essential new studies in STI for sustainable development.

More information about this series at http://www.springer.com/series/15883

Narasimman Sundararajan
Mehdi Eshagh • Hakim Saibi
Mustapha Meghraoui
Mansour Al-Garni • Bernard Giroux
Editors

On Significant Applications of Geophysical Methods

Proceedings of the 1st Springer Conference of the Arabian Journal of Geosciences (CAJG-1), Tunisia 2018

Springer

Editors
Narasimman Sundararajan
Department of Earth Sciences
Sultan Qaboos University
Muscat, Oman

Mehdi Eshagh
University West
Trollhättan, Sweden

Hakim Saibi
United Arab Emirates University
Abu Dhabi, United Arab Emirates

Mustapha Meghraoui
Université de Strasbourg
Strasbourg, France

Mansour Al-Garni
King Abdulaziz University
Jeddah, Saudi Arabia

Bernard Giroux
Centre Eau Terre Environnement
Institut National de la Recherche Scientifique
Québec, QC, Canada

ISSN 2522-8714 ISSN 2522-8722 (electronic)
Advances in Science, Technology & Innovation
IEREK Interdisciplinary Series for Sustainable Development
ISBN 978-3-030-01655-5 ISBN 978-3-030-01656-2 (eBook)
https://doi.org/10.1007/978-3-030-01656-2

Library of Congress Control Number: 2018958942

This Springer imprint is published by the registered company Springer Nature Switzerland AG
The registered company address is: Gewerbestrasse 11, 6330 Cham, Switzerland

Preface

Even with the advent and advancement of elegant tools and techniques coupled with sophisticated software and hardware, geophysical exploration for subsurface resources still poses a great challenge to the practicing geoscientists due to various known and unknown factors. The complex nature of geology, an improper choice of a geophysical tool or tools or even minute variations of physical properties between host rock and sources further complicate the problem of achieving the desired results. Therefore, geophysical exploration is a multifaceted task requiring a sound theoretical background with adequate field experience and a comprehensive knowledge of the geology of the area of study to yield reliable results. Further, all geophysical data are invariably corrupted with a wide variety of noise factors that complicate the interpretation. Therefore, data processing with appropriate mathematical and statistical tools that frees the noise from the acquired data is a major task. Interpretation of noise-free data with a correct choice of techniques ensures useable results in almost all geo-investigations.

This proceedings volume contains the best papers accepted for presentation during the 1st Springer Conference of the Arabian Journal of Geosciences (CAJG-1), Tunisia 2018. The book offers a variety of new case studies focused on mineral, groundwater, hydrocarbon, and environmental issues as well as a comprehensive study on recent earthquakes. In addition, there are significant studies on earthquake hazard assessment based on geophysical tools and techniques by experienced researchers mainly from research institutes or universities in the Mediterranean and Middle East region. The main topics include: Applications of gravity and magnetic methods, Electrical and Electromagnetic methods in mineral and groundwater exploration, Case studies on refraction and reflection seismic methods, Integrated geoscience applications in the exploration of subsurface resources, Hydrocarbon and petrophysical studies, Earthquakes and seismic hazard assessment and Tectonics. This volume gives new insights not only on the choice of particular geophysical methods in specific investigations but also about appropriate methods of analysis used to reach concise and concrete solutions and obtain desired results. In certain papers, the results of case studies are correlated with drilling data to substantiate the method of interpretation and its accuracy. Most of the studies presented here are from Mediterranean and Middle East and therefore, this volume will also provide an adequate understanding of the complexities of geology of this region, as well.

Muscat, Oman — Narasimman Sundararajan
Trollhättan, Sweden — Mehdi Eshagh
Abu Dhabi, United Arab Emirates — Hakim Saibi
Strasbourg, France — Mustapha Meghraoui
Jeddah, Saudi Arabia — Mansour Al-Garni
Québec, Canada — Bernard Giroux

July 2018

Acknowledgements

Our appreciation is extended to the authors of the papers for their hard and diligent work in producing high-quality contributions. We would like to thank the reviewers of the papers for their in-depth reviews and great efforts in improving the quality of the papers. Also, thanks are extended to Amjad Kallel who supervised and handled the evaluation process, to Sahbi Moalla who handled the submission and evaluation system for the ten conference proceedings volumes, and to the publishing staff of Springer headed by Nabil Khélifi, Senior Editor for their efforts and contributions in completing this conference proceedings volume. All the above-mentioned efforts were very important in making this book a success.

About the 1st Springer Conference of the Arabian Journal of Geosciences (CAJG-1), Tunisia 2018

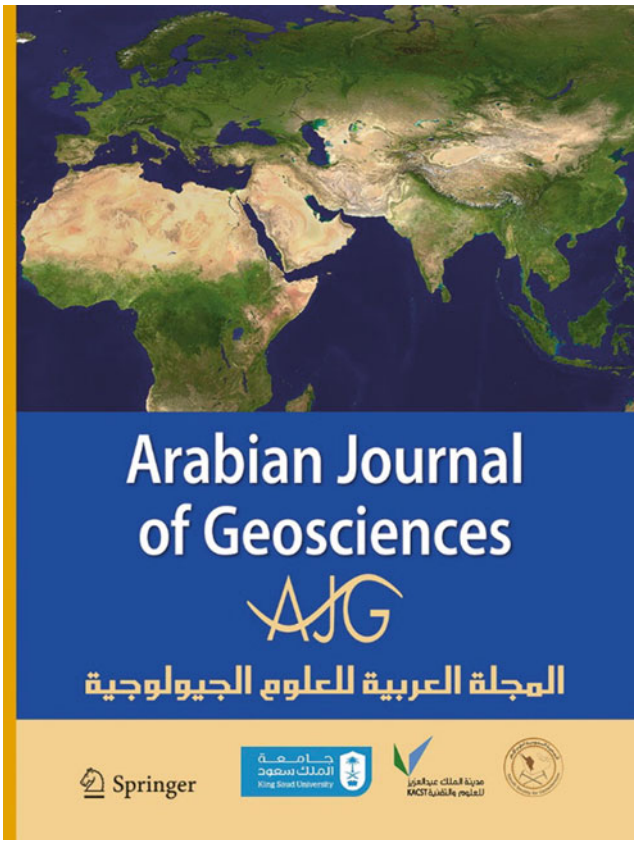

The *Arabian Journal of Geosciences (AJG)* is a Springer journal publishing original articles on the entire range of Earth sciences in partnership with the Saudi Society for Geosciences. The journal focuses on, but not limited to, research themes which have regional significance to the Middle East, the Euro-Mediterranean, Africa, and Asia. The journal receives on average 2000 submissions a year and accepts around 500 papers for publication in its 24 annual issues (acceptance rate 25%). It enjoys the participation of an editorial team of 100 international associate editors who generously help in evaluating and selecting the best papers.

In 2008, Prof. Abdullah Al-Amri, in close partnership with Springer, founded the Arabian Journal of Geosciences (AJGS). In this year, the journal celebrates its tenth anniversary. On this occasion and to mark this event, the Founder and Editor-in-Chief of the AJGS Prof. Al-Amri organized in close collaboration with Springer the 1st Conference of the Arabian Journal of Geosciences (1st CAJG) in Hammamet, Tunisia, from November 12 to 15, 2018 (www.cajg.org).

The conference was an occasion to endorse the journal's long-held reputation for bringing together leading authors from the Middle East, the Euro-Mediterranean, Africa, and Asia who work in the wide-ranging fields of Earth sciences. The conference covered all cross-cutting themes of Geosciences and focused principally on the following ten tracks:

- Track 1. Climate, paleoclimate and paleoenvironmental changes
- Track 2. Geoinformatics, remote sensing, geodesy
- Track 3. Geoenvironmental engineering, geomechanics and geotechnics, geohazards
- Track 4. Geography, geoecology, geoarcheology, geotourism
- Track 5. Geophysics, seismology
- Track 6. Hydrology, hydrogeology, hydrochemistry
- Track 7. Mineralogy, geochemistry, petrology and volcanology
- Track 8. Petroleum engineering and petroleum geochemistry
- Track 9. Sedimentology, stratigraphy, palaeontology, geomorphology, pedology
- Track 10. Structural/petroleum/mining geology, geodynamics, marine geology

The dynamic four-day conference provided more than 450 attendees with opportunities to share their latest unpublished findings and learn the newest geoscience studies. The event also allowed attendees to meet and discuss with the journal's editors and reviewers.

More than 950 short contributing papers to the conference were submitted by authors from more than 70 countries. After a pre-conference peer review process by more than 500 reviewers, 700 papers were accepted. These papers were published as chapters in the conference proceedings by Springer.

The conference proceedings consist of ten edited volumes, each edited by the following group of *Arabian Journal of Geosciences* (AJGS) editors and other guest editors:

Volume 1. Patterns and Mechanisms of Climate, Paleoclimate, and Paleoenvironmental Changes from Low-Latitude Regions

Zhihua Zhang (AJGS Editor): Beijing Normal University, Beijing, China
Nabil Khélifi (AJGS Editor): Earth Sciences Editorial Department, Springer, Heidelberg, Germany
Abdelkader Mezghani (Guest Editor): Norwegian Meteorological Institute, Norway
Essam Heggy (Guest Editor): University of Southern California and Jet Propulsion Laboratory, Caltech, USA

Volume 2. Advances in Remote Sensing and Geo Informatics Applications

Hesham M. El-Askary (Guest Editor): Schmid College of Science and Technology at Chapman University, USA
Saro Lee (AJGS Editor): Korea Institute of Geoscience and Mineral Resources, Daejeon, South Korea
Essam Heggy (Guest Editor): University of Southern California and Jet Propulsion Laboratory, Caltech, USA
Biswajeet Pradhan (AJGS Editor): University of Technology Sydney, Sydney, Australia

Volume 3. Recent Advances in Geo-Environmental Engineering, Geomechanics and Geotechnics, and Geohazards

Amjad Kallel (AJGS Editor): ENIS, University of Sfax, Tunisia
Zeynal Abiddin Erguler (AJGS Editor): Dumlupinar University, Kutahya, Turkey
Zhen-Dong Cui (AJGS Editor): China University of Mining and Technology, Xuzhou, Jiangsu, China
Ali Karrech (AJGS Editor): The University of Western Australia, Australia
Murat Karakus (AJGS Editor): University of Adelaide, Australia

Pinnaduwa Kulatilake (AJGS Editor): Department of Materials Science and Engineering, The University of Arizona, USA
Sanjay Kumar Shukla (AJGS Editor): School of Engineering, Edith Cowan University, Perth, Australia

Volume 4. Exploring the Nexus of Geoecology, Geography, Geoarcheology and Geotourism: Advances and Applications for Sustainable Development in Environmental Sciences and Agroforestry Research

Haroun Chenchouni (AJGS Editor): University of Tebessa, Algeria
Ezzoura Errami (Guest Editor): Chouaïb Doukkali University, El Jadida, Morocco
Fernando Rocha (Guest Editor): University of Aveiro, Portugal
Luisa Sabato (AJGS Editor): Università degli Studi di Bari "Aldo Moro", Bari, Italy

Volume 5. On Significant Applications of Geophysical Methods

Narasimman Sundararajan (AJGS Editor): Sultan Qaboos University, Muscat, Oman
Mehdi Eshagh (AJGS Editor): University West, Trollhättan, Sweden
Hakim Saibi (AJGS Editor): United Arab Emirates University, Al-Ain, Abu Dhabi, UAE
Mustapha Meghraoui (AJGS Editor): Université de Strasbourg, Strasbourg, France
Mansour Al-Garni (AJGS Editor): King Abdulaziz University, Jeddah, Saudi Arabia
Bernard Giroux (AJGS Editor): Institut National de la Recherche Scientifique, Québec, Canada

Volume 6. Advances in Sustainable and Environmental Hydrology, Hydrogeology, Hydrochemistry and Water Resources

Helder I. Chaminé (AJGS Editor): School of Engineering (ISEP), Polytechnic of Porto, Portugal
Maurizio Barbieri (AJGS Editor): University of Rome La Sapienza, Italy
Ozgur Kisi (AJGS Editor): Ilia State University, Tbilisi, Georgia
Mingjie Chen (AJGS Editor): Sultan Qaboos University, Muscat, Oman
Broder J. Merkel (AJGS Editor): TU Bergakademie Freiberg, Freiberg, Germany

Volume 7. Petrogenesis and Exploration of the Earth's Interior

Domenico Doronzo (AJGS Editor): Consejo Superior de Investigaciones Cientificas, Spain
Emanuela Schingaro (AJGS Editor): Università degli Studi di Bari Aldo Moro—UniBa, Italy
John S. Armstrong-Altrin (AJGS Editor): The National Autonomous University of Mexico, Mexico
Basem Zoheir (Guest Editor): Benha University, Egypt and University of Kiel, Germany

Volume 8. Advances in Petroleum Engineering and Petroleum Geochemistry

Santanu Banerjee (AJGS Editor): Indian Institute of Technology Bombay, Mumbai, India
Reza Barati (AJGS Editor): The University of Kansas, Lawrence, KS, USA
Shirish Patil (Guest Editor): Saudi Aramco and King Fahd University of Petroleum and Minerals, Dhahran, Saudi Arabia

Volume 9. Paleobiodiversity and Tectono-Sedimentary Records in the Mediterranean Tethys and Related Eastern Areas

Mabrouk Boughdiri (AJGS Editor): University of Carthage, Amilcar, Tunisia
Beatriz Bádenas (AJGS Editor): University of Zaragoza, Zaragoza, Spain
Paul Selden (AJGS Editor): University of Kansas, Lawrence, KS, USA
Etienne Jaillard (Guest Editor): University of Grenoble Alpes, France
Peter Bengtson (AJGS Editor): University of Heidelberg, Heidelberg, Germany
Bruno R. C. Granier (AJGS Editor): University of Bretagne Occidentale, Brest, France

Volume 10. The Structural Geology Contribution to the Africa-Eurasia Geology: Basement and Reservoir Structure, Ore Mineralisation and Tectonic Modelling

Federico Rossetti (Guest Editor): Università Roma Tre, Roma, Italy
Ana Crespo Blanc (Guest Editor): University of Granada, Spain
Federica Riguzzi (Guest Editor): National Institute of Geophysics and Volcanology, Roma, Italy
Estelle Leroux (Guest Editor): IFREMER, Unité Géosciences Marines, Plouzané, France
Kosmas Pavlopoulos (Guest Editor): Sorbonne University Abu Dhabi, Abu Dhabi, UAE
Olivier Bellier (Guest Editor): CEREGE, Aix-en-Provence, France
Vasilios Kapsimalis (Guest Editor): Institute of Oceanography, Hellenic Centre for Marine Research, Anavyssos, Greece

About the Conference Steering Committee

General Chair

Abdullah Al-Amri: Founder and Editor-in-Chief of AJGS, King Saud University, Saudi Arabia

Conference Supervisor

Nabil Khélifi: Senior Publishing Editor, Springer Middle East and North African Program Springer, a part of Springer Nature, Heidelberg, Germany

Scientific Committee Chair

François Roure: Guest of Editorial Board of AJGS, IFP—Energies Nouvelles, France

Walter D. Mooney: Guest of Editorial Board of AJGS, US Geological Survey Western Region, USA

Local Organization Chair

Mabrouk Boughdiri: Associate Editor of AJGS, University of Carthage, Amilcar, Tunisia

Evaluation Chair

Amjad Kallel: Assistant Editor of AJGS, ENIS, University of Sfax, Tunisia

Publication Chair

Biswajeet Pradhan: Associate Editor of AJGS, University of Technology Sydney, Sydney, Australia

Essam Heggy: Guest of Editorial Board of AJGS, University of Southern California and Jet Propulsion Laboratory, Caltech, USA

Program Chair

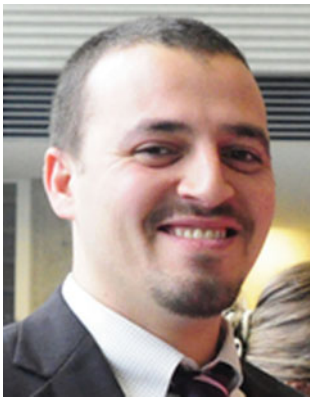

Hakim Saibi: Associate Editor/Assistant Editor of AJGS, United Arab Emirates University, Al-Ain, Abu Dhabi, UAE

Domenico Doronzo: Associate Editor/Assistant Editor of AJGS, Consejo Superior de Investigaciones Cientificas, Spain

Communication Chair

Mohamed Ksibi: Guest of Editorial Board of AJGS, ISBS, University of Sfax, Tunisia

English Language Advisory Committee

Abdelmajid Dammak: ENIS, University of Sfax, Tunisia
Chokri Khalaf: FMS, University of Sfax, Tunisia
Dhouha Mabrouk: FLSHS, University of Sfax, Tunisia
Mohamed Elbahi: ENIS, University of Sfax, Tunisia
Sami Shami: ENIS, University of Sfax, Tunisia
Yasmine Basha: FLSHS, University of Sfax, Tunisia

Conference Manager

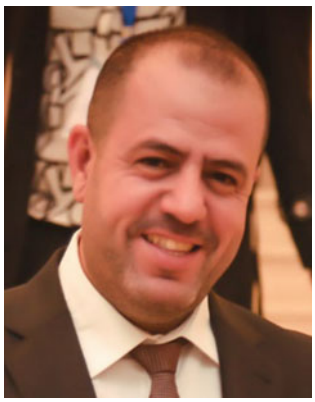

Mohamed Sahbi Moalla: Coordinator of AJGS, ISET, University of Sfax, Tunisia

Contents

About the Editors

Dr. Narasimman Sundararajan graduated in Mathematics from the University of Madras and then carried on with an M.Sc. (Tech) and Ph.D. in Exploration Geophysics from Osmania University, India. He began a career as a Research Scientist in the National Geophysical Research Institute under Council of Scientific & Industrial Research, Government of India and later switched over to teaching at the Centre of Exploration Geophysics, Osmania University, Hyderabad, India where he became a Professor in Geophysics in 2004. Presently, he is an Associate Professor of Geophysics in the Department of Earth Science, Sultan Qaboos University. He has published around 90 papers in the leading International journals and supervised several PhDs in Geophysics as well as Mathematics. He has published a book and a couple of book chapters during 2010–2012. He has implemented several research projects including Uranium exploration, earthquake hazard assessment studies, groundwater exploration, etc. He brought out a few innovative tools and techniques for the processing and interpretation of various geophysical data besides a mathematical equation called "*Sundararajan Transform*" (Exploration Geophysics, 2001) and a good deal of software including VLFPROS (Computers & Geosciences, 2007). He defined a valid and viable approach to multidimensional *Hartley transform* in contrast with the definition (Nature, 1991) of Prof. R. N. Bracewell, Stanford University, USA. Member of XIV Indian Scientific Expedition to Antarctica during 1994–1995 and carried out geophysical investigations, in which results were published in leading research Journals. Also, he was a member of IEEE transactions committee for the selection of best paper award in 2007. As a member of "Initiative for Research and Innovative in Science (IRIS)", he motivated young students in India during 2003–2007 to get involved in scientific research. For his overall significant research contribution, Govt. of India has conferred upon him the *Mineral Award now known as National Award for Geosciences in 2007*. His research interests are varied and wide including geophysical data processing, mineral and groundwater exploration, earthquake hazard assessment studies, applied mathematics, bio signal processing, etc. Currently, he is an Associate Editor of "Arabian Journal of Geosciences (Springer)", besides being a reviewer for many International Journals in multidisciplinary fields.

Dr. Mehdi Eshagh received his B.Sc. in Surveying Engineering 1999 from the Islamic Azad University, South of Teheran branch, M.Sc. in Geodesy 2002 from KNToosi University of Technology, and Ph.D. in Geodesy 2009 from Royal Institute of Technology (KTH) in Sweden. In October 2010, he was appointed as Docent/Associate Professor of Physical Geodesy/Space Geodesy at KTH and since September 2013 as professor of Geodesy at West University, Sweden. He has been a teacher of a variety of courses in Surveying Engineering at different levels of education from high school to Ph. D. programmes since 1999. His research interests include the fields of Physical Geodesy specially geoid and gravity field determination, satellite gravimetry and gradiometry, adjustment theory, satellite orbit determination, geodetic network optimization and design, theories of isostasy, Moho and density contrast determination, and sub-lithospheric stress modeling using gravimetric data. He has published and co-authored about 150 original articles, monographs, textbooks, edited books, special issues, and conference abstracts. He is the founder and senior managing editor of Journal of Geodetic Science. Also, he is cooperating as the editor of Journal Numerical Methods in Civil Engineering, Geodynamics Research International Bulletin, Journal of Applied Engineering Sciences, and Journal of Geodesy and Geomatics Engineering. In 2017, he joined the AJGS as an associate editor responsible for evaluating submissions in the fields of Geodesy and Solid Earth Geophysics.

Dr. Hakim Saibi holds a Ph.D. in Earth Sciences (2007) from Kyushu University (Japan). He is currently an Associate Professor at Geology Department, United Arab Emirates University (UAE). His research interests focus on exploration geophysics in general and developing new 2D and 3D geophysical codes for gravity and magnetic methods specially, 2D/3D Magnetotelluric for geothermal exploration, petroleum geosciences, hydrogeology & hydrochemistry, computational geosciences, volcanology, GIS, and remote sensing. He has developed new 2D and 3D methods for potential field data interpretation (modeling and inversion). He has published more than 46 International peer-reviewed journal papers, 65 proceedings in International Conferences, three books, and four book chapters. His publications covered 13 different countries from Asia, Africa, and Central America. He has supervised more than 10 M.Sc. and Ph.D. theses. In 2017, he joined the AJGS as an Assistant Editor supporting the Editor-in-Chief, and as an Associate Editor responsible for evaluating submissions in the fields of Geophysics. He is also Editor at ASEAN Engineering Journal for Geological and Geo-Resource Engineering.

Dr. Mustapha Meghraoui completed his Ph.D. (1988) at the University of Paris XI-Orsay (France) on Seismo-tectonics and Paleoseismology of the Tell Atlas in Algeria. He is a Senior Scientist at the "Institut de Physique du Globe" at the University of Strasbourg (France). His working group has achieved major strides, releasing pioneering studies on the identification of active faults in intra-plate Europe and inter-plate major continental active faults. They have developed paleoseismic studies in regions with fast active deformation and large earthquakes, and in regions with low-level seismicity in Europe. In particular, and for nearly 20 years now, the combination of micro-topography, shallow geophysics and trenching in active faulting studies has led the group to produce numerous peer-reviewed publications and internationally recognized research papers (ca. 90 articles in ISI-JCR journals, 2500 citations). These contributions focus on the development of paleoseismic and archeo-seismic studies and earthquake geology in different tectonic domains (North African Atlas, North and East Anatolian fault, and Dead Sea fault), and on the comparison between regions with slow active deformation and regions with fast seismic slip release. Furthermore, their research focuses on the development of a conceptual framework to deepen our understanding of long-term faulting behavior in earthquake-prone regions, and on studies of faults in regions with the potential for large or moderate earthquakes and related physical characteristics. He has contributed to many international scientific projects, supervised 12 Ph.D. theses, and coordinated several European and international (UNESCO) projects. He has served as an editorial board member for the Annals of Geophysics and Natural Hazards journals. He is currently an Associate Editor of the Euro-Mediterranean Journal for Environmental Integration (Springer). In 2016, he joined the AJGS as an Associate Editor responsible for evaluating submissions in the fields of Earthquake Geology, Paleoseismology, Archeo-seismology, Seismo-tectonics, and Neo-tectonics.

Dr. Mansour Al-Garni holds a B.Sc. (1993) in Geophysics from King Abdulaziz University (KAU, Saudi Arabia), a M. Sc. (1996) in Geophysics from Colorado School of Mines (Colorado, USA), and a Ph.D. (2001) in Geophysics from Texas A&M University (TAMU, College Station, USA). In 1993, he worked as a Geophysicist at the Ministry of Petroleum and Mineral Resources, United States Geological Survey in Jeddah (Saudi Arabia), and as a Demonstrator of Geophysics at KAU, where he became an Assistant Professor of Geophysics in 2002. He has been promoted to an Associate Professor in 2006 and to a full Professor of Geophysics in 2010. He has been nominated as the Chairman of Geophysics Department (2003–2011), Vice Dean (2014), and Vice Dean for graduate studies and scientific research (2015–Now). His research interests cover controlled-source electromagnetic induction, electrical methods, gravity and magnetic methods, near-surface applied Geophysics, forward and inverse model-

ing, environmental and engineering Geophysics, environmental site characterization, ground penetrating radar, hydrogeophysics, and mining Geophysics: theory, data processing, and interpretation. He has reviewed a lot of academic works and has been in many committees including those of M.Sc. and Ph.D. examinations. His remarkable efforts in the establishment and development of various projects were reflected in valuable academic and professional successes and achievements. He has conducted more than 15 research projects, the most recent of which involved EM, DC resistivity, SP, IP, and magnetic methods for mineral exploration in the Arabian Shield. He has published more than 50 research articles in international indexed and refereed journals. He has been listed in the "Marquis Who's who in the World" as one of the world's foremost achievers in the field of Geophysics in the 28th Edition (2011). In 2015, he joined the AJGS as an Associate Editor responsible for evaluating submission in the fields of Theoretical and Applied Exploration Geophysics.

Dr. Bernard Giroux holds a B.Sc.A. in engineering physics (1992) from Laval University (Canada) and a M.Sc.A. (1994) and Ph.D. (2001), both in applied geophysics from École Polytechnique de Montréal (Canada). He is currently Associate Professor at the Institut National de la Recherche Scientifique, Centre Eau-Terre-Environnement in Quebec city (Canada). His research interests include geophysical monitoring, near-surface geophysics, numerical modeling, geophysical inversion, and data assimilation. During the last years, his work focused largely on improving methods for quantitative interpretation and monitoring of CO_2 storage. In 2016, Dr. Giroux joined the AJGS as an Associate Editor responsible for evaluating submissions in Applied Geophysics.

Part I
Keynote

Rupture Dynamics and Seismic Radiation on Multi-scale Geometrically Complex Faults

P. Martin Mai

Abstract

Geological faults comprise large-scale segmentation and small-scale roughness that govern earthquake processes and associated seismic radiation. Recent large earthquakes demonstrate that standard techniques for seismic hazard assessment for such faults (fault systems) are insufficient. This problem can be overcome by numerical simulations for multi-scale geometrical complex faults to investigate their rupture dynamics and seismic radiation. In this review, I discuss recent work to understand effects of large-scale segmentation and small-scale roughness on rupture evolution and near-source shaking. Using numerical simulations, we find that rupture incoherence due to fault roughness leads to high-frequency spectral decay consistent with observations. Waveform characteristics and comparisons with empirical ground-motion relations show that rough-fault rupture simulations generate realistic synthetic seismogram that can be used for engineering applications. We also show that for segmented faults, the spatial distribution of the regional stress is of critical importance as it determines the initial stress on the fault system. Similarly, the rupture nucleation point has significant impact on the resulting rupture process and earthquake size. Consequently, seismic hazard assessment for such fault systems must include more earthquake physics to capture the possible near-source shaking levels of future earthquakes.

Keywords

Earthquake physics • Geometric fault complexity • Rupture dynamics • Seismic shaking • Seismic hazard analysis

P. Martin Mai (✉)
Division of Physical Science and Engineering,
King Abdullah University of Science and Technology,
23955 Thuwal, Saudi Arabia
e-mail: martin.mai@kaust.edu.sa

1 Introduction

Ground-motion estimation for seismic hazard assessment generally utilizes empirical methods based on ground-motion prediction equations (GMPEs) that are developed from strong-motion recordings of past earthquakes. GMPE's quantify the expected shaking level for an earthquake of given magnitude at some selected source-to-site distance, involving additional source, site, and path parameters. However, strong-motion databases are still limited for large ($M > 7$) earthquakes and the near-source region. In addition, recent damaging earthquakes highlight the geometrical complexity of faults and fault systems that is not included in any GMPE-parameterization. Therefore, GMPE-based ground-motion estimation for complex-faulting earthquakes, as for instance expected for the Gulf of Aqaba region, is likely to return inaccurate and unreliable forecasts of the possible shaking levels in future earthquakes.

The issue of complex-faulting earthquakes also must include an assessment of the likelihood whether or not several fault segments are activated (e.g. triggered) during a single event, and if so, how. Are such multi-segment ruptures common? What are the required initial and boundary conditions in terms of stress, geometry, friction, etc. for these events to happen? Can we include such information into the next-generation seismic-hazard-assessment (SHA) methods? How do the rupture evolution, the source dynamics, and the resulting seismic radiation depend on fault segmentation and, at a smaller scale, on fault roughness?

In this review, I summarize our recent work on rupture dynamics on segmented faults [4, 6, 8], the effects of fault roughness on rupture and seismic radiation [3], and kinematic ground-motion simulations on complex-geometry fault systems [7]. In the light of planned large infrastructural developments around the Gulf of Aqaba, our work has immediate impact for the region: the last large earthquake in the Gulf of Aqaba dates back to 1995 (M 7.3), but parts of

N. Sundararajan et al. (eds.), *On Significant Applications of Geophysical Methods*,
Advances in Science, Technology & Innovation, https://doi.org/10.1007/978-3-030-01656-2_1

the fault system have not ruptured for centuries. The region therefore needs to prepare for future large earthquakes through advanced seismic hazard assessment.

2 Method and Parameterization

We conducted numerical simulations using high-performance-computing (HPC) enabled numerical solvers that are capable to handle 3D Earth structure, topography, geometrically complex fault planes, and—depending on application—realistic friction parameterization on the fault surface. For rough-fault simulations, we used the second-order (in space and time) generalized finite-difference method that allows for complex fault geometries through a support-operator method (SORD-code by [1, 2]). For multi-segment fault-rupture simulation on the North Anatolian Fault, we used a 3-D explicit finite-element method [5] to model the spontaneous, dynamic rupture evolution for changing rupture-initiation points and varying regional stress directions. In addition, we employed the software package SeisSol (www.seissol.org) to simulate spontaneous rupture failure and subsequent seismic wave propagation on complex fault systems. SeisSol is well suited for handling complex geometries due to the use of tetrahedral mesh elements, while it is also highly optimized for the efficient use on modern high-performance computing infrastructure.

Both SORD and SeisSol were used for dynamic rupture simulations and kinematic ground-motion calculations. Dynamic rupture simulations require an initial stress on the fault and a friction law that acts on the rupture plane; solving the elastic dynamic equations of motions, the simulation then determines which point on the fault breaks, and when, and what its slip-rate function is. That is, the entire space-time evolution of the rupture process is determined through an "ab initio" simulation. The resulting ground-motions are then a by-product of the dynamic rupture simulation. In contrast, in kinematic simulations, the rupture model is prescribed on the fault, and the resulting seismic radiation is computed based on the prescribed slip and slip-rate distribution and the specified temporal rupture evolution.

Numerical stability was ensured choosing appropriate time-stepping for each method, given the 3D Earth model, the desired highest resolved frequency (that depends also the available computational resources), and the corresponding grid-size (mesh). Depending on the particular application and numerical method, our grid-size vary from 500m to 25 m, providing a frequency resolution from 0.25 Hz up to nearly 6 Hz.

3 Results

3.1 Dynamic Ruptures on Segmented Faults

Dynamic earthquake rupture models for the complex-geometry fault system in the Marmara Sea (considering the northern North Anatolian Fault) reveal that the earthquake size, rupture propagation, and near-fault ground motion strongly depend on the interplay between the initial regional stress, and the dynamic stresses radiated by the propagating rupture. Testing several nucleation locations, we found that nucleation far from an oblique normal-fault stepover near Istanbul leads to large through-going rupture on the entire fault system, whereas nucleation closer to the stepover tend to produce ruptures that die out in the stepover. This pattern changes in case a small rotation of the regional stress field is considered ($\pm 10°$). The complex fault geometry leads to a very complicated and asymmetric distribution of near-fault ground motion (including greatly amplified ground motion on the insides of fault bends) that cannot be modelled by standard GMPE's. Ground-motion patterns also change drastically with different hypocenters, in excess of what is expected from directivity effects, demonstrating that the dynamics of the source process must be included in ground-motion simulations as much as possible to adequately quantify the possible seismic shaking for future earthquakes.

3.2 Dynamic Ruptures on Rough Faults

Fault roughness strongly influences the dynamic rupture process, and with that also the resulting near-source seismic wavefield. Based on the 21 different rough-fault dynamic source models, with variations in roughness pattern, roughness degree, and rupture-nucleation points, we showed how roughness parameterizations affect rupture evolution. Even a small increase in roughness profoundly alters the rupture propagation and distribution of peak slip-rates, and consequently also near-field ground motions. The roughness-induced rupture incoherence naturally generates high-frequency radiation following the widely observed spectral ω^{-2}-decay in displacement. Broadband ground-motion simulations for earthquake-engineering purposes therefore are likely to benefit from the inclusion of an "effective fault-roughness parameterization" that generates natural ground-motion characteristics over the frequency range of interest.

3.3 Kinematic Rupture Simulations for Rough Faults

Dynamic rupture simulations are still computationally expensive, requiring access to HPC-architecture, while kinematic ground-motion calculations can be essentially done on a powerful desktop computer. Therefore, we develop a kinematic source approximation that emulates the observed dynamics. To avoid computations that require parameterizing the rough-fault geometry, we developed a planar-fault approximation for the kinematic source. Comparing dynamic and equivalent kinematic simulations, we observed that perturbations in local moment tensor orientation are important, while perturbations in local source location are not. Therefore, the planar-fault approximation is permissible if the local strike, dip, and rake are maintained. We found that the dynamic rake angle variations are anti-correlated with local dip angles. Using a dynamically consistent parameterization for a Yoffe source-time function, the seismic wavefield of the planar-fault kinematic rupture reproduces the seismic radiation of the full dynamic source process. Our findings suggest that an alternative "pseudo-dynamic" source characterization can be developed that captures fault-roughness effects on rupture dynamics and seismic radiation.

4 Conclusion

Current ground-motion estimation techniques using empirical relations (GMPEs) are insufficient to quantify the level and range of shaking levels expected in future earthquakes, in particular for complex-geometry faults that may generate large (M > 7) events. Dynamic and advanced kinematic (so called pseudo-dynamic) simulations provide an avenue to investigate how rupture on complex faults may behave and what their shaking levels will be. Parameter-space studies are needed for a given fault-system under investigation to realistically estimate the range of possible shaking levels, and to develop corresponding seismic design criteria. This will be particularly important for instance in regions of massive near infrastructural developments that are prone to large earthquakes, like the Gulf of Aqaba.

References

1. Ely, G.P., Day, S.M., Minster, J.-B.: A support-operator method for visco-elastic wave modeling in 3-D heterogeneous media. Geophys. J. Int. **172**, 331–344 (2008)
2. Ely, G.P., Day, S.M., Minster, J.-B.: A support-operator method for 3-D rupture dynamics. Geophys. J. Int. **177**, 1140–1150 (2009)
3. Mai, P.M., Galis, M., Thingbaijam, K., Vyas, J., Dunham, E.: Accounting for fault roughness in pseudo-dynamic ground-motion simulations. Pure Appl. Geophys. (2017). Published online April 03, 2017. https://doi.org/10.1007/s00024-017-1536-8
4. Oglesby, D.D., Mai, P.M.: Fault Geometry, rupture dynamics, and ground motion from potential earthquakes on the North Anatolian Fault Zone under the Sea of Marmara. Geophys. J. Int. (2012). https://doi.org/10.1111/j.1365-246x.2011.05289.x
5. Oglesby, D.D.: Earthquake dynamics on dip-slip faults. Ph.D. thesis, University of California, Santa Barbara, CA (1999)
6. Oglesby, D.D, Mai, P.M., Atakan, K., Pucci, S.: Dynamic models of earthquakes on the North Anatolian Fault under the Sea of Marmara: the effect of hypocenter location. Geophys. Res. Lett. **35**, L18302 (2008). https://doi.org/10.1029/2008gl035037
7. Passone, L., Mai, P.M.: Kinematic earthquake ground-motion simulations on listric normal faults. Bull. Seismol. Soc. Am. (2017). Published online October 2017, https://doi.org/10.1785/0120170111
8. Wollherr, S., Gabriel, A.-A., Mai, P.M.: An integrated dynamic rupture model for the 1992 Landers earthquake. In revision for J. Geophys. Res. (2018)

Part II
Applications of Gravity and Magnetic Methods

The Study of the Gravity Anomaly Maps of West and Southwestern Part of Ninawa Governorate (Iraq)

Ezzadin N. M. Amin Baban

Abstract

In this study we interpreted, the gravity maps of west and southwestern part of Ninawa governorate, where, the regional gravity maps show large and extended positive and negative anomalies. These anomalies may be reflecting the effect of high and low blocks within sedimentary rocks and extended into the Basement such as Mosul block. These blocks bounded by deep faults trending NW-SE, E-W and NW-SE trend. The local positive anomalies on residual gravity maps may refer to the subsurface anticlines within the sedimentary rocks having NW-SE, E-W and NE-SW directions. These anticlines might have been formed during Najd, Hejaz and Alpine orogeny. The negative anomalies on gravity residual maps may reflect the presence of synclines within the sedimentary rocks. The assumed Fault locations on the maps may have the trending NW-SE, E-W and NE-SW. The modeling of some anomalies supported that regional anomalies reflecting the high and low features within sedimentary and basement rocks while, most of the local anomalies reflect the effect of the features with the sedimentary rocks. The depth of Moho discontinuity map constructed using Woollard (The Crust of the Pacific Basin. AGU, Washington, D.C., pp. 60–80, 1962 [1]) equation and the depth of Moho ranges 33–35 km in the area.

Keywords

Gravity • Regional • Residual • Mosul • Ninawa • Iraq

1 Introduction

The study area is located in the northwestern part of Iraq, at the west and southwest of Mosul city. Geographically, the area is bounded by latitude (36° 52′–35° 78′) and longitude (42° 27′–43° 24′). The studied area is dominated by the following geological formations ranging from Lower Miocene to Quaternary [2, 3]; Jeribi formation, Lower Fars (Al-Fatha) formation, Upper Fars (Injana) Formation (Late Miocene) and Quaternary sediments. The subsurface geology can be obtained from Atshan-1 and Adyaya-1 deep wells.

2 Separation Methods

Bouguer anomaly map of the studied [4] area shows several broad and large-scale elongated and semi-circular high (called H1, H2 and H3) and low (Called L1, L2, L3 and L4) anomalies with obvious undulations of contour lines having a direction of NW-SE and W-E. The general decrease in gradient direction of the gravity is toward SW and NE.

Two separation methods were used for the preparation of regional-residual anomalies maps which are; moving average and inverse distance methods.

3 Results (Interpretation and Discussion)

3.1 Regional Gravity Anomaly Maps

In regional maps, the general decrease in gradient direction of the gravity is toward SW and NE. There are several broad and large-scale high and low anomalies having a direction of NW-SE and W-E. These regional anomalies may reflect the effects of geological structures (blocks) within sedimentary basement rocks, bounded by faults having NW-SE and NE-SW trends (F1–F6). Below, an explanation of the most important anomalies appear on the map (Fig. 1).

E. N. M. Amin Baban (✉)
Sulaimani University, Kurdistan Region, Iraq
e-mail: ezadin.mohamed@univsul.edu.iq

N. Sundararajan et al. (eds.), *On Significant Applications of Geophysical Methods*,
Advances in Science, Technology & Innovation, https://doi.org/10.1007/978-3-030-01656-2_2

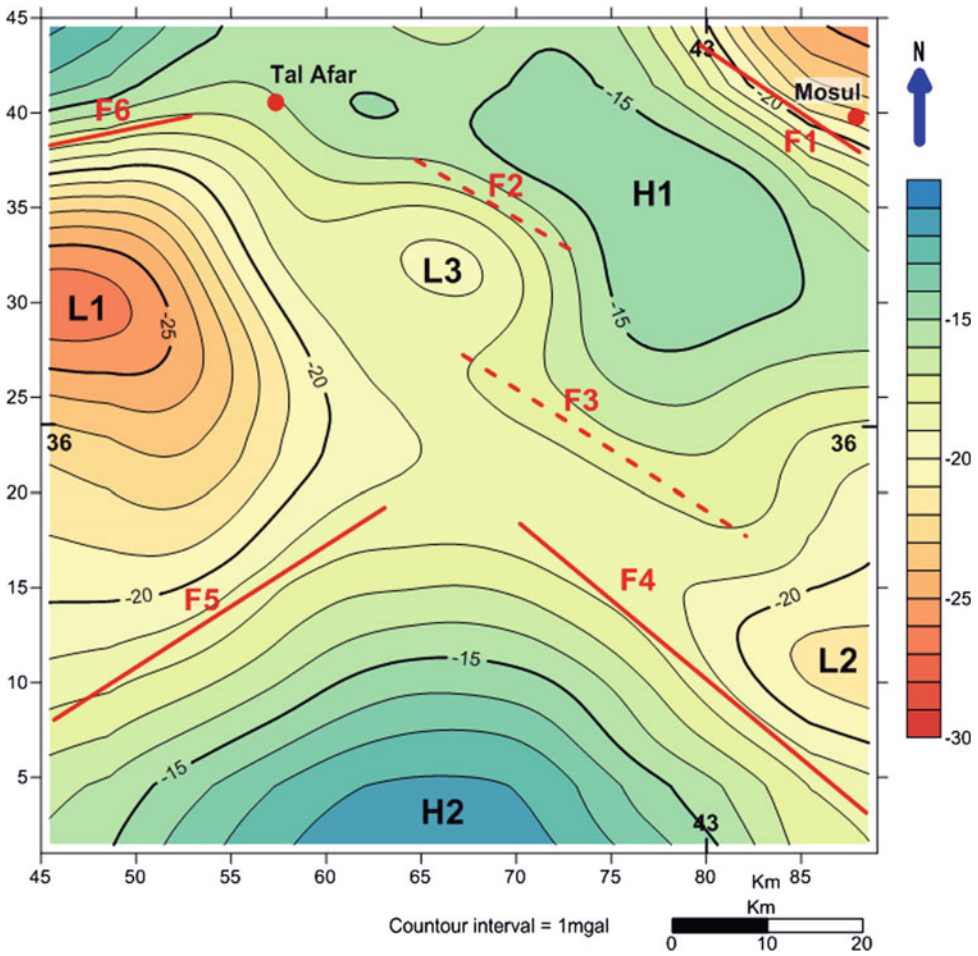

Fig. 1 Regional anomaly map of the studied area

Anomaly **H1** is a high anomaly appearing on regional anomaly maps and lies in the northern part, west of Mosul city. It is a broad, large elongated anomaly. The direction of the anomaly is NW-SE. This anomaly may reflect an elongated positive (high) block within the sedimentary cover and extended into the basement rocks too. Anomaly **H2**: Part of this high semi-circular very broad anomaly appears in the center of the southern part of the map. This high anomaly may reflect the effect of high block within the basement rocks and extended to sedimentary cover. Anomaly **L1**: It is a wide low anomaly that lies in the central part of the west of the maps having E-W direction and may refer to the existence of a low block within the sedimentary rocks and extend to the basement. Anomaly **L2**: It is low NW-SE elongated anomaly and may reflect the presence of low block within the sedimentary rocks and extending to the basement. Also several faults were recognized within the regional maps of the studied area and were marked by red color thick lines as shown on Bouguer anomaly map. Four of them (F1–F4) have NW-SE directions and the others are of NE-SW directions. F1 lies west of Mosul city. This fault may not extend to basement rocks. F2 lies northeast of L2 anomaly. Also may not extend to basement rocks. F3 lies in the central part of the map. F4 lies to the southwest of F3.

3.2 Residual Anomaly Map

The maps show several small-scale high (H1–H7) and low (L1–L3) anomalies most of them have NW-SE and E-W direction (formed during Alpine orogeny). These small and narrow anomalies may reflect the effects of shallow geological structures such as anticline and syncline within the sedimentary cover. These anomalies bounded by several NW-SE and NE-SW faults (F1–F9). Anomaly **H1** is positive anomaly lies at northern part of all the residual maps, southeast of Tal Afar town. It is elongated anomaly having a direction of NW-SE. The length of the anomaly exceeds 10 km and it is wide at the central part where it reaches 5 km. This anomaly may reflect an elongated surface and subsurface anticline within the sedimentary cover. Anomaly **H2** is positive anomaly that lies to the southeast of anomaly H1, in the northern part of all the residual maps. It is elongated anomaly with a NW-SE direction. The length of the

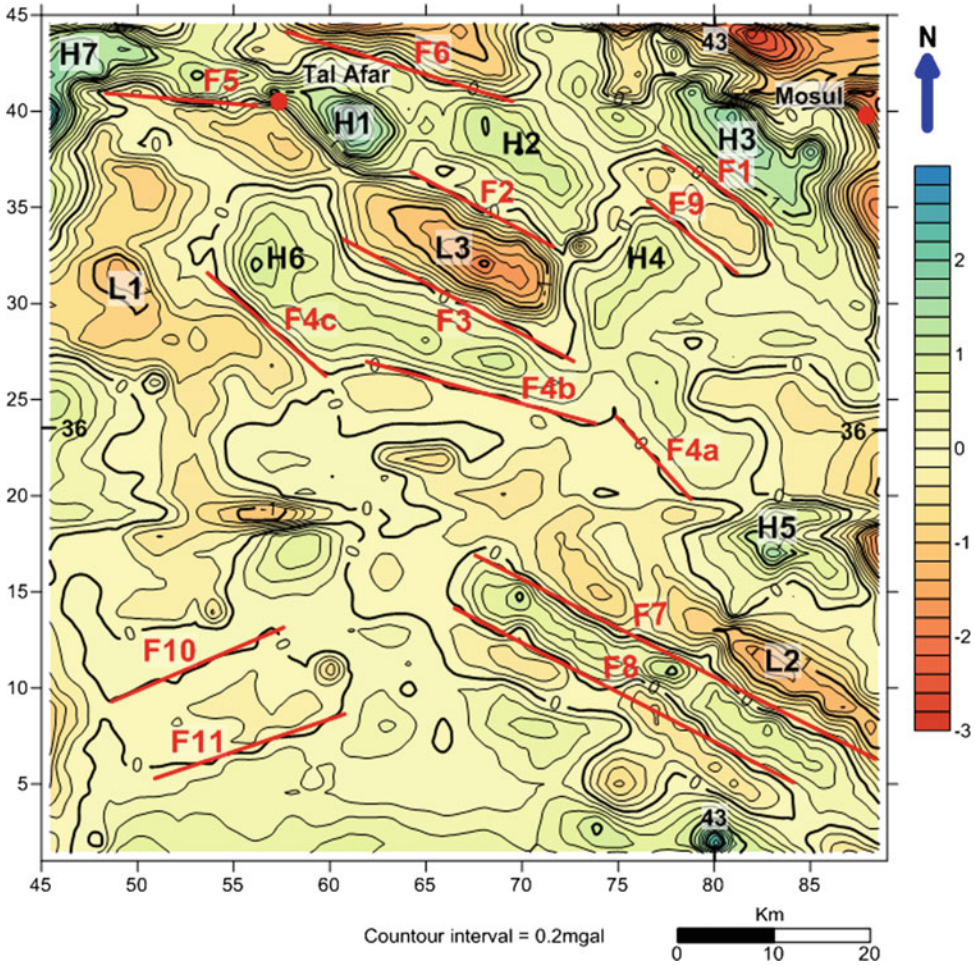

Fig. 2 Residual anomaly map of the studied area

anomaly exceeds 15 km and it is width reaches 5 km. This anomaly may reflect an elongated surface and subsurface anticline within the sedimentary cover. Anomaly **H3** is positive anomaly that lies to the southwest of Mosul city on all the residual maps. It is an elongated anomaly with a NW-SE direction. The length of the anomaly exceeds 15 km and its width reaches 6 km (Fig. 2).

Anomaly **L1**: It is a wide negative anomaly that lies at the central west part of the map trending E-W and may reflect the presence of a syncline within the sedimentary rocks. Anomaly **L2** is a negative NW-SE elongated anomaly that lies at the southeastern part of the map southwest of the positive anomaly (H5). The length of this anomaly reaches more than 50 km and its width exceeds 12 km. this anomaly consists of two domes and reflect the presence of a syncline within the sedimentary rocks.

4 Conclusion

On the regional anomaly maps, several broad positive and negative anomalies were detected. These anomalies may reflect high and low features within sedimentary rocks and extend to the Basement such as Mosul block. The length of the blocks exceeds 60 km. These blocks occurred during different orogeny such as Alpine orogeny which has NW-SE and E-W trends. The blocks bounded by faults trending NW-SE, E-W and NW-SE. The length of these faults ranges between 20 and 70 km.

The local positive anomalies on residual maps, may reflect the presence of anticlines within the sedimentary rocks having NW-SE, E-W and NE-SW trends and might have occurred during the Alpine orogeny. The modeling of some of these anomalies support this suggestion.

The negative anomalies on the residual gravity maps may reflect the effect of synclines within the sedimentary rocks trending NW-SW, E-W and NE-SW too. Most of them were assumed faults on the gravity maps trending NW-SE, E-W and NE-SW with different lengths. Some of them occurred within sedimentary rocks and extended into the Basement.

The depth of Moho discontinuity (crust thickness) map was constructed using Wollard [1] equation. It shows that the depth of Moho ranges between 33 and 35 km in the area.

References

1. Woollard, G.P., Strange, W.E.: Gravity anomalies and the crust of the Earth in the Pacific Basin. In: MacDonald, G.A., Kuno, H. (eds.) The Crust of the Pacific Basin. Geophysical Monograph Series, vol. 6, pp. 60–80. AGU, Washington, D.C. (1962)
2. Buday, T., Jassim, S.Z.: Final report and the regional geological survey of Iraq. Unpub. Report SOM. Library. Tectonic Frame Work Baghdad, 2 (1984)
3. Buday, T., Jassim, S.Z.: In: Kassab, I.I., Abbas, M.J. (eds.) The Regional Geology of Iraq, vol. 2. Tectonism Magmatism, and Metamorphism, Baghdad, 445 p (1987)
4. Al-Kadhimi, J.M., Abbas, M.J., Fathah, A.S.: Bouguer Anomaly Map of Iraq. Gravity Survey, Scale 1: 1000 000. GEOSURV, Baghdad, Iraq (1994)

High-Precision Gravity Measurements in Riyadh Using FGL Absolute Gravimeter

Saad Mogren

Abstract

This study presented the importance of the new absolute gravity measurements in bringing all gravity surveys of Saudi Arabia into one unified datum, absolute gravity was measured using FGL absolute gravity meter from 2008 to 2015, and the resultant data showed excellent coherences from 2008 to 2012 with small change of approximately 10 μGal. However, notable decrease of 31.77 μGal from 2012 to 2015 which was either due to water-level changes or the fact that the instrument was recently repaired and some parts were replaced. Nevertheless, the obtained accuracy was sufficient for geophysical and geoidal applications. A new correction value (13.117 mGal) for Potsdam datum was determined which can be used to adjust old gravity surveys tied to Potsdam datum to the new KSU gravity base station.

Keywords

Gravity measurements • FGL gravimeter
King Saud absolute gravity station

1 Introduction

High-precision repeated Absolute Gravity measurements for the Arabian Shield and Platform have several potential application areas, including the geoidal, geodynamic and hydrologic investigations. For the last two, geodynamic applications cover crustal movements whose origin is traceable to Red Sea spreading and Zagros seismicity in the region. The Arabian Shield and Platform experience tectonic movement and consequent mass deformation at crustal depths in direct consequence to lithospheric upwelling under the Red Sea and spreading. The hydrologic investigations however, relate to minor density variation primarily due to seasonal water-level changes in the subsurface at rather shallow depths. The new absolute gravity value was used now to adjust all existing gravity surveys of Saudi Arabia. Therefore, it is worth mentioning that only the ARAMCO surveys were tied to Potsdam datum whilst the other survey campaigns were tied to IGSN71 as seen in Fig. 1.

2 Research Procedure

The absolute gravity measurements were carried out using Microg™ FGL absolute gravity meter at KSU (Fig. 2), laboratory AB87 at the College of Sciences building 4 ground floor at the concrete basement this location was selected due to its quietness, room temperature stabilities between 20° and 25°, away from magnetic radiations and accessibilities to power supply. The precision of absolute gravity measurements is strongly dependent on the location of the stations. Therefore, most of the standard criteria for the absolute gravity stations were followed when selecting the station location, FGL absolute gravity measurements were observed at KSU during 2012 for 96 sets of 100 drops (shown in Fig. 3) results statistics and show the stabilities and reliabilities of the measurements. The second station was located at the Water Resources building at Hafer Al-Baten. These two stations are located on the ground surface of the building cellar at the two buildings (Results of the measurements was very accurate within ±10 μGal).

S. Mogren (✉)
Geology and Geophysics Department, King Saud University, Riyadh, Saudi Arabia
e-mail: smogren@ksu.edu.sa

N. Sundararajan et al. (eds.), *On Significant Applications of Geophysical Methods*,
Advances in Science, Technology & Innovation, https://doi.org/10.1007/978-3-030-01656-2_3

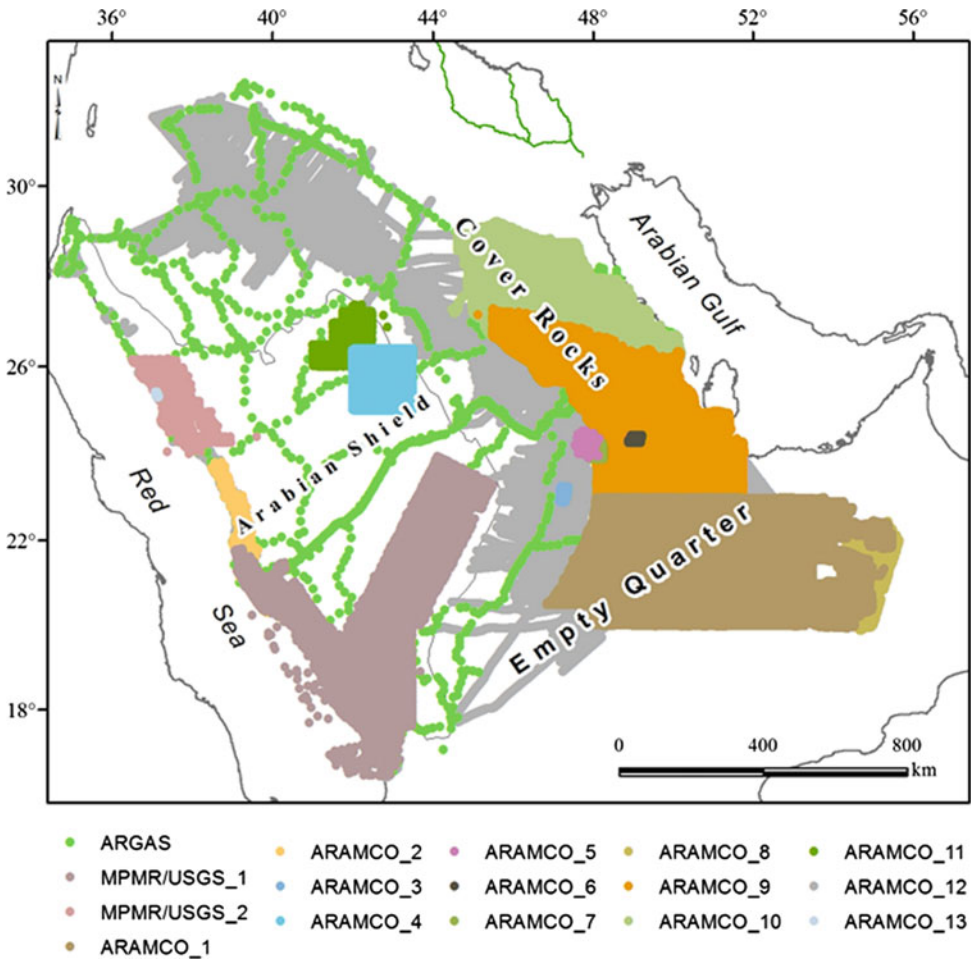

Fig. 1 Map showing the diverse existing gravity surveys, apart from ARGAS and MPMR/USGS all surveys were conducted by ARAMCO

3 Adjusting ARAMCO Gravity Surveys to KSU Absolute Gravity Station

An additional field survey trip was conducted to tie ARAMCO base stations to KSU absolute gravity station. In this trip only 5 ARAMCO base stations were resurveyed as many of them were destroyed or not accessible, calculating the median value of the differences in gravity values between old reading (which is tied to Potsdam gravity datum) and the new Absolute gravity reading at KSU base station that showed a median decrease of 13.117 mGal (Table 1) which can be considered as the difference between Potsdam gravity datum and the higher accuracy KSU gravity base station. Therefore 13.117 mGal was deducted from ARAMCO gravity readings. 13.117 mGal should be used in Saudi Arabia to convert any old gravity surveys with Potsdam datum instead of the old estimated value of 14 mGal to correct from Postdam to IGSN71 datum.

4 Discussion and Conclusion

A huge area of Saudi Arabia was not covered by gravity surveys. We think it is necessary now to start filling these empty gaps particularly in the Arabian Shield. All existing

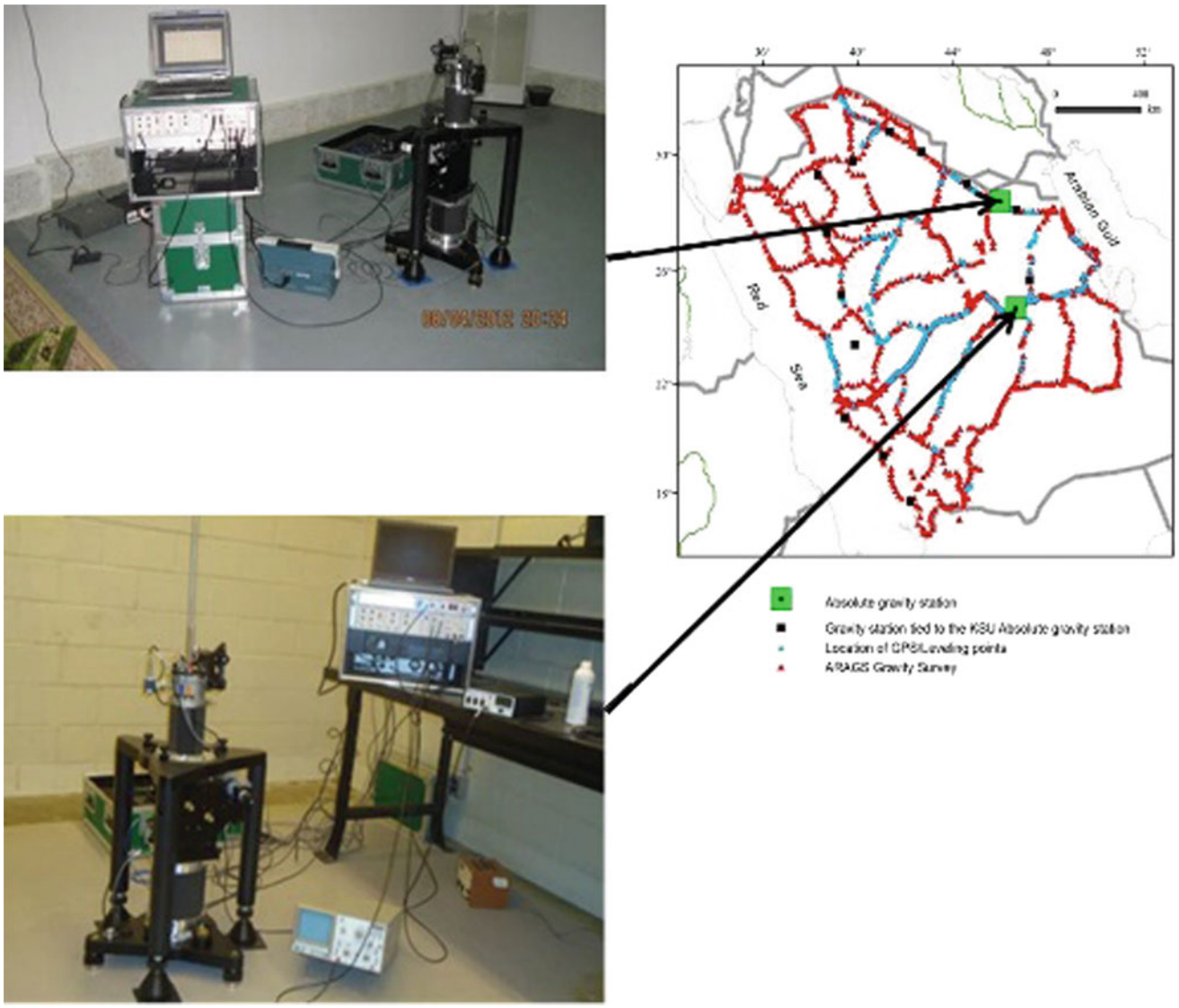

Fig. 2 FGL absolute gravimeter operating at KSU and at Hafer Al-Baten gravity base stations, these sites were selected based on their quietness and the facilities provided in these sites (electricity and air-conditioning)

gravity data need to be tied to the new absolute gravity stations. Corrections, mainly adjustments should be applied to the existing gravity surveys to get a seamless unified gravity grid. For absolute gravity measurements, increasing the number of sets more than 4 sets will not increase accuracy. 2008–2011 showed changes of 9.9 μGal probably due to hydrological effects. However, a notable decrease of 31.77 μGal from 2012 to 2015 which was either due to

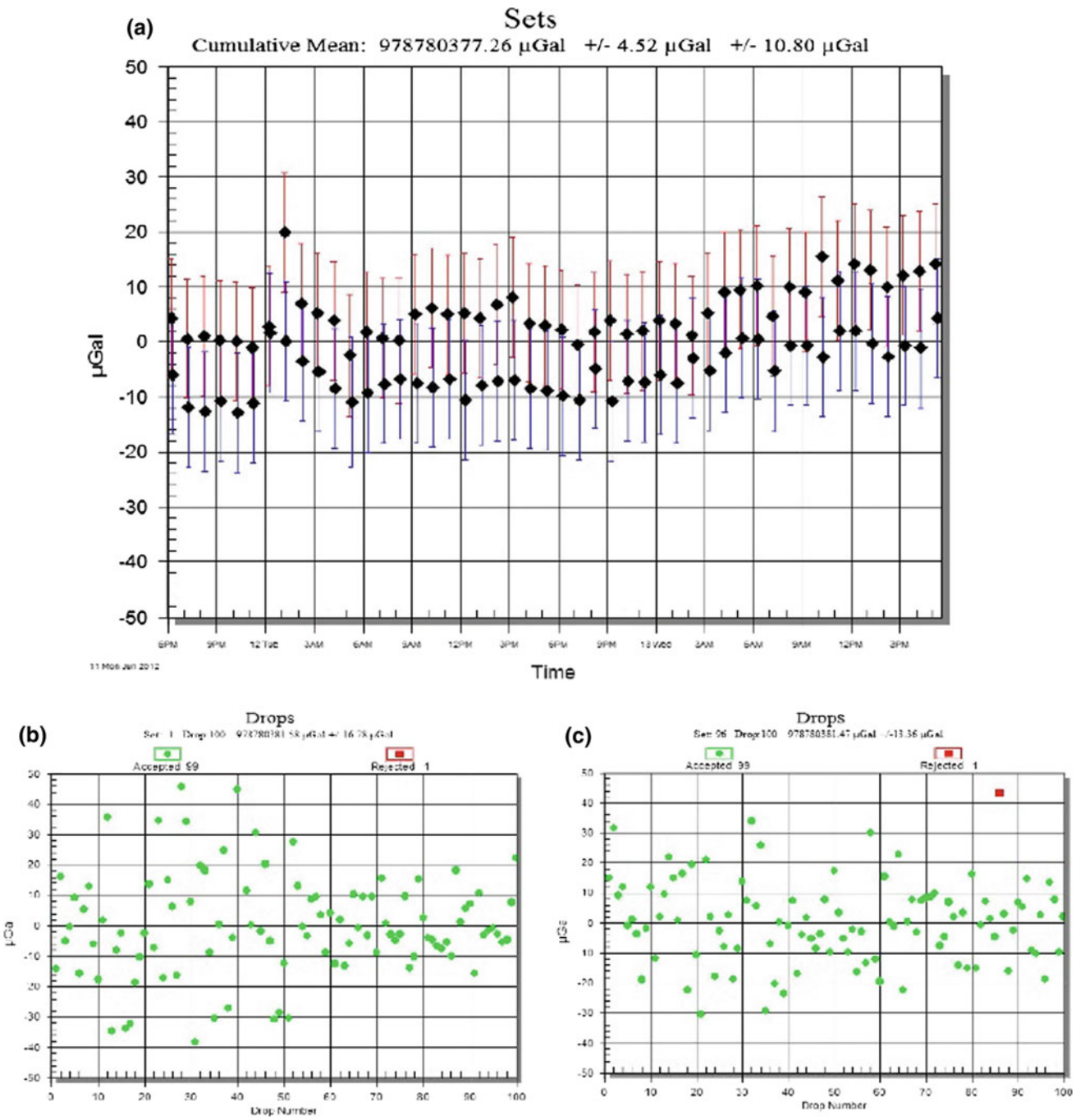

Fig. 3 Absolute gravity station at KSU using FGL for 96 sets, **a** is the cumulative mean, **b** and **c** are diagram showing the statistics of set 1 and set 96. Sets 1 and 96 were selected to show the stability and reliability of the gravity measurements

Table 1 The difference between Potsdam (datum used by ARAMCO) and the new KSU absolute gravity measurements, it can be seen from the table that a median value of 13.117 mGal should be used to adjust old ARAMCO gravity surveys

Station	KSU absolute gravity in mGal	L5808/S P1322	L5856/SP1 182	L5852/SP1368	L5624/SP10425	BARRAH GRAV. BASE
Tied to KSU station	978,780.3773	978,771.373	978,738.359	978,737.487	978,765.550	978,757.577
Tied to Potsdam datum		978,784.49	978,751.48	978,750.6	978,778.74	978,770.37
Differences		13.117	13.121	13.113	13.190	12.793
Median value	13.117 mGal					

water table level or to the fact the instrument was recently repaired and some parts were replaced at the factory. Absolute gravity measurement showed good stability apart from 2012 to 2015 which needs more investigations. A new value was determined to correct gravity surveys referenced to Potsdam (−13.117 mGal).

Geological Evolution of the Tefedest Terrane a Recorder of a Polycyclic Pan-African Amalgamation (Central Hoggar, Algeria): Evidence from Airborne Geophysics, Remote Sensing and Field Study

Massinissa Amara, Abderahmane Bendaoud, Toshiake Tsunogae, Mohamed Amrouche, Zakaria Hamimi, Gregory Dufrechou, Mark Jessell, Basem Zoheir, Mohamed Hamoudi, and Safouane Djemai

Abstract

Tuareg shield lies to the Pan-African domain that has recorded a complex orogenic evolution during the upper Neoproterozoic. It is bordered to the west by the West African craton (WAC) stable since 2 Ga and to the east by the East Saharan Metacraton. Referring to Previous works this shield recorded two main punching phases; an early collisional phase within the west with the WAC through mega N–S shear zone and last one to the East with the eastern Saharan metacraton. The main purpose of this work was to bring new geological and interpreted geophysical data by using remote sensing, airborne geophysics and fieldwork to produce an updated geological map. Moreover, it extracted tectonic features that encompass the kinematics evolution of N–S shear zones border of the Tefedest terrane that is part of central Hoggar. The integration of remote sensing data processing as well as airborne geophysics (Magnetic and Gamma ray spectrometry) data led to develop a 1/200,000 scale geological map. The extracted tectonic features (foliation, lineaments and main shear) through various processing techniques led to set chronological deformation steps as E–W foliation was relics of oldest deformation phases and D2 is N–S tight fold phase, while D3 was merely a brittle wrench feature. The Tefedest evolution was transpressive and slides through the main shear border led their squeezing toward north during Pan-African orogeny.

Keywords

Hoggar • Tectonic • Geological map • Remote sensing • Airborne geophysics

1 Introduction

The Tefedest terrane belongs to central Hoggar terranes south of Algeria (Fig. 2a and b). Its emplacement led that terrane to record a very complex orogenic process related at different stages to the Pan-African orogeny (630–520 Ma) [1]. Despite some old performed Geological works on the whole central Hoggar (Fig. 2c) [1]. Tefedest terrane was involved in very scarce studies, where the terrane was edified by an E–W compression accompanied by three main magmatic cycles [2]. Deformation Phases were defined as early tangential under amphibolite facies followed by a wrench brittle under green schist grade, which was sealed by NE–SW to E–W conjugated fault [3]. The main purpose of this work was to develop a new geological and interpreted geophysical data by using remote sensing (Landsat 8 Oli), coupled with airborne geophysics (magnetic and gamma ray) and fieldwork to produce an updated geological map as well as emphasize the tectonic evolution of the main border shear zones of the Tefedest terrane.

M. Amara (✉) · A. Bendaoud · M. Hamoudi · S. Djemai
University of Science and Technology Houari Boumediene, Algiers, Algeria
e-mail: maamara@usthb.dz

T. Tsunogae
Faculty of Life and Environmental Sciences (Earth Evolution Sciences), University of Tsukuba, Ibaraki, 305-8572, Japan

M. Amrouche
Schlumberger K.K Center, 2-2-1 Fuchinobe, Chuo Sagamihara, Kanagawa 252-0206, Japan

Z. Hamimi · B. Zoheir
Benha University, Benha, Egypt

G. Dufrechou
Géosciences Environnement Toulouse, 14 Avenue Edouard Belin, 31400 Toulouse, France

M. Jessell
Center of Exploration Targeting, Perth, Western Australia, Australia

N. Sundararajan et al. (eds.), *On Significant Applications of Geophysical Methods*,
Advances in Science, Technology & Innovation, https://doi.org/10.1007/978-3-030-01656-2_4

2 Data and Materials

This study was mostly based on using Landsat Oli 8 acquired on June 2015 and checked for acceptable cloud cover level (<1%), sensor errors such as banding and other geometric distortions.

It was geometrically orthorectified and calibrated to soil reflectance [4]. Band rationing (BR) enhancement was conducted with analysing prior data compiled from fieldwork (samples) and anterior maps together faced to spectral band response (exploitation of slope spectra extracted by referring to field observation and evaluation of spectral separability) of enhanced images to produce an updated map (Fig. 2b). A classification algorithm was applied as a supervised Maximum likelihood; this led to produce the Classified (Predictive map) of the outcropped lithological units. The training strategy used was based on existing geologic maps (i.e. Map Based sampling), reported lithologies from previous works [1, 2, 5] as well as location samples already collected in this work. Airborne geophysics as Magnetic and gamma ray spectrometry data were used. It consists of 2 km spaced flight line and 40 km tie line at 150 m above the ground level [6]. In the study region (Central Hoggar) the flight path was carried under E–W trending perpendicular to the N–S shape main structures, the raw data were compiled, spike noise removed and corrected from diurnal variation and heading path flight error levelled. Geomagnetic reference field (IGRF75) was removed [6] to obtain the main crustal remanence; acicular variation of 100 nT that is created during survey which introduced artefacts that may be considered lacking in this survey [7]. The TMI was then reduced to pole assuming induced magnetization using inclination I = 28.75 and declination D = −4.47 (Fig. 3a). Gamma ray was used in this study to well circumscribe the lack of granitoids and intermediate rocks reported from previous work, and were corrected from cosmic ray and atmospheric noise and converted to PPm or percentage for Potassium. Element ratio map was performed to highlight geochemical distribution of elements in various geological units (Fig. 3b). All the used data were compiled under GIS environment and faced to field investigation measurement carried in different parts of the Tefedest terrane and anterior geological work.

3 Results

3.1 Remote Sensing Results

Enhancement as Abrams ratio [8] performed on Landsat 7 ETM+ (R: 6/7, G: 4/2, B: 5/6) in Landsat 8 Oli were successfully conducted (Fig. 1a). This ratio seems to operate in steep slope absorption between Band 6 and Band 7 for Taourirt alkaline granite, Archechoum amphibolitic orthogneiss, quartzitic rocks as well as metavolcanic, rhyolites and orthogneiss. The predicted final map was checked statistically and compared to generalized collected data based on previous published geological works, and maps gave the accuracy of map-based and field-based training area as 60.72% and Kappa coefficient of 0.58. Further using Landsat 8 data was successful in extracting foliation path and sense of shearing of the main fault of the Tefedest terrane (Fig. 1a).

3.2 Airborne Geophysics Results

Several Processing filters were applied to magnetic data as Tilt derivative applied on Magnetic reduced to pole (RTP) anomaly map or upward RTP anomaly map, that allowed us to highlight deep structures and report most important lineaments and large scale shear zones (Fig. 2a). However airborne gamma ray data were helpful to adjust the interpreted predictive map, report several lithologies as Ternary U, Th and K shaded to magnetic data (Fig. 2b) and finalize the 1/200,000 scale geological map of Tefedest terrane (Fig. 2b).

4 Discussion and Conclusion

Field work investigation and compiled remote sensing and geophysical data have led us to 1/200,000 geological map; as Taourirt post orogenic granite were well highlighted with Ternary Gamma ray spectrometry as well as most geological unit limits have been well reported by remote sensing enhancement and classification. However, predicted remote

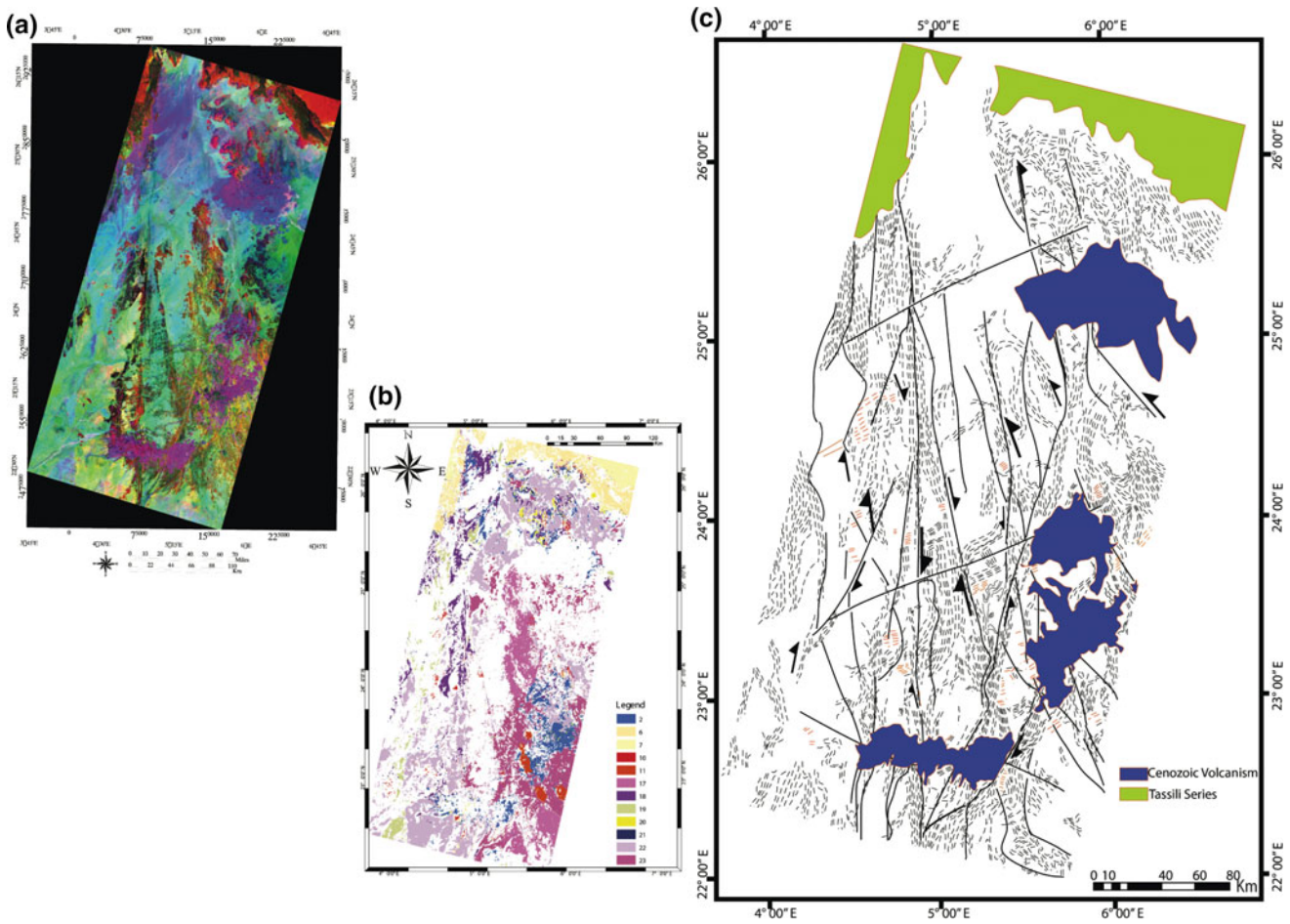

Fig. 1 **a** Band ratio color composite displayed as R: 6/7, G: 4/2, B: 5/6, and its supervised classification results on the Tefedest terrane with an RMS < 20% (**b**). **c** Foliation path and structural sketch of the Tefedest terrane derived from directional filter and enhancement processing results leading to kinematic interpretation

sensing classification output led to an average result of the reality even though class code of each lithology was assessed for best class separability during spectral enhancement, while airborne gamma ray led to geochemical and mineralogical features classification. Various magnetic processings and interpretations and textural information derived from remote sensing data led us to report the whole structural character of the Tefedest terrane. More field investigation is needed to understand more accurately the deformation phases and tectonic evolution of the Tefedest block; however, compiling several data performed in this work allowed us to report some stages as described below:

- E–W foliation is relics of an oldest deformation phase (D1), while N 150° direction seems to be guidance for setting place of early Pan-African granites as oldest structural direction (Fig. 3f) [2–8].
- D2 is ductile and operates under Amphibolites facies [2] propped by N–S with N–S tight fold with stip dipping toward the north (Fig. 3e).

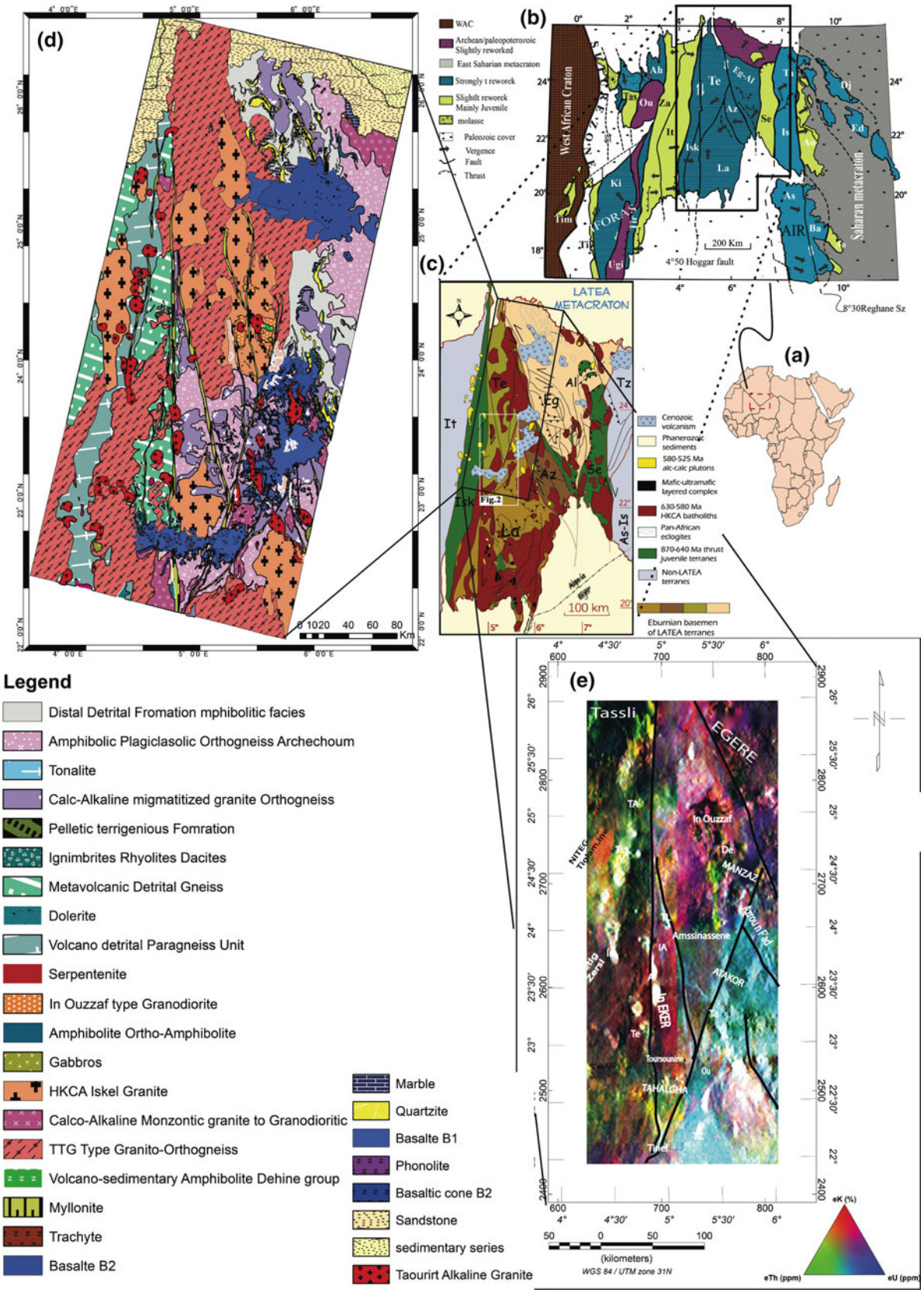

Fig. 2 **a** Central Hoggar position map; **b** Combined Tuareg shield mam from [9] and [1] . Solid arrow movement direction. From east to west, of the 23 terranes, **c** sketch map of central Hoggar terranes (from Liégois et al. 2003). **d** Geological map in GIS environment of the Tefedest terrane. **e** Ternary U, Th and K gamma ray spectrometry with different blocs of Tefedest terrane which shows different types of granitoids and various lithologies the lead to compile the geological map

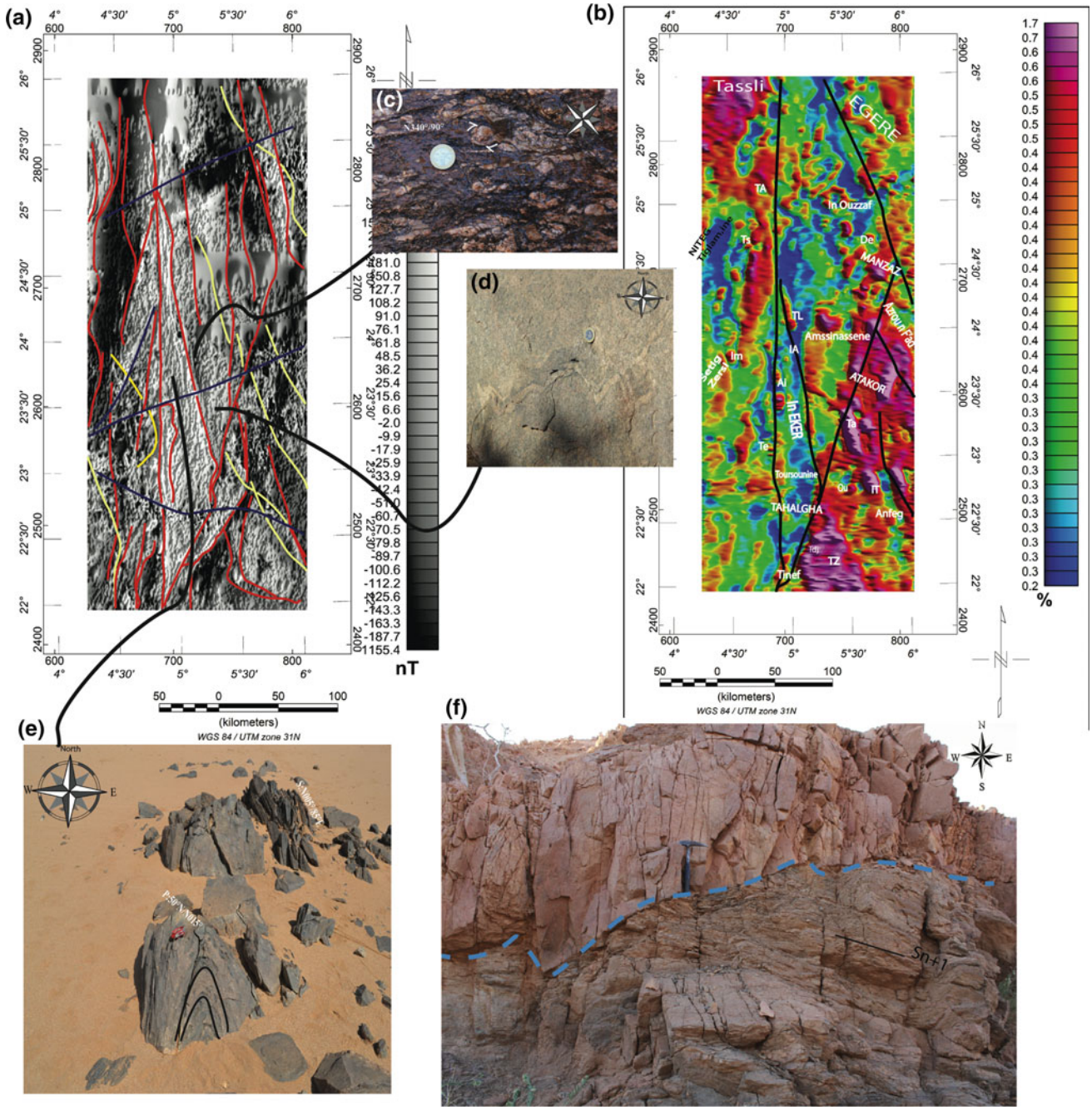

Fig. 3 **a** Magnetic reduced to pole anomaly map of the Tefedest terrane, with chronological lineament interpretation respectively from the oldest to younger as yellow, red and blue. **b** U/K ratio gamma ray map of Tefedest terrane which shown limits of TTG, granitoids and older basement signature. **c** In Amguel-Amssinassene shear indicator in ultra mylonitic band, **d** thrusting toward west indicator underlined by a leucosome in migmatites. **e** Tight fold in amphibolitic orthogneiss with axial plan dipping of 50° N. **f** E–W foliation in orthogneiss described by [3] as Sn+1 is used as guidance for emplacement of Pan-African granites

- D3 seems to be fragile deformation with vertical component considered as reactivation of all N–S south faults as wrench character of In Amguel and 4°50 faults associated to low-grade metamorphism [3].
- D4 is characterized by E–W to NE–SW fault seems to be started as early as the Post orogenic granite intrusion to later eras as guidance for Cenozoic volcanism, with reactivation after Cambrian age probably.
- Tefedest terrane presented features of N–S half sigmoid shape and related a transpressive deformation feature (Fig. 3c, d and e) and witnessed the squeezing of the Hoggar toward the north during the Pan-African shortening [1].

References

1. Liégeois, J.P., Latouche, L., Boughrara, M., Navez, J., Guiraud, M.: The LATEA metacraton (Central Hoggar, Tuareg shield, Algeria): behaviour of an old passive margin during the Pan-African orogeny. J. Afr. Earth Sci. **37**, 161–190 (2003)
2. Vitel, G.: La region Tefedest Atakor du Hoggar central (Sahara). Evolution d'un complexe granulitique précambrien. Unpublished Thesis, University of Paris, France, 324 pp (1979)
3. Boullier, A.M., Bertrand, J.M.: Tectonique tangentielle profonde et couloirs mylonitiques dans le Hoggar central polycyclique (Algérie). Bull. Soc. Géol. Fr. **23**, 17–22 (1981)
4. Chander, G., Markham, B.L., Helder, D.L.: Summary of current radiometric calibration coefficients for Landsat MSS, TM, ETM and EO-1 ALI sensors. Remote Sens. Environ. **113**, 893–903 (2009)
5. Azzouni-Sekkal, A., Liégois, J.P., Bechiri-Benmerzoug, F., Belaïdi-Zinet, S., Bonin, B.: The "Taourirt" magmatic province, a marker of the closing stages of the Pan-African orogeny in the Tuareg shield: review of the available data and Sr–Nd isotope evidence. J. Afr. Earth Sci. **37**, 337–350 (2003)
6. Boubekri, H., Hamoudi, M., Bendaoud, A., Priezzhev, I., Allek, K.: 3D structural cartography based on magnetic and gravity data inversion—case of South-West Algeria. J. Afr. Earth Sci **112**, 471–484 (2015)
7. Schnetzler, C.C., Taylor, P.T., Langel, R.A., Hinze, W.J., Phillips, J.D.: Comparison between the recent U.S. composite magnetic anomaly map and Magsat anomaly data. J. Geophys. Res. **90**, 2543–2548 (1985)
8. Abrams, M.J., Rothery, D.A., Pontual, A.: Mapping in Oman ophiolite using enhanced Landsat Thematic Mapper images. Tectonophysiscs **151**, 387–401 (1988)
9. Black, R., Latouche, L., Liégeois, J. P., Caby, R., Bertrand, J. M.: Pan-African displaced terranes in the Tuareg shield (central Sahara). Geology **22**(7):641 (1994)

Structural Setting of Western Mali Insights from Magnetic Data Analysis

Adama Youssouf Kone, Imen Hamdi Nasr, Wajdi Belkheria, Mohamed Hedi Inoubli, Adnen Amiri, and Saïdou Ly

Abstract

Within the Western African Craton, the Kedougou-Kenieba Inlier lodges the Senegalo-Malian Shearing-Zone, with its secondary structures, control the gold mineralization. The magnetic method is of great interest in structures determination and characterization. Many techniques were applied to the airborne magnetic data (Field Residual, Reduction to Equator, Derivations, and Euler Deconvolution) in order to reveal magnetic structures related to mineralization. Lineaments of different directions (N–S, NE–SW, NW–SE and E–W) have been identified and coincided with the known faults and intermediate to basic magmatic dykes. These lineaments have low magnetic intensity signatures, generally negative. A large NE–SW overlapping corridor contains the majority of the Artisanal Mining Sites testifying the controllability of gold deposits by the NE–SW structures. Euler solution led to a brief estimate of the depth of different structures. This led to propose additional targets so as to help exploration activities in Western Mali.

Keywords

Aeromagnetic data • Geophysics • West Africa Craton (WAC) • Kedougou-Kenieba Inlier (KKI) • Western Mali

A. Y. Kone (✉) · I. H. Nasr
Faculty of Sciences of Bizerte (FSB), University of Carthage, Bizerte, Tunisia
e-mail: konenos@gmail.com

A. Y. Kone · I. H. Nasr · W. Belkheria · M. H. Inoubli · A. Amiri
Research Unity of Applied Geophysical at Ore and Material (UR-GAMM), Tunis, Tunisia

A. Y. Kone
Faculty of Sciences and Technics (FST), University of Sciences, Technics and Technological of Bamako (USTTB), Bamako, Mali

S. Ly
Ecole Nationale d'Ingénieurs Abdaramane Baba Toure (ENI-ABT), Bamako, Mali

1 Introduction

In the West African Craton (WAC), and within the Precambrian land, the structural characterization is inaccurate and difficult. The airborne magnetic data were carried out in order to determine the magnetic behavior of Paleoproterozoic structures of the Kossanto region, within the Kedougou-Kéniéba Inlier (KKI). This work allowed to identify structures controlling the gold mineralization in the Birimian of western Mali.

2 Geological Setting

The Kossanto region is located in the Kedougou-Kéniéba Inlier (KKI) within the West African Craton (WAC). The WAC is this part of Africa stabilizing around 1700 Ma [1] at the end of the eburnean orogeny [2, 3]. The WAC is made up with the plutonic, volcano-sedimentary, metamorphic and migmatites formations. These formations are located in the Reguibat Mountain to the north and that of Leo to the South as well as the Precambrian base inlier, named Kayes (Mali) and Kedougou-Kenieba (Senegal and Mali). A large Paleozoic basin (Taoudeni, Illemeden, Tindouf, Volta …) distributed through those Precambrian terranes.

3 Methodology

Aerodat collected geophysical data in 1996 using the «Geometrics G-822A cesium streams» magnetometers. Flight lines interval was 200 m, flight height 120 m and direction of N65-245°. Quality assessment and quality control were completed by SYSMIN (Mining System) project in 2001. Flight characteristics are/line interval: 3000 m; height: 120 m, line direction: N155-335. Different filters were used: Residual anomaly, Reduced to Equator Field

N. Sundararajan et al. (eds.), *On Significant Applications of Geophysical Methods*,
Advances in Science, Technology & Innovation, https://doi.org/10.1007/978-3-030-01656-2_5

(RTE) and Euler Deconvolution. This work aim to specify different geological structures and estimate depth of causative sources.

4 Data Analysis and Interpretation

The residual anomaly and Reduction to Equator maps give similar features showing NE–SW lineaments and in some places NW–SE trend. These lineaments have negative magnetic signatures (Fig. 1a). There is also a central lineament with an N–S trending, which corresponds to the Senegalo-Malian Sheared zone (SMS). Some associated magnetic signal, corresponding to intrusive bodies, are outlined.

In Kossanto, lineaments coincide with intermediate to basic rocks dykes. The central accident N–S (SMS) appears to be perturbated by magmatic intrusions. Euler Deconvolution technique allows a quantitative interpretation of dykes (SI = 1) related previously defined lineaments above (NE–SW, NW–SE and E–W). It appears that the majority of NE–SW and E–W directions are located less than 250 m depth.

Magnetic interpretation of Kossanto area led to highlight the main structural trend of Western Mali globally N–S trending, known as Senegalo-Malian Shear zone (Fig. 2). NE–SW, NNE–SSW, NW–SE and E–W lineaments were also identified and thought to be secondary structures of the SMS (Fig. 2). NE–SW and E–W faults are filled up with intermediate to basic rock dykes [3].

Previous studies confirm the gold controllability by SMS and its secondary structures in the KKI [4, 5]. Secondary lineaments (NE–SW; NNE–SSW; NW–SE and E–W) are crosscut or intersected by SMS [6]. This is approved by geological observations in the field [3].

Interpreted lineaments are recognized as Birimian. They present negative anomalies (Fig. 1). They correspond to a NE–SW shear zones, NE–SW and E–W dykes and NW–SE contact zones in the field. NE–SW lineaments, N5-60° bearing, frame lineaments (N10 to 45°) and thus establish a large NE–SW corridor from the village Naragui to Netekoto (Fig. 2), bordering the majority of gold Artisanal Mining Sites (AMS).

NE–SW lineaments can be detected in the surface geology. However, the quantitative interpretation testifies for their rooting up to 500 m depth (Fig. 2).

5 Conclusion

Aeromagnetic data analysis led to the identification of lineaments with trending corresponding highlighted structures (faults and dyke) defined by previous researchers in KKI. The distribution of Artisanal Mining Sites (AMS) in the study area confirms that gold mineralization is controlled by NE–SW trending structures (Fig. 2). This was proven by various studies at the KKI scale. In Kossanto south-west part, the identified dextral shear zone, N24° bearing, over 3 km, is similar to D3 phase fault. According to previous works, this would be a component of Riedel type corridor in Senegal. Interpretation shows a similar corridor but larger in Western Mali (Fig. 2).

Lineaments with negative magnetic signatures were defined. NE–SW and N–S trending structures seem to control gold mineralization in KKI. There is a large NE–SW corridor, which includes partly the one defined in eastern Senegal. This corridor frames is known as gold deposits and artisanal mining sites. Among the new proposed targets, some are rather shallow.

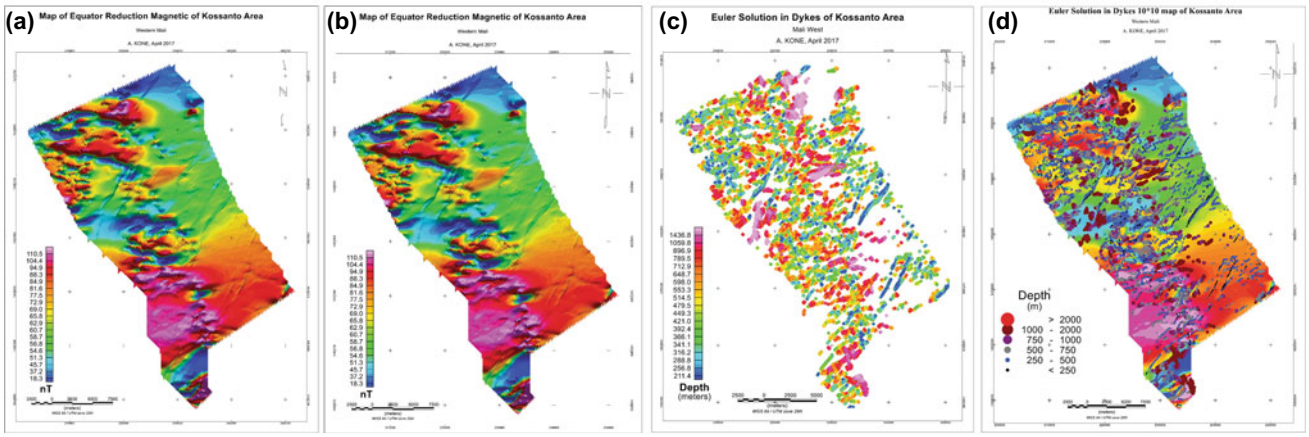

Fig. 1 Residual anomaly (**a**), reduction to equator magnetic (**b**) and both map solution (**c**) and plot point solution in RTE (**d**) are Euler deconvolution

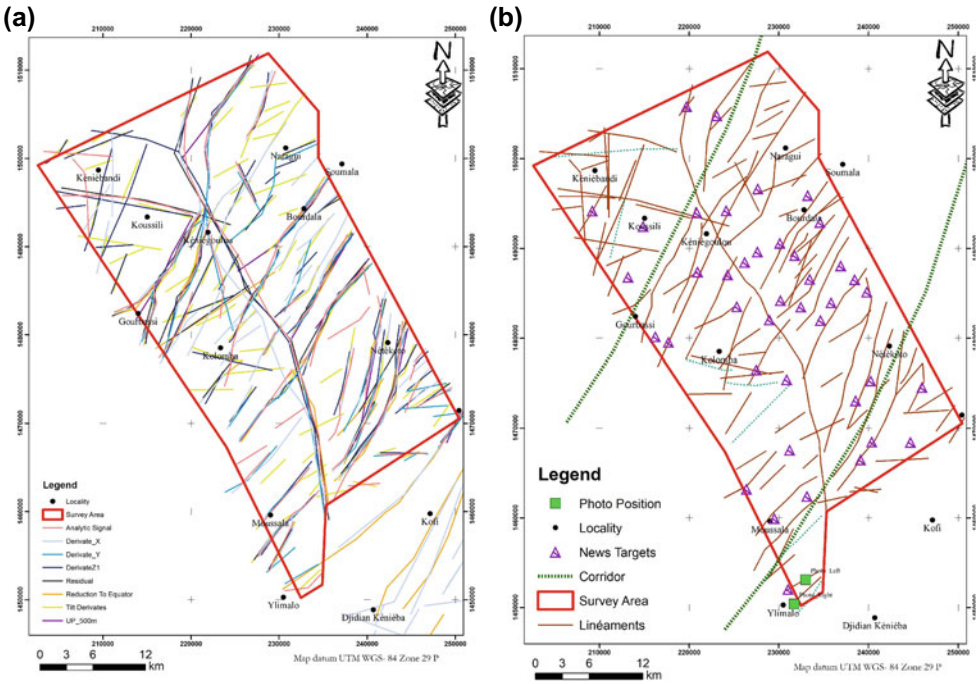

Fig. 2 **a** Lineaments map of different magnetic filters, **b** magnetic lineaments with Kossanto new targets proposal

References

1. Rocci, G.: Essai d'interprétation des mesures géochronologiques de la structure de l'Ouest africain. Science de la Terre **10**(3–4), 461 (1966)
2. Allibone, A., Teasdale, J., Cameron, G., Etheridge, M., Uttley, P., Soboh, A., Appiah-Kubi, J., Adanu, A., Arthur, R., Mamphey, J., Odoom, B., Zuta, J., Tsikata, A., Pataye, F., Famiyeh, S.: Timing and structural controls on gold mineralization at the Bogoso gold mine, Ghana, West Africa. Econ. Geol. **97**, 949–969 (2002)
3. Feybesse, J.M., Sidibé, Y.T., Konaté, C.M., Lacomme, A., Zammit, C., Guerrot, C., BRGM, CPG, DNGM.: Notice explicative de la Carte géologique de la République du Mali à 1/200 000, Feuille n° ND-28-XII/ND-29-VII, Dalafi—Kossanto Bamako (MALI), 2ième édition, 34 pp. Ministère des Mines, de l'Énergie et de l'Eau (2006)
4. Lambert-Smith, J.S., Lawrence, D.M., Vargas, C.A., Boyce, A.J., Trelaor, P.J., Herbert, S.: The Gounkoto Au deposit, West Africa: constraints on ore genesis and volatile sources from petrological, fluid inclusion and stable isotope data. Ore Geol. Rev. **78**, 606–622 (2015)
5. Masurel, Q., Miller, J., Hein, A.A.K., Hanssen, E., Thébaud, N., Ulrich, S., Kaisin, J., Tessougue, S.: The Yatela gold deposit in Mali, West Africa: the final product of a long-lived history of hydrothermal alteration and weathering. J. Afr. Earth Sci. **113**, 73–87 (2016)
6. Dabo, M., Aïfa, T.: Late Eburnean deformation in the Kolia-Boboti sedimentary basin, Kédougou-Kéniéba Inlier, Senegal. J. Afr. Earth Sci. **60**, 106–116 (2011)

Improved Internal Geomagnetic Field Selection Using Artificial Neural Network

Ayoub Boudelaa and Mohamed-Cherif Berguig

Abstract

Data selection is a very important step for Earth's magnetic field modelling. Many measurements were taken through many different kinds of observations, leading to a huge amount of geomagnetic data. However, many of these observations are of poor quality due to the disturbances caused by either the solar winds or even worse the Coronal Mass Ejection (CME) phenomenon. For this reason, the resulting data must be filtered before modelling, by excluding any sort of disturbance. Using geomagnetic indices is a common way to locate these disturbances based on their values at a specific time interval. In this work, we introduced a new approach using the ability of Artificial Neural Network (ANN) to learn patterns within data and make predictions, and also some geomagnetic indices to train the prediction model.

Keywords

Artificial Neural Network • Data selection
Geomagnetic indices

1 Introduction

Several satellites were launched through the years, such as CHAMP (Challenging Minisatellite Payload) in 2000 and Swarm in 2013, providing us with an enormous amount of uninterpreted and disturbed data for the Earth's magnetic field modelling. Thus, in order to eliminate the disturbances caused by the solar activities, the data must be filtered first before modelling, keeping only the quiet-time data.

There are many approaches and algorithms for data selection. A common way to filter data is to use geomagnetic indices. Each index describes a specific geomagnetic activity at a specific time interval. A wide range of algorithms, such as BGS/G/L/0706 filters [1] was introduced to improve the quality of the selection and the model as well.

In the last few years, the usage of Artificial Neural Network (ANN) in geophysics has highly increased. Mohamed et al. [2] have used ANN to develop a geothermal gradient map based on gravity and corrected bottom-hole temperature data. Another work by Watanabe et al. [3] has also taken advantage of ANNs to predict Dst index two hours in advance from solar wind parameters.

In this paper, we introduced a new different approach for geomagnetic data selection using ANN. For the training process, we used geomagnetic indices data to label our training and testing sets. Besides, we fed our prediction model with a large amount of data (Swarm 2013.0 data set) to increase its accuracy as much as possible.

2 Methodology

An ANN consists of learning patterns within data to build a decision and prediction model based on weighted connections between neurons. A neuron is a computational unit which takes an input and produces an output using the following formula: $y = \sum_i^n X_i w_i$ where n is the number of inputs, X is the input and w is the weight. For nonlinearity an activation function is used to modify the output. An ANN has typically three layers of neurons: the input (raw data), hidden and output layers.

In the present study, we used the ANN to filter geomagnetic data by evaluating each row to determine whether it is disturbed or not. Our learning process has two main steps: preprocessing and training. The first step consists in labeling the geomagnetic data (Swarm data in our case) in the context of supervised learning, so our ANN can learn from it. Therefore, we leaned on the described geomagnetic activity and used the following geomagnetic indices for labeling: *Kp*, *ap* and *Dst* for global geomagnetic storm activity, and *PC* (Polar Cap) and *AE* (Auroral Electrojet) for

A. Boudelaa (✉) · M.-C. Berguig
University of Science and Technology Houari Boumediene, Algiers, Algeria
e-mail: ayoub.boudelaa@etu.usthb.dz

N. Sundararajan et al. (eds.), *On Significant Applications of Geophysical Methods*,
Advances in Science, Technology & Innovation, https://doi.org/10.1007/978-3-030-01656-2_6

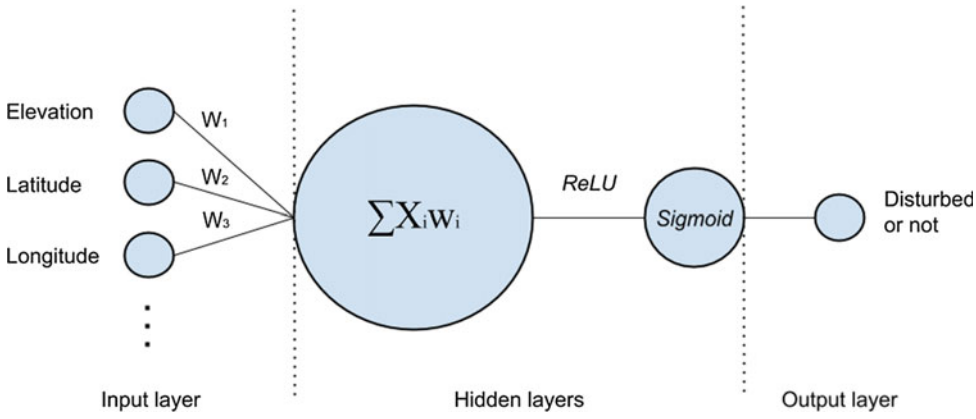

Fig. 1 The flow diagram of the ANN used to filter geomagnetic data

high latitude currents and substorms [4]. Using multiple indices allows us to identify any sort of disturbance and increase the quality of the learning as well. The criteria on which we labeled a data row as disturbed or not (1 or 0) was based on the conjunction of these indices. For instance, if $Kp < 2$, $|Dst| < 20$ and $PC < 0.8$ for a given row, we mark it as quiet (not disturbed).

In the training step, we constructed our ANN starting with selecting the right inputs for the input layer. Thus, we used the following inputs for Swarm 2013.0 data set: *date*, *time*, *latitude*, *longitude*, *altitude*, F, dF, B_x, B_y, B_z, dB_x, dB_y and dB_z. However, we converted *date* and *time* to *sun elevation*, which we believe that it is better for the learning than handling them directly. For the hidden layers, determining the number of layers and the neurons within them is data-dependent and requires testing and tuning to find the most satisfied network design. The activation function used in these layers is the ReLU (Rectified Linear Unit) function: $max(0, y)$. To produce a probability outcome in the output layer, we changed the activation function from ReLU to a Sigmoid function: $\frac{1}{1+e^{-y}}$ (Fig. 1).

The way that the geomagnetic data was split for training and testing, which is very important. Feeding the ANN with only quiet-time data in the training will result in a poor prediction and vice versa. So, in order to ensure balanced data, we divided them by months, instead of days, using three months for training and one for testing.

3 Results

3.1 Evaluation Metrics

Using accuracy and AUROC (Area Under the Receiver Operating Characteristic curve) metrics with K-Fold Cross Validation, we obtained the following results for 10 iterations (K = 10) (Table 1).

Table 1 Accuracy and AUROC metric outputs

Iteration	Accuracy	AUROC
1	0.834	0.911
2	0.836	0.824
3	0.826	0.912
4	0.841	0.914
5	0.837	0.873
6	0.798	0.907
7	0.847	0.922
8	0.802	0.915
9	0.783	0.926
10	0.797	0.912

The accuracy metric is the ratio of correct predictions to all predictions made, whereas the AUROC metric represents the ability of our model to discriminate between disturbed and quiet rows. It is a performance metric used for binary classification problems. The obtained mean AUROC is about 0.902, which means that our ANN is well trained.

4 Discussion

Using ANNs for data selection opens new doors for the application of Artificial Intelligence in geophysics. Learning from data instead of dealing with it roughly allows a better understanding. With geomagnetic indices being well suited to isolate quiet-time data, using them to accomplish the learning leads to a quite good decision and prediction model capable of performing a selection of quality on its own. However, the model can be allowed to improve the model continuously not only through the quality of the data but also the quantity.

5 Conclusion

The use of ANN to filter geomagnetic field data has proved to be fast and efficient. Using different geomagnetic indices to label the data, does not only ensure a quality training for the prediction model, but also improves the quality of modeling by eliminating as much as possible the disturbances caused by the solar activities.

References

1. Thomson, A.W.P., Lesur, V.: An improved geomagnetic data selection algorithm for global geomagnetic field modelling. Geophys. J. Int. **169**, 951–963 (2007)
2. Mohamed, H.S., Abdel Zaher, M., Senosy, M.M., Saibi, H., El Nouby, M., Fairhead, J.D.: Correlation of aerogravity and BHT data to develop a geothermal gradient map of the northern western desert of Egypt using an artificial neural network. Pure Appl. Geophys. **172**, 1585–1597 (2014)
3. Watanabe, S., Sagawa, E., Ohtaka, K., Shimazu, H.: Prediction of the Dst index from solar wind parameters by a neural network method. Earth Planets Space **54**, 1263–1275 (2002)
4. Kauristie, K., Morschhauser, A., Olsen, N., Finlay, C.C., McPherron, R.L., Gjerloev, J.W., Opgenoorth, H.J.: On the Usage of Geomagnetic Indices for Data Selection in Internal Field Modelling. Springer (2016)

Lithospheric Structure Along a Transect from Red Sea to Arabian Shield Using a Potential Data (Gravity and Aeromagnetic Data)

Akrem Nahali, Hakim Gabtni, and Chokri Jallouli

Abstract

There is an evidence that the crustal thickness from the Red Sea coastal plain to the interior of Saudi Arabia increases dramatically from 10 km in the Red Sea to about 42 km. In order to give more insights on crustal configuration of the Arabian plate, we proposed to analyze available gravity and aeromagnetic data. The gravity data was analyzed and interpreted within a profile A-B perpendicular to the Red Sea coast along the western margin of the Shield. The analysis included the construction of Bouguer gravity and residual anomaly maps, regional gravity and magnetic anomaly maps based on wavelength filtering and derivative techniques, and 2.5D gravity models were constructed in an integrated method constrained by surface geology and previous work such as the available seismic refraction and broadband models [Hansen et al. in Earth Planet. Sci. Lett., 2007 1]. Our observations of lithospheric structure showed a relative complexity of the gravity and aeromagnetic anomaly controlled by structural complexity and variable lithology of the transect and support a two-stage rifting history along the Red Sea and suggest that the Moho and LAB topography is the result of extension and erosion caused by asthenosphere flow where the thinnest lithosphere is coincident with the rift axis.

Keywords

Red Sea • Arabian shield • Gravity • Aeromagnetic • Model • Rifting

1 Introduction

The Arabian shield and the Red Sea (Fig. 1) are areas with a huge potential in natural resources. One of the main targets in mineral and petroleum exploration is to characterize the structure of the sedimentary cover and the topography of the crystalline Precambrian basement [2]. During the last decade, different transect from the Arabian shield to the Red Sea have been subject of numerous geophysical surveys to unravel the crustal and lithospheric structure of the region [3–6]. All these studies show a variable resolution depending on the particular area subject to analysis and the method used. In our case, gravity modelling was combined with additional techniques and data sets in order to build the regional gravity and magnetic anomaly maps based on wavelength filtering and derivative techniques. The aim of this work is to provide a first-order estimate of the crustal and lithospheric mantle geometries of the transect Arabian Shield-Red Sea and bring new insights on the large-scale geodynamics of this segment.

2 Materials and Methods

In order to model the lithospheric structure of the studied area, two methods were referred to namely gravity and aeromagnetic methods.

A. Nahali (✉)
Geological Department, Faculty of Sciences, University Tunis El Manar, Campus Universitaire, 2092 Manar 2, Tunis, Tunisia
e-mail: akrem93@hotmail.com

A. Nahali · H. Gabtni
Georessources Laboratory, Centre de Recherches et des Technologies des Eaux (CERTE), BO 273 Soliman, 8020, Tunisia

C. Jallouli
Department of Geology and Geophysics, College of Sciences, King Saud University, P.O. Box. 2455 Riyadh, 11451, Saudi Arabia

N. Sundararajan et al. (eds.), *On Significant Applications of Geophysical Methods*,
Advances in Science, Technology & Innovation, https://doi.org/10.1007/978-3-030-01656-2_7

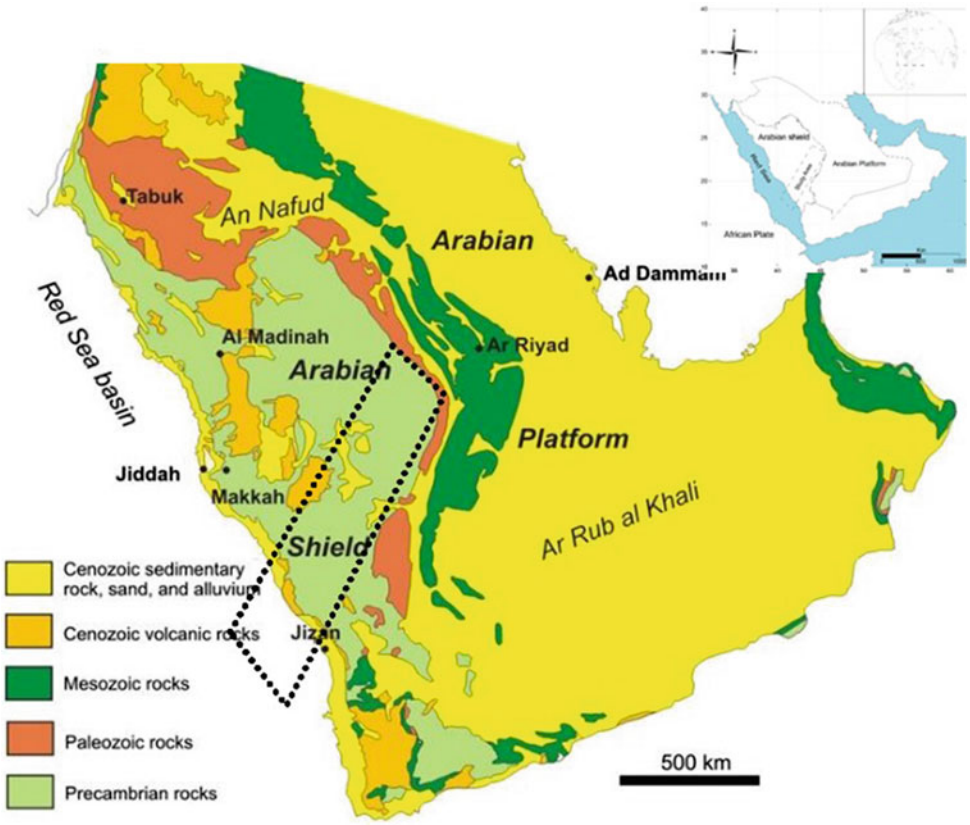

Fig. 1 Location of the study area with different geological domains

- Gravity method: The gravity data used in this work are from International Gravimetric Bureau (BGI), collected by United States geological survey (USGS) at a station density of 1 per 100 km^2. The gravity survey was carried out in 1976, covering approximately 202,100 km^2 and including a total of 2477 gravity stations. Free air and Bouguer gravity corrections were performed using sea level as a datum and 2.67 g/cm^3 as a reduction density.
- Aeromagnetic method: We used the aeromagnetic data from the International Gravimetric Bureau (BGI). Several aeromagnetic surveys were carried out from 1962 to 1983 by commercial companies under the auspices of the Ministry of Petroleum and Mineral Resources of the Kingdom of Saudi Arabia and supervised by BRGM and USGS. The surveys were conducted over individual blocks. They had round clearances of 150, 300, or 500 m and a line spacing of about 800 m [7].

3 Results

3.1 Gravity Results

We were able to identify the Bouguer anomaly (Fig. 2) with several anomalies in the transect indicating two major directions: NorthWest–SouthEast and North–South.

2.5D regional gravity model (Fig. 4) using a 3D forward modeling algorithm that calculates the gravitational attraction due to an ensemble of right, rectangular prisms.

Crust, lithospheric mantle and asthenosphere densities were estimated from average seismic velocities and previous studies [1, 5, 8] in order to convert them to densities using the Nafe–Drake relationship. Sediment thickness was extracted from a global sediment model. The model was broken up into three layers: Crustal structure (2.85 g/cc in the interior of the

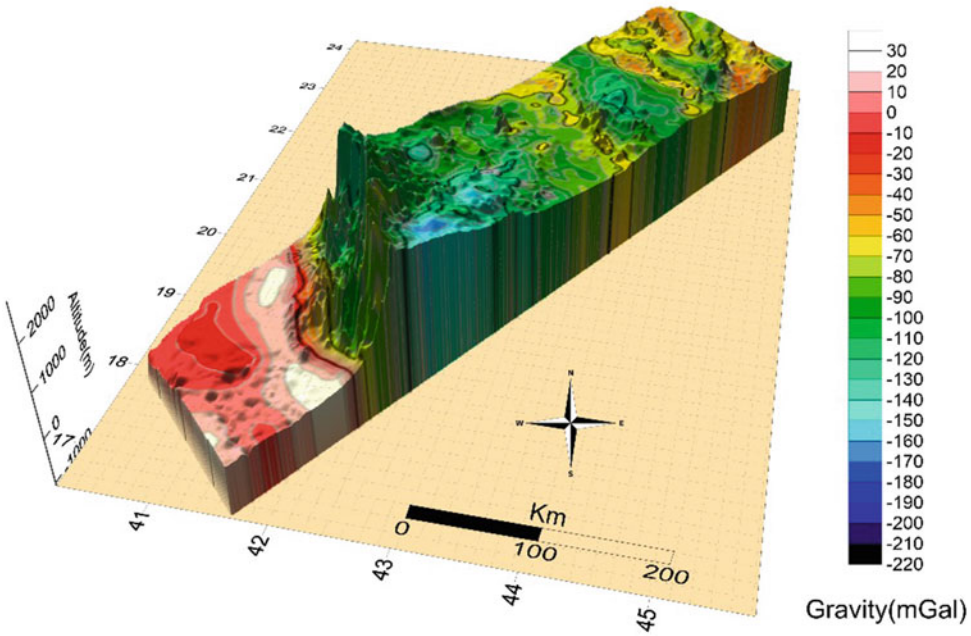

Fig. 2 3D representation shows Bouguer anomaly superimposed over topographic model of the study area

shield), lithospheric mantle (3.2 g/cc) and asthenospheric structure (3.12 g/cc) (Fig. 4). We chose 2.67 g/cc as a reference density. Gravity modeling indicates a high density heterogeneities within Asir province that represents the transition zone represented by a typical mafic crust below the coastal plain [9] and provides insight on mass distribution, lithospheric configuration and their significant changes. The model shows a mean global thickness of 45 km beneath the Shield areas that decreases to 12 km beneath the Red Sea.

We have managed to distinguish the delimitation in our study area (Red Sea, Asir tectonic province and Najd tectonic province) from the upper crustal structure (Figs. 3 and 4).

3.2 Aeromagnetic Results

A general examination of Reduction to the pole (RTP) anomaly (Fig. 5) shows the solid white lines coinciding with the High aeromagnetic axis, dashed white lines coinciding with the Low aeromagnetic axis, AP and AN are labels for the solid and dashed white lines, respectively. Contour interval is 10 nT, AP and AN are labels for the solid and dashed white lines respectively.

In comparison with the Bouguer gravity anomaly (Fig. 2) that reflects the northward shift in the positions of the inherited magnetic anomalies due to the elimination of the inclination and the declination effect of the magnetic field. Also, the sizes of the anomalies become larger and centered over their respective causative bodies.

4 Discussion

Based on gravity and magnetic analysis, there is evidence of several anomalies in two major directions: North West–South East and North–South. We interpret them as changes in bulk composition of rocks.

There are big differences in lithospheric buoyancy, thinner and denser beneath the Red Sea; thicker and more buoyant beneath the Arabian Shield. Our gravity model confirms the results of previous geophysical studies [1, 3, 5, 9, 10]. The Moho and Lithosphere, Asthenosphere Boundary (LAB) are shallowest near the Red Sea and become deeper towards the Arabian interior. Near the coast, the Moho is at a depth of about 12.5–15 km. Crustal thickening continues until an average Moho depth of about

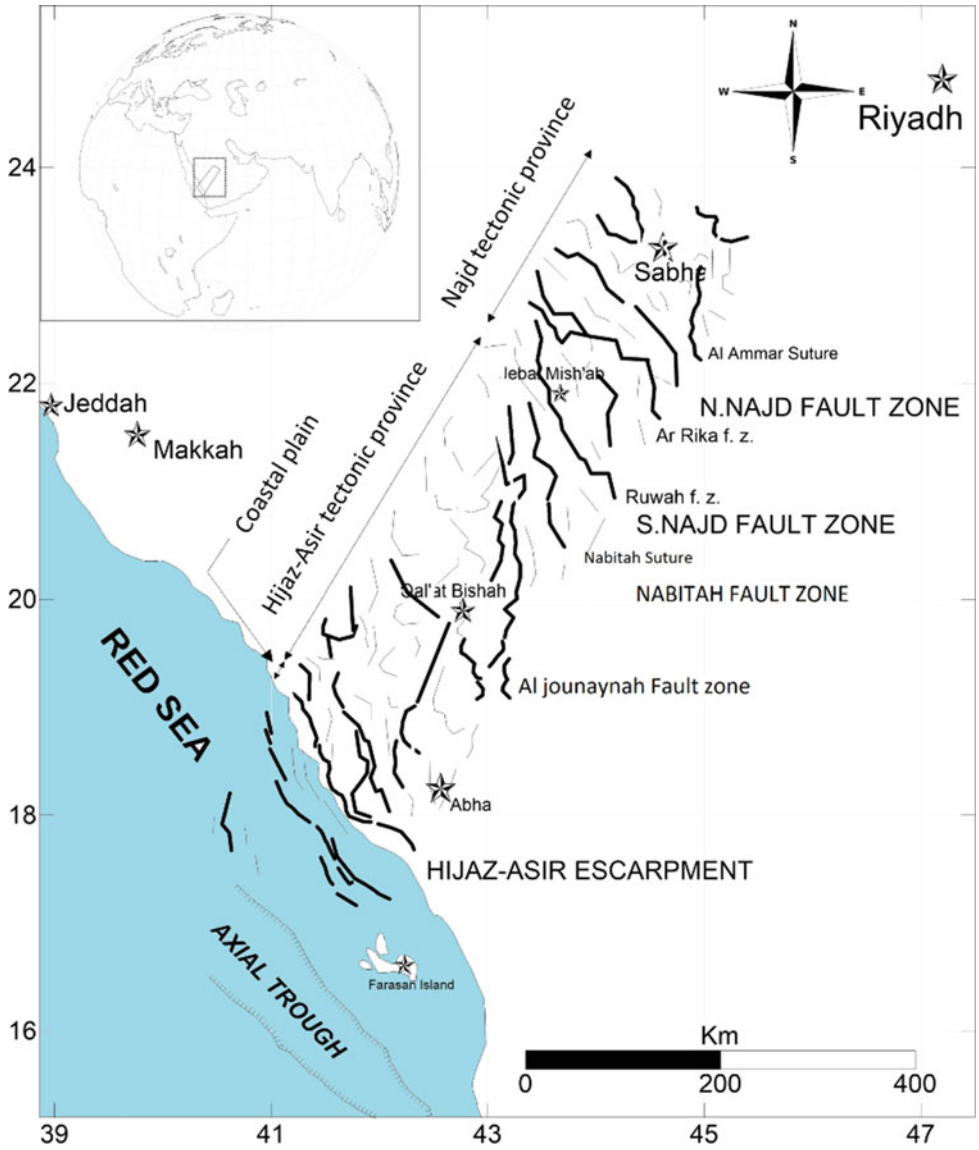

Fig. 3 Results of the gravity modeling that provides some basic insight into the mass distribution and crustal configuration

40–45 km is reached beneath the interior Arabian Shield. The LAB near the coast is at a depth of about 35 km; however, it also deepens beneath the Shield to attain a maximum depth of 145 km. Signatures of rifting and crustal thinning are evident here: The crustal and lithospheric configuration derived from the gravity modeling for the entire transect supports the consensus view on Red Sea spreading for the region.

Our observations of lithospheric structure support a two-stage rifting history along the Red Sea and suggest that the Moho and LAB topography are the results of extension and erosion caused by asthenospheric flow where the thinnest lithosphere is coincident with the rift axis. Previous studies [1] speculated the existence of such topography and suggested that it may direct asthenospheric flow beneath the Arabian Shield and the Red Sea Rift.

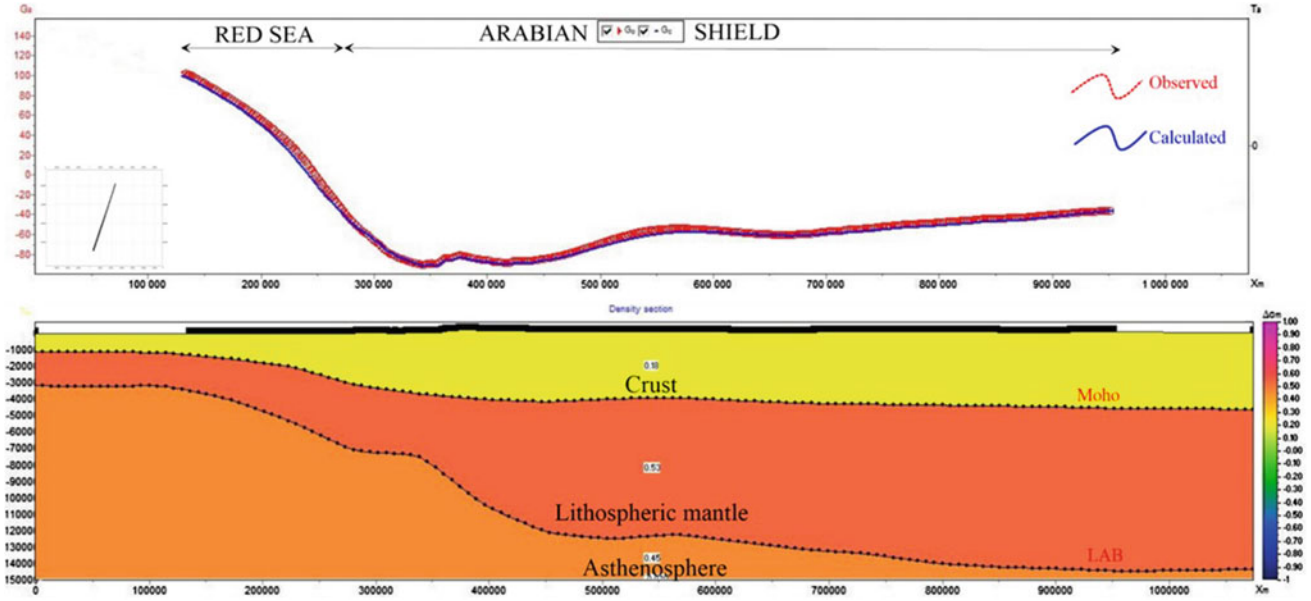

Fig. 4 NorthEast–SouthWest cross-section of the 2.5D regional gravity model. The cross-section consists of three layers: asthenospheric structure, lithospheric mantle and crustal structure

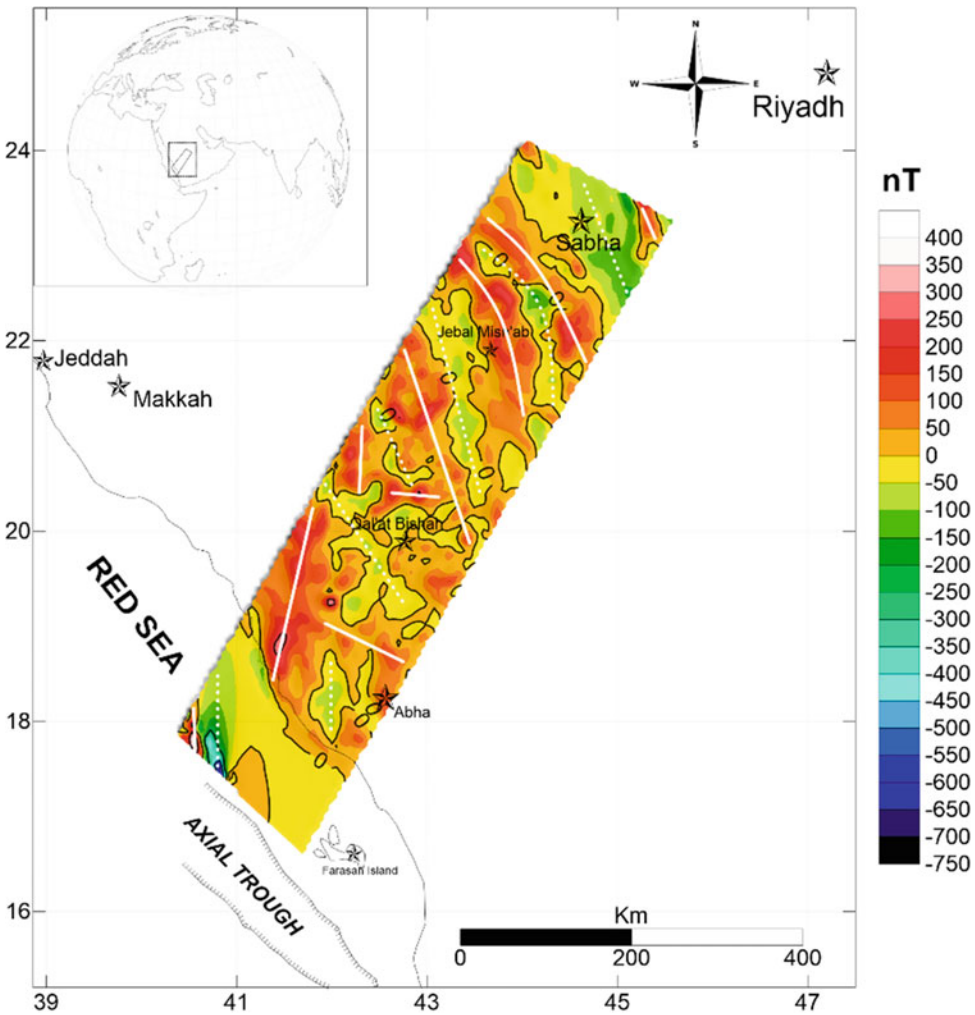

Fig. 5 RTP anomaly map of the study area

5 Conclusions

The transect Arabian Shield-Red Sea represents an excellent example of passive margin with little relative complexity of the Bouguer and RTP anomaly controlled by structural complexity and variable lithology of the study area.

Finally, it is thought that further models (velocity model, aeromagnetic model) are required in order to give more insights on crustal configuration of the Red Sea margin.

References

1. Hansen, S., Rodgers, A., Schwartz, S., Al-Amri, A.: Imaging ruptured lithosphere beneath the Red Sea and Arabian Peninsula. Accepted for publication in Earth Planet. Sci. Lett. (2007)
2. Jiménez-Munt, I.: 3-D lithospheric structure and regional/residual Bouguer anomalies in the Arabia-Eurasia collision (Iran). Geophys. J. Int. (2012)
3. Al-Amri, A.: Crustal and Upper Mantle Structures Beneath the Arabian Shield and Red Sea. Springer International Publishing AG (2017)
4. Mooney, W.D., Gettings, M.E., Blank, H.R., Healy, J.: Tectonophy. **136**, 173–246 (1995)
5. Sandvol, E., Seber, D., Barazangi, M., Vernon, F., Mellors, R., Al-Amri, A.: Lithospheric seismic velocity discontinuities beneath the Arabian shield. Geophys. Res. Lett. **25**, 2873–2876 (1998)
6. Stern, R.: Arc assembly and continental collision in the Neoproterozoic East Africa Orogen: implications for the consolidation of Gondwanaland. Annu. Rev. Earth Planet. Sci. 319–351 (1994)
7. Aboud, E.: Magnetic and gravity data analysis of Rahat Volcanic Field, El-Madinah city, Saudi Arabia. NRIAG J. Astron. Geophys. (2015)
8. Rodgers, A., Walter, W., Mellors, R., Al-Amri, A., Zhang, Y.: Lithospheric structure of the Arabian shield and platform from complete regional waveform modeling and surface wave group velocities. Geophys. J. Int. **138**, 871–878 (1999)
9. Mogren, S., Mukhopadhyay, M.: Gravity modeling for the rifted crust at the Arabian shield margin—further insight into Red Sea spreading, open. J. Geol. **3**, 28–33 (2013)
10. Gettings, M., Blank, H., Mooney, W., Healey, J.: Crustal structure of southwestern Saudi Arabia. J. Geophys. Res. **91**, 6491–6512 (1986)

Neotectonic Deformation Model of the Northern Algeria from Paleomagnetic Data: Preliminary Results from Northwestern Areas

Mohamed El-Messaoud Derder, Saïd Maouche, Philippe Robion, Bernard Henry, Mohamed Amenna, Boualem Bayou, Yves Missenard, Rafik Bestandji, and Salamet Mahboubi

Abstract

Previous paleomagnetic studies, performed in central North-Algeria (Chelif and Mitidja basins) on Neogene formations, pointed out some tectonic clockwise rotations of large blocks, sometimes of large amplitudes. Narrow zones represent also important shear zones with strong rotations. The preliminary results of a new paleomagnetic study undertaken in Northwestern Algeria (Aïn Temouchent–Ghazaouet area) suggest the presence of clockwise block-rotations of lower magnitude. That confirms that the northern Algeria is organized as tectonic blocks, accommodating by transpression and blocks rotations, the Africa-Eurasia convergence. A gradient of "deformation" appears from the NNE to the SSW, i.e. from the Mitidja basin affected by strong rotations to Aïn Temouchent–Ghazaouet area where the rotations are limited.

Keywords

Northwestern Algeria • Paleomagnetism
Neotectonics • Block rotation • Transpression

M. E.-M. Derder (✉) · S. Maouche · M. Amenna · B. Bayou
R. Bestandji · S. Mahboubi
CRAAG, BP 63, 16340 Bouzaréah, Alger, Algeria
e-mail: m.e.m.derder@gmail.com

P. Robion
Geosciences Environnement Cergy, 5 Mail Gay-Lussac,
95031 Cergy-Pontoise Cedex, France

B. Henry
Paléomagnétisme, IPGP and CNRS, 4 Avenue de Neptune,
94107 Saint-Maur Cedex, France

Y. Missenard
GEOPS, Université Paris-Sud, CNRS, Université Paris-Saclay,
Rue du Belvédère, Bât. 504, 91405 Orsay, France

1 Introduction

The convergence between Africa and Eurasia plates in northern Algeria involves transpression tectonics with N–S to NNW–SSE shortening direction. This shortening is reflected by active deformation along the plate borders. Northern Algeria is structured by regional major E–W to WNW–ESE dextral shear zones, in which active structures affect Neogene to Quaternary sedimentary basins (e.g. Chelif and Mitidja Plio-Quaternary basins). Within this context, the NE–SW trending folds and NE–SW sinistral transpressive faults delimit NE–SW oriented blocks. A kinematic model describing the active deformation in northern Algeria could be that of blocks rotation, the NNW–SSE trending direction of convergence (resulting from the transpressive tectonics) implying clockwise rotations of these blocks [1].

Paleomagnetism represents an efficient approach to point out rotations. So, previous paleomagnetic studies, performed in North Central Algeria (Chelif and Mitidja basins), on Neogene sedimentary and magmatic formations [2–4], highlighted tectonic clockwise rotation of large blocks, sometimes of important amplitude, in agreement with the kinematic model. Narrow zones represent also significant shear zones with strong rotation of smaller blocks [5]. In order to check the validity of this kinematic model in other regions, a new paleomagnetic study was carried out on the Neogene-Quaternary rocks (mostly magmatic) outcropping in the Aïn Temouchent–Ghazaouet area (Northwestern Algeria).

2 Paleomagnetic Sampling

The geophysical method used in this study is the paleomagnetism [6]. Volcanic large bodies, of different ages, outcrop in 6 main areas [7] in the northwestern Algeria (Fig. 1). They were extensively sampled for the paleomagnetic investigations: 800 cores distributed over 75 sites were oriented using magnetic and sun compasses and collected (Fig. 1).

N. Sundararajan et al. (eds.), *On Significant Applications of Geophysical Methods*,
Advances in Science, Technology & Innovation, https://doi.org/10.1007/978-3-030-01656-2_8

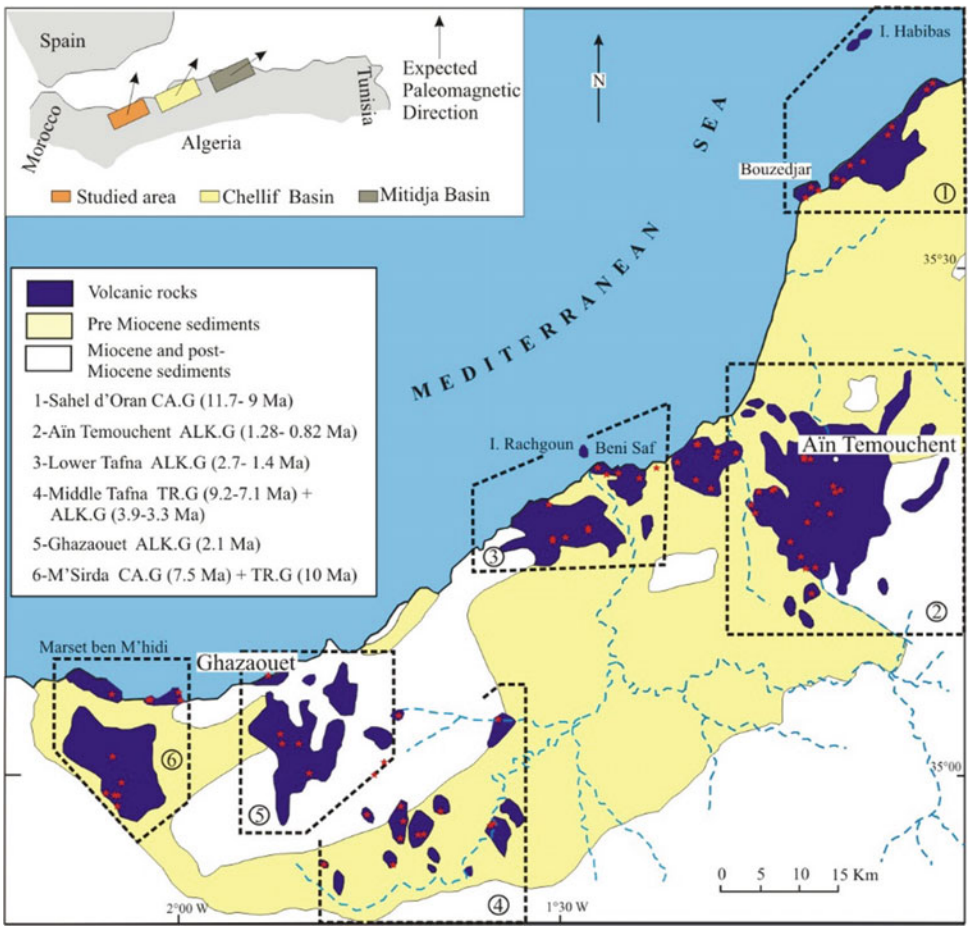

Fig. 1 Geological map (from Coulon et al. [7], modified) of the studied area showing the sampling sites (red stars). The inset indicates the location of the studied area with respect to Mitidja and Chelif basins; the arrows point out the obtained mean paleomagnetic direction from each basin

3 Paleomagnetic Results

Following the selection from pilot specimen investigation and until today, 616 samples have been demagnetized. During the demagnetization procedure, two different main cases were observed from Zijderveld diagrams. The first one, obtained from most samples, is described by a single stable magnetic B direction obtained after elimination of a secondary viscous A component. The Characteristic Remanent Magnetization (ChRM) B is of normal or reversed polarity according to the sites. Ti-poor titanomagnetite is the principal magnetic mineral carrier of this B magnetic component. The second type is related to other samples displaying erratic evolution during demagnetization process, not allowing reliable paleomagnetic results. The mean B ChRM direction, not significantly different before and after bedding correction, is indicated on Fig. 2.

4 Discussion

The structural interpretation of the paleomagnetic results obtained from the NW Algeria (Fig. 2) suggests (as in the other basins—Fig. 1—inset), the presence of clockwise blocks rotations. However, the magnitude of these rotations should be much lower than those obtained in the Chelif [3] and Mitidja [4] basins. Rotations, though all clockwise, are not homogeneous in north Algeria (Fig. 1—inset).

A gradient of "rotation" magnitude appears from the Mitidja basin [4] affected by strong rotations (in average 56°) to Aïn Temouchent–Ghazaouet area, located more westward, where rotations are limited around 15° (this study). For the Chelif basin, 30° average rotation was assessed by Derder et al. [3]. This important result lies with the sampled rocks age and the position of the zones with regard to the Africa-Europe plate boundary.

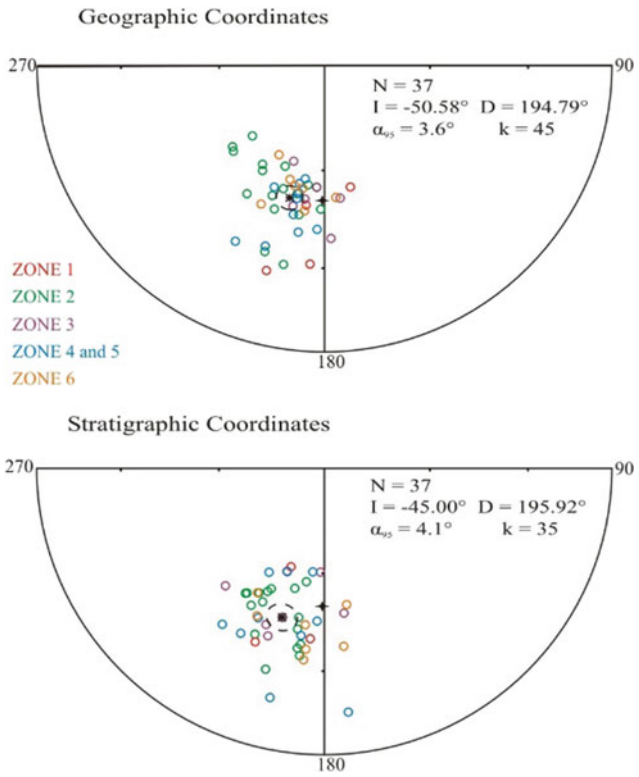

Fig. 2 Equal-area plot (upper hemisphere) showing the paleomagnetic directions obtained from the different mean-sites B ChRM (all data are presented as with reversed polarity) of the 6 zones (see Fig. 1) and the total mean paleomagnetic direction (in black) associated with its confidence zone. The black star represents the expected paleomagnetic direction

5 Conclusion

The different rotation values pointed out by the paleomagnetic tool in northern Algeria cannot be precisely quantified by the classical geological methods. However, they corroborate the tectonic model of Meghraoui and Pondrelli [1] and, confirm that the northern Algeria is organized as tectonic blocks and that the Africa-Eurasia convergence would be partially accommodated by transpression and rotations. The tectonic block rotation model evidenced and promoted the importance of future works in northern Africa marge, particularly in eastern Algeria, Morocco and Tunisia.

References

1. Meghraoui, M., Pondrelli, S.: Active faulting and transpression tectonics along the plate boundary in North Africa. Ann. Geophys. **55**, 5 (2012). https://doi.org/10.4401/ag-4970
2. Aïfa, T., Feinberg, H., Derder, M.E.M., Merabet, N.: Rotations paléomagnétiques récentes dans le bassin du Chéliff (Algérie). C. R. Acad. Sci. Paris **314**, II, 915–922 (1992)
3. Derder, M.E.M., Henry, B., Amenna, M., Bayou, M., Maouche, S., Besse, J., Abtout, A., Boukerbout, H., Bessedik, M., Bourouis, S., Ayache, M.: Tectonic evolution of the active "Chelif" basin (Northern Algeria) from paleomagnetic and magnetic fabric investigations. In: New Frontiers in Tectonic Research at the Midst of Plate Convergence Intech Publisher Book, pp. 3–26. Intech (2011). ISBN 978-953-307-594-5
4. Derder, M.E.M., Djellit, H., Henry, B., Maouche, S., Amenna, M., Bestandji, R., Ymel, H., Gharbi, S., Abtout, A., Dorbath, C.: Strong neotectonic block-rotations, related to the Africa-Eurasia convergence, in northern Algeria: paleomagnetic evidence from the Mitidja basin. Submitted to Tectonics (2018)
5. Derder, M.E.M., Henry, B., Maouche, S., Amenna, M., Bayou, B., Besse, J., Bessedik, M., Belhai, D., Ayache, M.: Transpressive tectonics along a major E–W crustal structure on the Algerian continental margin: block rotation revealed by paleomagnetic investigations. Tectonophysics **593**, 183–192 (2013)
6. Butler, R.F.: Paleomagnetism: Magnetic Domains to Geologic Terranes. Blackwell Scientific Publications (1992)
7. Coulon, C., Megartsi, M., Fourcade, S., Maury, R.C., Bellon, H., Louni-Hacini, A., Cotten, J., Coutelle, A., Hermitte, D.: Post-collisional transition from calc-alkaline to alkaline volcanism during the Neogene in Oranie (Algeria): magmatic expression of a slab breakoff. Lithos **62**, 87–110 (2002)

Geothermal Reconnaissance of Southeastern Nigeria from Analysis of Aeromagnetic Data

Ema M. Abraham and Onyekachi E. Itumoh

Abstract

The West African Rift System led to the formation of the Benue Trough in Nigeria, creating sub-basins within the Trough. These basins were subjected to synsedimentary tectonic deformations during Cretaceous to Neogene times and were affected by magmatic—volcanic episodes leading to multiple areas of geothermal anomalies within sedimentary basins. We performed a geothermal reconnaissance of the lower Benue Trough using aeromagnetic data. Estimates of depths to the bottom of magnetized crust (assumed Curie point depth) were determined from spectral analysis of magnetic anomalies. The estimated average Curie point depth in the region is 13.16 ± 1.20 km with an average geothermal gradient of 46.04 ± 1.45 °C km^{-1}. The average geothermal gradient reckoned from our estimated CPD data is in agreement with average geothermal gradient achieved from deep wells drilled in the region for oil exploration. Results are useful for further geothermal explorations in the region.

Keywords

Curie point • Magnetic anomaly • Geological structures • Geothermal gradient • Heat flow

1 Introduction

Exploitation of geothermal resources in Nigeria is essential given the Country's daunting energy challenges and its status as a developing nation. Geothermal resources abound in Nigeria and some surface manifestations in the form of warm springs have been located.

E. M. Abraham (✉) · O. E. Itumoh
Department of Physics/Geology/Geophysics, AE—Federal University Ndufu Alike, Ikwo, P.M.B. 1010, Abakaliki, Ebonyi State, Nigeria
e-mail: ema.abraham@funai.edu.ng

2 Settings, Materials and Methods

The geology of Nigeria is widely classified into the sedimentary Basins and the basement complex rocks (Fig. 1). The sedimentary Basins include the Benue Trough, a synclinal structure trending NE–SW and the oil-rich Niger Delta Basin as well as the Nupe or Bida, Sokoto and Chad or Borno Basins. The sediments of these Basins are largely Cretaceous to recent and occupy a Y-shaped structure which extends from the north-western and north-eastern part of the country into the Atlantic Ocean where they form a delta [1]. This study investigated the depth to the bottom of magnetic sources herein referred to as the Curie Point Depth (CPD) using recently acquired high-resolution aeromagnetic data. These depths, when contoured for an area, could provide a picture of the spatial variation of Curie isotherm level.

This picture should correlate to a significantly high degree with various known indices of geothermal activity in the area under consideration [3]. For the magnetic data analysis, we followed the procedures of [4, 5].

The average surface heat flow and geothermal gradient values were computed and were based on the possible Curie-point temperature of 580 °C with an average thermal conductivity of 1.80 W m^{-1} °C^{-1} [6] for the region. Aeromagnetic data used was acquired by the Nigerian Geological Survey Agency (NGSA) using a mean terrain clearance of 80 and 500 m line spacing. We applied the RTE correction assuming a magnetic declination of −2.15° and an inclination of −13.91° for the study area utilizing the Fast Fourier Transform algorithm for spectral analysis in the estimation of depth from aeromagnetic anomalies. Figure 2 shows the RTE geomagnetic anomaly field map of the study area. We divided the magnetic anomaly map into subregions of dimension 110 × 110 km ensuring at least 50% overlap of the blocks. We, then, sampled additional blocks placing center points of subregions within notable geological provinces following [7].

N. Sundararajan et al. (eds.), *On Significant Applications of Geophysical Methods*,
Advances in Science, Technology & Innovation, https://doi.org/10.1007/978-3-030-01656-2_9

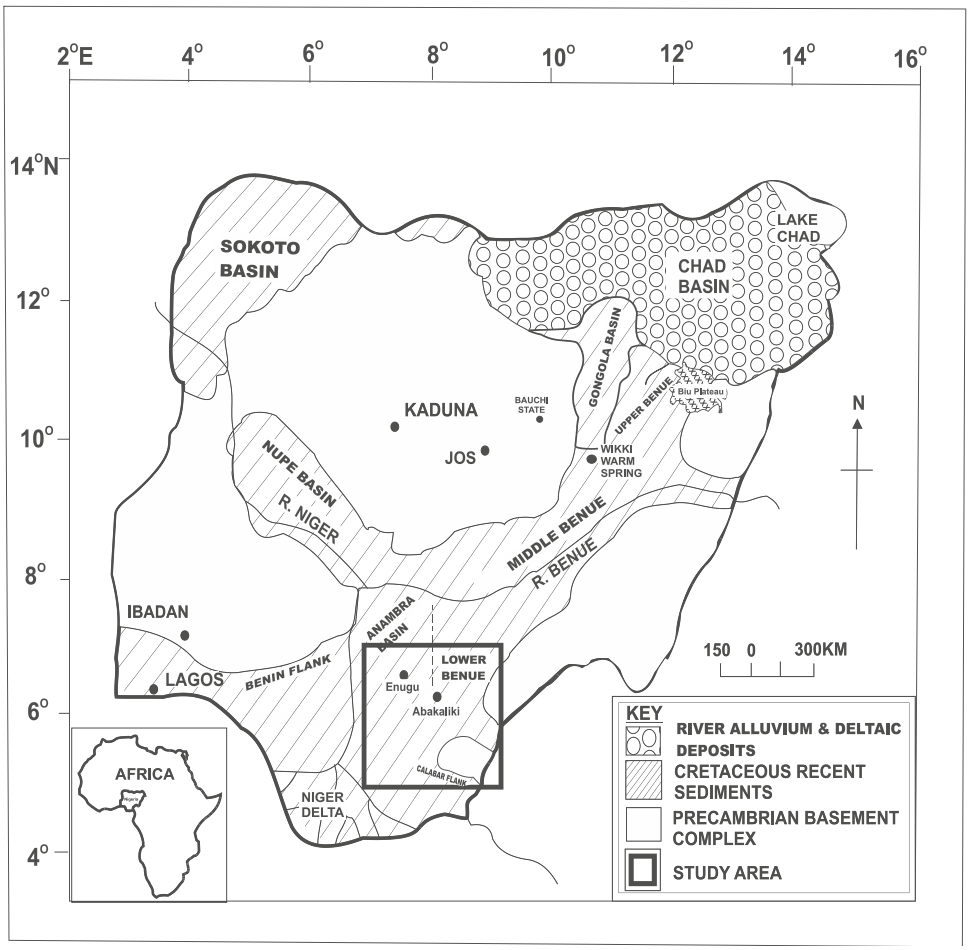

Fig. 1 Map of Nigeria showing the general geology, location and coverage area of our study (modified from [2])

3 Results

Figure 3 displays the map of estimated CPD for the study area.

4 Discussion

The estimated CPD in Fig. 3 shows deeper depth results within an approximate range of 18 and 20 km towards the central and southern regions of the map (Okposi, Afikpo and Biase regions).

Shallow depths within an approximate range of 6 and 17 km were also estimated for the Ugbodo, Obubra and Abakaliki locations, NE of the study area. General appraisal shows that a minimum depth of 6.33 ± 0.27 km and maximum depth of 19.33 ± 1.98 km with an average value of 13.16 ± 1.20 km was estimated for the study area. The deeper depths around the Afikpo region is related to the structural inversion of the Benue trough that led to the subsidence of the Afikpo syncline. We attribute the shallow CPDs obtained around Ugbodo, Obubra, and Abakaliki regions to the Basic and Intermediate intrusions within the subsurface. Some of these intrusions were mapped on a geological map. This region is located northwards of the

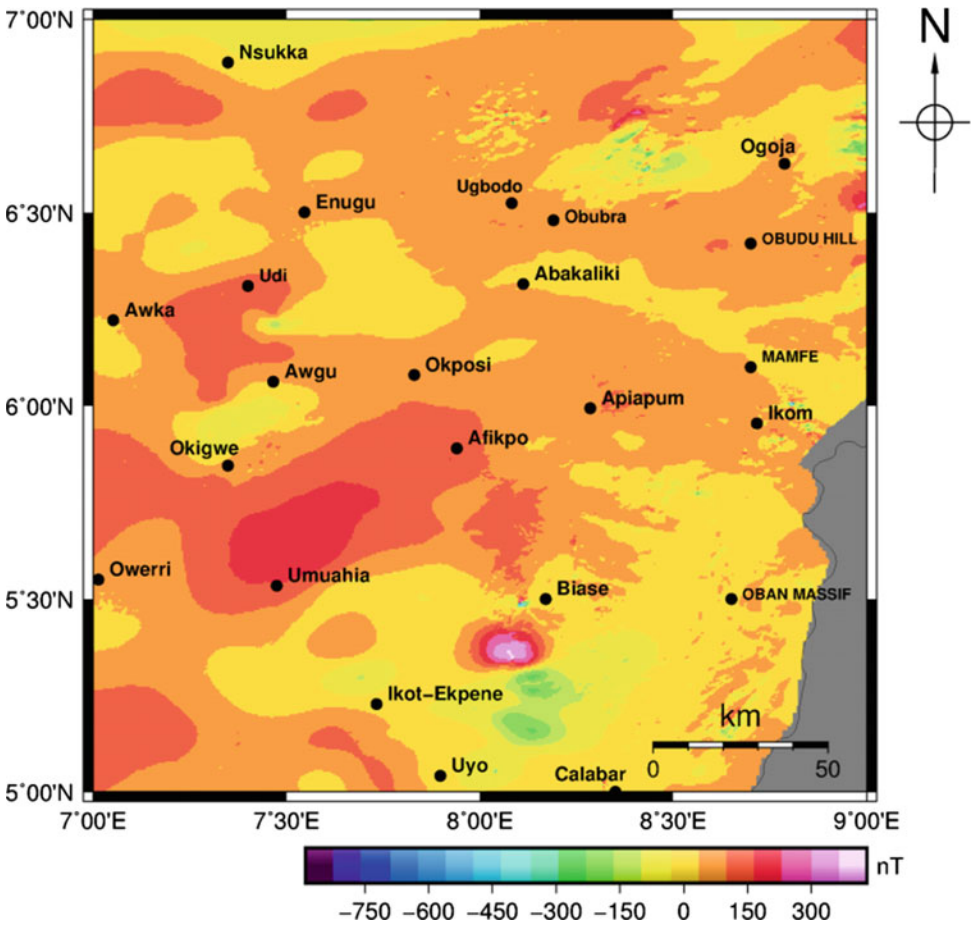

Fig. 2 Geomagnetic anomaly map of the study area. Positive anomalies (90–400 nT) are noticeable at Udi, Umuahia and Biase regions, and negative anomalies (−20 to −800 nT) around Uyo, Ikot Ekpene, Northeastern Obubra and Nsukka regions

Abakaliki Anticlinorium and is of the Asu River group formation, believed to have been formed during the Santonian. The events in the late Santonian were accompanied by pronounced igneous activities accounting for the occurrence of a large number of intermediate and basic intrusions in the Asu River Group. We believe parts of these subsurface intrusions are responsible for the lower CPDs obtained in our calculations. Our average geothermal gradient of 46.04 ± 1.45 °C km^{-1} and heat flow of 82.88 ± 1.94 mW m^{-2} agrees with the geothermal gradients and heat flow variations evaluated from deep wells drilled for oil exploration in the Anambra Basin by [6].

5 Conclusion

The spectral analysis technique applied on the data enabled the estimation of depths to the bottom of magnetic sources herein assumed CPD. The study area is characterized by deeper and shallow CPDs and high geothermal gradients.

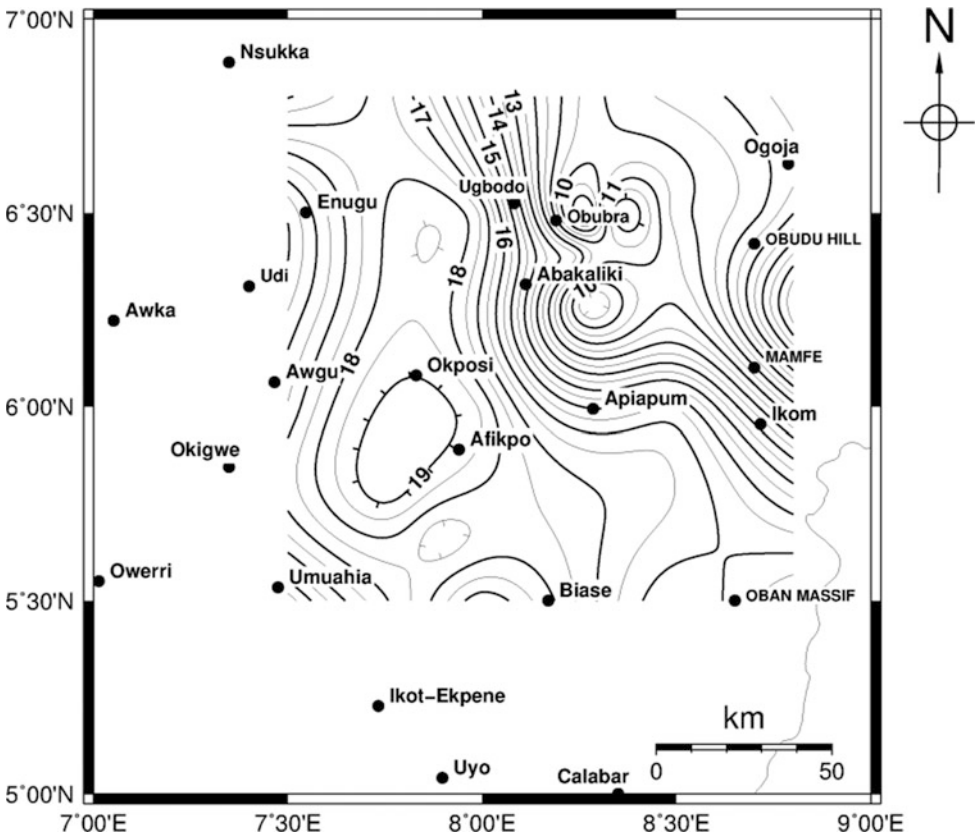

Fig. 3 Curie point depth map of the study area. Depths were obtained from two-dimensional spectral analysis of the geomagnetic data using 23, 50% overlapping square blocks

We proposed that the shallow CPDs are due to basic and intermediate intrusions within the subsurface. The identified region with shallow CPDs is recommended for further geothermal exploration.

References

1. Benkhelil, J.: The origin and evolution of the Cretaceous Benue Trough (Nigeria). J. Afr. Earth Sci. **8**(2–4), 251–282 (1989)
2. Abraham, E.M., Lawal, K.M., Ekwe, A.C., Alile, O., Murana, K.A., Lawal, A.A.: Spectral analysis of aeromagnetic data for geothermal energy investigation of Ikogosi Warm Spring—Ekiti State, southwestern Nigeria. Geotherm. Energy **2**, 1–21 (2014)
3. Bansal, A.R., Gabriel, G., Dimri, V.P., Krawczyk, C.M.: Estimation of depth to the bottom of magnetic sources by a modified centroid method for fractal distribution of sources: an application to aeromagnetic data in Germany. Geophysics **76**, L11–L22 (2011)
4. Okubo, Y., Graf, R.J., Hansen, R.O., Ogawa, K., Tsu, H.: Curie point depths of the island of Kyushu and surrounding areas, Japan. Geophysics **53**(3), 481–494 (1985)
5. Tanaka, A., Okubo, Y., Matsubayashi, O.: Curie-temperature isotherm depth based on spectrum analysis of the magnetic anomaly data in east and southwestern Asia. Tectonophysics **306**, 461–470 (1999)
6. Onuoha, K.M., Ekine, A.S.: Subsurface temperature variation and heat flow in the Anambra Basin, Nigeria. J. Afr. Earth Sci. **28**(3), 641–652 (1999)
7. Ross, H.E., Blakely, R.J., Zoback, M.D.: Testing the use of aeromagnetic data for the determination of Curie depth in California. Geophysics **71**(5), L51–L59 (2006)

Part III

Electrical and Electromagnetic Methods in Mineral and Groundwater Exploration

A Complete Solution to Self-potential Anomalies Due to 2D Inclined Sheets Using Whale Optimization

Mohamed Gobashy, Maha Abdelazeem, and Mohamed Abdrabou

Abstract

A new heuristic solution to self-potential anomalies due to 2D inclined sheets of infinite horizontal extent is presented. This technique is based on using whale optimization algorithm (WOA) in order to infer the optimum solution of the problem. The inverted parameters are polarization amplitude (k), the half-width (a), the inclination angle (α) and the depth (h). The WOA has been tested on a synthetic example, the effect of random noise is analyzed as well and the method depicted good results using MATLAB code. The method has also been applied on two real examples from India. The inversion parameters illustrate that WOA accurately detects model parameters, and show good validation when compared with other inversion methods in the published literature.

Keywords

Self-potential • WOA • 2D inclined sheet • Artificial intelligence • Inversion

1 Introduction

Self-potential (SP) method is used for mineral exploration. It is a passive method that mainly based on the measurement of the natural potentials resulted from electro-kinetic or electrochemical reactions. The two-dimensional (2-D) inclined sheet model is one of the most commonly used models to interpret SP anomalies generated by ore deposits [1]. Modular neural networks technique was used to solve this problem. This work shows the application of whale optimization algorithm (WOA) [2] to completely solve this inverse problem for the unknown parameters.

M. Gobashy · M. Abdrabou
Cairo University, Giza, P.O. 12613 Egypt

M. Abdelazeem (✉)
National Research Institute of Astronomy and Geophysics (NRIAG), Helwan, Cairo, Egypt
e-mail: maazeem03@hotmail.com

2 Methodology

2.1 Problem Formulation

The formula expressing the self-potential anomaly at any surface point $V(x)$ along a line normal to the strike of a 2-D inclined sheet of infinite horizontal extent (Fig. 1) [1, 3] is given as:

$$V(x) = k \ln \left[\frac{\{(x - x_a) - a\cos\alpha\}^2 + (h - a\sin\alpha)^2}{\{(x - x_a) - a\cos\alpha\}^2 + (h + a\sin\alpha)^2} \right] \quad (1)$$

In the above equation k is the electric dipole moment, x_a is the horizontal location of the sheet center, h is the depth to the sheet center, a is the half width of the sheet and α is the inclination angle in anticlockwise direction from positive x-axis. The unknown parameters k, x_a, h, a, and α can be calculated through the minimization of an objective function Eq. (2), which is defined by [4] as:

$$Q = \frac{2\left\|V_i^o - V_i^c\right\|}{\left\|V_i^o - V_i^c\right\| + \left\|V_i^o - V_i^c\right\|} \quad (2)$$

where V_i^o and V_i^c are the observed and computed self-potential field, respectively.

Whale Optimization Algorithm (WOA)

WOA is a global optimization algorithm proposed by [2]. It is a meta-heuristic algorithm inspired from nature that mimics the humpback whales hunting behavior. The WOA algorithm presumes that the best solution is the prey (i.e. target) or is close to the optimum. The other search agents (solutions) will try to enhance their positions following the best search agent. Such position update is represented by:

N. Sundararajan et al. (eds.), *On Significant Applications of Geophysical Methods*,
Advances in Science, Technology & Innovation, https://doi.org/10.1007/978-3-030-01656-2_10

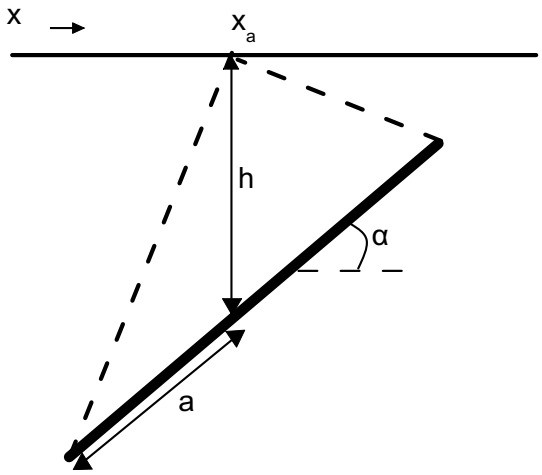

Fig. 1 Geometry of a 2-D inclined sheet model

$$D = |C.X^*(t) - X(t)| \tag{3}$$

$$X \leftarrow t + 1 \leftarrow \psi\Im \leftarrow X^*(t) - \text{A.D} \tag{4}$$

where, t refers the iteration, A and C are coefficient vectors, X^* is the current best solution position vector, X is the new position vector, D refers to the distance separate between the whale and prey, $|\,|$ means the absolute value, and '·' is an element-wise multiplication. It is important to note here that X^* is upgraded in each iteration if a better solution is found. The coefficient vectors A and C are calculated as follows:

$$\text{A} = 2\ \text{b.r} - \text{b} \quad \text{and} \quad \text{C} = 2\text{r},$$

where b is reduced linearly from 2 to 0 through the iterations and r is a random vector in the range [0,1].

3 Results

3.1 Synthetic Example

The WOA has been used to invert the SP data assuming the target have the parameters $k \equiv 50$ mV, $a \equiv 12$ m, $\psi \equiv 150^\circ$, $x_o \equiv 55$ m and, $h \equiv 10$ m and the resulted parameters and inverted field are identical to the assumed ones. Then, we added random noise to the SP anomaly in two levels (10 and 30%) to test the constancy of the method (Fig. 2). It proves that the inversion from WOA is acceptable.

3.2 Real Examples

1. **Surda Field Anomaly**

The WOA is applied to the measured SP anomaly (Surda area) of the Rakha mines, India [5]. The model response resulted depicts a good fitness with the observed data. Table 1 shows previous results compared to our results.

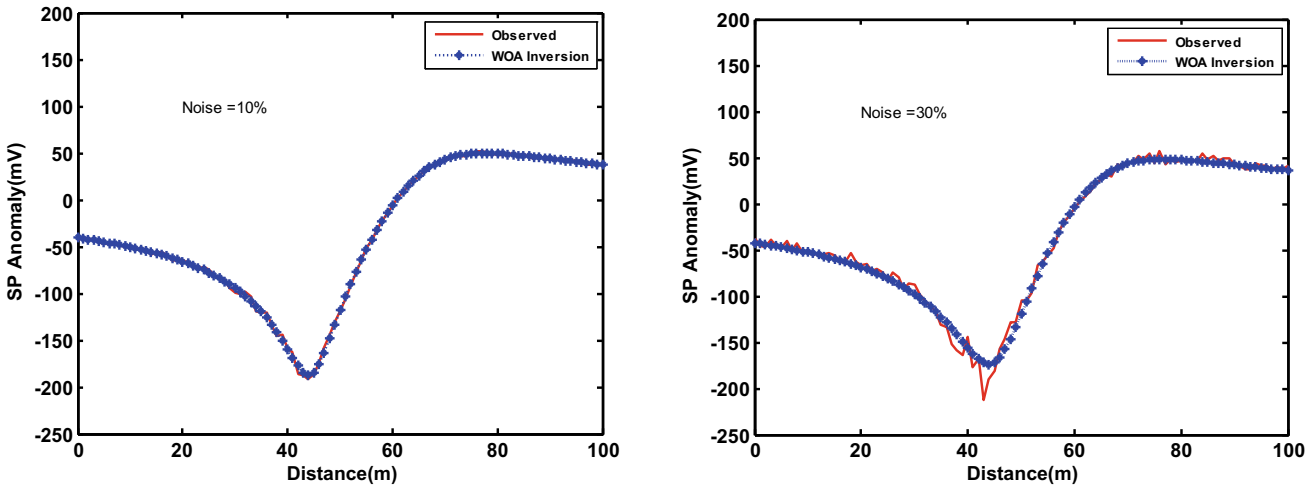

Fig. 2 Observed SP anomaly of an inclined sheet (10% noise) left, and (30% noise) right and their WOA inversion

Table 1 A comparison among the inverted parameters using WOA and previous inverted parameters by different authors

Methods	k (mV m)	X_0 (m)	a (m)	α (°)	h (m)
El-Kaliouby and Al-Garni [2]	130.86	5.86	19.51	50.96	27.78
Monteiro Santos [5]	98.38	−3.87	28.8	45.98	31.4
Di Maio et al. [7]	128.67	1.72	21.92	52.47	31.94
WOA	94.57	−4.17	29.91	45.94	31.29

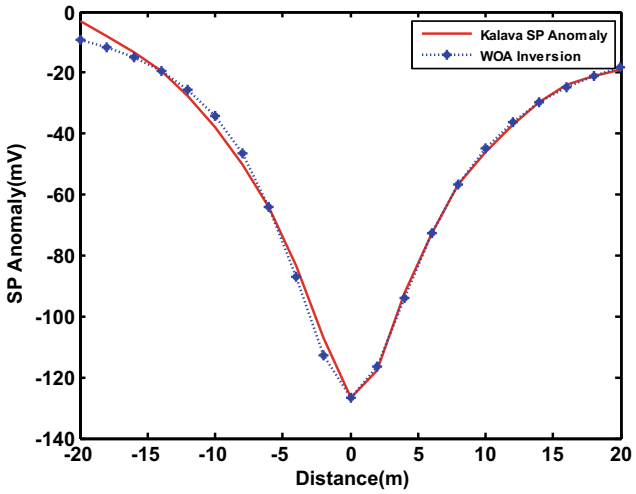

Fig. 3 Observed Kalava SP anomaly with inverted field using WOA

Table 2 A comparison among the inverted parameters using WOA and previous inverted parameters by different authors

Methods	k (mV)	X_0 (m)	a (m)	α (°)	h (m)
Jagannadha Rao et al. [8]	–	0.4	3.75	80	7.59
El-Kaliouby et al. [2]	68.29	−0.9	3.15	78.72	7.2
Biswas and Sharma [9]	−867	−0.8	–	81.8	7
WOA	64.62	−0.455	3.35	82.42	7.35

2. Kalava Field Anomaly

Figure 3 illustrates SP anomaly profile that is taken from the Kalava fault zone, India [6]. The inverted parameters from WOA showed good fit with other methods (Table 2).

4 Conclusions

We have studied the utilization of WOA as a meta-heuristic algorithm to solve the inverse problem of self-potential resulted from 2D inclined sheet. WOA Inversion is applied to solve for 5 SP unknowns, where it is tested on noise free synthetic example and on noisy example, and showed good outcomes until 30% noise. The inversion outcomes from WOA of the two real examples showed good fit with those published in literature.

References

1. Murty, B.V.S., Haricharan, P.: Nomogram for the spontaneous potential profile over sheet-like and cylindrical two-dimensional sources. Geophysics **50**, 1127–1135 (1985)
2. El-Kaliouby, H.M., Al-Garni, M.A.: Inversion of self-potential anomalies caused by 2D inclined sheets using neural networks. J. Geophys. Eng. **6**, 29–34 (2009). https://doi.org/10.1088/1742-2132/6/1/003
3. Mirjalili, S., Lewis, A.: The whale optimization algorithm. In: Advances in Engineering Software (in press). J. advengsoft.2016.01.008
4. Biswas, A., Sharma, S.P.: Optimization of self-potential interpretation of 2-D inclined sheet-type structures based on very fast simulated annealing and analysis of ambiguity. J. Appl. Geophys. **105**(2014), 235–247 (2014)
5. Monteiro Santos, F.A.: Inversion of self-potential of idealized bodies' anomalies using particle swarm optimization. Comput. Geosci. **36**, 1185–1190 (2010)
6. Rao, R.M., Babu, H., Sivakumar Sinha, G.: A Fourier transform for the interpretation of self-potential anomalies due to two-dimensional inclined sheet of finite depth. Pure Appl. Geophys. **120**, 365–374 (1982)
7. Di Maio, R., Rani, P., Piegari, E., Milano, L.: Self-potential data inversion through a Genetic-Price algorithm. Comput. Geosci. **94**, 86–95 (2016)
8. Jagannadha Rao, S., Rama Rao, P., Radhakrishna Murthy., I.V.: Automatic inversion of self-potential anomalies of sheet-like bodies. Comput. Geosci. **19**(1), 61–73 (1993)
9. Biswas, A., Sharma, S.P.: Interpretation of self-potential anomaly over idealized body and analysis of ambiguity using very fast simulated annealing global optimization. Near Surf. Geophys. **13** (2), 179–195 (2015)
10. Murthy, I.V.R., Sudhakar, K.S., Rao, P.R.: A new method of interpreting self potential anomalies of two-dimensional inclined sheets. Comput. Geosci. **31**, 661–665 (2005)

Contribution of Electrical Tomography to the Study of Landslides in Texenna Region (Northeast Algeria)

Hassiba Kherrouba, Mohammed Lamara, and Riad Benzaid

Abstract

Landslides are complex and evolving phenomena that are difficult to characterize. The region of Texenna, like all the regions of northern Algeria, records several sites affected by these land movements. The morphology of the region makes it exposed to a high risk of landslides, controlled by the combined action of various geological, geomorphological, hydrological and structural factors. This work aimed to study a landslide in the city of Texenna, located 20 km southeast of the city of Jijel, in a metamorphic terrain with a steep gradient greater than 30°. The adopted approach was to process the available data on the electrical resistivity of the formations encountered by exploiting these data in the form of electrical images. The correlations of these electrical images with the results of the core holes allowed us to distinguish the unstable mass from the underlying substratum. The precise determination of the depth of the shear zone was of vital use to carry out the stabilization work of this unstable zone.

Keywords

Texenna • Landslide • Tomography • Soil resistivity

1 Introduction

Slope stability problems are frequently encountered in the construction of roads, canals, dikes and dams. In addition, some natural slopes may become unstable. A sudden rupture of an embankment can be catastrophic and very dangerous on human lives [1, 2]. The same is true of the instabilities in the Texenna region of northeastern Algeria. The present work relied on field investigations characterizing the affected areas by landslides. Geophysical methods, such as electrical tomography, are suitable for studying such phenomena. Indeed, the electric tomography makes it possible to obtain a scan of the underground precising the depths of the various formations and the weak zones such as the faults and the planes of slip.

2 Location of the Studied Area

The study landslide is located in the center city of Texenna (Fig. 1). Geologically the region of Texenna belongs to the domain of the volcano-sedimentary complex and the crystallophyllian formations of the Kabyle basement [2, 3].

3 Materials and Methods

The method of electrical prospecting is a method to measure the electrical resistivity of geological formations (Fig. 2). The interpretation is based on the analysis of resistivity contrasts, which makes it possible to locate and apprehend the geometry of the various prospected geological formations [4–6].

The electrical survey or the electrical resistivity measurement of a geological structure consists in injecting a continuous electric current into the structure by means of two electrodes (named A and B) and measuring the potential difference with two other electrodes (named M and N) are shown below. The number and arrangement of the electrodes defines the electrical device used. In practice there are several devices: Schlumberger, Wenner …, and the device was chosen according to the problem to study [4, 6].

The vertical electrical sounding (VES) technique was used to study the variation of resistivity as a function of depth. The achievement of the VES in the field was

H. Kherrouba (✉) · R. Benzaid
Laboratory of Geological Engineering, Mohammed Seddik Benyahia University, Jijel, Algeria
e-mail: Kherrouba_hassiba@yahoo.fr

M. Lamara
Laboratory of Civil Engineering and Environment, Mohammed Seddik Benyahia University, Jijel, Algeria

N. Sundararajan et al. (eds.), *On Significant Applications of Geophysical Methods*,
Advances in Science, Technology & Innovation, https://doi.org/10.1007/978-3-030-01656-2_11

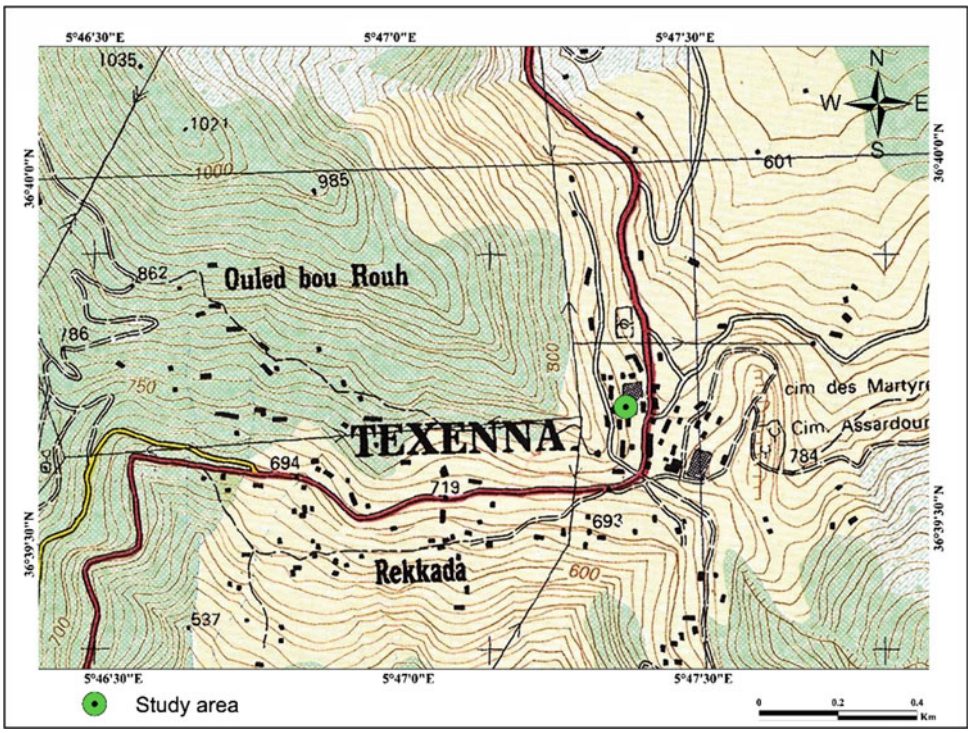

Fig. 1 Location of the studied landslide

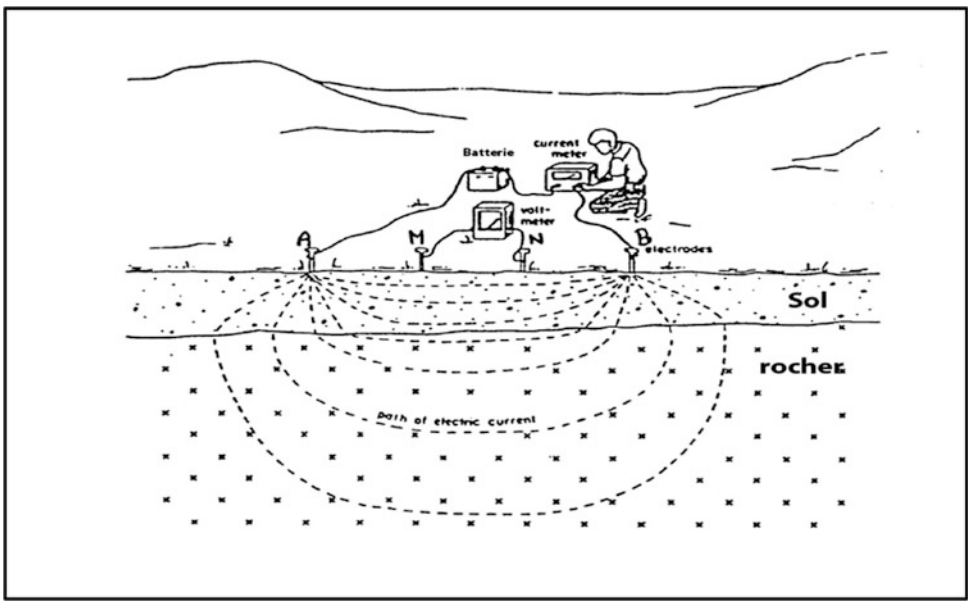

Fig. 2 Device of electrical prospecting

performed by removing the injection electrodes while keeping the center fixed, which allowed each time a greater depth of investigation [4, 6].

The technique of electrical profiling or electric dragging makes it possible to study the lateral variation of the resistivity for a fixed slice of soil. The achievement of the electrical profiling in the field was performed by moving the entire device while keeping its fixed dimensions [4, 6].

The combination of these two techniques made it possible to obtain an electrical panel (electrical imaging) which represents the 2D spatial variation of the apparent resistivity. The 2D acquisition uses several electrodes connected to a multi-electrode cable placed according to a profile and a pre-selected device depending on the problem. Once the pseudo-section of the apparent resistivities measured was obtained, modeling was performed by the inversion method.

Inversion consists in minimizing, by an iterative method, the differences between the measured relative resistivities and those calculated from the direct model [4, 6].

The pseudo-section of the calculated resistivity must converge to the pseudo-section of the measured resistivity, and therefore, a field model is obtained, thus giving the distribution of true resistivity. This resistivity model can then be interpreted geologically. This interpretation will be based on the resistivity contrast that can exist between the different formations of the subsoil [4, 6].

Two profiles were achieved on the area landslide of Texenna [7]. The pseudo-sections were established with the Schlumberger-Wenner device, comprising 24 electrodes each spaced apart from the other by 5 m totaling a length of 115 m and a depth of investigation of 25 m [7].

4 Results and Discussion

Relying on the results of the various pseudo-sections, 2 selected pictures in the context of our work are represented in Figs. 3 and 4. The different pseudo-sections allowed showing:

- A gradual change in resistivity values that indicates the facies change this is practically visible in all pseudo-sections.
- The appearance of water-saturated areas showing that the ground is very permeable in some places and also indicating that these areas present a preferential path of water circulation.
- A line that shows the boundary between two environments of different resistivities, this limit can be a boundary between the natural terrains (Bed-Rock) and the terrain that has been displaced.

As stated above, we gave in what follows the interpretation of the selected profiles. The correlation between the electrical image and the data of the mechanical soundings made it possible to recognize three levels of grounds.

Profile N° 01: From top to bottom, we have—Horizon1: this horizon is characterized by a resistivity varying between 40 and 68 Ω m and a depth ranging from 12 to 24 m which corresponds to shale. Horizon2: this horizon is characterized by a low resistivity varying between 5.73 and 8.16 Ω m and a depth ranging from 1.3 to 6.2 m which corresponds to very altered shale. This low resistivity is due to the presence of water and a clay matrix. Horizon3: this horizon is characterized by a resistivity varying between 11.6 and 35 Ω m and a depth 1–12 m corresponds to clogging zones.

Profile N° 02: From top to bottom, we have—Horizon1: this horizon appears as a block with a depth ranging from 10.5 to 22.8 met with a resistivity varying between 31.7 and 57.5 to 189 Ω m corresponding to shale. Horizon2:

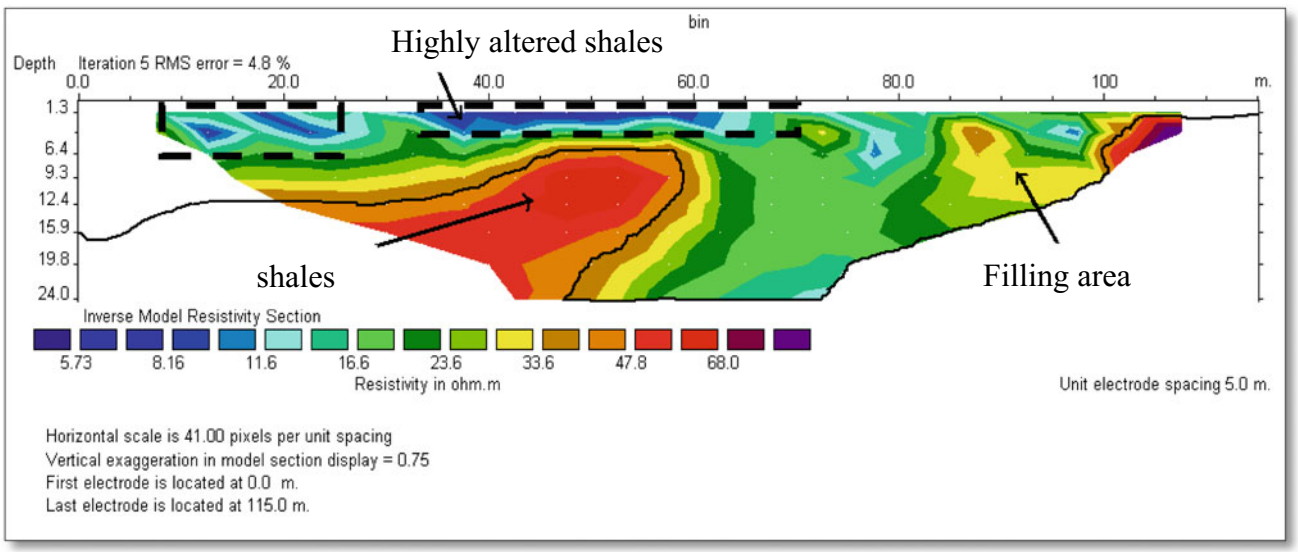

Fig. 3 Pseudo-section of the profile N° 01 [7]

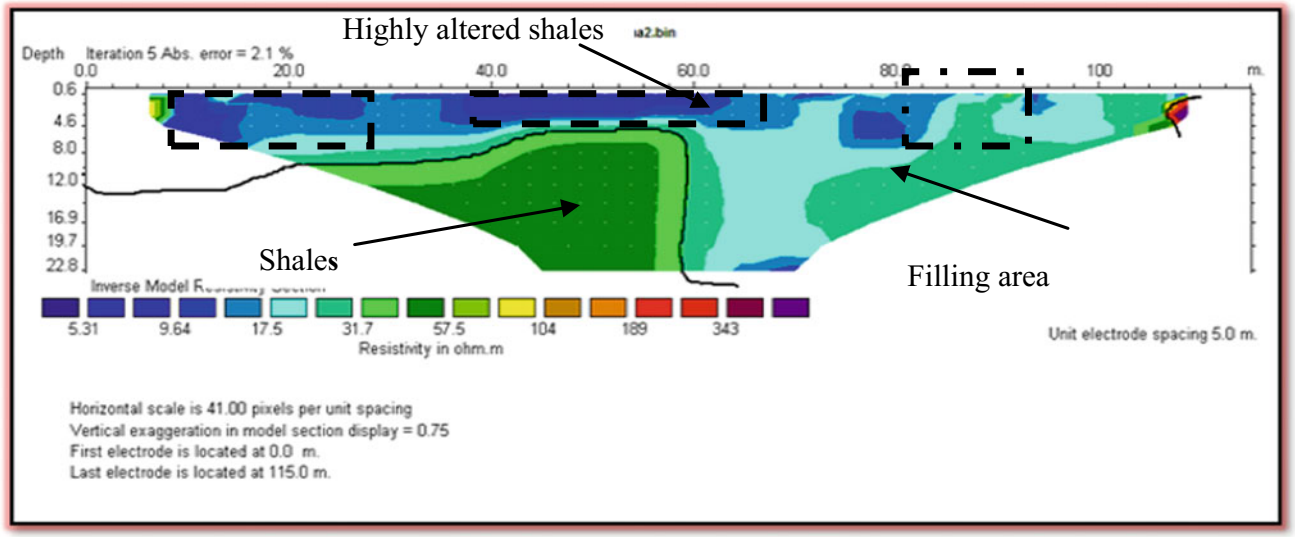

Fig. 4 Pseudo-section of the profile N° 02 [7]

this horizon is characterized by a low resistivity which varies between 5.31 and 15.5 Ω m and a depth of 0.6–7.5 m which corresponds to very altered shale. Horizon3: this horizon appears at varying depths and with resistivity varying between 17.5 and 31.7 Ω m, which corresponds to clogging zones.

5 Conclusion

The purpose of this study was to characterize the internal structure and the hydroelectric state of the study landslide area. The electrical resistivity along these profiles revealed a structure composed of two layers of displaced material superimposed on the shaly bedrock.

The geophysical prospecting by electrical imaging made it possible to distinguish three types of formations that are different from an electrical and lithological point of view. The pseudo-sections obtained show that the main cause of instability is due to the presence of groundwater at a depth of 4 m combined with the irregular morphology and the geological nature of the site.

References

1. Djerbal, L., Melbouci, B.: Le glissement de terrain d'Ain El Hammam (Algérie): causes et évolution. Bull. Eng. Geol. Env. **71**(3), 587–597 (2012)
2. Kherrouba, H.: Etude géologique et géotechnique des zones instables de la région de Texenna-Djimla, wilaya de Jijel, (Algérie). Mém de Magister. Univ. Jijel. Algérie, 2008, 173 p
3. Kherrouba, H.: Les mouvements de sols dans la wilaya de Jijel (Nord-Est Algérien): impact sur les infrastructures. 1er SIE-MATGRSC. Univ Batna, Algérie (2010)
4. Bouaziz, N., Melbouci, B.: Apport de la tomographie electrique a l'etude des glissements de terrains en Grande Kabylie, Algerie, 33èmes Rencontres de l'AUGC, ISABTP/UPPA, Anglet, 27–29 mai 2015
5. Friedel, S., Thielen, A., Springman, S.M.: Investigation of a slope endangered by rainfall-induced landslides using 3D resistivity tomography and geotechnical testing. J. Appl. Geophys. **60**, 100–114 (2006)
6. Jongmans, D., Garambois, S.: Geophysical investigation of landslides: Areview. Bulletin de la Société Géologique de France **178**, 101–112 (2007)
7. Laboratoire de Géologie et de Géotechnique BOUIBAOUNE Lakhdar (L.G.G Sétif, 2012): Rapport de l'étude géotechnique et suivi des travaux de stabilisation d'un glissement de terrain à Texenna village. 103P. Source: Direction l'Urbanisme et de la Construction (DUC) de la wilaya de Jijel, Algérie (2012)

Effectiveness of DC Resistivity Imaging and Shallow Seismic Refraction Techniques Around El Giza-Pyramid Plateau, Egypt

Adel Mohamed, Hosni Ghazala, and Hany Mesbah

Abstract

The Giza plateau is considered the most characteristic examples of the ancient Egyptian civilization. It still attracts archeologists just like any other historical sites. Therefore it is important to carry out a geophysical survey representing seismic refraction and direct current resistivity imaging methods for mapping the different rock units around the pyramids and studying any groundwater infiltration that might have a bad impact on the archeological remains. The results have shown the presence of geoseismic layer of high velocity value corresponding to the dolomitized limestone, the main lithologic unit of the pyramid plateau. It is covered at some localities by moderate and\or low velocity geoseismic layers. The low velocity layer is interpreted as friable sand and fragments of limestone. The moderate velocity layer is interpreted as fractured-marly limestone that might be caused by the percolation of groundwater resulting from rainfall and drainage systems indicating relatively low resistivities as illustrated in 2D resistivity imaging results. The possibilities of the presence of archeologically small anomalies representing caves, mysterious tombs and/or secret rooms are indicated by localized anomalous resistivitities.

Keywords

Geoseismic layer • Resistivity imaging • Giza plateau • Percolation of groundwater

1 Introduction

Egypt has a deeply rooted civilization that extends over thousands of years. This civilization has left a huge amount of traces and antiquities. The study area (Giza Pyramids Plateau) is one of the most important areas among those interesting archeological locations in Egypt. It is located at the northern extension of the necropolis of Memphis, situated on the west bank of the River Nile and today part of the suburb of modern Cairo (Fig. 1). The three great Pyramids are the most famous and prominent monuments at Giza plateau. They are still the interest for tourists and for every scientific works because of its historical background.

2 Materials and Methods

Two geophysical techniques were applied around the Giza Pyramids Plateau; shallow seismic refraction and geoelectrical resistivity techniques using Wenner-Schlumberger array. The shallow seismic refraction method was carried out in the form of profiles, 38 for the longitudinal P-wave and the same number of profiles for the shear S-wave at the same locations. The P-wave profiles were acquired using the seismographs StrataView (Geometrics, USA) 24 channels while the S-wave profiles were conducted using DOLANG (Dolang, ITALY) with 12 channels. Forward, reverse and central shooting surveys were conducted for most of the profiles. A sledge hammer of 15 kg weight was used for both seismographs. The length of the profiles was controlled by the validity and access of the area. It ranges between 50 and 75 m while the geophones interval was spaced 1 and 3 m and the shot point was 3 m from the nearest geophone. On the other hand, thirty four-geoelectric resistivity profiles have been carried out at the pyramids area using a multi-electrode system consisting of the equipment Syscal/R2 resistivity meter, remote control multiplexer (RCM), multi-electrode cable, 12 V battery and 3 Node Boxes, each Box contains 16 nodes (c.f. [1–3]).

A. Mohamed (✉) · H. Ghazala
Geology Department, Faculty of Science, Mansoura University, Mansoura, Egypt
e-mail: mohamedemamm79@yahoo.com

H. Mesbah
National Research Institute of Astronomy and Geophysics, Helwan, Cairo, Egypt

N. Sundararajan et al. (eds.), *On Significant Applications of Geophysical Methods*, Advances in Science, Technology & Innovation, https://doi.org/10.1007/978-3-030-01656-2_12

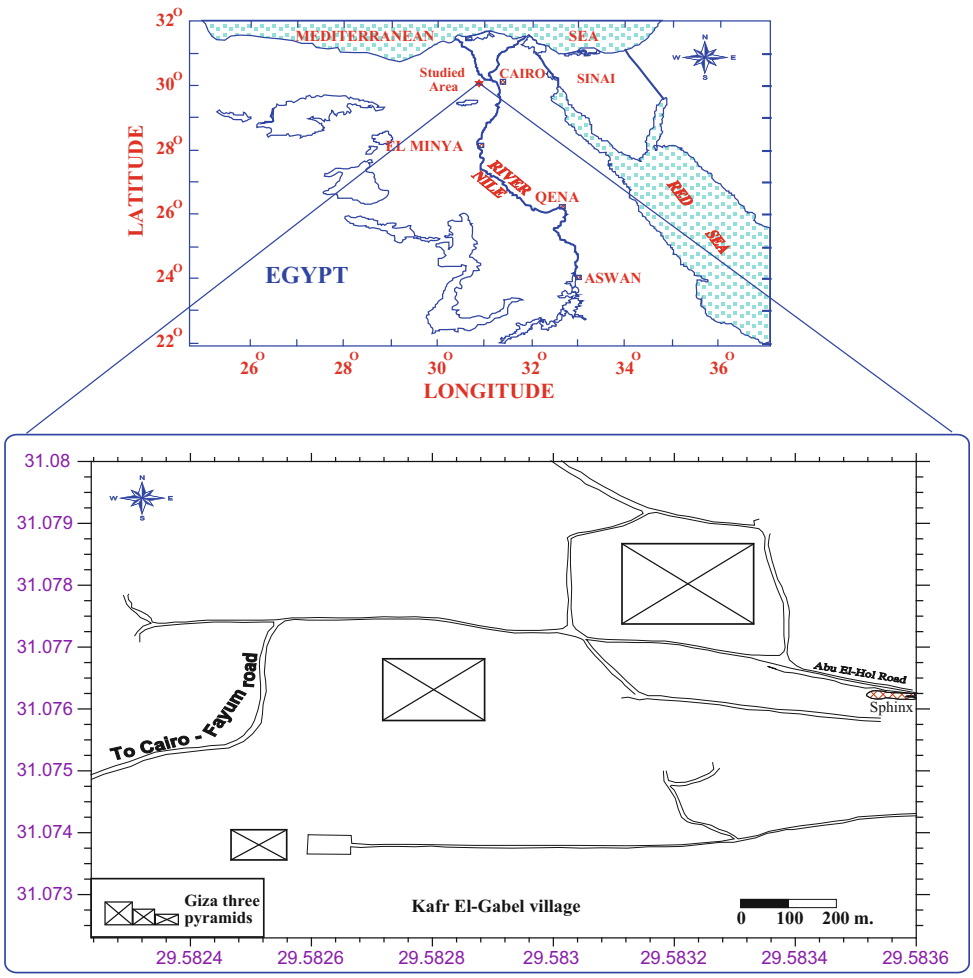

Fig. 1 Base map of the study area

3 Results and Discussion

The results of seismic data were presented vertically in the form of velocity–depth profiles (Fig. 2). Generally, there are three geoseismic layers in the area, the high velocity one representing the bedrocks are covered at some localities by moderate and/or low velocity layers. The first and top geoseismic layer is characterized by low seismic velocity values ranging from 900 to 1300 m/s for the P-wave while its S-wave velocity ranges from 450 to 710 m/s. It has a variable thickness ranging from 0.5 to 13.5 m. This layer is corresponding to the accumulation of loose sand and some fragments of limestone rock as indicated from given lithology. It generally appeared at the seismic profiles far from the pyramids themselves and passes through constructed roads for pedestrians. The second geoseismic layer that was remarked along most of the seismic profiles is characterized by a moderate seismic velocity values ranging from 1400 to 2000 m/s for the P-wave while its S-wave ranges from 840 to 1220 m/s. It has a variable thickness with minimum and maximum values of 1 and 20 m, respectively. This moderate seismic velocity layer is related to fractured marly limestone. The third geoseismic layer, on which the three pyramids were constructed, is characterized by high seismic velocity values of ≥ 2010 m/s for the P-wave and reaches up to ≥ 1230 m/s for S-wave. This seismic velocity layer is correlated to dolomitized limestone as illustrated in the given lithology [4]. Besides, some of the time-distance curves reveal shallow and small local high velocity zones. These zones might be corresponding to the presence of archeological remains that cannot be quantitatively represented by the software used in this study.

On the other hand, 2-D resistivity imaging profiles were produced (Fig. 2b). They also portray three geoelectric layers. The first one is indicated by high resistivity values from 550 to 3000 Ω m. This resistive zone might reflect the effect of the aridity. The second geoelectric layer is characterized by relatively low resistivity values ranging from 15 to 150 Ω m. This layer corresponds to the marly limestone layer that might be wetted as a consequence of percolation of rainfall, particularly this DC resistivity survey was carried out in the rainy season, and/or the seepage of unmanaged domestic waste causing the low resistivity zones. The third

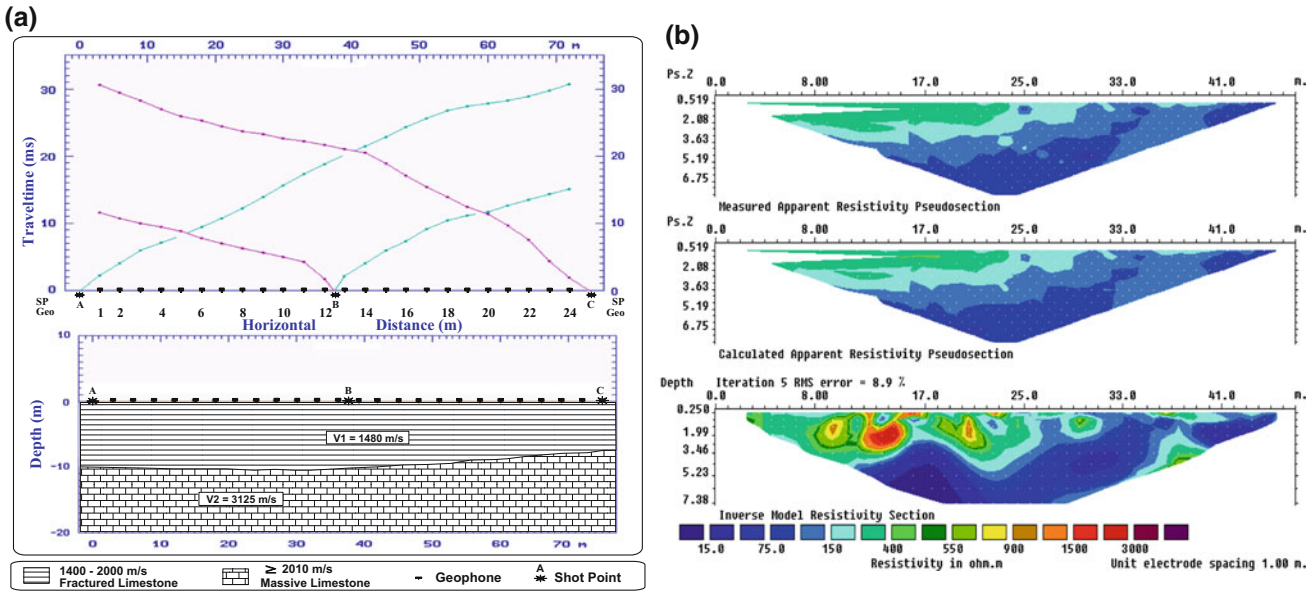

Fig. 2 **a**, **b** 2-D electrical resistivity section along profile P-12

layer of dolomitic limestone is detected only along few geoelectric profiles, which go through a greater depth to reach that layer. It is indicated by high resistivity values ranging from 550 to 3000 Ω m. Moreover, small local high resistivity features appear within the first and second geoelectric layers. They could represent the existence of cavities and/or archeological remains as inferred from the above seismic data and have been confirmed by the field observation and archeologists in the area.

4 Conclusion

Two geophysical techniques were applied around the Giza Pyramids Plateau; shallow seismic refraction and geoelectrical resistivity techniques. Seventy-two shallow seismic refraction profiles were carried out, 38 for the longitudinal wave and 38 for the shear wave at the same locations. On the other hand, Thirty-four resistivity imaging profiles have been conducted at the pyramids area using a multi-electrode system with Wenner-Schlumberger array. The output results of the seismic data have shown the presence of three geoseismic layers, the highest velocity one representing the main rock unit appears very shallow or exposed around the pyramids. Moreover, there is an indication of the presence of local and archeological leftovers. The calculated Bearing Capacity and Poisson ratio of the third layer that constitutes the main lithologic units portrayed its high hardness.

On the other hand, most of the 2-D geoelectric resistivity imaging results have portrayed two resistive layers sandwiched by relatively a low resistivity one which might be affected by runoff of rainwater through the fractures and joints and/or the result of leakage of domestic wastes causing the low resistivity zones. However, measurements at different seasons (monitoring) are highly recommended to delimit the origin of wetting agent. The resistivity imaging results indicated the possibility of the presence of cavities and/or archeological residue; however detailed 3-D survey and modeling software should be applied for these prospective localities. The seismic and geoelectric resistivity techniques were generally consistent and have shown their efficiency as costly effective and non-invasive methods for archeological applications in the area of study.

References

1. Loke, M.H.: Tutorial of 2-D and 3-D electrical imagining surveys. Penange, Malaysia University, Sains Malaysia, unpublished course notes, www.abem.com, 129 p (2001)
2. Loke, M.H., Barker, R.D.: Rapid least squares inversion of apparent resistivity pseudo-sections by a Quasi-Newton method. Geophys. Prospect. **44**, 131–152 (1996)
3. Loke, M.H., Dahlin, T.: A comparison of the Gauss-Newton and Quasi-Newton methods in resistivity imagining inversion. J. Appl. Geophys. **49**(3), 149–162 (2002)
4. Yehia, M.G.: The geomorphological and geological mapping of the Giza pyramids (Al-Ahram) area. Environmental and Remote Sensing Services Center (ERSS) (1995)

Magnetotelluric Investigation of the Underlying Structure of Manzaz Volcanic District (Hoggar, Southern Algeria)

Abderrezak Bouzid, Amel Benhallou, Abdenaceur Lemgharbi, Abdelhamid Bendekken, Walid Boukhlouf, Zakaria Boukhalfa, Aboubakr Deramchi, Abdeslam Abtout, and Khaled Aghanbilou

Abstract

The main objective of this study was to model the lithospheric structure of the Manzaz volcanic district (Hoggar) using the magnetotelluric (MT) method. For this purpose, eleven MT stations forming a 70-km long NW-SE profile, intersecting the Manzaz, were modeled. The 2D resistivity model shows an anomalously conductive crust resting on a lithospheric mantle of normal resistivity. The anomalously high conductivity of the middle and lower crust results probably from magma ascent from the asthenosphere to the surface. It could correspond to the presence of partial melting, trapped fluids released by the magma and/or precipitation of mineralization. The conductive structures underlying the Manzaz could correspond to intracrustal magmatic chambers or to magmatic underplating zones at the Moho or at lower/upper crust discontinuities.

Keywords

Manzaz volcanic district • Hoggar • Magnetotellurics Algeria

1 Introduction

The volcanic episodes in the Tuareg Shield are Eocene to Quaternary in age (35 Ma to recent) [1]. The last episode, in the Hoggar, began 1.9 Ma ago and lasted until the present, with exclusively basanite lava flows and associated scoria cones. The Manzaz massif belongs to this episode [1]. Few geophysical studies have been performed on Manzaz's underlying structure counter to Atakor volcanic district located some tens km to the south [2]. Thus, to highlight its lithospheric structure, a Magnetotelluric (MT) field survey has been conducted recently. MT is a passive electromagnetic geophysical method, that infers the distribution of the electrical conductivity in the lithosphere by recording the natural telluric current fluctuations and the magnetic field variations [6]. Electrical conductivity is a geological marker that can reflect geodynamic conditions in the Earth. It can also be strongly affected by the presence of fluid, mineralization or partial melting in the crust. MT is thus a suitable method for the investigation of the underlying structure of the Manzaz volcanic district. In this work, we presented the preliminary 2D modeling of a NW-SE MT profile.

2 Geological Settings

The Manzaz volcanic district covers an area of approximately 1500 km^2, bounded by 5° 00′–6° 00′E longitudes and by 23° 00′–24° 00′N latitudes. It is located north of the Atakor Massif near the boundary between Azrou N'Fad and Tefedest terranes [1]. Lava flows were emitted on a fairly flat basement made up of mostly Eburnean gneiss and Pan-African granitic intrusions. Numerous recent and well-preserved monogenetic scoria cones are associated with rare polygenetic cones, Oukcem twin maars and Iteghrene spatter cone, decorate the landscape. They emitted peridotite enclave-rich basic flows, overlying older lava flows. Volcanic bombs of various sizes and shapes, thick tuff deposits and pouzzolane layers constitute and cover crater flanks [1].

3 MT Data Survey, Analysis and Modeling

MT reconnaissance survey was conducted in December 2016 at 7 sites and were supplemented by four stations collected in a previous field survey. The whole forms ~70 km long NW-SE profile (Fig. 1). MT time series were recorded for about 20 h, while AMT recordings were

A. Bouzid (✉) · A. Benhallou · Z. Boukhalfa · A. Deramchi
A. Abtout
CRAAG, BP 63, Route de l'Observatoire, Algiers, 16340, Algeria
e-mail: a.bouzid@craag.dz

A. Lemgharbi · A. Bendekken · W. Boukhlouf · K. Aghanbilou
U.R. Tamanrasset, CRAAG, BP 32, Tamanrasset, 11000, Algeria

N. Sundararajan et al. (eds.), *On Significant Applications of Geophysical Methods*,
Advances in Science, Technology & Innovation, https://doi.org/10.1007/978-3-030-01656-2_13

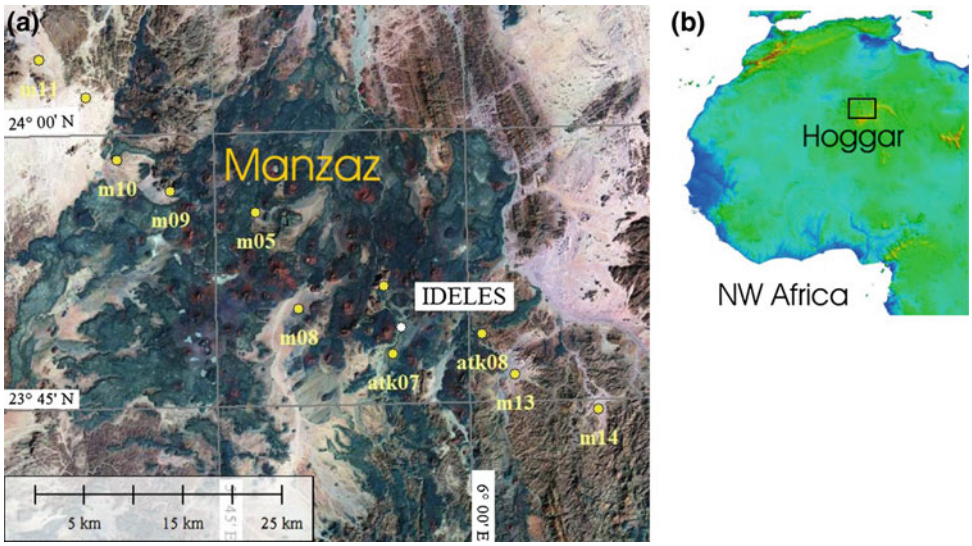

Fig. 1 **a** MT sites (yellow solid circles) distribution along a NW-SE profile plotted on satellite image of MrSID™ file format from www.lizardtech.com. The volcanic lava field appears in dark blue while the volcanic cones are red. **b** Study area location on the North-West Africa topographic map

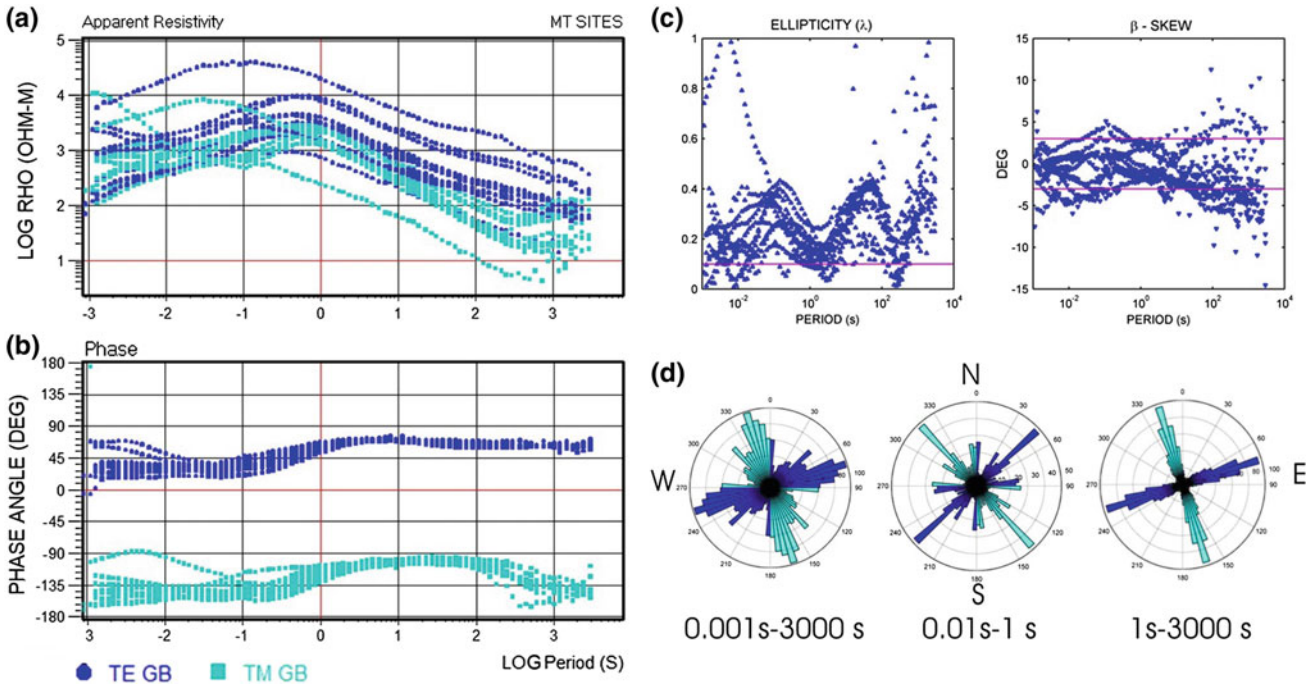

Fig. 2 Apparent resistivity (**a**) and phase (**b**) curves of the TE (dark blue) and TM (light blue) modes of all 11 MT stations. Ellipticity (**c**, left panel) and β-skew (**c**, right panel) of all MT sites calculated using the Caldwell et al. [3] method. Rose diagrams of strike angles obtained by the phase tensor method for all sites and all periods (**d**, left), for short periods (**d**, center) and for long periods (**d**, right)

measured for only 30–45 min. Combining both types of recording provided broadband data. The time series were processed using robust software supplied by the manufacturer [5]. The transfer functions were then extracted in the period range of 0.001–3000 s (Fig. 2a, b). Given the remoteness of the study area from any inhabited region, the use of a reference station was not necessary and the data obtained were of good quality.

The phase tensor method [3] was used to analyze the dimensionality of the geoelectric structure as well as to determine its strike. The analysis of β-skew and ellipticity values showed a roughly 2D structure geometry under the

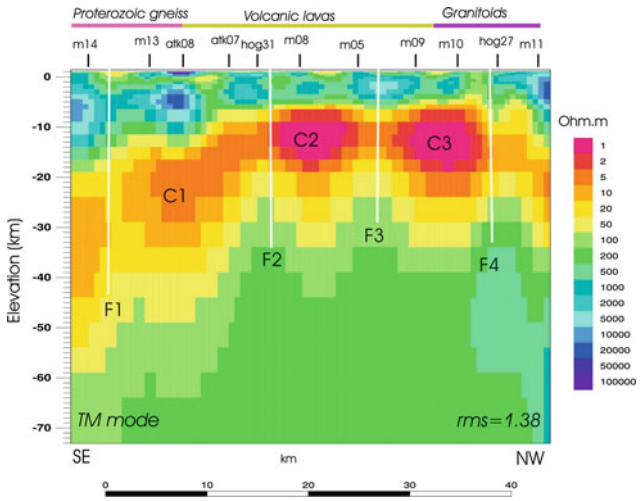

Fig. 3 2D resistivity model obtained by inversion of the TM mode apparent resistivity and phase data of all the MT sites. C1–C3 are mid- to lower-crust conductive structures. F1–F4 are crustal faults inferred from the resistivity 2D model. The surface traces of F1 and F4 are visible on the geological map. The volcanic lavas do not allow seeing the traces of F2 and F3

study area (Fig. 2c). The strike is at N50°E for the short period data (T < 1 s) and then becomes N70°E for the long period data (T > 1 s, Fig. 2d). The 90° ambiguity inherent to the MT method was removed by using induction vectors. A strike of N70°E was adopted for all the stations. The impedance tensor was then decomposed according to the method of Groom and Bailey [4]. TE and TM mode data were then extracted. Since the TM mode data are less affected by 3D effects [8], they were chosen to calculate a 2D model. The 2D model was obtained by inversion of apparent resistivity and phase data of the TM mode using the NLCG algorithm [7]. The inversion process was initiated by a starting model consisting of a half-space of 100 Ω m. Data corresponding to 18 periods (0.0022, 0.0046, 0.01, 0.022, 0.046, 0.1, 0.22, 0.46, 1, 2.2, 4.6, 10, 22, 46, 100, 220, 460, and 1000 s), were selected for the inversion. After several iterations, a model was obtained with a good enough root mean square (rms) of 1.38 (Fig. 3). The inversion of the TE mode data and that of the two simultaneous modes gave 2D models with higher rms values of respectively 6.26 and 4.66.

4 Discussion

The 2D resistivity model reveals a moderately resistive upper crust of a few hundred to a few thousand Ω m, about 10–15 km thick. In spite of its Precambrian age, this upper crust is of an order of magnitude less resistive than that of other Hoggar areas [2]. Then, there was an anomalously conductive middle and lower crust with resistivity reaching 20 to up to 1 Ω m (Fig. 3). The crust is about 35 km thick beneath the center and the NW end of the profile, and reaches a thickness of ∼45 km under its SE end. The whole crust rests on a relatively homogeneous lithospheric mantle with a normal resistivity of 100–200 Ω m. Furthermore, the resistivity model reveals several vertical faults that dissect the crust over its entire thickness. The surface traces of F1 and F4 were visible on the geological map (Fig. 3). On the other hand, the volcanic lavas do not allow seeing the traces of F2 and F3 (Fig. 1). Moreover, the conductive structure associated with the middle and lower crust dips below the SW end of the profile. This anomaly is connected to the deep anomaly highlighted south of the study area [2]. The drastic drop in electrical resistivity in the middle and lower crust probably results from magma circulation and ascent from the asthenosphere to the surface. It could correspond to the presence of partial melting, trapped fluids released by the magma and/or precipitation of mineralization. The conductive structures C1–C3 could correspond to intracrustal magmatic chambers [1] or to zones of magmatic underplating at the discontinuities of Moho or under the upper crust.

References

1. Benhallou, A.-Z., Azzouni-Sekkal, A., Bonin, B., Ikhlef-Debabha, F., Ben El Khaznadji, R., Liégeois, J.-P.: Le district volcanic du Manzaz (Hoggar, Sahara algérien): Géologie, pétrologie et minéralogy. Bulletin du Service Géologique de l'Algérie **27**, 3–42 (2016)
2. Bouzid, A., Bayou, B., Liégeois, J.-P., Bourouis, S., Bougchiche, S.S., Bendekken, A., Abtout, A., Boukhlouf, W., and Ouabadi, A.: Lithospheric structure of the Atakor metacratonic volcanic swell (Hoggar, Tuareg Shield, southern Algeria): Electrical constraints from magnetotelluric data. in Foulger, G.R., Lustrino, M., and King, S.D., eds., The Interdisciplinary Earth: A Volume in Honor of Don L. Anderson: Geological Society of America Special Paper 514 and American Geophysical Union Special Publication 71, p. 239–255 (2015)
3. Caldwell, T.G., Bibby, H.M., Brown, C.: The magnetotelluric phase tensor. Geophys. J. Int. **158**, 457–469 (2004)
4. Groom, R.W., Bailey, R.C.: Decomposition of magnetotelluric impedance tensor in the presence of local three-dimensional galvanic distortion. J. Geophys. Res. **94**, 1913–1925 (1989)
5. Jones, A.G., Chave, A.D., Egbert, G., Auld, D., Bahr, K.: A comparison of techniques for magnetotelluric response function estimation. J. Geophys. Res. **94**, 14201–14213 (1989)
6. Kerbadj, N., Bouzid, A., Saibi, H., Bounif, M.O., Bougchiche, S. and Kebede, Y.: 2-D inversion of magnetotelluric data at Dar-Chioukh region (Djelfa, Algeria). The 4th International Conference on Engineering Geophysics, Al-Ain, UAE, 9–12 October 2017, pp 366-369 (2017)
7. Mackie, R., Rieven, S., and Rodi, W.,: User's manual and software documentation for two-dimensional inversion of magnetotelluric data: Earth Resources Laboratory Rpt.: Cambridge, Massachusetts Institute of Technology, 13 p. (1997)
8. Siripunvaraporn, W., Egbert, G., Uyeshima, M.: Interpretation of two-dimensional magnetotelluric profile data with three-dimensional inversion: synthetic examples. Geophys. J. Int. **160**, 804–814 (2005)

Characterization of Layers Saturated with Biogenic Gas Using Electromagnetic Geophysical Method

Mohamed Sbeaa, Hamza Khmiri, Ferdaws Ouakad, and Younes Ferchichi

Abstract

During a geotechnical survey recognition phase of a project in Raoued region, gas release has been observed. This shallow gas presence, even in small amount, represents a serious obstacle during the project execution. An exhaustive study has been conducted to better understand the phenomenon and insure the security of works: (i) Geotechnical campaign (18-cored holes) completed by a detailed measure of gas nature and properties and (ii) Geophysical electromagnetic prospection using NANOTEM. On this paper, we focused on the geophysical survey process and methodology. A high-density geophysical prospection was performed: 588 measure stations were distributed in 17 lines, leading to an investigation depth between 50 and 60 m. This prospection allowed us to elaborate the average resistivity map. In order to increase the model credibility, an adjustment was done using cores data. The model shows gas-filled layers mainly in the southeast and smaller anomalies scattered on the rest of the site. This information was the key to success of the degassing operation.

Keywords

Geophysics • Resistivity • Electromagnetic prospection • Gas satured layer detection

1 Introduction

During the geotechnical reconnaissance phase of a project in Raoued region, Ariana Governorate, Tunisia, which is a down lifted zone [1] known as the "Deltaic Mejerda Plain": a marine domain corresponding to the southern part of the Utica ancient Gulf, before it got totally filled by the Mejerda alluvial sediments, some incidents of gas emission (essentially CH_4) from the geotechnical surveys have been observed. In order to characterize the phenomenon extension, a geophysical study by electromagnetic prospection adopting the NANOTEM soundings (very short turn-off Transient Electro-Magnetic) was carried out.

This study focused on the gas problem in the project area. Its main aim was to recognize the existing structures, and determine the gas zones so the degassing process would be optimized and the security of the works and buildings could be ensured.

2 Methods

In the study area, several geotechnical surveys of variable depths (20–50 m) and random locations have been achieved. The examination of the cuttings and carrots led to the recognition of the lithology in the zone, the gas saturated layers and the gas properties. However, these surveys were not sufficient to evaluate the risk and understand the phenomenon due to the geological complexity and the surveys random locations. Therefore, an electromagnetic sounding method in the time domain (NANOTEM) was chosen for its reliability, low cost and timeliness.

This method uses the diffusion phenomenon of a transient EM field to determine the electrical resistivity of the terrain as a function of depth. This transient EM field was created by the abrupt breaking of a current flowing in a transmitting coil placed on the ground. If a conducting body is crossed by the vertical primary magnetic field (Hp), it becomes a source of secondary field (Hs). The TDEM (Time Domain Electro-Magnetic) method was established on the measurement of disturbances created at the surface by this secondary field. The depth of investigation increased with the time during which the secondary field was measured, obviously after the primary field cut-off.

M. Sbeaa (✉) · H. Khmiri · F. Ouakad · Y. Ferchichi
General Geosciences Service, 03 Hasdrubal Streets, 2083 El Ghazela City, Ariana, Tunisia
e-mail: med.sbeaa.ggs@gmail.com

N. Sundararajan et al. (eds.), *On Significant Applications of Geophysical Methods*, Advances in Science, Technology & Innovation, https://doi.org/10.1007/978-3-030-01656-2_14

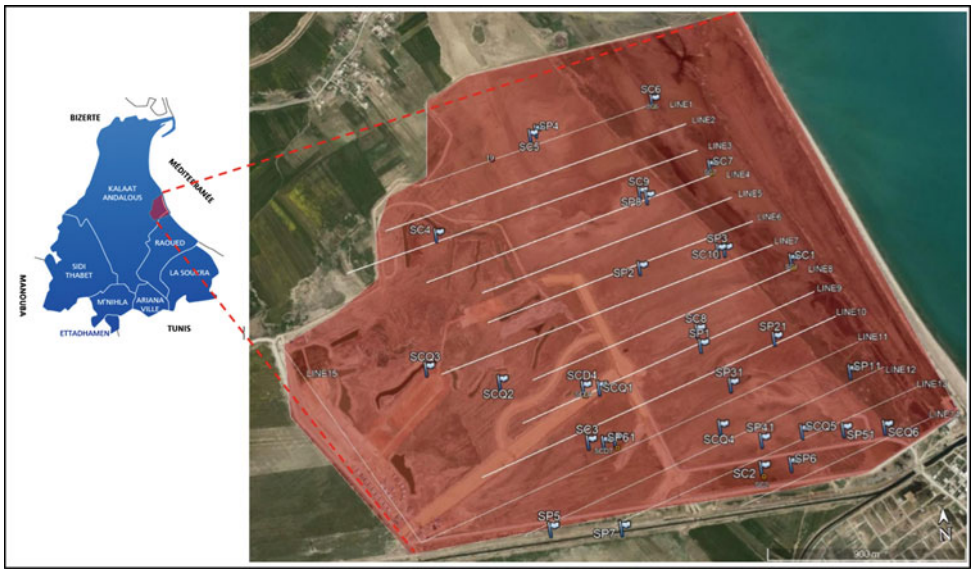

Fig. 1 Project zone and NANOTEM lines

The apparent resistivity "ρa" (late time) is expressed by the following formula[1]:

$$\rho a = \left(\frac{I.At.Ar}{V}\right)^{(2/3)} \left(\frac{1}{t}\right)^{(5/3)} \times 6.3219.10^{-3} (\Omega\,\mathrm{m})$$

Depth investigation:

$$\mathrm{D} = 28\sqrt{\rho}.t \quad (\mathrm{m})$$

With

At transmitter moment in m^2,
Ar Receiver moment in m^2,
I Transmitter current in A,
V Received voltage in μV,
t Time in ms.

In the project zone, an In-loop set has been achieved with a transmitting loop measuring 20 per 20 m and a receiving loop measuring 5 per 5 m, leading to an investigation depth between 50 and 60 m. The signal was measured with 3A intensity and 3 μs cut-off time to identify the time response since the first decimeters. The time decreasing curves were saved by a 1.6 μs sampling steps receiver.

With the above-described configuration, the measuring stations were distributed as follows:

– 02 rigging lines on geotechnical soundings containing gas (38 stations).
– 15 lines systematically scan the entire proposed site totaling 550 stations.

Figure 1 shows the field of study and the measurement stations locations.

A lithological model was elaborated based on the bibliography and the information given by the study of the geotechnical surveys. Then the row data were treated assembled and organized in pseudo-sections.

In order to elaborate a valuable geological model, a rigging was carried out using the geotechnical surveys in order to relate the geophysical model to the lithological model. Finally, after rectifying the model, the distribution was located.

3 Results

In general, the resistivity spectrum obtained varied between 0.3 and 1.4 Ω m in the whole area. The subsurface was divided into 3 horizons (Fig. 2):

– A high conductive roof which resistivity was between 0.4 and 0.7 Ω m and of 5–20 m depth.
– A high conductive substratum of 0.4–0.8 Ω m resistivity.
– An intermediate layer relatively resistant (0.7–1.4 Ω m) with a remarkable facies heterogeneity marked by a developed spectrum of resistivity, its average depth was 25 m.

The average resistivity map shows gas-filled layers in the construction zone especially in the southeast. The other anomalies were scattered on the rest of the site, as it could be seen on the map (Fig. 2).

[1] http://zonge.com/geophysical-methods/electrical-em/tem/

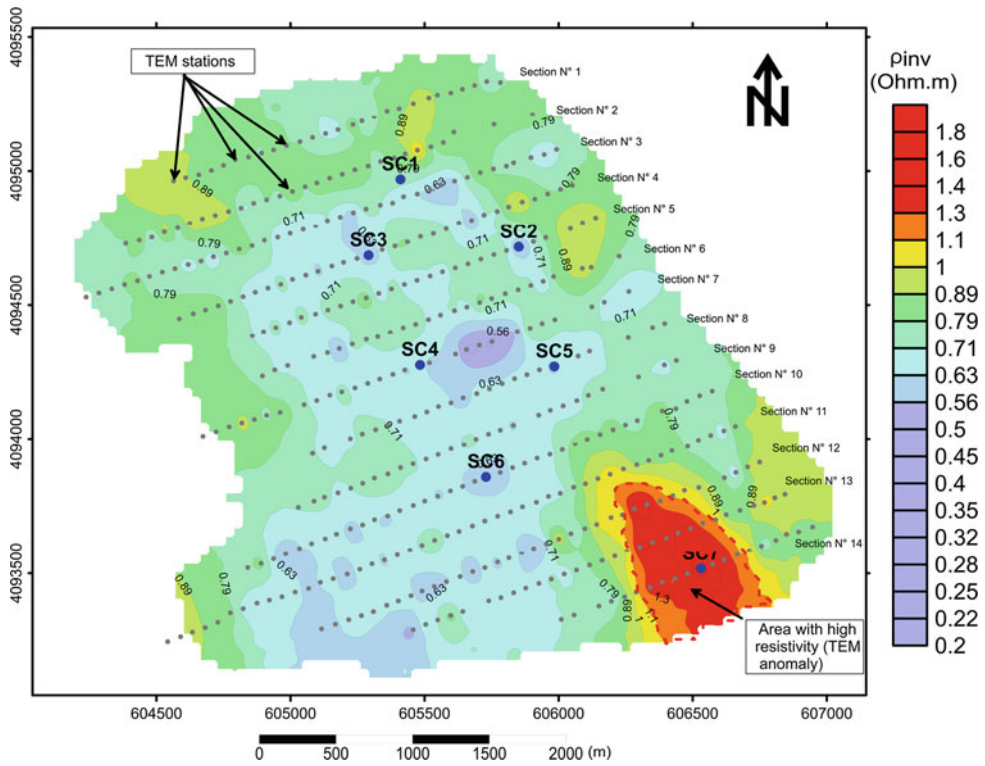

Fig. 2 Resistivity map at 30 m depth

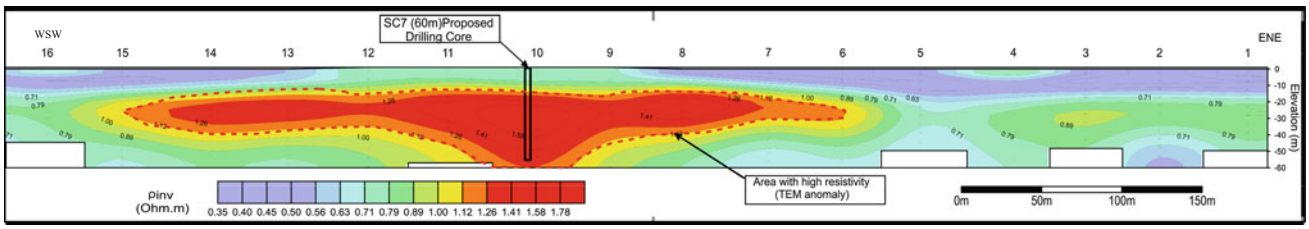

Fig. 3 Vertical resistivity cross section (Line 14)

4 Discussion

The interpretation of the results obtained by the TEM surveys made it possible to distinguish the limits of the geological structure and its shape. In this area, it is recommended to consider conducting additional reconnaissance campaigns by geotechnical surveys. Seven drill holes by mechanical coring were proposed (from SC1 to SC7). The SC7 (see Fig. 3) drilled on the core of the main anomaly proved the gravity of the situation and the high risk of such amount of methane. These holes were used for the degassing of the area and thus ensuring the stability of the structures that will be built later.

5 Conclusion

NANOTEM method proved its efficacy and efficiency in detecting gas-saturated layers. The pseudo-section developed was a useful way to display lateral changes in resistivity. The high density of the measuring stations provided a macroscopic measure of gas distribution for the region rather than a microscopic or point measurement given by cored boreholes in geotechnical survey.

References

1. Balch, S.J., Boyko, W.P., Paterson, N.R.: The AeroTEM airborne electromagnetic system. Lead. Edge, 562–566 (2003)
2. Ben Ayed, N.: Evolution tectonique de l'avant-pays de la chaîne alpine de Tunisie du début du Mésozoïque à l'actuel; Thèse d'Etat, éditions du service géologique de Tunisie (ONM), 286 p (1993)

Integration of Aeromagnetic Interpretation and Induced Polarization Methods in Delineating Mineral Deposits and Basement Configuration Within Southern Bida Basin, North-West Nigeria

Ayatu Ojonugwa Usman, Chukwudi Chris Ezeh, Aurelius Ojoina Omali, and Augustine Ifeanyi Chinwuko

Abstract

Aeromagnetic data interpretation and induce polarization (IP) method have been integrated, analyzed and interpreted in a view of delineating magnetic minerals within some part of the Southern Bida Basin, Nigeria. Spectral analysis method was used in delineating the magnetic properties of rock which were used to determine the depth to magnetic basement, model prominent magnetic anomaly, determine the basement topography, estimate the Curie point depth isotherm, evaluate the geothermal gradient and calculate the heat flow. The Analysis of induced polarization data was used in delineating the potential fractures zones of mineralization from the pseudosections of resistivity and chargeability contour maps. Visual inspection of the magnetic anomalies and first vertical derivative maps reveal that the area is highly faulted with major faults trending East-West (E-W) and minor ones Northeast-Southwest (NE-SW) directions. The qualitative interpretation results of both resistivity and chargeability pseudosections reveal potential fractures zones trending East-West (E-W) and the depth to the anomalous body ranges from (0.3 to 2.5 km) with average overburden thickness of 2.1 km. The average resistivity and chargeability values ranges from (5.17 to 42.4 Ω m) and (1.10 to 42.3 ms) respectively. Two depth source models were interpreted using Discrete Fourier Transform method (spectral analysis) namely; the shallower sources which range from 0.45 to 1.49 km and the deeper ones which range from 1.81 to 3.24 km. The quantitative interpretation of the aeromagnetic data, depict that the average sedimentary thickness ranges from (2.3 to 3.2 km) and the average depth to the Curie isotherm in the area is 24.76 km. The results also show that the Curie temperature isotherm within the basin is not a horizontal level surface, but undulating. The regional average results for both geothermal gradient and heat flow across the study area are 23.07 °C/km and 57.66 mW m^2 respectively. Based on the computed sedimentary thicknesses (2.3–3.2 km), the geothermal gradient (22.27 and 37.00 °C/km.) and the prevalent fractures, the possibility of hydrocarbon accumulation in the northern and southeastern parts of the study area is feasible, whereas other parts of the study area with low sedimentary thicknesses will favour magnetic mineral deposits such as the prevalent ooilitic iron ore deposits at Agbaja and Kotonkarifi axes. The deductions were reached after due consideration of qualitative and quantitative interpretations of both the aeromagnetic and IP data which was supported by geology of the study area.

Keywords

Spectral analysis • Geothermal gradient • Curie isotherm • Heat flow • Chargeability and resistivity psuedosection

1 Introduction

There is no doubt that petroleum has contributed substantially to Nigerian revenue since its discovery in 1956. The perennial crash of crude oil prices all over the world pushed the attention of stakeholders and researchers towards non-oil revenue generation such as solid minerals. Again, greater part of Nigerian landmass is underlain by basement rocks but the search for geothermal energy has not received enough attention [1,10], thus, there is gap in crustal temperature information across the country. In view of increasing environmental pollution associated with

A. O. Usman (✉) · A. O. Omali
Department of Earth Sciences, Kogi State University, Anyigba, Nigeria
e-mail: ayatuusman@gmail.com; usmanao@ksu.edu.ng

C. C. Ezeh · A. I. Chinwuko
Department of Geology and Mining, Enugu State University of Science and Technology, Enugu, Nigeria

A. O. Usman · C. C. Ezeh · A. O. Omali · A. I. Chinwuko
Department of Geology, Federal University Gusau, Gusau, Zamfara State, Nigeria

N. Sundararajan et al. (eds.), *On Significant Applications of Geophysical Methods*, Advances in Science, Technology & Innovation, https://doi.org/10.1007/978-3-030-01656-2_15

exploration and consumption of hydrocarbon as well as decline in its production in Nigeria, it is prudent to explore renewable and cleaner sources of energy such as geothermal energy for the satisfaction of human energy needs [11].

It should be noted however that target detection is usually impossible using a single geophysical method [2, 4], since identical geophysical anomalies may be related to an anomaly source with different physical properties, mode of occurrence pattern and nature. Thus, the integration of geophysical methods is necessary in order to reveal and characterize hidden targets like the simultaneous measurement of induced polarization and aeromagnetic anomaly interpretation for better interpretation of the observed anomalies. The study focused on integrating induced polarization method and aeromagnetic interpretation over the Bida basin. This would delineate the configuration of the Basin itself by determining the depth to magnetic basement. It would also establish the structural features and possibly obtain a 3-Dimensional view of the Basin, the geothermal gradient and the Curie-point isotherm depth of the basement rocks and mineral deposits respectively. It is within this background that this study has become necessary.

2 Methodology

The methodology involved the use of nine aeromagnetic maps which were collated and digitized in order to produce total magnetic intensity map that formed the input data for the separation of both regional and residual magnetic anomalies in this study. The residual anomaly formed the input data for spectral analysis. This was used to compute depth to the basement, deduce the prevalent igneous terrain, delineate Curie-temperature isotherm, geothermal energy potential and mantle heat flow. Finally, the potential zones of mineralization were delineated using spectral analysis and IP interpretation deductions (Fig. 1).

3 Results

The spectral analysis result in the study area revealed two depth sources; the shallower sources such as intrusive (0.45–1.49 km) and the deeper sources (1.81–3.24 km). The computed Curie point depth and geothermal gradients ranged from 16.0 to 32.0 km and 17.77 to 37.00 °C/km, respectively across the study area. The corresponding mantle heat flow values varied between 42.93 and 92.50 mW m^2 within the study area. The Curie point depth map of the study area showed that the area is an undulating surface. The results of IP and aeromagnetic interpretations revealed potential fracture zones trending east-west (E-W) directions and minor ones in northeast-southwest (NE-SW) directions.

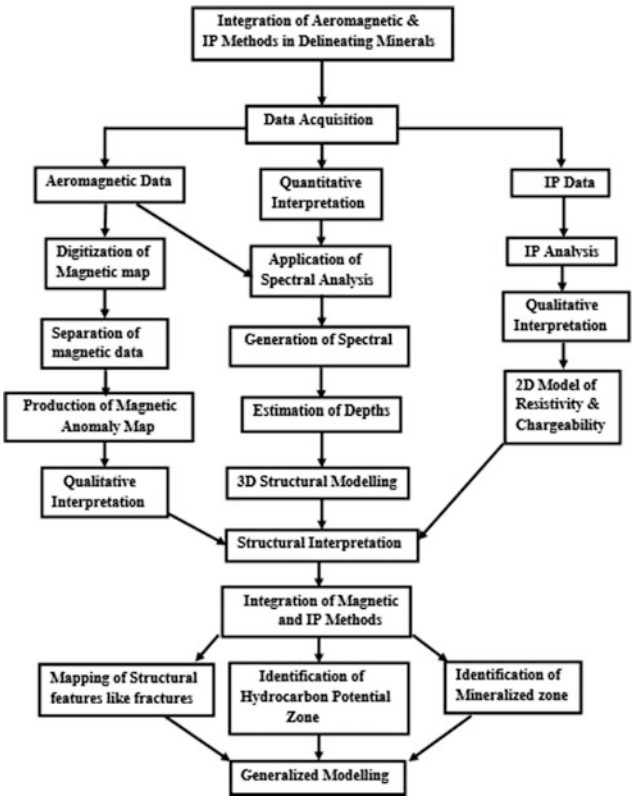

Fig. 1 The workflow of the study

Based on the computed sedimentary thicknesses (2.3–3.2 km), the geothermal gradient (22.27–37.00 °C/km) and the prevalent fractures, the possibility of hydrocarbon accumulation in the northern and southeastern part of the study area is feasible; while other parts of the study area with low sedimentary thicknesses will favour mineral ore deposits of magnetic origin [3, 7].

4 Discussion

All the previous studies in the Bida Basin were preliminary in nature. None of these studies discussed the mineral potential of the Bida Basin in details. This is because the data were scanty and did not include detailed geophysical interpretations and there was no detailed ground survey such as IP to map the mineral deposits and delineate the configuration of the basin [6, 8]. Also, the study area lacked records of crustal temperature. The present study revealed the Curie point depth in conjunction with geothermal energy and heat flow assessments within the study area in order to bridge the gap of scarce records of crustal temperature data. The study also identified high sedimentary thicknesses and considerable geothermal potentials which could serve as basis for hydrocarbon accumulation as it compared favourably with the work of Emujakporue and Ekine [5]. Again,

the present study managed to identify areas with igneous intrusives (the southern part of the study area which includes, Lokoja, Kabba and Kontonkarifi areas) which are to be avoided during search for hydrocarbon. Furthermore, the study produced a model for ease identification of potential areas for magnetic ore mineral deposits which are areas with high Curie isotherm depth and low geothermal gradient and hydrocarbon accumulation.

5 Summary and Conclusion

Analyzing of induced polarization (IP) and aeromagnetic anomalies over the southern Bida Basin has been carried out in order to pinpoint zones of high mineral potential and the conclusions are as follows:

The maps show that the total magnetic field and residual anomalies range from 7500 to 8800 nT and −1200 to 400 nT respectively. Both maps revealed that at the south-eastern parts comprising Ikole-Kabba-Kotonkarifi axis, there is strong evidence of higher magnetic intensity as well as numerous anomalous bodies within the area. The result also revealed contour lines are closely spaced signifying that the depths to basement around these areas are relatively shallow based on the visual interpretation, whereas at the central and northern parts, the contour lines are widely spaced signifying that the depths to basement are relatively high in these areas namely: Isanlu, Aiyegunle, Pategi, Baro and Gulu areas. The qualitative interpretation results reveal that the area is intensely faulted with major faults trending east-west (E-W) and minor ones northeast-southwest (NE-SW) directions.

The spectral analysis results reveal two depth sources in the area namely; the shallower sources which range from 0.45 to 1.49 km at the Southeastern and Southern parts (including Ikole, Kabba, Kotonkarifi and Lokoja areas) while the deeper ones which range from 1.81 to 3.24 km at the northwestern and northern parts (including Isanlu, Pategi, Baro and Gulu areas). Qualitative interpretation of both resistivity and chargeability pseudosections also reveal potential fractures zones trending East-West (E-W) and the depth to the anomalous body ranges from (0.3 to 2.5 km) with average overburden thickness of 2.1 km. The average resistivity and chargeability values ranges from (5.17 to 42.4 Ω m) and (1.10 to 42.3 ms) respectively. The result of the analysis also shows that depths to the centroid and magnetic bodies (sedimentary thicknesses) range from 9.09 to 16.84 km and 0.5 to 3.2 km, respectively. The Curie isotherm depth is shallower at the northwestern part (precisely at Isanlu and Pategi areas) with a Curie depth ranging from 16.0 to 23.0 km while at the other parts, the Curie isotherm depth is deeper and it ranges from 24.0 to 32.0 km. The average depth to the Curie isotherm in the area is 24.76 km. Our results also reveal that the Curie temperature isotherm within the basin is not a horizontal level surface, but undulating and the obtained geothermal gradients across the study area ranges between 18.82 and 32.03 °C/km. Based on the computed sedimentary thicknesses (2.3–3.2 km), the geothermal gradient (18.82 and 32.03 °C/km) and the fractures which serve as migratory pathway for hydrocarbon or hydrothermal fluids, then the possibility of hydrocarbon generation in the northern and Southeastern parts of the study area is feasible [9, 12–14].

References

1. Akande, S.O., Ojo, O.J., Ladipo, K.O.: Upper Cretaceous Sequences in the Southern Bida Basin, Nigeria, p. 78. Mosuro Publishers, Ibadan (2005)
2. Anakwuba, E.K., Chinwuko, A.I.: One dimensional spectral analysis and Curie depth isotherm of Eastern Chad Basin, Nigeria. J. Nat. Sci. Res. **5**(19), 14–22 (2015)
3. Bhattacharryya, B.K., Leu, L.K.: Spectral analysis of gravity and magnetic anomalies due two dimensional structures. Geophysics **40**, 993–1031 (1975)
4. Chinwuko, A.I., Usman, A.O., Onwuemesi, A.G., Anakwuba, E.K., Okonkwo, C.C., Ikumbur, E.B.: Interpretations of aeromagnetic data over Lokoja and environs, Nigeria. Int. J. Adv. Geosci. **2**(2), 66–71 (2014)
5. Emujakporue, G.O., Ekine, A.S.: Determination of geothermal gradient in the Eastern Niger Delta Sedimentary Basin from bottom hole temperatures. J. Earth Sci. Geotech. Eng. **4**(3), 109–114 (2014)
6. Johnmary, K.: Induced polarization and resistivity measurements on a suite of near surface soil samples and their empirical relationship to selected measured engineering parameters, pp. 19–137. M.Sc. thesis, the International Institute for Geo-information Science and Earth Observation (2002)
7. Likkason, O.K.: Angular spectral analysis of aeromagnetic data over the Middle Benue Trough, Nigeria. J. Min. Geol. **43**(1), 53–62 (2007)
8. Obaje, N.G.J., et al.: Preliminary integrated hydrocarbon prospectively evaluation of the Bida Basin in North Central Nigeria. Int. J. **3**(2), 36–65 (2013)
9. Obiora, D.N., Ossai, M.N., Okwoli, E.: A case study of aeromagnetic data interpretation of Nsukka area, Enugu State, Nigeria, for hydrocarbon exploration. Int. J. Phys. **10**(17), 503–519 (2015)
10. Ojo, O.J., Akande, S.O.: Sedimentary facies relationships and depositional environments of the Maastrichtian Enagi Formation, Northern Bida Basin, Nigeria. J. Geogr. Geol. **4**(1), 136–147 (2012)
11. Onwuemesi, A.G.: One dimensional spectral analysis of aeromagnetic anomalies and Curie depth isotherm in the Anambra Basin of Nigeria. J. Geodyn. **23**(2), 95–107 (1997)
12. Petters, S.W.: Stratigraphic evolution of the Benue Trough and its implications for the upper cretaceous paleogeography of West Africa. J. Geol. **86**, 311–322 (1978)
13. Spector, A., Grant, F.S.: Statistical models for interpretation of aeromagnetic data. Geophysics **35**, 293–302 (1970)
14. Tanaka, A.Y., Okubo, Y., Matsubayashi, O.: Curie point depth based on spectrum analysis of the magnetic anomaly data in East and Southeast Asia. Tectonophysics **396**, 461–470 (1999)

Study of an Aquifer in a Semi-arid Area Using MRS, FDEM, TDEM and ERT Methods (Youssoufia and Khouribga, Morocco)

Fatim-Zahra Ihbach, Azzouz Kchikach, Mohammed Jaffal, Driss El Azzab, Konstantinos Chalikakis, Naomi Mazzili, Roger Guerin, and Es-said Jourani

Abstract

To improve the knowledge on available groundwater and to better characterize the aquifers on the phosphate deposits at Youssoufia and Khouribga (Morocco), several geophysical surveys using Magnetic Resonance soundings (MRS), Frequency Domain Electromagnetic Method (FDEM), Time Domain Electromagnetism (TDEM) and Electrical Tomography (ERT) were performed. The goal was to test the capability of these methods to localize an aquifer and estimate its hydrogeological properties. The first experimental results indicate the presence of highly conductive zones that could be related to the presence of water. MRS data has permitted to better constrain the aquifer parameters. The hydrogeological model provided by these methods is similar to the one obtained by piezometric data.

Keywords

Geophysical methods • Groundwater resources • Aquifers characterization • Arid areas • Morocco

F.-Z. Ihbach (✉) · A. Kchikach · M. Jaffal
L3G Laboratory, Cadi Ayyad University, 40000 Marrakech, Morocco
e-mail: ihbachfatimzahra@gmail.com

D. El Azzab
Sidi Mohamed Ben Abdellah University, 30050 Fès, Morocco

K. Chalikakis · N. Mazzili
UAPV University, 84029 Avignon, France

R. Guerin
UMR 7619, METIS, Pierre et Marie Curie University, Paris, France

E. Jourani
OCP Groupe, Casablanca, Morocco

1 Introduction

In arid and semi-arid regions, water resources are often limited to groundwater. The recognition of this resource by drilling is often difficult and expensive. The need for water arises because of the successive droughts over several years. The local authorities and the Office Cherifien of Phosphates (OCP) were particularly interested in the exploitation of the water accumulated in the old underground phosphate series aquifers in order to supply the agglomerations with drinking water and also use it on the production factories.

Different geophysical methods were conducted at two sites: Khouribga and Youssoufia. The purpose was to localize and characterize the aquifer parameters on the phosphate series and use it for drinking water supply in rural areas, and also determine the flooded areas of the phosphate series in order to optimize the exploitation of phosphates. The first geophysical survey was conducted in Bouchane, near to Youssoufia city, using magnetic resonance sounding (MRS). The second investigation was performed in khouribga using FDEM, TDEM and ERT methods.

2 Settings and Methods

2.1 Investigation Areas

This study was performed at two sites in semi arid areas. The first one was carried out at Bouchane, located at about 26 km east of the city of Youssoufia. The climate is semiarid with an average annual rainfall of 199.6 mm and the average monthly temperature is 19.9 °C; this area belongs to the Gantour deposit [1]. The second was performed at Khouribga located 120 km Southeast of Casablanaca and the average annual rainfall is 432 mm, and the annual temperature average is 17.2 °C. The basin represents an important morphological unit of the Moroccan Mesetian domain, quasi-tabular and slightly corrugated; the altitudes are varied from 500 to 800 m (Fig. 1) [2].

N. Sundararajan et al. (eds.), *On Significant Applications of Geophysical Methods*,
Advances in Science, Technology & Innovation, https://doi.org/10.1007/978-3-030-01656-2_16

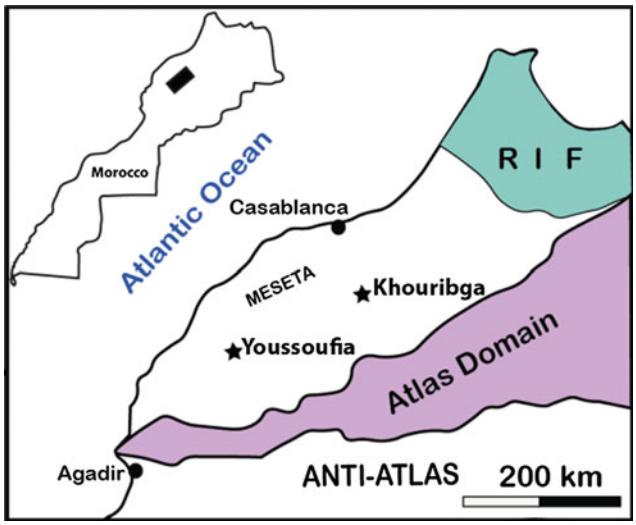

Fig. 1 Location of the study areas

2.2 Materials and Methods

The MRS technique is based on the ability of protons in groundwater molecules to have magnetic moments. These moments, normally oriented towards the directions of the Earth's magnetic field, are excited by an electric current at a specific frequency (larmor frequency). After cutting off the electric current, the protons return to their initial state by emitting a magnetic field recorded on the surface. The main geophysical parameters derived from MRS survey are the amplitude of the signal (E_0) proportional to the water content (θ_{MRS}) and relaxation times (T^*_2 and T1) versus depth related to the pore size [3]. In this study, an MRS survey was conducted at Youssoufia using Numis Pro (Iris Instruments). The measured parameter was the magnetic field of protons relaxation and the physical parameter that we tried to determine was the water content of the different layers of the subsoil. The resulting data were inverted and compared with the hydrogeological data provided by surveys.

The FDEM method is an electromagnetic technique that uses low frequency. The measured values of apparent conductivity provide an effective depth of investigation of about six meters [4]. In our study this method was carried out in khouribga using EM31 technique. Several profiles were conducted with a sampling step of 5 m and a spacing of 10 m, thus 137,322 measurements were recorded.

TDEM technique is based on the broadcasting of current that generates a primary electromagnetic field that interacts with subsoil materials [5]. When this current is suddenly cut-off it provokes a secondary field that recedes with time and is recorded on the surface [6]. In this study a total of 2500 TDEM surveys were conducted in Khouribga using Temfast Prosystem material. The mean measured parameter was resistivity and the aim was to identify the high conductivity structures that could be related to water content.

The ERT method is based on the measurement of the ground response against the propagation of an artificially generated current. This method was carried out in Khouribga using ABEM Terrameter LS12 equipment. Two profiles of 400 m and another of 800 m were conducted. The inversion of the data by suitable program made it possible to establish the resistivity pseudo-sections of the subsoil.

3 Results and Discussion

The survey MRS results accomplished in Youssoufia (Fig. 2a) shows that the signal is clearly distinguished from the electromagnetic noise, its amplitude changes according to the pulse excitation and so the depth; the values prove groundwater existence with a water content that changes from one level to another. The inversion allowed us to present the depth of aquifer layers with the estimated free water content corresponding to each aquifer. In general we had two aquifer layers, the first one was located between 20 and 30 m depth and the second was situated from 30 to 50 m, with a water content respectively 2.5% and 5%. In fact these two aquifers match with the aquifer of Ypresian and Lutitian formations [7]. The model provided by the MRS inversion is similar to the one obtained with piezomtric data. Considering the saturated layers, we estimated an average porosity of 3.75%; with an average thickness of 30 m, an area of about 19,242,500 m^2; we deduced a volume of 22,512,700 m^3 which is very comparable to the volume obtained from piezometric analysis.

Apparent conductivity map (Fig. 2b) provided by FDEM shows areas with high conductive values, since the investigation depth of FDEM is about 6 m, those areas could be related to infiltration zones. This interpretation should be confirmed with other studies as geological lineament maps to see if these conductive structures corresponded to geological lineament.

The apparent resistivity map obtained from TDEM indicated areas with low resistivity that might be also linked to the presence of water. The inversed section of TDEM indicated a conductive layer situated beyond 30 m depth. This layer was also revealed with ERT pseudo-sections conducted in the same areas (Fig. 2d); the three ERT profiles are all showing a conductive bottom beyond 30 m depth. In fact this level coincided with the first aquifer layers in the phosphate series.

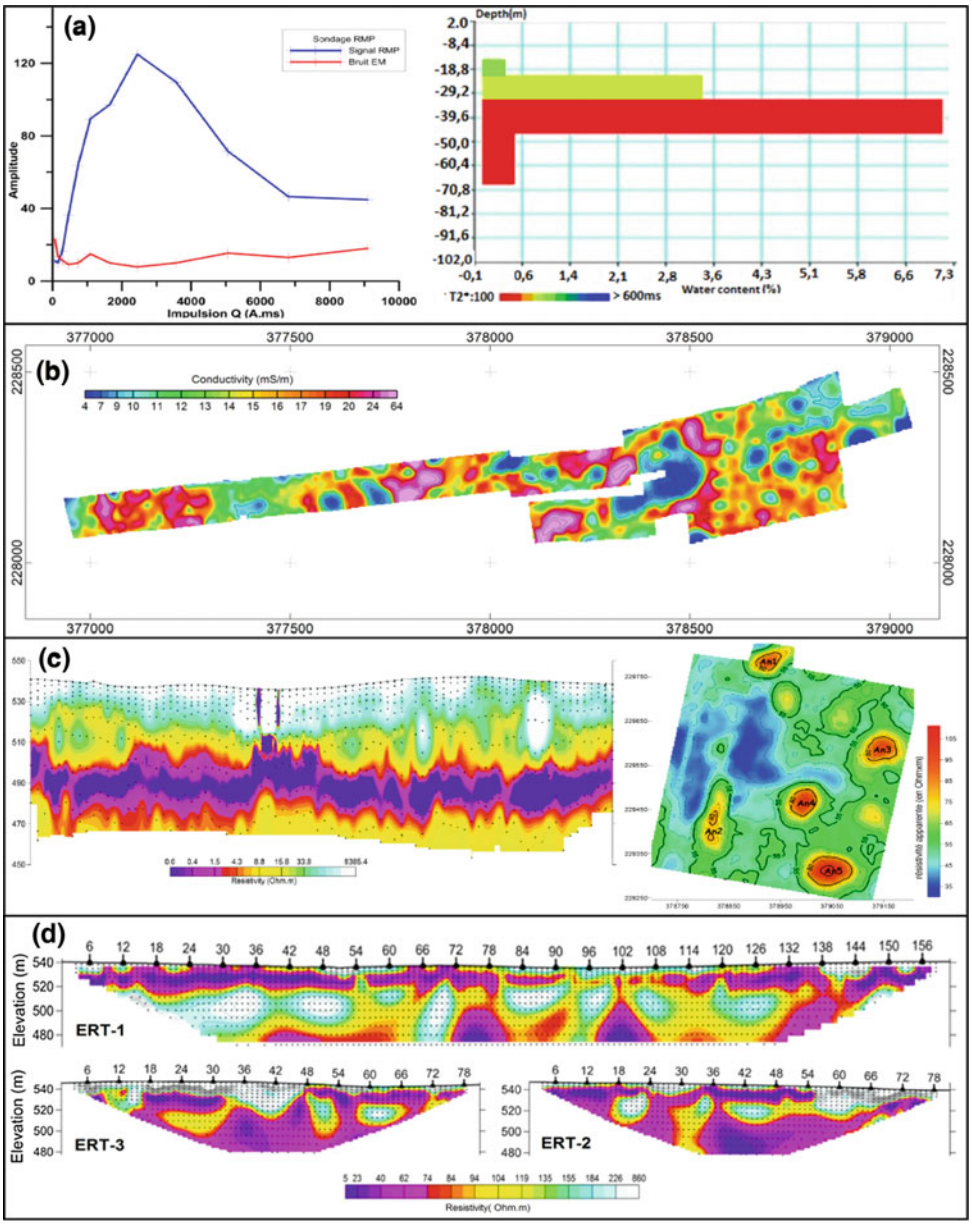

Fig. 2 Results obtained from different methods. **a** MRS signal obtained at Youssoufia. **b** FDEM map executed at Khouribga. **c** TDEM inverse section and map obtained at Khouribga. **d** ERT pseudo-sections at Khouribga

4 Conclusion

This case presented important information using non-invasive geophysical techniques to explore groundwater. The first results indicated the presence of highly conductive zones that may be related to the presence of water.

TDEM and ERT methods proved to be well adapted to detect deep aquifers whereas FDEM can reveal near-surface lateral effects that could be related to infiltration zones. These three methods showed information about the entire characteristics of the environment but those results could be related to other things than water (minerals …) and this is why it is really important to confirm them using other methods.

The MRS method seems to be the best technique to explore groundwater, since it gave direct information of the presence of water, the only limitation of this method is that it requires special conditions of electromagnetic noise, which is not usually the case. The MRS can give an estimation of the volume of free groundwater retained in aquifers. In our case the volume estimated by MRS was very comparable to the one calculated by piezometric data.

The combination of these methods would be a good tool to better define the geometric limits and hydrodynamic properties of aquifers in arid and semi-arid regions.

References

1. Hakkou, R., Benzaazoua, M., Bussière, B.: Valorization of phosphate waste rocks and sludge from the Moroccan phosphate mines: Challenges and perspectives. Procedia Eng. **138**, 110–118 (2016)
2. El Haddi, H.: Les silicifications de la série phosphatée des Ouled Abdoun (Maastrichtien-Lutétien Maroc): Sédimentologie, Minéralogie, Géochimie et Contexte Génétique: Université Hassan II de Casablanca; Faculté des Sciences Ben M'Sik (2014)
3. Chalikakis, K.: Investigation of sedimentary aquifers in Denmark using the magnetic resonance sounding method (MRS): Comptes Rendus Geosci. **341**(10), 918–927 (2009)
4. Geonics Homepage: http://www.geonics.com/html/em31-mk2.html. Last accessed 3 Oct 2018
5. Nabighian, M.N.: Time domain electromagnetic prospecting methods. Electromagn. Methods Appl. Geophys. Part A (2), 427–509 (1991)
6. Descloitres, M.: Improvement in TDEM sounding interpretation in presence of induced polarization. A case study in resistive rocks of the Fogo volcano, Cape Verde Islands. J. Appl. Geophys. **1**(45), 1–18 (2000)
7. Ait Khouya, J.: Synthèse hydrogéologique de la zone noyée de Youssoufia. Rapport géol. inédit N°455, Service géologique de Youssoufia, 45 p (2008)

2-D Earth Resistivity Imaging for Subsurface Characterization in Srinagar, Garhwal Himalaya

Pradeep K. S. Chauhan, Abha Mittal, Gayatri Devi, and Philip O. Falae

Abstract

Resistivity imaging technique is a geo-electrical method used to image the subsurface, water bearing zone, bedrock and layer thickness. The 2-D resistivity imaging method is a non-invasive technique which provides reliable picture of the subsurface at shallow depths. The application of this method for site investigation is becoming common nowadays. In the field of civil engineering site investigations, it is frequently used along with seismic refraction survey. In the present study, 2D electrical resistivity imaging has been used as a tool for subsurface geological characterization and delineation of sub-surface strata in Srinagar, Garhwal Himalaya, India. The aim of this survey was to map the shallow subsurface and geophysical properties i.e. resistivity and layer thickness. The survey was carried out on both sides of the river Alaknanda which flows through the city using ABEM Terrameter LS equipment. The data was processed using RES2DINV software. Three boreholes were also drilled in the area of study to evaluate the results obtained from the imaging survey. The results of the models show that the study area is predominantly of sand formation however, some clayey sand is also present in some areas as indicated by both the imaging and the borehole drilled.

Keywords

2D resistivity • Subsurface geology • Lithology • Borehole

1 Introduction

Srinagar is one of the major towns in the Garhwali Himalayas. Its geology has been controlled by both erosional and depositional activities [2]. The slope elements, evolution of drainage pattern, mass wasting activities, all these are controlled by the character of the bed rock and its structural configuration which has influenced the geology of the area. Adequate knowledge of these factors is necessary for the development of engineering structures as the quest for urbanization within this area is on the increase on daily basis.

The application of geophysical method for subsurface investigation has been applied to investigate engineering construction site such as roads, dams, high rise buildings, tunnels among others [3]. The subsurface characterization is a complex phenomenon dependent upon numerous factors. The direct investigations such as geological and geotechnical techniques can be applied along side with indirect assessment like geophysical method in order to ease the process of subsurface exploration with low cost and effective methods [1]. Since geophysics in civil engineering is an application of the principles and methods of physics in the measurement of subsurface characteristics and properties, the techniques were used to establish ground properties and profile for the engineering and development processes. The understanding of the nature of rock type and its weathering profile is crucial and very significant in site investigation processes.

This study aimed to delineate the subsurface geology of Srinagar in order to assess its engineering implication on civil engineering constructions (Fig. 1).

2 Methodology

The data acquisition for the 2D resistivity survey was carried out using ABEM Terrameter LS with electrode spacing range from 1.5 to 3 m depending on the available space and

P. K. S. Chauhan (✉) · A. Mittal · G. Devi · P. O. Falae
CSIR-Central Building Research Institute, Roorkee, 247667, Uttarakhand, India
e-mail: pkschauhan@cbri.res.in

N. Sundararajan et al. (eds.), *On Significant Applications of Geophysical Methods*,
Advances in Science, Technology & Innovation, https://doi.org/10.1007/978-3-030-01656-2_17

Fig. 1 Location of study area on google imagery

Table 1 Survey parameters

Parameter/ERT	L1	L2	L3	L4
Electrode spacing (m)	2	1.5	2.5	3
Length of profile (m)	96	72	120	144
Depth of investigation	15.2	13	18.9	26
No of electrodes	48	48	48	48

four survey lines were occupied within Srinagar Township (Table 1). GD 3X16 Protocol was used for data collection due to its reasonable sensitivity to changes in both horizontal and vertical directions as well as higher signal-to noise ratio [4]. The raw data collected from field of the apparent resistivity was processed using RES2DINV proposed by Loke and Barker [5] for gridding and presentation of the final result. Three boreholes were drilled in the study area to validate the results of electrical resistivity imaging. The results of the imaging were further classified based on the number of layers and their thicknesses.

3 Results and Discussion

The results of the inversion of resistivity pseudo section carried out from the data acquired from four locations are characterised by resistivity value range from very low to very high as indicated in Fig. 2a–d. This resistivity range is an indication of clayey sand, sand, sandstone, and conglomerate while the very low resistivity indicates high degree of water saturated zone. The higher resistivity is termed to be some boulders within the predominate sandy soil lithology

The first profile located in ITI ground Srinagar indicates the resistivity inversion results that the upper layer is made up of clayey sand as identified by the resistivity range from 200 to 400 Ω m up to a depth of 4 m followed by sandy soil having a resistivity of 1000–4000 Ω m. One bore was drilled on this profile and the results are in agreement with resistivity imaging results (Fig. 2a).

The second profile located in the premises of Anchal dairy, comprises two basic lithologies. The first layer is predominately made up of clayey sand owing to the low resistivity of 200–700 Ω m up to the depth of 4 m. This layer was underlain by sandstone with a resistivity value between 1500 and 3500 Ω m for a depth of 9 m. A saturated zone was noticed along the profile. The borehole along this profile indicates a pure cohesionless sand soil which corresponds to the results obtained from the inversion model on the profile (Fig. 2b).

The third profile located at GIC Chauras campus shows two main lithologies. The first layer is of clayey sand soil

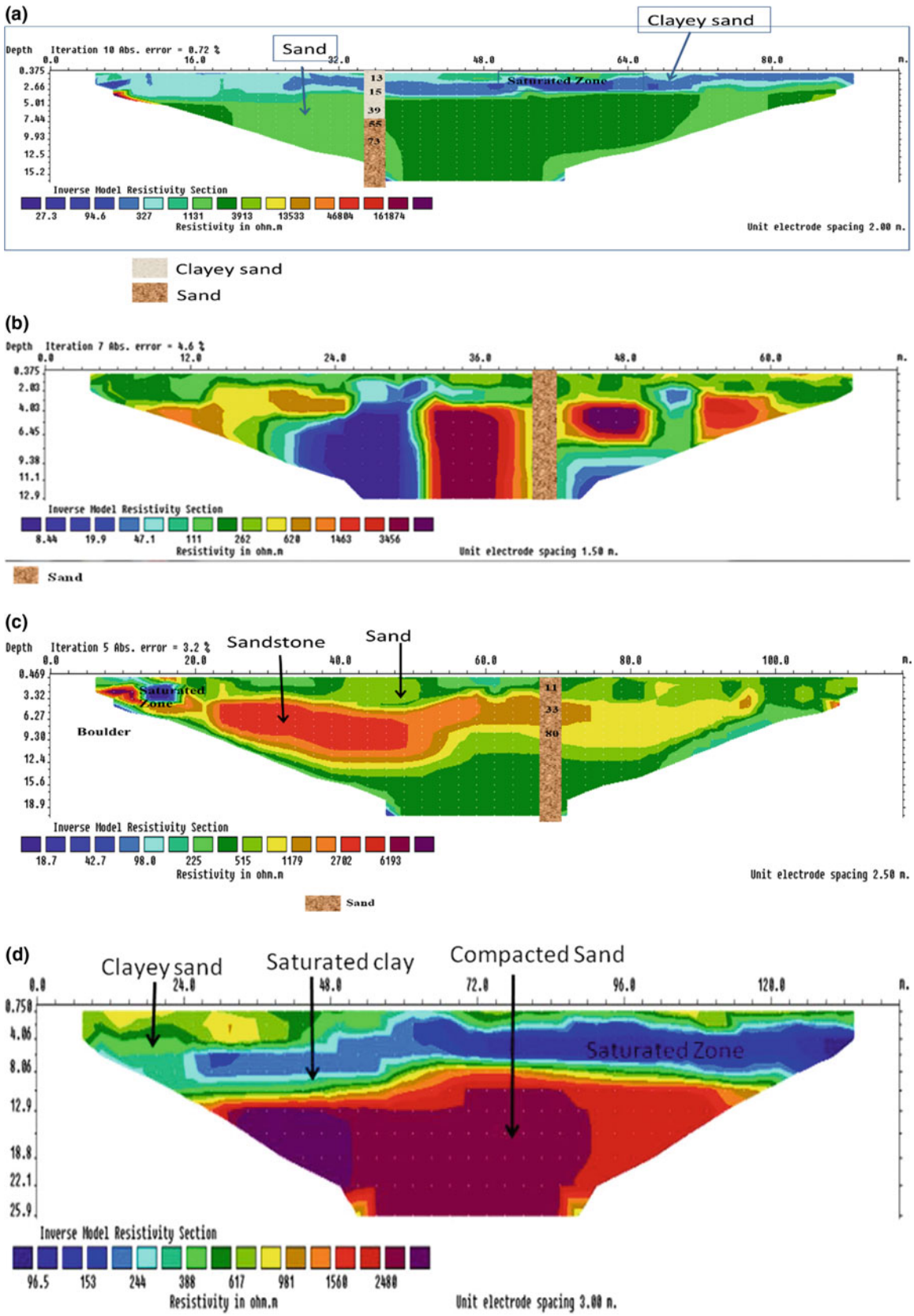

Fig. 2 **a** Profile of location 1. **b** Profile of location 2. **c** Profile of location 3. **d** Profile of location 4

Table 2 Summary of interpreted data

Location	Layers	Resistivity (Ω m)	Thickness (m)	Depth (m)	Probable lithology
L1	I	200–400	4	4	Clayey sand
	II	2400–4500	13	17	Sandstone
L2	I	200–700	4	4	Clayey sand
	II	1500–3000	9	13	Sandstone
L3	I	200–600	3.4	3.4	Clayey sand
	II	1200–5000	9.6	13	Sandstone
	III	600	8.5	21.5	Sand
L4	I	400–700	4	4	Sand
	II	100–300	9	13	Clayey sand
	III	1000–3000	13	26	Compacted sand

underlain by sandstone having a depth of 3.4 m and 9.6 m with recessitivity of 200–600 and 1200–5000 Ω m, respectively. The third layer is of sand with a resistivity of 600 Ω m and thickness of 8.5 m. The borehole drilled along this profile confirms this as indicated in Fig. 2c.

The fourth profile located along the river side Ranihat results a three layer subsurface. The first layer resistivity range from 400 to 1000 Ω m and having a depth up to 4 m with lithology as sand. This was directly underlain by saturated clayey sand of low resistivity between 100 and 300 Ω m having about 9 m in thickness. The third layer is made of compacted sand with a high resistivity of 1000–3000 Ω m and a depth of up to 13 m (Fig. 2d and Table 2).

4 Conclusions

The 2D electrical resistivity assessment of Srinagar was carried out in order to understand the subsurface formation and condition which are essential in determining the inherent engineering suitability of the subsurface variations. The resistivity inversion model clearly shows that Srinagar has undergone several oceanic depositions and transformations over the years, which has resulted into a variation in the consistency of the subsurface lithology. The models show that the study area is basically of sand formation; however, some clayey sand is present in some areas which generally fall within almost the same elevation. The results did not show any fractures, faults or voids in the study area which can be a great constraint in engineering constructions. Generally, the centre of study area has lower resistivity when compared to both the Northern and the Southern parts of the area which could have been the result of elevation differences.

References

1. Tan, S.N., Mohamad, E.T., Saad, R., Nordiana, M.M.: Assessment of subsurface profile at SILC, Nusajaya by 2D resistivity method. Appl. Mech. Mater. **695**, 823–827 (2015)
2. Islam, R., Ghosh, S.K., Vyshnavi, S., Sundriyal, Y.P.: Petrography, geochemistry and regional significance of crystalline klippen in the Garhwal Lesser Himalaya, India. J. Earth Syst. Sci. **120**(3), 489–501 (June 2011)
3. Nordiana, M.M., Azwin, I.N., Saad, R., Jia, T.Y., Anderson, A.B., Tonnizam, E., Zakaria, M.T.: 2-D resistivity assessment of subsurface characterisation and its engineering and environmental implications at SiLC. In: South Asian Conference on Geophysics IOP Conference Series: Earth and Environmental Science, vol. 62, no. 201, 012011
4. Falae, P.O., Kanungo, D.P., Chauhan, P.K., Kumar, R.D.: Recent trends in application of electrical resistivity tomography in Landslide investigation (2017)
5. Loke, M.H., Barker, R.D.: Rapid least-squares inversion of apparent resistivity pseudosections by a quasi-Newton method. Geophys. Prospect. **44**, 131–152 (1996). https://doi.org/10.1111/j.1365-2478.1996.tb00142.x

Two-Dimensional Resistivity Imaging of Migmatized Gneiss Basement Rock in Kaduna Polytechnic Main Campus, Kaduna Nigeria

Ani Chinedu and Gabriel Gabarko

Abstract

An environmental assessment was carried out in Kaduna Polytechnic to delineate and map the water bearing formations underlying some subsurface basement rocks that protrude on the surface as outcrops. There was a particular need to ascertain the extent of deformations of the migmatized gneiss basement complex at depths and obtain detailed geological information mainly for addressing environmental and engineering problems. To obtain a proper imaging of these geologic features, a 2-D Electrical Resistivity Tomography was adopted for the investigation. Data acquisition was achieved via six profiles spanning 200 m each, traversing parallel and even diagonally to the azimuth of the featured outcrops. The intent was to ascertain the depth and extent of weathering of the basement majorly overlain by unconsolidated materials. The tomographic images from the processed resistance data displayed intermingling of patches of low resistivity zones indicating highly saturated sections that may likely be aquifers and high resistivity zones in the overburden revealing shallow bedrock respectively. However, the study revealed that the Northern Nigerian basement complex is highly deformed due to weathering at depth and widely overlain by consolidated and unconsolidated materials. It also confirmed the convenience of the study area for engineering constructions.

Keywords

Aquifer • Basement outcrops • Downthrown faults
Electrical resistivity tomography • Migmatized gneiss

A. Chinedu (✉)
Department of Physics and Astronomy, University of Nigeria, Nsukka, Nigeria
e-mail: bedrock969@yahoo.com

G. Gabarko
Department of Mineral Resources Engineering, Kaduna Polytechnic, Kaduna, Nigeria

1 Introduction

Kaduna Polytechnic is geologically situated on the migmatized gneiss basement complex of Northern Nigeria. Due to the last tectonic events that affected the North central part of Nigeria, deformation of the gneiss basement complex has manifested in a nearly N-S major fracturing pattern with minor east-west components. At the northern part of the Study Area (Fig. 1), an outcrop of migmatized gneiss can be seen (Fig. 2) occupying a substantial portion of the area. It appears that this might be due to weathering and erosion, the gneissic outcrop stands out with a NW-SE orientation and the area west and north thereof are low lying.

Electrical resistivity has proved to be relevant in mapping geologic features [1] and monitoring changes of electrical properties in the subsurface and geotechnical investigations [2]. This is largely dependent on saturation, porosity, permeability, ionic content of the pore fluids, and clay content. However, applications of Two-Dimensional Electrical Resistivity inversions provided effective and reliable models of geologic features and the subsurface [3, 4].

The primary objective of this study was to use Electrical Resistivity Tomography for quantitative assessment of the portion of the Northern Nigerian Basement complex within the Study Area, map the water table and determine the extent of deformations due to weathering and erosion, hence the outcrops.

2 Data Acquisition

The Northern Nigerian basement complex is highly deformed due to weathering at depth and widely overlain by consolidated and unconsolidated materials. It is worth bearing in mind while planning the profiling pattern (Fig. 2) and general data acquisition in the area need to be recalled.

The acquisition of 2-D Electrical Resistivity data is fundamentally nondestructive and maybe relatively

N. Sundararajan et al. (eds.), *On Significant Applications of Geophysical Methods*,
Advances in Science, Technology & Innovation, https://doi.org/10.1007/978-3-030-01656-2_18

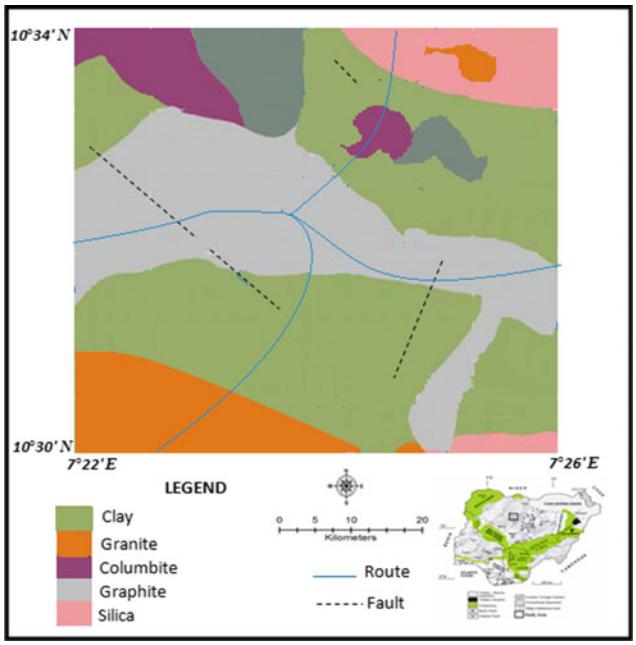

Fig. 1 Geological Map of the Study Area

Fig. 2 Satellite imagery of the study area showing 2D electrical resistivity profiles

inconvenient if collected manually. The sequence of measurements as described in [5, 6, 1] was adopted. The resistivity equipment includes SAS 4000 Terrameter and 42 electrodes spread across profile lengths, 200 m each, spaced at 10 m interval. The profiles were taken along the field geometry profile as shown in Fig. 2, and were planned parallel, perpendicular and diagonally to the azimuths of the visible outcrops, in order to delineate possible microstructures or features within the area.

The Wenner protocol format for the control file [6] was adopted for data acquisition. The acquired set of data was processed with RES2DINV program. The Geotomo Software modified by [6], was used to automatically determine a two dimensional resistivity model for the subsurface.

3 Results

The acquired set of 2D electrical resistivity field data were processed to image the existing geological structures within the study area. The presence of discontinuities, highly permeable zones and low resistivity associated with Fault zones, can easily be mapped using electrical properties compared to their surroundings. These characteristics have aided the detection of the highly saturated zones that may likely be the water table or aquifer at the downthrown part of the fault within the study area. The nearest available borehole log data was used as a control over the interpretation of the resistivity pseudosections (Table 1). Meanwhile, the results obtained from the 2D inversion of field data and borehole information, were interpreted to determine the depth and extent of deformations of the shallow bedrock and thickness of the overburden.

Figure 3 is one of the six ERT images from the various 2D profiles undertaken around the gneissic outcrop. More Figures for the remaining results (profiles) will be shown on the main paper.

4 Discussion

The combined tomographic sections of the inverted field resistivity data revealed and imaged the true signature of the subsurface within the study area and also in good agreement with the correlated borehole log from the area. The profiles as depicted in the pseudo-sections have identified the water table and shallowness of the basement complex. However, the ERT results have confirmed the depth to the water table in the area, to be at, between 8 and 25 m, and in good agreement with the borehole log data of 40 m depth.

5 Conclusion

The purpose of this study was to image the migmatized gneiss basement complex, the extent of bedrock deformations during the epierogenic era and eventually map the water bearing formations within the study area. However, the combined interpretations of ERT and borehole log survey data have been useful in providing a more interesting and accurate understanding of the subsurface geology of the

Table 1 The results of electrical resistivity and depths correlated with available borehole log data

Depth	Electrical resistivity	Borehole log
0–8	7.88–14.8	Top soil, unconsolidated lateritic clay
8–13	31.8–432	Weathered and partly weathered Basement complex. Schists with Granitic pebbles
12–25	128–1256	Saturated sand stones with mica schists. Partly weathered basement
24–40	516–3654	Granitic basement complex

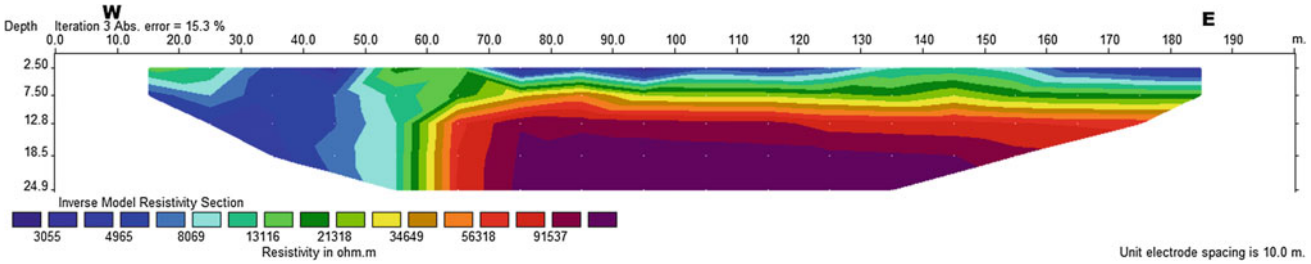

Fig. 3 2D resistivity section of W-E1 profile

study area. It can be deduced from the study that the basement in the study area is highly undulating and as shallow as 2 m and deeper than 30 m which might have been caused by tectonic forces. By extension, the paper also shed more light on the water table and the general stability of the study area for engineering constructions.

References

1. Dahlin, T.: 2D resistivity surveying for environmental and engineering applications. First Break **14**, 275–284 (1996)
2. Ward, S.H.: Resistivity and induced polarization methods in Geotechnical and environmental geophysics. In: Ward, S.H. (ed.) Society of Exploration Geophysics, vol. 1 pp. 147–189, Tulsa, Okla, (1990)
3. Chinedu, A.D., Ogah, J.A.: Electrical resistivity imaging of suspected seepage channels in an Earthen Dam in Zaria, North-Western Nigeria. Open J. Appl. Sci. **3**, 145–154 (2013)
4. Griffiths, D.H., Barker, R.D.: Two-dimensional resistivity imaging and modelling in areas of complex geology. J. Appl. Geophys. **29**, 211–222 (1993)
5. Loke, M.H.: Electrical imaging surveys for environment and engineering studies (a practical guide to 2D and 3D surveys) (1999) www.terraplus.com.info@terraplus.com,mhloke@pc.jaring.my
6. Loke, M.H.: Tutorial: 2D and 3D Electrical Imaging Surveys (2004). www.geoelectrical.com

2-D Resistivity Model of Magnetotelluric Inversion from M'rara Area, Algerian Sahara

Djabir Foudili, Abderrezak Bouzid, and Mohamed Chérif Berguig

Abstract

The M'rara region belongs to the North-Eastern basin of the Algerian Sahara. Indeed, this area is the locus of two major aquifer systems. The main objective of this research was to obtain a two-dimensional (2D) resistivity model of the structures, based on the 2D inversion method that was performed by means of the algorithm Occam for 08 sites. The resistivity and phase data for both TE and TM modes, in addition to the tipper data, were jointly inverted. Additionally, the dimensionality of the data was analyzed by the phase tensor method, which allows us to obtain the 2D dimensionality below the period of 0.5 s. The resulting model of the 2D inversion was successfully used to identify the two aquifer systems; it also reveals the two horizontal superficial layers which are conductive and resistive, respectively.

Keywords

Magnetotelluric • 2D inversion • Phase tensor • M'rara region

1 Introduction

The MT method is a geophysical technique based on the emission and propagation of natural electromagnetic waves. This technique has been widely used in groundwater investigations [1, 2]. The hydrographic representation of the region of M'rara shows the existence of two large groundwater systems [3]. The first is the deep continental intercalaire (CI) aquifer whereas the second is the complex terminal (CT) aquifer, located at a shallower depth [4]. The large difference in depth between these aquifer systems is accompanied by changes in pressure, water temperature and chemical composition. Indeed, the salinity and temperature of the CI aquifer are 1.7 g/L and 55 °C, respectively; they are much lower in the CT aquifer [4]. The main purpose of the present paper was to suggest a new 2D resistivity model in 8 MT sites distributed in the North-South direction in order to identify these aquifer systems in this basin. This model was performed through an algorithm Occam [5, 6].

2 MT Data

The Broadband MT (BBMT) data for all 18 MT sites in the M'rara region were collected during seventeen days, using a V5 System 2000® of Phoenix Geophysics. These sites were divided according to two orthogonal profiles, i.e. along the N-S direction and the W-E direction (Fig. 1). The raw time-series data were processed using the Jones-Jödicke code [7], in order to determine the four components of the impedance tensor, as well as the apparent resistivity and phase data. We used the phase tensor method [8] to analyze the MT data. In this study we used just the 08 sites which were selected along the N-S profile.

3 Dimensionality and Inversion Results

From the phase tensor method [8], the 3D subsoil structure was found when the absolute skew angle ($|\beta|$) is larger than the threshold angle of 3°. Thus, at the periods range 0.01–0.5 s (above the dashed line Fig. 2a), our regional structure can be described by the 2D model. Also, over long periods (under the dashed line Fig. 2a) it indicates that the MT data were the responses of the 3D regional structures. Therefore, the strike angle of the 2D regional structures is along the N20°E direction (Fig. 2b).

D. Foudili (✉) · M. C. Berguig
Department of Geophysics, USTHB University, BP 32 El Alia, Algiers, Algeria
e-mail: foudilidjabir@gmail.com

A. Bouzid
CRAAG, Route de l'Observatoire, BP 63 16340 Bouzaréah, Algiers, Algeria

N. Sundararajan et al. (eds.), *On Significant Applications of Geophysical Methods*,
Advances in Science, Technology & Innovation, https://doi.org/10.1007/978-3-030-01656-2_19

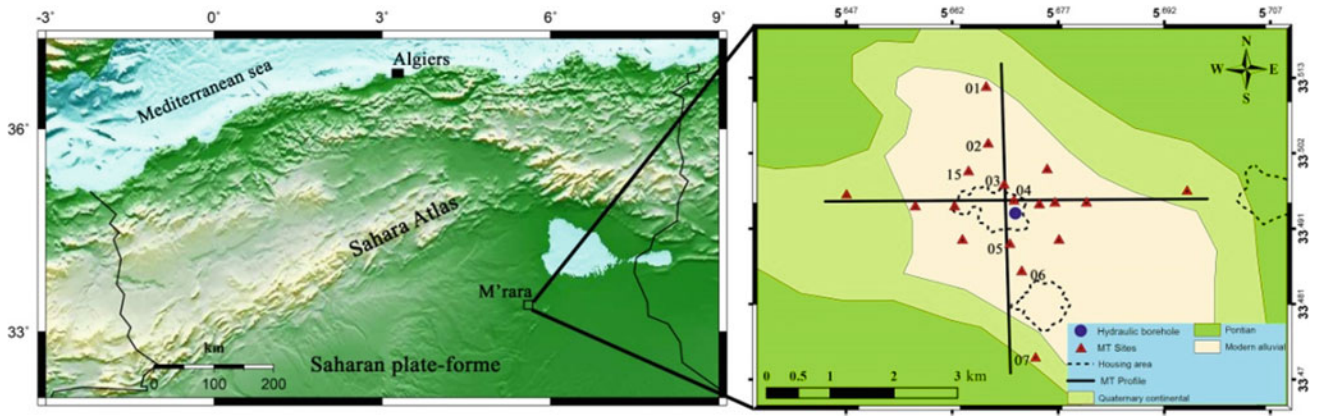

Fig. 1 Location of the M'rara area (left panel). MT sites distribution on the simplified geological map (Right panel). The locations of the MT sites are represented as triangles. The black straight lines indicate the location of the E-W and N-S profiles

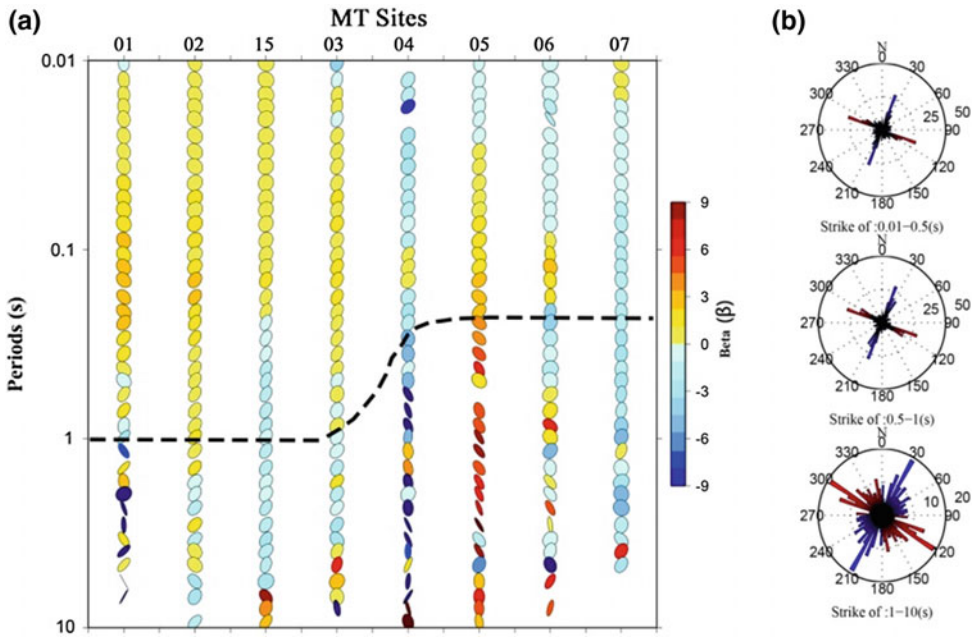

Fig. 2 **a** Pseudo section of phase tensor ellipses, the color concerns the β values. **b** Shown the rose diagrams of the Strike angles at three different period ranges of all sites

In the 2D inversion, the data of all 08 MT sites (sites MT: 01, 02, 15, 03, 04, 05, 06 and 07, see Fig. 1) rotated through the strike angle (N20°E) of the 2D regional structure. The resistivity and phase data for both TE and TM modes, in addition to the tipper data (VTFs), were jointly inverted, for a set of 10 periods, logarithmically distributed between 0.0531 and 1.96 s. The specified error floor was set at 10% of TE and TM modes, and to 0.1 of VTFs. Our 2D mesh grid was discretized into 160 × 46 nodes in the y and z directions; the vertical grid increases by a factor of 1.5 starting from the initial width of 1 m. The uniform horizontal rectangular prisms of the mesh have a width of 40 m. The inversion process ran with the initial model, with a resistivity equal to 20 Ωm. The final and preferred model converged after 19 iterations starting from the normalized RMS Misfit of 5.14 to below 2.35 (Fig. 2).

4 Discussion and Interpretation

The 2D model (Fig. 3) is found at a shallower depth of 500 m below surface, shows two horizontal geoelectrical layers that have specific conductive and resistive features (the black and white horizontal dashed lines in Fig. 3). The first low-resistivity layer, extending from surface to a depth of approximately 130 m, may be interpreted as the CT

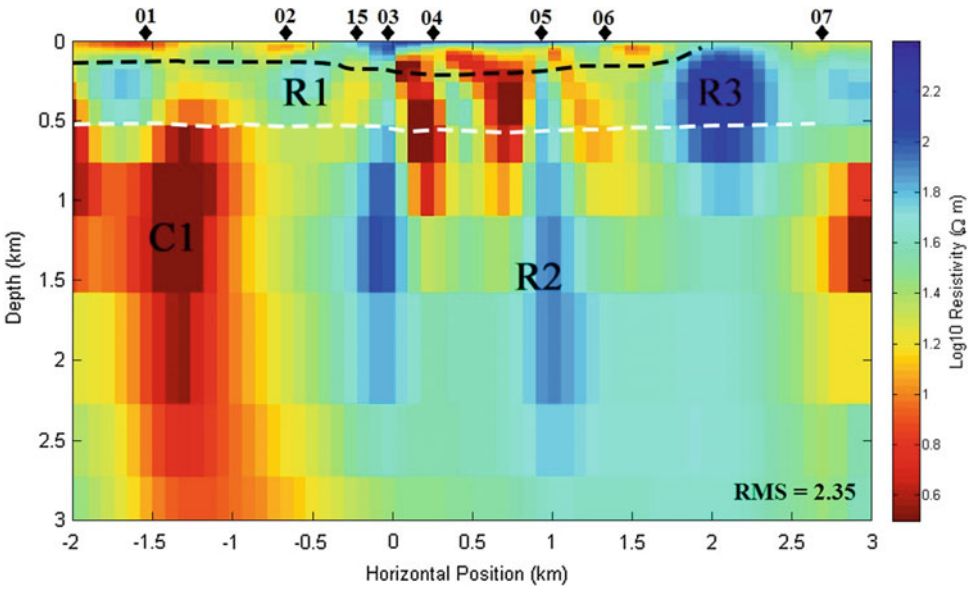

Fig. 3 2D model of the resistivity underground structures obtained from the 2D inversion for 08 MT sites. C and R denote the conductive and resistive anomalies, respectively

aquifer located at a shallower depth. Also, the 2D model is clearly visualized beneath stations 01 and 02 the conductive anomaly C1 that is located at a depth between 500 and 1500 m. This anomaly is interpreted as the CI aquifer which contains very salty water (1.7 g/L). This is the reason for the sharp drop in resistivity (0.1–2 Ω m). In particular, the 2D model (Fig. 3) did not clearly highlight the resistive anomaly R2 in the central and southern parts, beyond the depth of 500 m. In reality, the 2D inversion based on the Occam algorithm was influenced by the 3D structures; this may be confirmed by the large value of the RMS Misfit of the preferred model (RMS Misfit = 2.35). This explanation is supported by the analysis of the impedance tensor, which shows 3D structures along the N-S profile.

5 Conclusions

The 2D resistivity model allows highlighting two superficial horizontal layers which are conductive and resistive, respectively. Fortunately, the interpretation of the 2D inversion results allows us to identify the two aquifer systems as the CI aquifer and the CT aquifer. In addition, we found the data affected by the 3D structures cannot be correctly interpreted by the 2D inversion algorithm. Therefore, all the above allows us to say that the 3D model is more realistic than the 2D model in our area.

References

1. Abdelzaher, M., Nishijima, J., Saibi, H., El-Qady, G., Massoud, U., Soliman, M., Younis, A., Ehara, S.: A coastal aquifer study using magnetotelluric and gravity methods in Abo Zenema, Egypt. Pure Appl. Geophys. **169**, 1679–1692 (2012)
2. Kerbadj, N., Bouzid, A., Saibi, H., Bounif, M., Bougchiche, S., Kebede, Y.: 2-D inversion of magnetotelluric data at Dar-Chioukh region (Djelfa, Algeria). In: International Conference on Engineering Geophysics, Al Ain, United Arab Emirates, 9–12 Oct 2017, pp. 366–369. SEG Global Meeting Abstracts. Society of Exploration Geophysicists (2017)
3. Edmunds, W.M., Guendouz, A.H., Mamou, A., Moulla, A., Shand, P., Zouari, K.: Groundwater evolution in the Continental Intercalaire aquifer of southern Algeria and Tunisia: trace element and isotopic indicators. Appl. Geochem. **18**(6), 805–822 (2003)
4. Guendouz, A., Moulla, A.S., Edmunds, W.M., Zouari, K., Shand, P., Mamou, A.: Hydrogeochemical and isotopic evolution of water in the complexes terminal aquifer in the Algerian Sahara. Hydrogeol. J. **11**, 483–495 (2003)
5. Constable, S., Parker, R., Constable, C.: Occam's inversion: a practical algorithm for generating smooth models from electromagnetic sounding data. Geophysics **52**(3), 289–300 (1987)
6. deGroot-Hedlin, C., Constable, S.: Occam's inversion to generate smooth, two-dimensional models from magnetotelluric data. Geophysics **55**(12), 1613–1624 (1990)
7. Jones, A., Jödicke, H.: Magnetotelluric transfer function estimation improvement by a coherence? based rejection technique. In: SEG Technical Program Expanded Abstracts 1984, edited, pp. 51–55. Society of Exploration Geophysicists (1984)
8. Caldwell, T.G., Bibby, H.M., Brown, C.: The magnetotelluric phase tensor. Geophys. J. Int. **158**(2), 457–469 (2004)

Magnetotelluric Imaging of Subsurface Structure in Rahat Volcanic Field, Madinah City (Saudi Arabia)

Essam Aboud, Peter Wameyo, Faisal Alqahtani, and Mohammed Rashad Moufti

Abstract

Rahat volcanic field, Saudi Arabia, has three major geohazard events; the historical eruption, the fissure eruption, and seismic swarm. A magnetotelluric survey was carried out to evaluate these hazards. The results revealed four major resistivity zones. The first is a layer of intermediate resistivity (40–250 O m) which is thicker to the south-west and thinner to the eastern edge. This layer is underlain by a resistant (>1000 O m) granitic basement. Intruding into the resistive basement are two near-vertical conductive (<20 O m) structures. One is located west of the historic eruption (1256 AD) center, at a depth of about 15 km. The other intruder is on the southern end of the survey area, at the same depth. Two conductive "channels" trending NW-SE and NE-SW were observed at depths of about 18 km. The NE-SW aligned "channel" runs through the northern intrusive while the NW-SE trending "channel" runs in the middle of the study area and connects both intrusive structures. The conductive intrusive structures and "channels" may be attributed to partial melts stored in the pre-existing structures within the lower crust. Although the youngest known trachytic eruptions from the study area are several hundred thousand years old, recent and ongoing seismicity strongly suggests there may be magmatic activities in the lower and probably upper crusts.

Keywords

Magnetotelluric • Rahat volcanic field • Madinah • Saudi arabia

1 Introduction

Volcanic fields in Saudi Arabia extend across the western regions of the Arabian Peninsula. They define different phases of magmatic activity that took place during the 30 million year history of the Red Sea–Gulf of Aden rift system [1–2].

Rahat volcanic field (RVF) is one of the Cenozoic lava fields in the Kingdom that covers a 50 km wide plateau extending from north to south for almost 300 km between the Hejaz coastal range on the west and the high plains of Najd on the east [3, 4]. It has an approximate volume of 2000 km^3 volcanic flows with an estimated average thickness of about 150–400 m flows [5]. The most recent eruption of AD 1256 (historic eruption), which lasted 52 days, extruded 0.5 km^3 of alkali-olivine basalt forming a 2.25 km long fissure, produced 6 scoria cones, and a 23 km-long lava flow that came to within 8 km of Madinah city [6, 7]. Three volcanic hazards are located within the study area: the historic eruption of AD 1256, fissure eruption or five fingers eruption, and the earthquake swarm in 1999 [8]. In the current study, we used magnetotelluric (MT) data to evaluate the above-mentioned hazards.

KAU and UoA jointly collaborated to evaluate the geohazards in RVF via the Volcanic Risks in Saudi Arabia (VORiSA) project. This project carried out geophysical and geological surveys over 3 years. Gravity, MT, and seismic surveys were the most important tasks in the VORiSA project. Aboud et al. [9] published the results of gravity data combined with the available aeromagnetic data. Abdelwahed et al. [10] published the seismic results. Currently, we would discuss the analysis and interpretation of MT data taking into consideration the previously published works.

E. Aboud (✉) · F. Alqahtani
Geohazards Research Centre, King Abdulaziz University, Jeddah, 21589, Saudi Arabia
e-mail: eaboudeshish@kau.edu.sa

E. Aboud
National Research Institute of Astronomy and Geophysics (NRIAG), Cairo, Egypt

P. Wameyo
Pemura Geoscience & Engineering, Auckland, New Zealand

F. Alqahtani · M. R. Moufti
Faculty of Earth Sciences, King Abdulaziz University, Jeddah, 21589, Saudi Arabia

N. Sundararajan et al. (eds.), *On Significant Applications of Geophysical Methods*,
Advances in Science, Technology & Innovation, https://doi.org/10.1007/978-3-030-01656-2_20

In RVF, we used Phoenix MTU-5A to record long period (~24 h) MT stations. In this survey, after we recorded the MT stations, some sites were selected for high frequency measurements using MTU-8 MT system, for static shift correction. Finally, 65 MT stations were recorded to map subsurface resistivity variations, identify major structures, map minor and major fault systems and possible intrusive bodies that could be related to local volcanism.

2 Materials

As a part of the VORiSA project, 65 MT soundings covering an area of about 1050 km^2 were collected to image deep resistivity structures. 56 MT sites were selected on profiles trending in NE, perpendicular to the main NW direction of RVF, 5 km spacing between stations (Fig. 1). The remaining, 9 MT sites, were selected around the AD 1256 historical eruption to improve coverage in the north. In each station, the measurement equipment consisted of 5-channel MTU-5A MT data acquisition systems, 24-bit data logger with a signal recording band from 10 kHz to 1000 s, 3 magnetic coils with frequency sensitivities between 400 Hz and 1000 s, and 5 non-polarizing, PVC-protected, broadband and low noise/offset/DC drift Pb-PbCl2 electrodes.

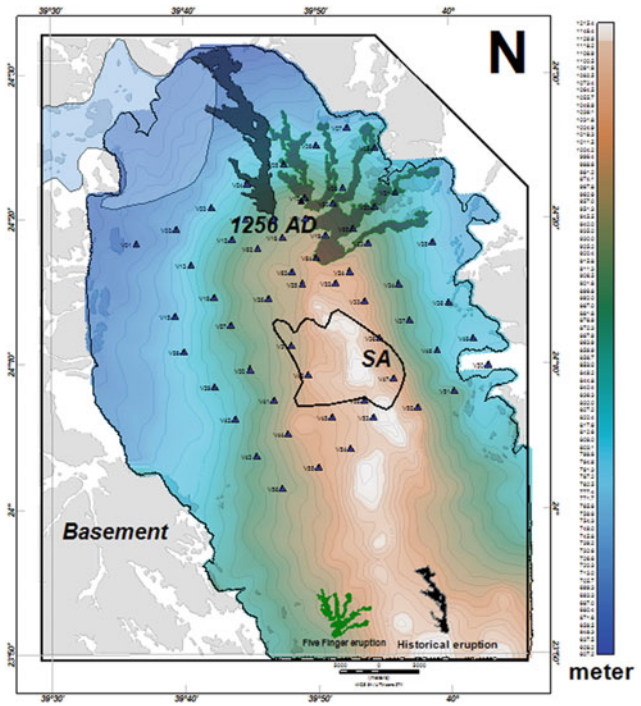

Fig. 1 Location of MT stations (blue triangles). Red asterisks = Volcanic vents. 1256 A.D = historic eruption (near Madinah city and airport), Transparency polygon = Almadinah city, SA = Swarm Area of 1999 [8]. P1–P10 are the selected profiles for 2D inversion of MT data. Light greys = basement rocks are on both sides of RVF. Background colored grid = ASTER data

For all MT stations, a cross-dipole array was used with dipole length between 60–70 m, using magnetic north as the north reference. In each deployment, all sensors were buried to minimize cultural noise. Additionally, all MT time-series data were evaluated in the field and data that did not meet a pre-set quality threshold (i.e., good records for periods > 100 s) were repeated upon modifying station layout to minimize cultural noises. Finally, all MT station duration times were 24 h to get greater depths.

3 Results

The results from the 3D inversion of the MT data are presented in Figs. (2) and (3). These clearly illustrate the thick resistive zone and the irregular-shaped low resistivity zones seen at depth below ~12 km. The view in Fig. 2a is of the low resistivity body as seen through the resistive zone. The northern peak is shown in Fig. 2a–c; resistivity values in this zone range from just 10–100 Ωm. Figure 2e also shows a low resistivity zone, in which the low resistivity abuts the edge of the survey area. The southern peak is seen in Fig. 3d; resistivity values in this zone average around 100 Ωm.

The high resistivity layer (>1000 Ωm) at the surface is likely to reflect unaltered basaltic lava flows. The layer of moderate to low resistivity (50–200 Ωm) beneath this surface zone that extends to the east where it ends on contact with outcropping Precambrian basement (Fig. 3a) may be interpreted as old and altered lava. The resistive zone below the top layers is inferred to reflect the basement; it is shallower to the east and dips to the west (Figs. 2c and 3a). Discontinuities observed in the basement (Figs. 2c and 2d), could reflect extensions of fault systems observed outside the volcanic field and may continue beneath the volcanic cover.

Two near-vertical bodies of low resistivity (<20 Ωm) are observed at about 12 km depth, one immediately south-west of the 1256 AD eruptive centre (Fig. 2a, b), and the and other at the southern end of the survey area (Fig. 2a, d). These structures are connected by a NW-SE aligned zone of low resistivity at a depth of about 18 km (Fig. 3a). The northernmost low-resistivity body may reflect a remnant of the magmatic system that fed the 1256 AD eruption.

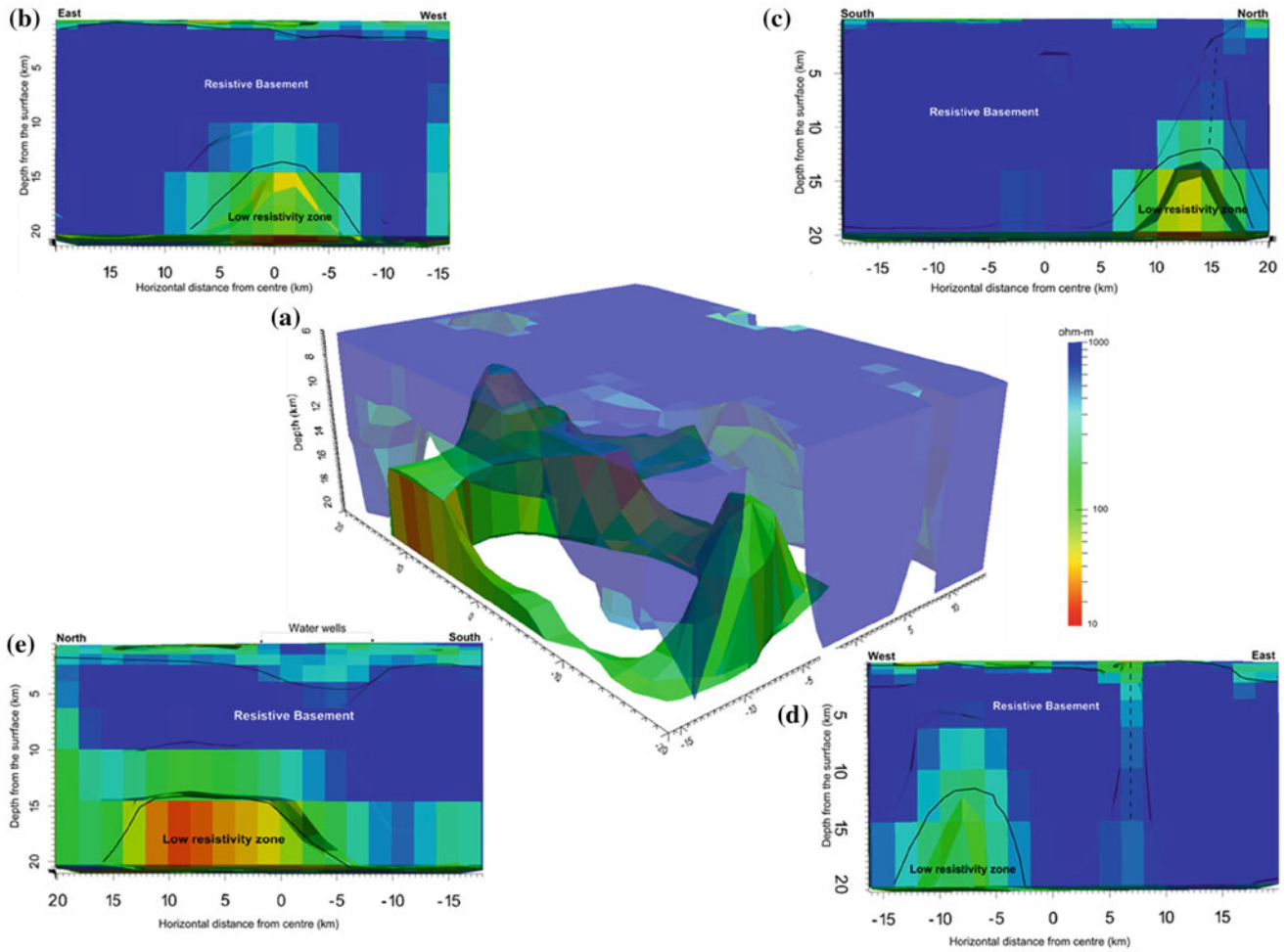

Fig. 2 3D resistivity volume of with top 4 km chopped off (**a**), side-view from NW (**b**), side-view from East (**c**), side-view from SE (**d**) and side-view from West (**d**)

4 Conclusion

The low resistivity zone at the southern end of the survey area lies beneath the area of trachytic volcanism and coincides with the seismicity of 1999. We do not know the lower bound of the low resistivity zone; we just know that only the upper bound is ~12 km deep. We tentatively interpreted this low resistivity zone as a zone of partial melt, reflecting stalled and crystallizing magma.

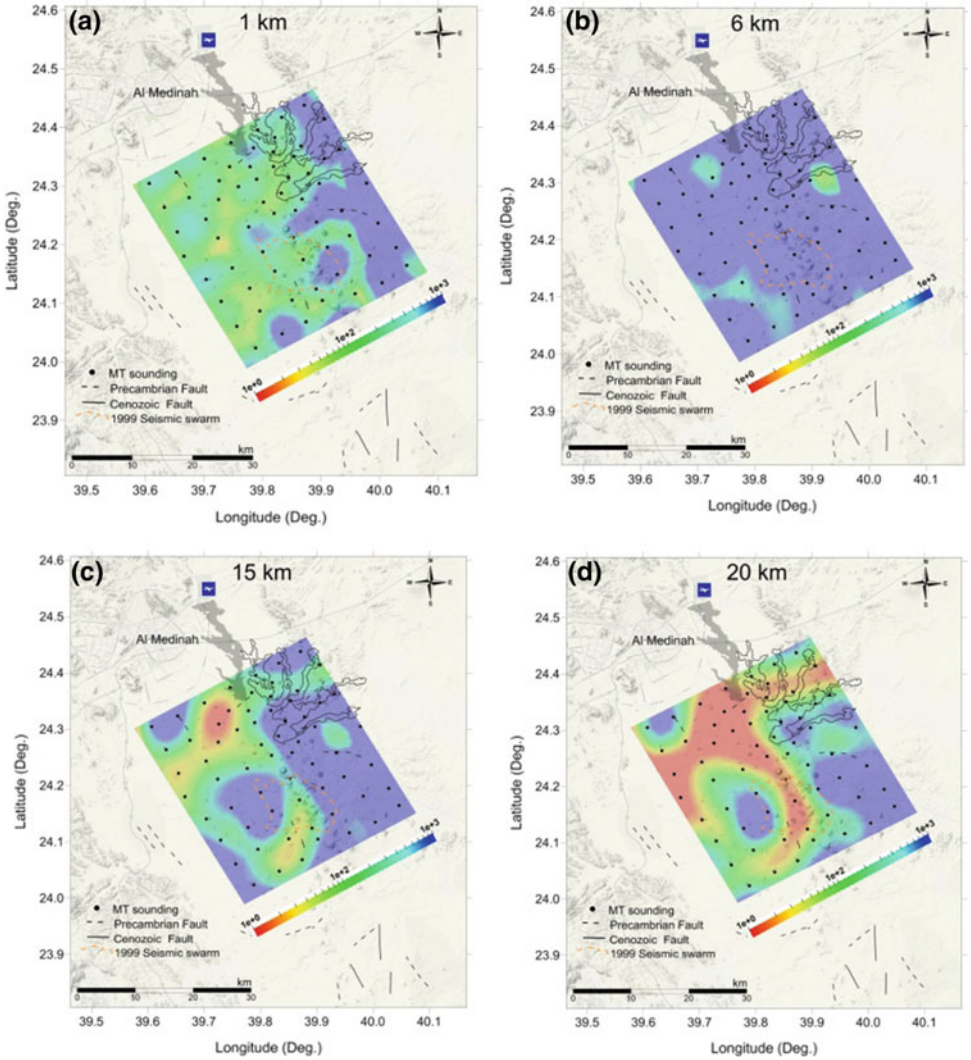

Fig. 3 Resistivity distribution in northern Harrat Rahat at different depths. **a** 1 km, **b** 6 km, **c** 15 km and **d** 20 km

References

1. Bosworth, W., Huchon, P., McClay, K.: The Red Sea and Gulf of Aden Basins. J. Afr. Earth Sci. **43**(1–3), 334–378 (2005)
2. Camp, V.E., Roobol, M.J.: Upwelling asthenosphere beneath western Arabia and its regional implications. J. Geophys. Res. Solid Earth **97**(B11), 15255–15271 (1992)
3. Berthier, F., Demange, J., Iundt, F., Verzier, P.: Geothermal resources of the Kingdom of Saudi Arabia. Saudi Arabian Deputy Ministry for Mineral Resources Open-File Report BRGM-OF-01-24, p. 116 (1981)
4. Durozoy, G.: Groundwater geology of the basalt on the Harrat Rahat plateau. Bureau de Recherche's Geologicques et Minieres (BRGM), Saudi Arabian Mission. (Open-File Report, 70 JED 24, p. 31) (1970)
5. Blank, H.R., Sadek, H., Hamdy.: Spectral analysis of the 1976 aeromagnetic survey of Harrat Rahat, Kingdom of Saudi Arabia. pp. 83–640 (1983)
6. Camp, V.E., Hooper, P.R., Roobol, M.J., White, D.L.: The Madinah eruption, Saudi Arabia: magma mixing and simultaneous extrusion of three basaltic chemical types. Bull. Volcanol. **49**(2), 489–508 (1987)
7. Camp, V.E., Roobol, M.J.: The Arabian continental alkali basalt province: part I. Evolution of Harrat Rahat, Kingdom of Saudi Arabia. Geol. Soc. Am. Bull. **101**(1), 71–95 (1989)
8. El Difrawy, M.A., Runge, M.G., Moufti, M.R., Cronin, S.J., Bebbington, M.: A first hazard analysis of the Quaternary Harrat Al-Madinah volcanic field, Saudi Arabia. J. Volcanol. Geoth. Res. **267**, 39–46 (2013)
9. Aboud, E., El-Masry, N., Qaddah, A., Alqahtani, F., Moufti, M.R.H.: Magnetic and gravity data analysis of Rahat Volcanic Field, El-Madinah city, Saudi Arabia. NRIAG J. Astron. Geophys. 154–162 (2015)
10. Abdelwahed, M.F., El-Masry, N., Moufti, M.R., Kenedi, C.L., Zhao, D., Zahran, H., Shawali, J.: Imaging of magma intrusions beneath Harrat Al-Madinah in Saudi Arabia. J. Asian Earth Sci. **120**, 17–28 (2016)

Indices of Energy and Appraisal for Electrical Current Signal at Polarising Frequency Using Electrical Drilling: A Novel Approach

Nyakno George and Aniekan Ekanem

Abstract

Despite the rapidity in the use of vertical electrical drilling in the study of hydrology, mineralogy, contamination and other geophysically based studies over decades, it appears that our ability to identify the relationships between the energy loaded in direct currents injected into the ground between two electrodes at low polarizing frequency is impeded. This study was undertaken to address this problem by establishing the novel links from the existing theories between resistivity and the two complementary energies, the voltage-driven energy called charging energy and the charge-driven energy called the discharging energy. This was achieved by sorting the resistivity values achieved from electrical drilling into regimes and plotting each regime in a location against the signal current low polarizing frequency measured from the relationship between power line frequency and the ratio of potential to current separations. The two energies, which are determinable from the slopes of regressed resistivity-period plots and the novel relations established in this work depend on the dynamic parameters β_v and β_q which are respectively called the voltage geometric index of energy and charge geometric index of energy. These indices connect earth resistivity to energy and frequency/relaxation period.

Keywords

Energy • Electric current • Resistivity • Polarizing frequency • Charging energy • Discharging energy

1 Introduction

During electrical drilling, details of the distribution of electrical conductivity in the subsurface can be explored by examining the magnitude of current flow in the geo-formation. The method of direct current flow in the earth, which enables the measurement of resistivity, is all about the injection of a stable electrical current into the subsurface. The trend of the injected current is observed in the resulting distribution of potential difference within a borehole or on surface. Interestingly, due to existing polarization in partially/fully saturated geo-units, the flow of currents shows variations at low frequencies/relaxation periods. As it is applicable in other methods of geophysics, the direct current method of exploration can be viewed on the basis of input energy, which is the current, the geohydraulic properties, and the measured parameters [1]. This process leads to the transfer of energy within the geological units. The energy source in this case, is the two electrodes injecting a known low frequency current into the ground in the study area. The compositions of the subsurface affect the injected energy due to the noticeable variations in the subsurface resistance which influences the pattern of the lines of current flow. The measured energy-loaded voltage within a borehole or at the earth's surface is polarization dependent. These measured signals contain clues on how charges are distributed within a formation boundary characterized by changes in electrical conductivity/resistivity. The energy index that penetrates the geological units depend on the amount of current sent into the ground; the composition of the geological formation, which determines the energy loss factor and the depth of investigation. The depth of penetration is frequency dependent and it is predetermined by electrical properties of the formation [2]. Formations with similar geological geo-units show consistency in the resistivity values. Hence the need to decipher the energy index of direct current signal sent into the geologically consistent geo-unit at a known low frequency caused by

N. George (✉) · A. Ekanem
Department of Physics, Geophysics Research Group (GRG), Akwa Ibom State University, Ikot Akpaden, PMB 1169, Uyo, Akwa Ibom State, Nigeria
e-mail: nyaknogeorge@aksu.edu.ng

N. Sundararajan et al. (eds.), *On Significant Applications of Geophysical Methods*, Advances in Science, Technology & Innovation, https://doi.org/10.1007/978-3-030-01656-2_21

polarization during vertical electrical drilling is necessary as this leads to the generation of energy expression from primary geo-electrical data. Besides, it is possible to establish the earth's resistivity/conductivity-energy relation at specific frequency based on the geological factors that affect the energy of the current signal using appropriate determining factors.

2 Materials and Methods

Vertical electrical drillings designed to send electrical current into sizably thick geo-materials in order to assess the current in terms of the total energy and the polarizing energy at very low frequencies [1]. The measurements of the very low frequency in the dc current signal was possible due to the polarization between the two pairs of electrodes connected to current electrodes and potential electrodes in resistivity measuring instrument. The dc currents were sent into the geomaterials of different electrical conductivities and permittivities using the vertical electrical drilling, which employs Schlumberger electrode arrangements. The cables carrying the current were extended in some places up to 800 m. This was done to ensure sizable exploratory depth of investigation beyond 160 m. The separation of the potential electrode (MN) ranged from 0.5 m at AB = 2 m (a minimum separation) to 20 m at AB = 800 m (maximum separation). With the known geology of the study area, unique geo-stratigraphy comprising arenaceous materials and argillites were expected to be assessed by the polarizing current signals [1–3]. Equation 1 was used in transforming the apparent resistance *Ra* to its appropriate apparent resistivity ρ_a.

$$\rho_a = \pi.\left((AB/2)^2 - (MN/2)^2 \Big/ MN\right).Ra \tag{1}$$

The signal currents for each measurement which was automatically varying by the resistivity metre were read in milliampere (mA) while their corresponding polarizing signal frequencies f were estimated from the known power line frequency f_o, of 50 Hz, using Eq. 2. The current signal relaxation period, T in seconds was calculated from the polarising signal frequencies f.

$$f = \left(\frac{MN}{AB}\right) f_o \tag{2}$$

The potential difference, V across the potential electrodes were calculated by finding the product of measured current, I and resistance, R in Ohm while polarising charge, Q in Coulomb was computed using Eq. 3

$$Q = IT \tag{3}$$

The resistivity regimes were obtained by sorting the geologically consistent resistivity values at their corresponding frequencies. The observed overlaps were due to the variations in grained size, fluid saturation, pore spaces, mineralogy and the generality of heterogeneous nature of sediments within a geological formation and inter-bedding.

3 Results and Discussion

In order to assess the loaded energy in the current signals sent into the ground at specific signal of low frequencies, the resistivities and the current relaxation periods with similar geo-electrical properties were sorted out through the $\rho - T$ plots in the locations considered. In locations 1 for instance, Fig. 1, three geologically consistent regimes were identified. In this case, irrespective of the geological regimes, the resistivity and the current relaxation time increases proportionally while for instance in $\rho - f$ plot for location 1, the relation is reversed.

Using the expression deduced from the basic principles in electrical drilling, given below, the energy loaded in the current was estimated

$$\rho = \frac{KV^2}{E_v} \times \frac{1}{f} = \beta_v \times \frac{1}{f} \tag{4}$$

where $\beta_v = \frac{KV^2}{E_v}$, f =polarizing frequency, E_v = charging energy due to source in Joules. K = geometric constant and ρ is the resistivity.

β_v was deduced as the slope from the plots in Fig. 1 and the numerical value of the charging energy E_v were calculated through the measured parameters in the Eq. 4.

The discharging was also measured from the expression in Eq. 4.

$$\rho = \frac{KE_q}{Q^2} \times \frac{1}{f} = \beta_q \times \frac{1}{f} \tag{5}$$

where $\beta_q = \frac{KE_q}{Q^2}$, Q = charge in coulomb and E_q= discharging due to loss factor of formation in Joules.

β_q was deduced as the slope from the plots in Fig. 1 and the numerical value of discharging energy E_q, was calculated through the measured parameters in the Eq. 4.

4 Conclusion

The inability to examine the convertibility of injected dc current in milliamperes at polarizing low frequency to energy in Joules and the insightful understanding of the links between energy and resistivity and other geo-unit parameters are really issues that have led to ambiguity within data

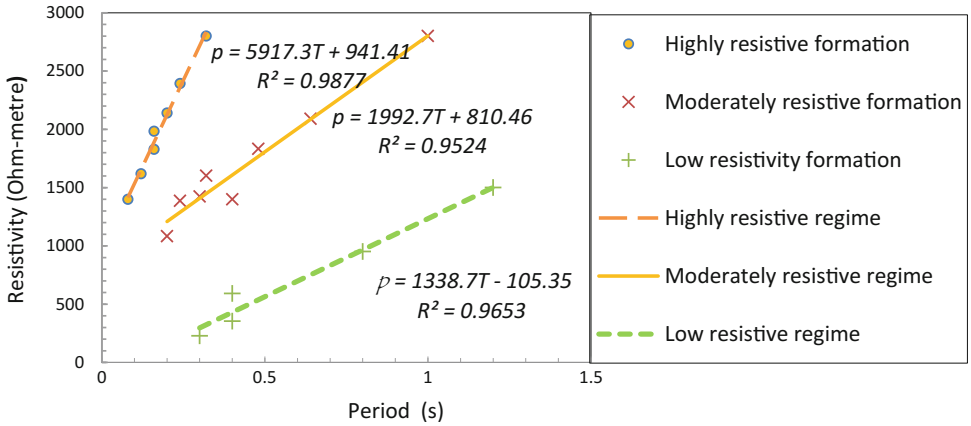

Fig. 1 A representative graph showing the spread of the three resistivity regimes with period in the study location

collection and interpretation in dc electrical resistivity drilling. Sometimes this knowledge gap makes vertical electrical drilling methods unsuitable when exploring for some geo-resources at geo-electrically possible depth of investigation. This study, which involved sorting the resistivity values into geologically consistent regimes and analyzing them in terms of the charging and discharging energies at low polarizing frequency dc signal, underpins more robust and dynamic models that govern electrical geoscientists on how to trade between geological formations and depths of penetration in order to achieve valid conclusions regarding data acquisitions and interpretations.

References

1. George, N.J., Obiora, D.N., Ekanem, A.M., Akpan, A.E.: Approximate relationship between frequency-dependent skin depth resolved from geoelectromagnetic pedotransfer function and depth of investigation resolved from geoelectrical measurements:A case study of coastal formation, southern Nigeria. J. Earth Syst. Sci. **125**(7), 1379–1390 (2016a). https://doi.org/10.1007/s12040-016-0744-4
2. George, N.J.A., Akpan, A.E., Ekanem, A.M.: Assessment of textural variational pattern and electrical conduction of economic and accessible quaternary hydrolithofacies via geoelectric and laboratory methods in SE Nigeria: a case study of select locations in Akwa Ibom State. J. Geol. Soc.of India, **88**(4), 517–528 (2016b)
3. George, N.J., Ekanem, A.M., Ibanga, J.I., Udosen, N.I.: Hydrodynamic Implications of Aquifer Quality Index (AQI) and Flow Zone Indicator (FZI) in groundwater abstraction: a case study of coastal hydrolithofacies in South-eastern Nigeria. J. Coast. Conserv. **21**(6), 759–776 (2017). https://doi.org/10.1007/s11852-017-0535-3

Part IV

Case Studies on Refraction and Reflection Seismic Methods

Refraction Seismic Study Over a Proposed Landfill Site in South West Bank, Palestine

Radwan El-Kelani and Abdelhaleem Khader

Abstract

A refraction seismic survey was used at a proposed landfill site in Al Minya basin south of West Bank in an effort to delineate the thickness of the soil cover and the distribution of rock types underneath, and to detect the subsurface structures that can act as contaminant pathways. One hundred seismic refraction traverse lines were run on the ground surface using the reverse profile techniques with a geophone interval between 3–5 m. From the seismic data analysis and the geological interpretation of the results, three main velocity zones were detected, ranging between 192–1085 m/s of the first two layers, representing the unconsolidated materials, to a moderately high velocity of the fresh bedrock, varying between 1100–2400 m/s. The velocity zones found, within the investigated seismic refraction sections were found to be compatible with the changes in the lithology of the study area. The general characteristics of the subsurface geology seem suitable for the proposed landfill site, yet light fracturing traced within the bedrock requires some remediation to prevent seepage. However, the landfill site is underlain by an aquitard layer of marl and chalk that will attenuate naturally the leachate infiltration.

Keywords

Landfill • Geophysical assessment • Seismic refraction • West Bank • Palestine

1 Introduction

Land-use planning represents an attempt to reduce some conflicts and environmental impacts in relation to both society and nature [1]. In the context of research program activities to develop the rural regions in West Bank, Palestine, sites were proposed for finding suitable areas for landfills [2]. The increasing demand of larger space for domestic and industrial wastes from urban areas makes waste disposal by landfill a necessary part of the human cycle of activities. Finding suitable sites for landfills is one of the most difficult tasks in solid waste management that is experienced by all countries in the world. Developing countries started to establish such agencies and institutions to take care of this field [3]. It is considered as one of the most serious environmental and social problems challenging municipalities [4]. The sanitary landfill site selection must address social, environmental and technical concerns. Thus, a significant amount of work is required to accurately define the relevant parameters of a covered landfill site.

This work focused on a geophysical seismic assessment of a proposed landfill site in Al Minya basin south of West Bank (Fig. 1). The seismic velocity models were used to delineate the soil cover thickness and the existing bedrock unit types beneath the study area. An attempt was also made to detect fractured zones which may provide contaminant pathways for the leachate [5].

2 Materials and Methods

The study area is located in Al Minya basin south of the West Bank between Bethlehem and Hebron Governorate (Fig. 1) at a distance of 10 km to the southeast of Bethlehem city, 16 km north east of Hebron, 5 km east of the regional road between the two cities. The proposed landfill site is spread over a land of about 250,000 m^2 of almost flat area with gentle slopes. The exposed sequence of rocks that covers the basin (Pleistocene to upper Cretaceous) consists of alluvium with poorly sorted gravels, dolomite and thin bedded limestone, karst dolomite and chalky limestone, marl, chalk and clay [6].

A refraction survey was conducted on more than 100 seismic profiles in the study area (Fig. 2). The survey lines were between 50–70 m long with 3–5 m geophone intervals

R. El-Kelani (✉) · A. Khader
An-Najah National University, Nablus, Palestine
e-mail: radwan@najah.edu

N. Sundararajan et al. (eds.), *On Significant Applications of Geophysical Methods*,
Advances in Science, Technology & Innovation, https://doi.org/10.1007/978-3-030-01656-2_22

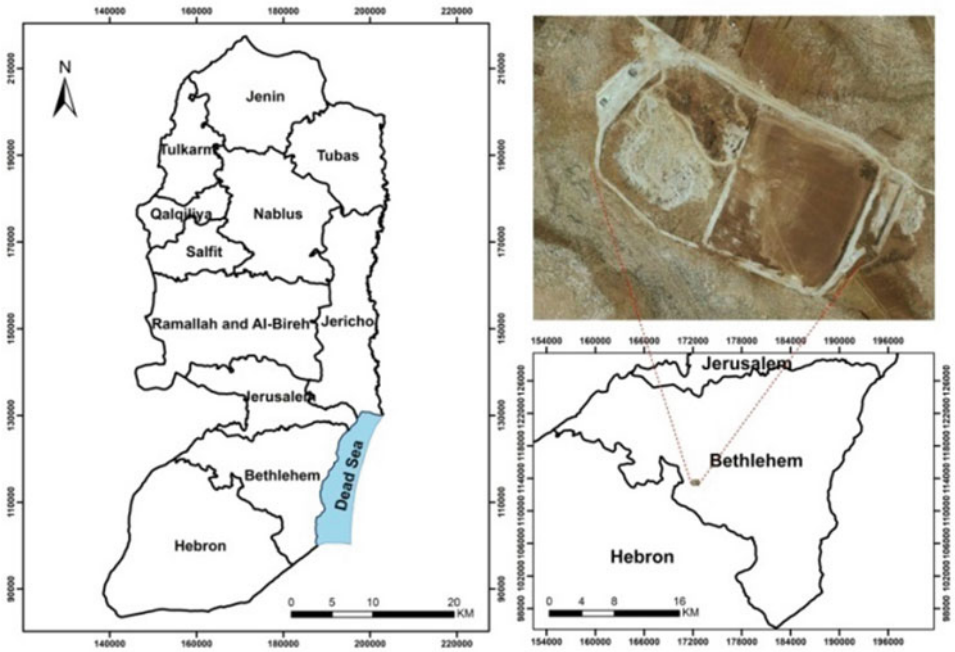

Fig. 1 Location map of the study area

and each successive refraction line overlapped with the previous one by two geophone positions. The survey type used was the reversed profile; it consists of two shot points at the extreme ends of the spread geophone and one in the middle. The recording system used for carrying out the survey was the 24 channels Smart Seis Exploration seismograph model S/N 70253. The system is equipped with 28 Hz natural frequency detectors each of which consists of an amplifier and a filter. A sledge hammer (12 kg) was used to generate seismic signals, where they are fed into a recording unit after selecting the suitable amplification and filtering the undesirable frequencies.

3 Results

The seismic refraction survey is an important geophysical technique used in the investigation of the subsurface characteristics based on the interpretation of the first arrival time of the P-waves. In the present study, the seismic refraction data were analyzed and interpreted using the modeling and the interactive ray techniques. The travel time-distance curves and the corresponding ground models for the P-waves were obtained beneath the seismic profiles. Velocity values determined from the shots were indicative of three-layer case (Fig. 2). Using classification of seismic velocity values of friable soil [7], two main velocity zones were defined: low velocity values of the first two layers between 192 and 1085 m/s, representing the unconsolidated materials, and a refractor, with an irregular interface moderately high seismic velocities of the fresh bedrock, varying between 1100 and 2400 m/s.

4 Discussion

The analysis of the seismic data from the conducted profiles indicated that the thickness of the unconsolidated materials increased towards the east, where the rocks crop out in the western part of the study area (Fig. 2). Seismic velocities ranged from 192–1085 m/s corresponding to the surface layers, and from 1100 to 2400 m/s in the bedrock, which is in agreement with the geology in the study area [6]. Adopting Kilty et al. [8], the bedrock in this study, characterized by higher velocity values, is interpreted as consolidated carbonate materials of limestone, chalky limestone and dolomite. The low velocity material represents the first and the second layer. The surface layer is interpreted as unconsolidated weathered material consisting of alluvium with poorly sorted gravels with a depth that ranged from 0.3 to 2.1 m, whereas the second layer is explained as chalk and marly sediment material and reaches a maximum of 13 m. The changes of the seismic velocities in the third layer, the bedrock, could be attributed to differences in the degree of weathering and fracturing.

5 Conclusion

The results of the seismic refraction surveys conducted over the proposed landfill site in Al Minya basin showed that the velocity zones within the investigated sections were found to be compatible with the changes in the lithology of the study area, and the general characteristics of the materials seem

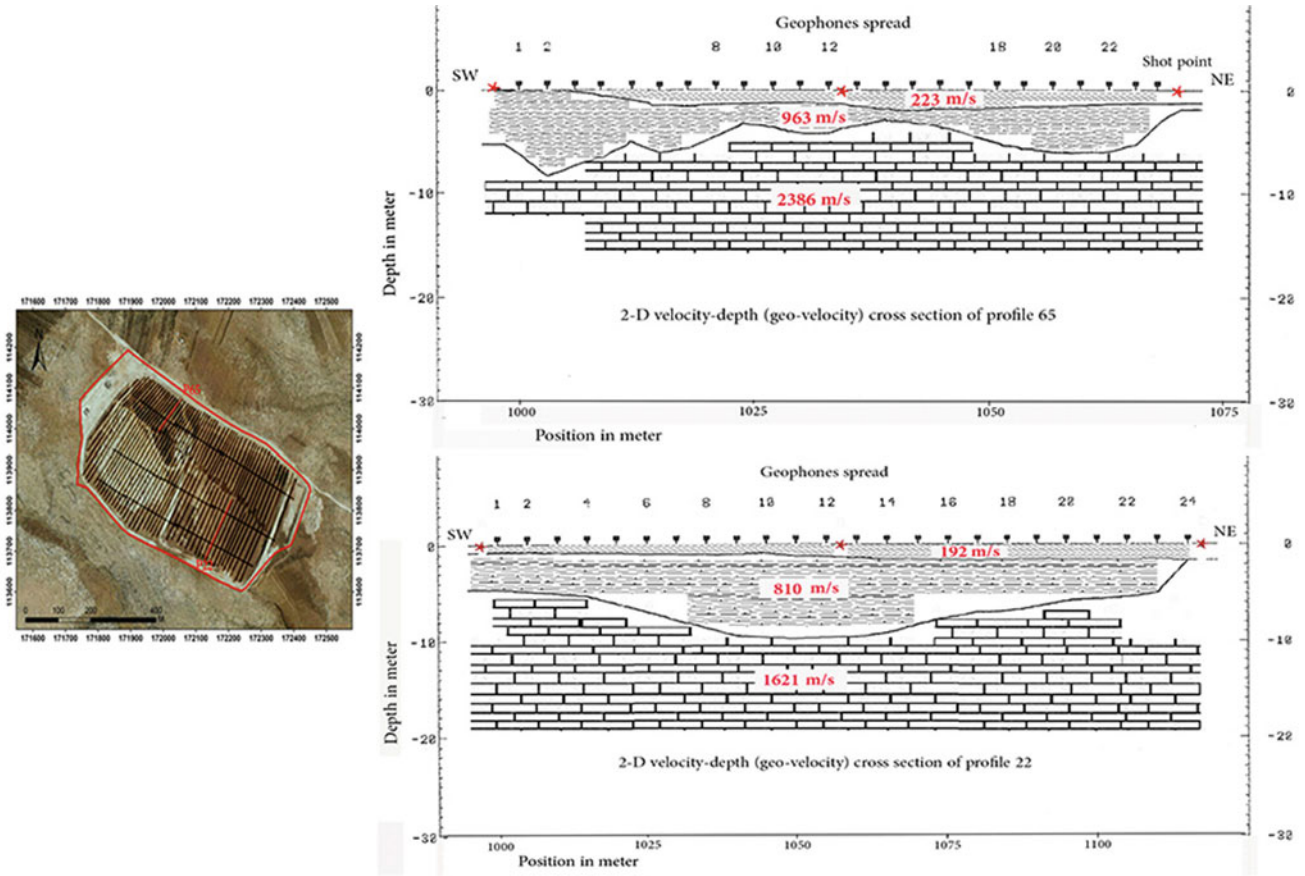

Fig. 2 Location map of the seismic refraction traverse lines, also shown 2-D velocity depth sections of profiles P22 and P65

suitable for a landfill. The geo-velocity sections generated for the seismic profiles show velocity values of 192 to 1085 m/s related to overburden materials. The overburden is underlain by a moderate velocity layer with values varying between 1100 and 2400 m/s, characterized by slight fracturing with possibilities for seepage. However, the landfill site underlain by an aquitard layer of marl and clay will naturally attenuate the leachate infiltration. In addition, the thick layer of clay soil cover, at the landfill site can be excavated and also used during the daily operation as lining material between wastes in landfill cells.

References

1. Bell, F.: Geological Hazards, Their assessment, Avoidance and Mitigation, 1st edn. E & FN Spon, London (1999)
2. El-Kelani, R., Shadeed, S., Hasan, A., Hasan, A., Ghodieh, A., Burqan, M.: Geospatial implications assessment of Zahrat Al Finjan solid waste landfill, North of West Bank, Palestine, IUG. J. Nat. Stud **25**(2), 1–9 (2017)
3. Al-Khatib, I., Arafat, H., Basheer, T.H., Shawahneh, H., Salahat, A., Eid, J., Ali, W.: Trends and problems of solid waste management in developing countries: a case study in seven Palestinian districts. Waste Manag **27**, 1910–1919 (2007)
4. Abdullahi1, N., Osazuwa, I., Sule, P., Onugba, A.: Geophysical assessment of an active open dump site in basement complex of Northwestern Nigeria. Int. J. Eng. Sci. Invention **2**(5), 12–21 (2013)
5. Berisa, G., Birhanu, Y.: Municipal solid waste disposal site selection of Jigjiga town using GIS sand remote sensing technique. Int. J. Sci. Res. Publ. **3**, 1–17 (2015)
6. Abed, A., Wishahi, S.: Geology of palestine: the West Bank Gaza Strip, Palestine, 1st edn. Palestine Hydrology Group (PHG), Ramallah (1999)
7. Palmer, D.: Measurement of rock fabric in shallow refraction seismology. Explor. Geophys. **51**(2), 266–257 (2001)
8. Kilty, K.T., Norris, R.A., McLamore, W.R., Hennon, K.P., Euge, K.: Seismic refraction at Horse Mesa Dam: an application of the generalized reciprocal method. Geophysics **51**(2), 266–275 (1986)

Application of Seismic Refraction Tomography to Map Bedrock: A Case Study from Al-Amrat, Oman

Mohammed Farfour and Talal Al-Hosni

Abstract

In this study, a seismic refraction survey was conducted to map the topography of bedrock in Al-Amrat, North of Sultanate of Oman. The targeted rock lies beneath unconsolidated rocks. A number of seismic profiles in the area were acquired, analyzed, and interpreted. The tomographic inversion of the data produced high resolution velocity models that contributed to understand the formations of interest. The formations are found to be characterized by variation in thickness and velocity which indicates variation in lithology and consolidation. The velocity sections were then used to build 3-D depth map that helped to understand the distribution of porous and permeable formations responsible for charging a water-producing well in the area. To support our interpretation, the data were calibrated with the exposed rocks in the survey area and showed good correlation.

Keywords

Seismic refraction • Bedrock • Tomography

1 Introduction

Seismic refraction methods are based on Snell's law, which governs the refraction of propagating waves across the boundary between layers of different physical properties. Once these waves at surface are recorded, they can be used to derive the properties of the rock along which they have traveled. The list of properties are, velocities of the rock, its depth, thickness etc.

Recent advances in seismic equipment, software packages, and interpretation techniques have led seismic refraction methods to be an effective and economical tool for numerous hydrological applications, engineering operations, in addition to mineral and petroleum exploration. The simplicity of the methods and their applicability in different environments have played key roles in their popularity. In literature, an increasing number of published papers such as: Avalos et al. [1], Zhao and Xu [2] and Osazuwa and Chinedu [3] among many others, have demonstrated the success of refraction tomography in characterizing near surface formations.

In this study, seismic data were acquired from 8 profiles crossing a dry valley in Al-Amrat, north of Sultanate of Oman. The main objective of the survey was to map the surface of the refracting bed rock and overlying unconsolidated rocks which allow ground water to charge a well in the area.

2 Methods

The survey was designed to image the depth of the bedrock surface. It consists of 8 lines with twenty four 4.5 Hz geophones. The geophones were spaced at 3 m intervals and planted for optimum physical contact with the ground. The lines were distributed on the area to ensure a good coverage of the area around the well. For calibration purposes, some lines crossed the bedrock which was exposed on surface. The well is located in the southern part of the survey area as displayed in Fig. 1. For each line, 5 shots were recorded. The data were then loaded to a software and prepared for inversion by correcting the geometry and picking first arrivals for all the shots. Tomography would allow lateral velocity variations and vertical gradients to be imaged, as opposed to most conventional refraction interpretation methods, which produce constant velocity layers.

3 Results and Discussion

First arrival times for the lines were used to build an initial model for the tomographic inversion. In this type of inversion, the final model depends heavily on the characteristics of the

M. Farfour (✉) · T. Al-Hosni
Earth Science Department, Sultan Qaboos University, Muscat, Oman
e-mail: m84.farfou@gmail.com

N. Sundararajan et al. (eds.), *On Significant Applications of Geophysical Methods*,
Advances in Science, Technology & Innovation, https://doi.org/10.1007/978-3-030-01656-2_23

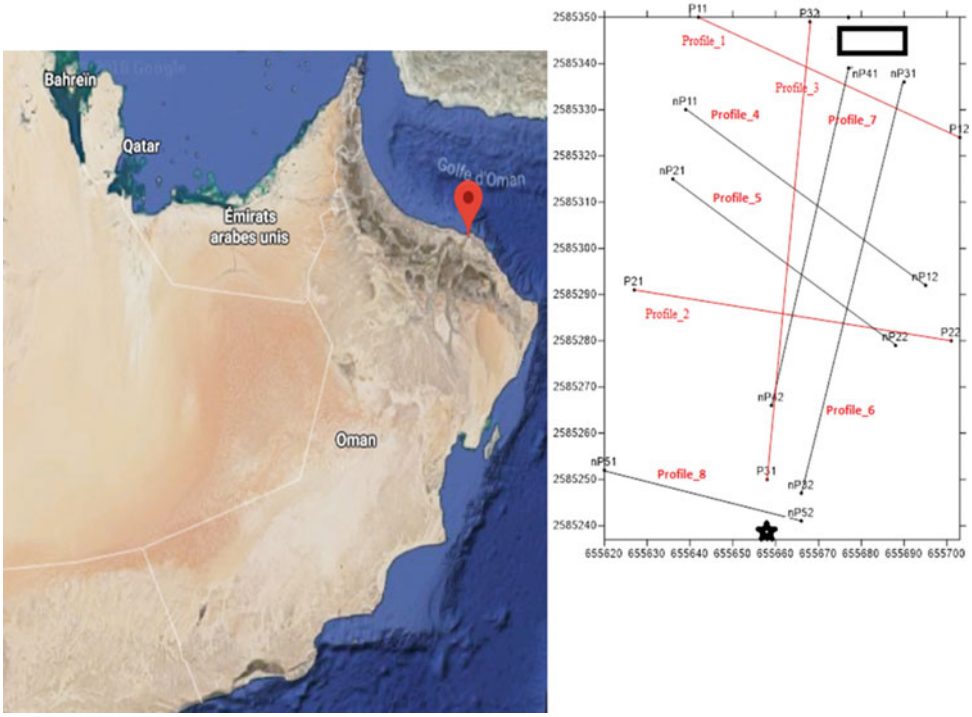

Fig. 1 Map showing the location of the study area and survey map showing the profiles location and orientations. The red lines have been recorded first then the black lines next. The black rectangle is porous and permeable zone. The star depicts the well location

initial velocity model. After several tests, a velocity model was obtained for each line. The observation of inverted sections revealed that the hard basement rock and the overlying formations both vary in velocity and thickness. The variation in velocity can be associated with the degree of consolidation of these sediments, their porosity and permeability. In fact, the low velocity is an indication of low consolidation, high porosity and permeability while high velocity indicates high consolidated and less porous material. Line 1, for example, shows a very clear depression in a form of low velocity trend that appears in other lines that have been shot in the same direction (Figs. 2 and 3). This indicated the presence of low

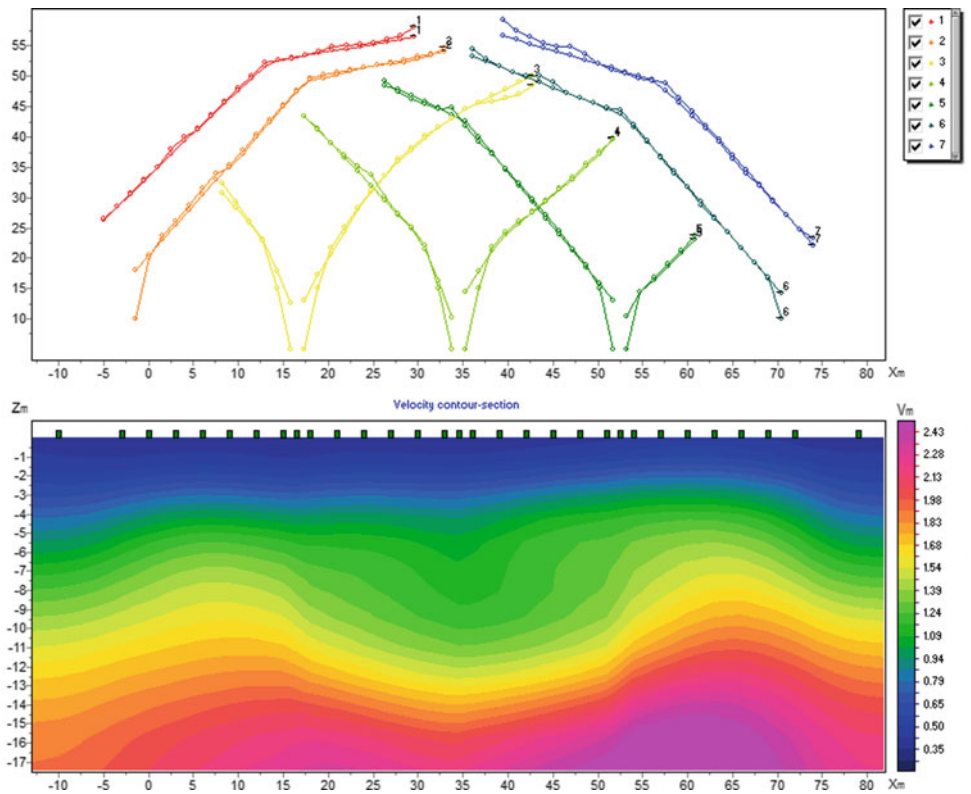

Fig. 2 The travel-time and the velocity model obtained from the inversion of profile 2. Velocities are in km/s

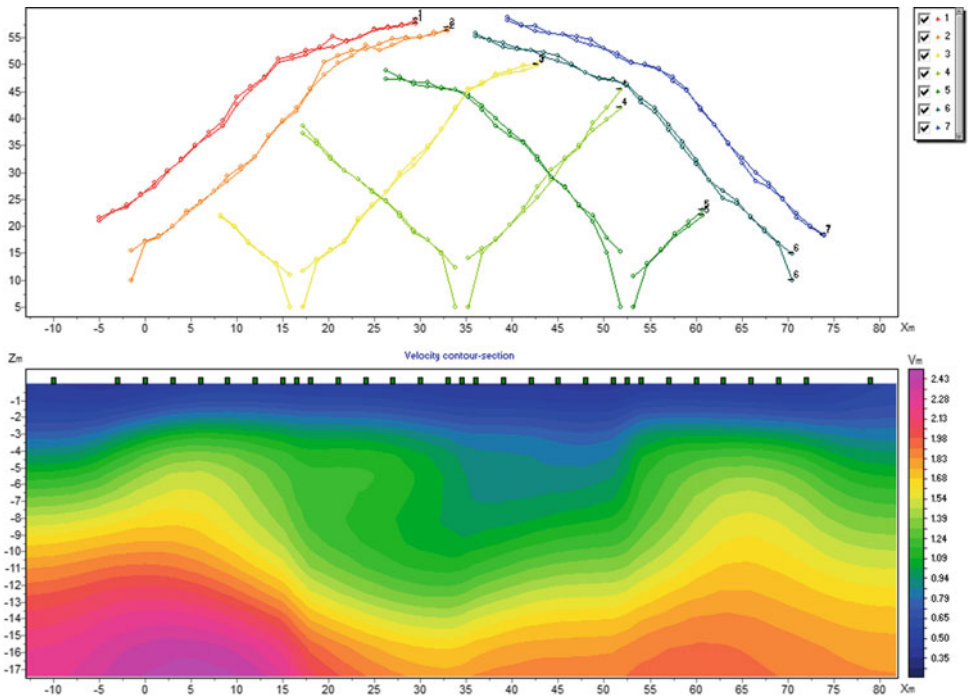

Fig. 3 The travel-time and the velocity model obtained from the inversion of profile 3. Velocities are in km/s. Note that a similar velocity trend to that of profile 2 is oberved in the model from profile 3

consolidated like-channel structure that possibly allows the water to pass to the well.

At later stage, the 2-D velocity models derived from tomographic inversion were used to produce a 3-D map of the targeted bed. The resulting map is displayed in Fig. 4. The map provided another reliable interpretation of the target. As the bedrock was exposed on surface, this has allowed us to calibrate the obtained images with the real geology.

Note that several tests were conducted to evaluate the accuracy of the above tomographic models. This includes solution robustness and stability in addition to the direct comparison with geology and exposed formations.

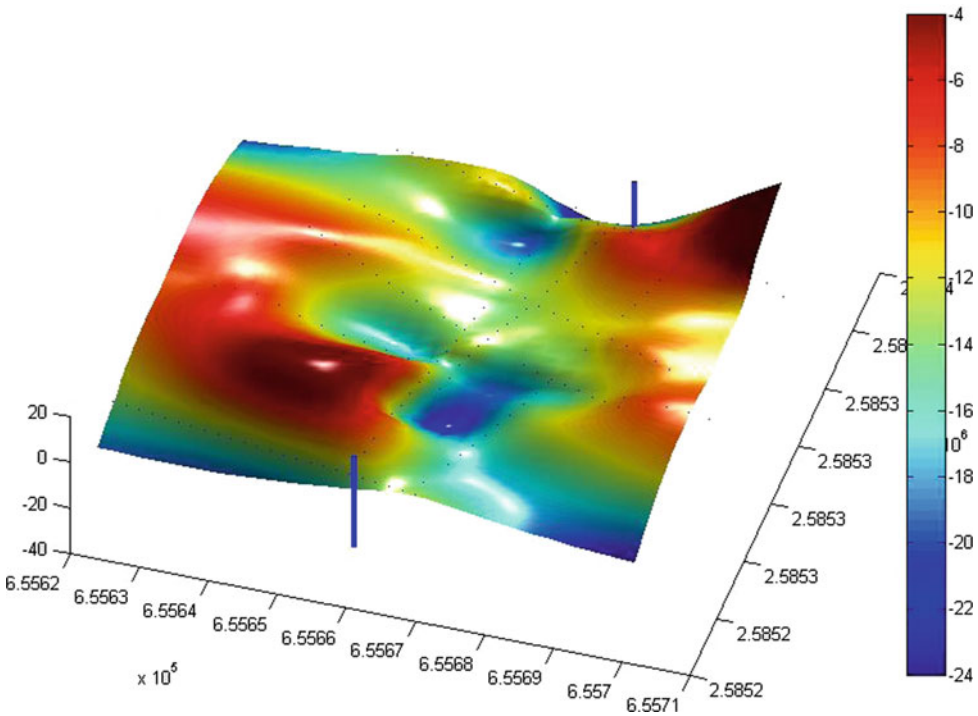

Fig. 4 3-D map view of the targeted bedrock. The upper and lower blue lines show the porous permeable zone and the well location respectively

4 Conclusion

Seismic refraction tomography was applied to map the topography of consolidated rock and overlying zones in Al-Amrat, Sultanate of Oman. The consolidated rock was characterized by high velocity and thickness variation. The overlying layers showed low velocity trend that was observed in different lines and interpreted to be porous channel that might be responsible for the water passage to charge water-well in the area. The 3-D map obtained from the velocity sections calibrated with the exposed formations on surface have provided more support to our interpretation.

References

1. Avalos, E., Malone, D., Peterson, E., Anderson, W., Gehreles, W.: Two dimensional seismic refraction tomography of a buried bedrock valley at Hallsands beach, Devon, United Kingdom. Environ. Geosci. **23**, 179–193 (2016)
2. Zhao, Z., Xu, J.: Geological structure investigation of shallow layers by the explosion seismic survey tomographic technique. J. Environ. Eng. Geophys. **15**(1), 21–28 (2010)
3. Osazuwa, I.B., Chinedu, A.D.: Seismic refraction tomography imaging of high permeability zones beneath an earthen dam, in Zaria area, Nigeria. J. Appl. Geophys. **66**, 44–58 (2008)

Q Factor Estimation and Validation: A New Link Between VSP and Seismic Lines

Jean-Luc Mari and Béatrice Yven

Abstract

In this paper, a new approach to estimate Q factor of geological formations on seismic lines was proposed. The purpose was to evaluate the amplification of ground motion on a site dedicated to store radioactive waste. Attenuation introduced dissipative dispersion which could be measured from the frequency-dependent phase velocity of the VSP down-going wave. The variation of velocity ΔV due to the variation of frequency was estimated from a residual variation $d\Delta t$ of the arrival times of the down-going wave. A scan procedure in $d\Delta t$ has been implemented to estimate the quantity ΔV and the Q factor, the search being done in realistic domain of Q values. The methodology was checked on VSP and then extended from well data to surface seismic data, using a predictive law with uncertainties estimations. The methodology was applied to estimate Q factors of the Callovo-Oxfordian claystone (host rock) and limestone formations, using both VSP and seismic lines.

Keywords

Q factor • Velocity • Dispersion • Instantaneous frequency • Elastic inversion • Velocity model • Depth conversion • Claystone • Limestone

1 Introduction

In the framework of Cigéo, a French project dedicated to store high-level and intermediate-level long-lived radioactive waste in a reversible deep geological repository, Andra (French national radioactive waste management agency) has conducted an extensive characterization of the claystone and limestone formations in eastern Paris Basin. In 2010, a 3D reflection seismic survey was recorded in a zone of interest for deeper research called ZIRA (30 km^2). Additionally to the 3D seismic work, drilling and geophysical borehole measurements including Vertical seismic profiles (VSP) and up-hole investigations were performed in order to calibrate the 3D seismic blocks, perform the time to depth conversion and evaluate the Q factor of the formations. The paper shows how the methodology developed to estimate the Q factor per layer [1] was validated on VSP data sets, and extended to estimate the Q factor on seismic lines.

2 Method

A number of discussions has always existed in the literature that use different approaches leading to a general form for the frequency dependence of the phase velocity, a synthesis was carried out by Varela [2]. The resulting expression, which is valid for a relatively large and constant Q, is given by:

$$V(f_1)/V(f_2) = 1 + (1/\pi Q) \cdot Ln(f_1/f_2) \qquad (1)$$

where Q is the constant Q factor, $V(f_1)$ is the propagation velocity at frequency f_1, $V(f_2)$ is the propagation velocity at frequency f_2.

Equation 1 can be written as follows:

$$Q = (1/\pi) \cdot (V/\Delta V) \cdot Ln(f_1/f_2) \qquad (2)$$

where $\Delta V = V(f_1) - V(f_2) = \Delta z/\Delta t - \Delta z/(\Delta t + d\Delta t)$ and $V = \Delta z/(\Delta t + d\Delta t) = V(f_2)$.

J.-L. Mari (✉)
IFP Energies Nouvelles, Rueil Malmaison, France
e-mail: jean-luc.mari@ifpen.fr

B. Yven
Andra, Châtenay-Malabry, France

N. Sundararajan et al. (eds.), *On Significant Applications of Geophysical Methods*,
Advances in Science, Technology & Innovation, https://doi.org/10.1007/978-3-030-01656-2_24

The procedure was successfully used on VSP data [1]. Q was computed from Eq. 2. For 2 geophone positions (Δz apart), ΔV was estimated from the variation Δt of the arrival times of the downgoing wave over a distance Δz and from $d\Delta t$ the residual variation of Δt due to the variation of frequency between f_1 and f_2.

3 Results

Figure 1 (top left) shows the VSP recorded in well Est 433. The first step in the processing was the wave separation. The downgoing waves, shown Fig. 1 (top right), were used to measure both velocity and frequency logs versus depth. The down-going waves were filtered in a low frequency band (8–28 Hz). A scan procedure in $d\Delta t$, equivalent to a velocity scan, was implemented to estimate the quantity ΔV and the Q factor (Eq. 2), the search being done in realistic domain of Q values, as example between 20 and 100. If the f_1/f_2 ratio is close to a constant, the $V/\Delta V$ ratio is a linear function of Q (Fig. 1, bottom left). Figure 1(bottom left) shows from top to bottom: the $V/\Delta V$ curve for an f_1/f_2 ratio of 3.5; the $d\Delta t$, ΔV and $V/\Delta V$ curves versus the level of the borehole geophone. Figure 1 (bottom right) shows the computed Q factor log. Q values vary between 33 and 96. Due to standard deviation low values of the ΔV curve (4 m/s) and of the f_2 frequency curve (2 Hz), the Q factors can be predicted using constant values for ΔV and f_2.The predicted Q-factor curve is shown in Fig. 1 (bottom right) with a relative uncertainty of 10% in average. The result was validated on a second well Est 412 (Fig. 2, top), the predicted Q values being estimated from the law defined at well Est 433. The uncertainties between the 2 Q-logs were weak, ranging between 0.5 and 30%. Consequently, the predicted Q log can be applied to surface seismic data if interval velocities $V(f_1)$ and instantaneous frequencies f_1 are measured.

Figure 2 (Bottom left) shows the Pre Stack Time Migrated section. The PSTM section was transformed in an instantaneous frequency f_1 seismic section, using the analytic signal. A model-based elastic inversion applied to the angle migrated stacks, provides impedance sections (*Ip* and *Is* sections) and *Vp* sections after calibration on logging data (sonic and density logs) Mari and Yven [3] showed that a single *Ip to Vp* relationship could be used whatever the range of acoustic impedance and whatever the geological unit to obtain a high resolution velocity model *Vp* in time which was integrated in time to obtain a time-depth conversion model [3].

The predicted Q section in depth (Fig. 2, bottom right) was computed using Eq. 2 with constant values for ΔV and f_2. The Q factor of the Cox formation (650–850 m) varies between 35 and 50 while the Q factors of the Oxfordian and Dogger limestone directly located above and below were higher, ranging between 65 and 100. The difference in depth between the VSP and the seismic line was due to the change of datum plane (ground level for the VSP and seismic datum plane for the seismic line).

4 Conclusion

Q factor of geological formations can be obtained from VSP data. We used the fact that attenuation introduced dissipative dispersion which could be measured from the frequency-dependent phase velocity of the VSP down-going wave. The methodology was validated, using 2 VSP data sets. The two VSPs were processed independently in order to obtain two Q-logs. One of the VSPs was used as a reference to define the law for Q-prediction. The comparison between the measured Q-log and the predicted one at the second well shows a very good fit between the 2 logs, with a relative uncertainty ($\Delta Q/Q$) smaller than 12% in average. Consequently, the procedure was then extended from well data to surface seismic data.

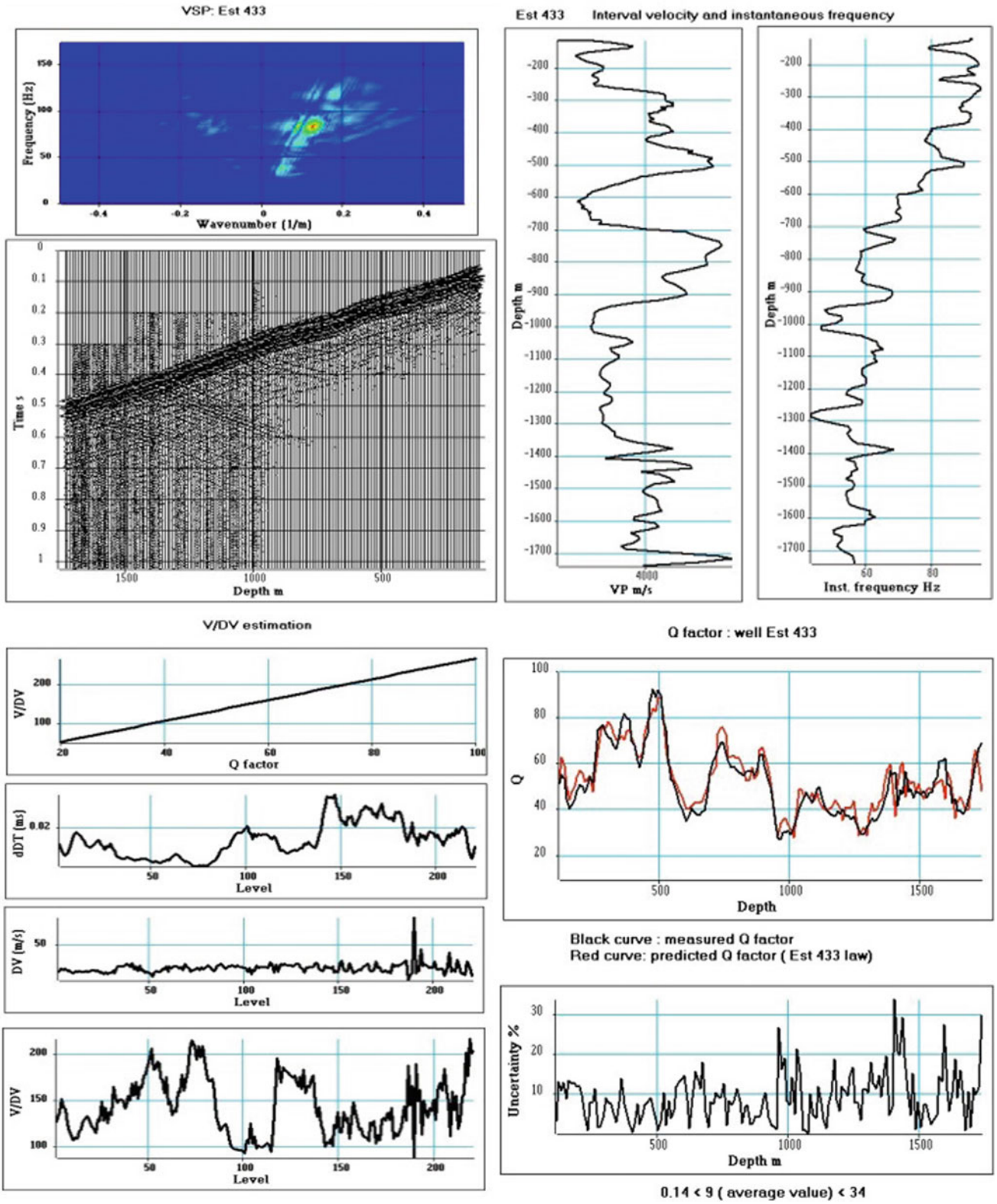

Fig. 1 VSP and Q factor. Top left: VSP and its associated *f-k* diagram; Top right: Velocity ($V(f_1)$) and frequency (f_1) logs. Bottom left: $V/\Delta V$ estimation: Bottom right: Q factors (measured, predicted) and uncertainties

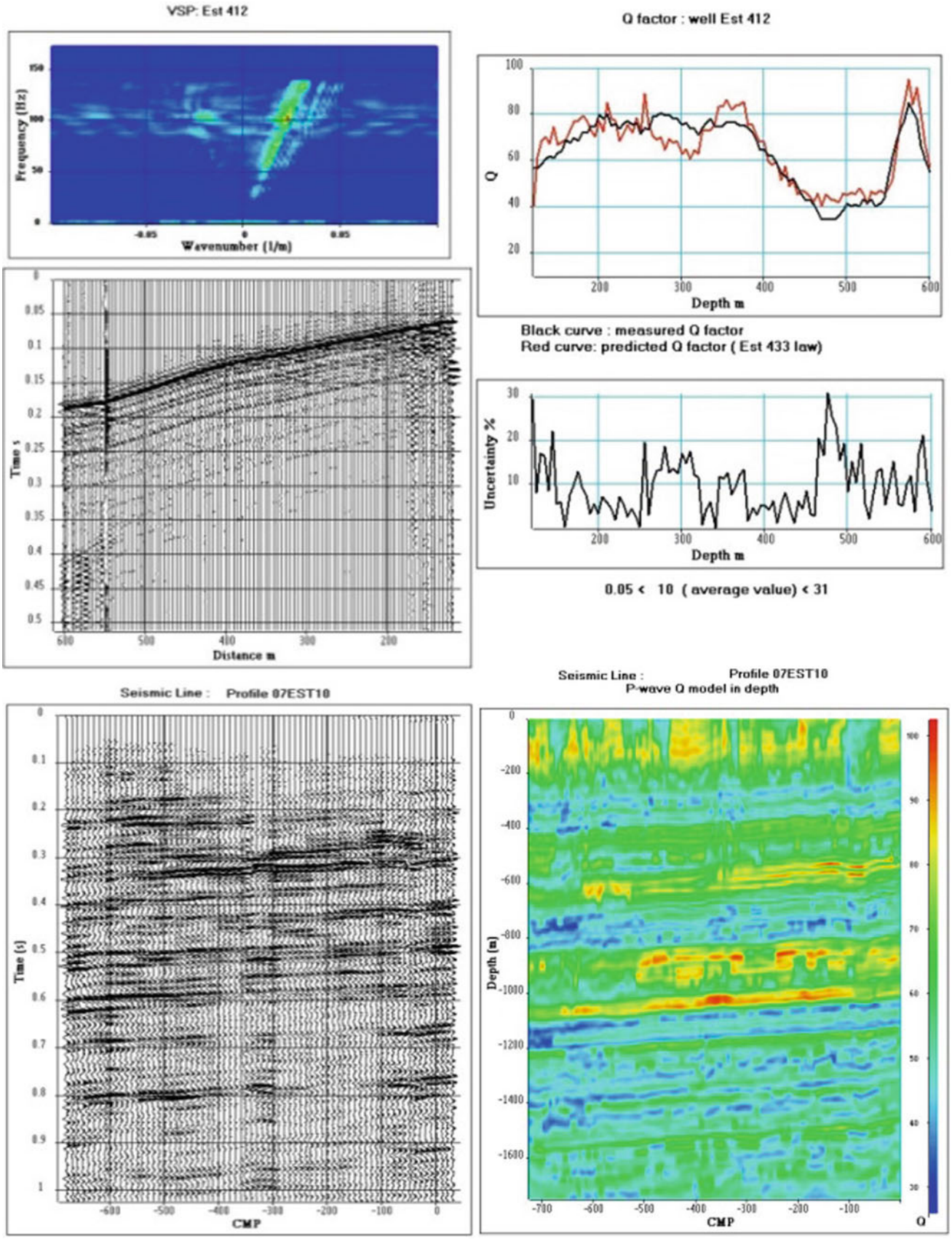

Fig. 2 Q factors from VSP and seismic line. Top: VSP and Q factor with uncertainties. Bottom: Time migrated section and Q factor section in depth

References

1. Mari, J.L., Yven, B.: Q factor: from VSP to seismic line, We P1 08. In: 79th EAGE Conference, Paris, 13–15 June 2017
2. Varela, C.L., Rosa, A.L.R., Ulrych, T.J.: Modeling of attenuation and dispersion. Geophysics **58**(8), 1167–1173 (1993)
3. Mari, J.L., Yven, B.: The application of high resolution 3D seismic data to model the distribution of mechanical and hydrogeological properties of a potential host rock for the deep storage of radioactive waste in France. Mar. Pet. Geol. **53**, 133–153 (2014). https://doi.org/10.1016/j.marpetgeo.2013.10.014

Young's Modulus: From Core and Logging to Seismic Lines

Béatrice Yven and Jean-Luc Mari

Abstract

To prepare the construction and operation of a deep geological disposal facility, the mechanical behaviour of the rock formations has to be well known. One of the studied parameters is the Young's modulus. A workflow has been developed to estimate static Young's moduli in claystone and limestone formations on seismic lines. First, the dynamic Young's moduli have been obtained by elastic inversion of the seismic data after calibration on well data. Then static Young's moduli have been estimated from dynamic Young's moduli using core and logging data. Finally, the procedure has been extended to evaluate static from dynamic moduli on seismic lines. This procedure can be generalized to all the seismic lines of the 3D seismic cube. The spatial variability of the elastic moduli can now be studied at high resolution and on the entire area dedicated to build a repository for radioactive waste.

Keywords

Young's modulus • Static moduli • Dynamic moduli
Elastic inversion claystone • Limestone

1 Introduction

Cigeo is the French high-level (HL) and intermediate-level long-lived (IL-LL) nuclear waste reversible storage project in the Callovo-Oxfordian clay formation. The investigated area is located at the eastern part of the Paris basin and has been extensively studied by the French national radioactive waste management agency (Andra) for the past 25 years.

From 1994 to 2008, forty-four wells were drilled from 400 up to 2000 m in depth, and 200 km of 2D seismics were acquired. In 2000, following a 3D seismic survey (4 km^2), Andra started to build the Meuse/Haute-Marne Underground Research Laboratory (URL) at Bure in the argillaceous layer where more than 30 experiments were carried out. Even though the boreholes help to characterize the geological, hydro-geological, geochemical, structural and mechanical properties of the host rock, the URL is necessary to analyze and understand the hydro-mechanical (HM) behavior of the rock to different drift excavation and construction methods and to test and optimize repository concepts at full scale on site.

In 2010, a zone of interest for detailed survey located a few kilometres from the URL, was defined to host the underground facilities and a 3D seismic survey (40 km^2) was recorded to verify the geometry and properties of the clay formation and the underlying and overlying limestones formations. Additionally to the 3D seismic work, drilling and geophysical borehole measurements including Vertical seismic profiles (VSP) and up-hole investigations were performed in order to calibrate the 3D seismic blocks and perform the time to depth conversion.

This paper presents a methodology to estimate static mechanical moduli per layer on seismic lines. It is based on the result of a previous study dedicated to estimate density, velocity and dynamic mechanical parameters distributions from the 3D seismic data, core and logging data [1]. The main purpose of these parameters estimations was to analyze the spatial evolution of the key parameters in the entire 3D seismic block and demonstrate the suitability of the site to host the repository.

2 Method

The mechanical properties of Callovo-Oxfordian clay formation were characterized in the laboratory (deformation modulus, compressive strength, tensile strength, etc.) using

B. Yven (✉)
Andra, Châtenay-Malabry, France
e-mail: beatrice.yven@andra.fr

J.-L. Mari
IFP Energies nouvelles, Rueil Malmaison, France

N. Sundararajan et al. (eds.), *On Significant Applications of Geophysical Methods*,
Advances in Science, Technology & Innovation, https://doi.org/10.1007/978-3-030-01656-2_25

conventional triaxial or uniaxial compression tests. The samples that were significantly desaturated (Sr < 90%) or damaged have been eliminated from the analysis.

On the other hand, the dynamic Young's modulus was obtained by elastic inversion of the seismic data after calibration on well data (VSP and acoustic logs) [1].

A description of the methods for determining the relation between static and dynamic Young's moduli can be found in a number of standard texts. A synthesis was given by Eissa and Kazi [2]. In laboratory, it was shown that there is a possibility to predict the static modulus values E_S from dynamic values E_D. The appropriate function relating to the high correlation coefficient between measured and predicted static values is the linear function:

$$E_S = a\,E_D + b \tag{1}$$

However, Eissa and Kassi [2] have shown that the value of the static modulus of elasticity can be best predicted from the relationship:

$$\text{Log } 10\,(E_S) = a.\text{Log } 10\,(\rho\,E_D) + b \tag{2}$$

with ρ the density.

Equation 2 was used to compute the static Young's modulus using logging data (acoustic and density logs) and core data (static modulus obtained in laboratory). The coefficients a and b were evaluated to obtain an optimum fit between static modulus from core with predicted static modulus from logging data.

3 Results

Figure 1 (top left) shows the Pre Stack Time Migrated section. VSP and logging data were recorded in the well Est433 located near the CMP point 600. A model-based elastic inversion (a priori impedance model obtained from well data), applied to the angle migrated stacks, provided impedance sections (*Ip* and *Is* sections). In our field case, three angle migrated stacks were generated (0–14°, 14–28°, 28–42°) to perform the elastic inversion in order to compute *Ip* and *Is* sections. The procedure used to obtain a high resolution velocity model, was described in Mari and Yven [1].

The results have shown that the *Vp* log and the predicted P-wave velocity from the acoustic impedance log are strongly correlated (Fig. 1, top right). The correlation coefficient and the Taner-Kohler coefficients between the two velocity logs are very high (>0.98). A single law can be used whatever the range of acoustic impedance and whatever the geological unit to obtain a high resolution velocity model *Vp* in time. The *Vp*, *Ip* and *Is* sections can then be used to obtain density and shear velocity *Vs* sections and to compute the dynamic mechanical moduli. The velocity model *Vp* was integrated in time to obtain a time-depth conversion model. The time-depth conversion model was used to convert in depth any type of sections such as density or dynamic Young's modulus (Fig. 1, bottom).

An attempt to convert dynamic Young's modulus into static Young's modulus was achieved using Eq. 2. In this paper, only data coming from borehole EST433 located on the 2D seismic line 07EST10 was used. The obtained results after core calibration (measurements of static Young's modulus on core samples) are shown in Fig. 2. The Static to Dynamic Young's modulus ratio varied between 0.51 and 0.56. In the future, the relationship between static to dynamic will be analysed with other boreholes.

4 Conclusion

The example shows the benefit of combining elastic inversion of seismic data, acoustic logging and measurements of static Young's modulus on a core to obtain the distribution of static Young's modulus at a seismic scale. In the 3D seismic area, dynamic young moduli have already been estimated. In a future work, a similar procedure will allow to estimate static young moduli distribution in the host formation and to evaluate the variability of the mechanical

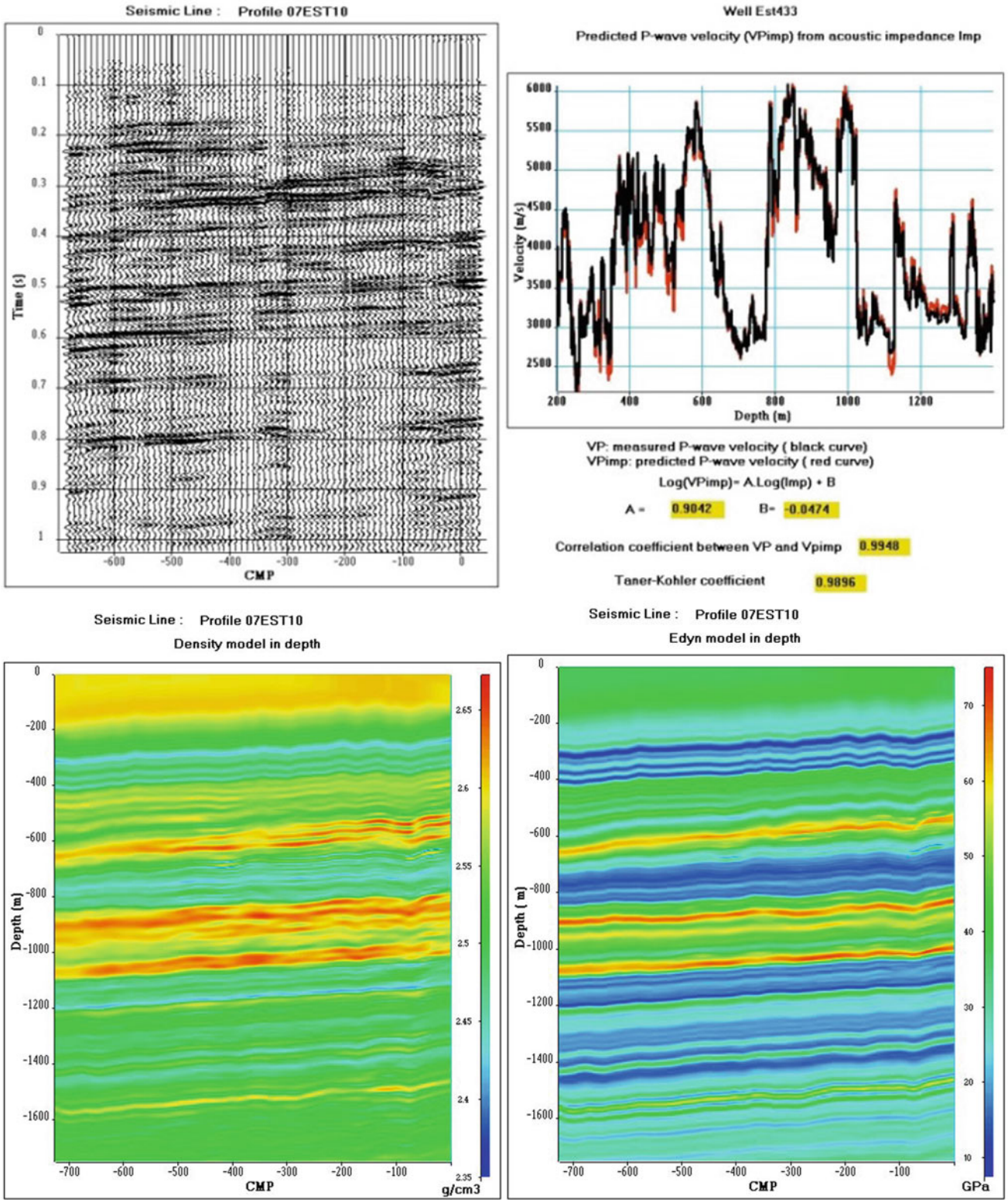

Fig. 1 Seismic line and mechanical moduli. Top left: migrated section; Top right: predicted P-wave velocity from acoustic impedance Ip. Bottom left: density model in depth; Bottom right: dynamic Young's modulus in depth

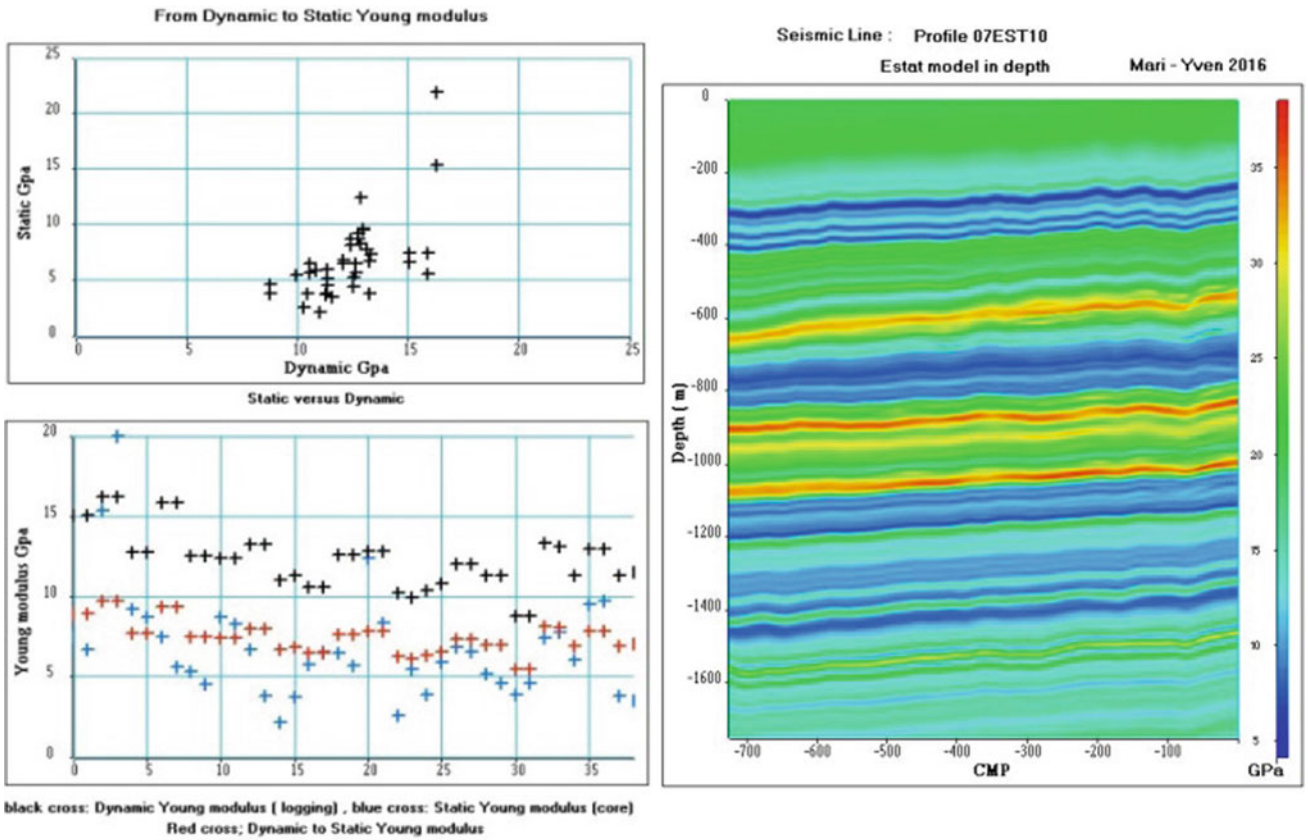

Fig. 2 From dynamic to static moduli. Left: dynamic to static moduli in the claystone formation (logging and core data). Right: static Young's modulus section in depth (seismic line: 07Est10)

parameters at the repository scale. This evaluation will help with the design of the underground nuclear waste disposal.

References

1. Mari, J.L., Yven, B.: The application of high resolution 3D seismic data to model the distribution of mechanical and hydrogeological properties of a potential host rock for the deep storage of radioactive waste in France. Mar. Petrol. Geol. **53**, 133–153 (2014)
2. Eissa, E.A., Kazi, A.: Relation between static and dynamic Young's moduli of, rocks. Int. J. Rock Mech. Min. Sci. Geomech. Abstr. **25**(6), 479–482 (1988)

Application of Varying Geometric Spreads in Seismic Refraction Studies to Characterize the Overburden Strata on the Flanks of Zaria Dam, Northwestern Nigeria

Ani Chinedu

Abstract

A geophysical investigation was carried out on the flanks of Zaria Dam using Seismic Refraction Tomography. The aim was to analyze the data provided to characterize the different strata of the subsurface within the overburden. To this end, varying geometric spreads were used with optimum geophone spacing of 5 m reduced to 4, 3 and 2 m successively for different traverses on the same profile line. Using the Tomographic inversion, it was possible to derive the picture of the subsurface layering mapped from the Tomograms despite the geologically complex environment. The results gave velocities of 1356, 2543 and 3743 m/s for the overburden, weathered basement and fresh basement, respectively. However, the depth of probe differed as the geophone spacing varied. In some profiles, the model suggested a sedimentary thickness of not less than 20 m overlying the basement. The results showed that as the geometric spread is reduced, the shallow structures within the overburden strata become enhanced. Hence, making it possible to recover hidden and undetected layers with such ranges of velocities as 778–998 m/s and 2197–2439 m/s in the overburden and weathered basement, respectively.

Keywords

Tomography • Overburden deposits • Varying geophone spacing • Hidden layers • Seismic refraction

1 Introduction

Zaria Dam is a zoned earth-fill embankment dam made from dissimilar compacted earth materials with a watertight clay core. The level of water in the reservoir plain is usually flooded to its crest during the rainy season (April to October) and partially dried during the dry season (November to March). This may be as a result of the presence of permeable zones that conduct suspected anomalous seepage within the dam subsurface. Excess sedimentation in the reservoir may also be considered amongst the factors contributing to water reduction in the dam reservoir [1–3].

However, a study was carried out by Chinedu and Osazuwa [4] and Osazuwa and Chinedu [5] at approximately latitude 11°00′00″ N to 11°08′25″ N and longitude 7°45′40″ E to 8°00′00″ E (Fig. 1), on the flanks of the Dam, whereby amongst the findings are loose and unconsolidated grounds mapped as depressions in the tomography models. The Seismic Refraction Tomography (SRT) investigation showed some characteristic responses to anomalous zones that may be responsible for the seasonal water loss in Zaria dam. The zones delineated by each profile agreed with each other, confirming that these anomalies are directly related to the weak zones that may be a contributory factor to the problems in the dam. The SRT images implied that anomalous seepage might be taking place in the internal part and thus contributes to making the dam seasonal. This raised a serious question that led to further investigations and characterizations of the overburden structures through this study. Meanwhile, this study was meant to provide tentative data using a single profile but with different take-outs of varying geophone spacing and lengths of spread. However, this was meant to further investigate and assess this threatening problem by using a technique that may enhance these features. It would assist in mapping weak and unconsolidated layers that may constitute hidden and blind zones within the study area.

2 Data Acquisition

The technique of varying geophone separations on the same profile enables the delineation of undulating refractor surfaces, the detection of lateral velocity variations in layers and most important, the recognition of hidden layers [6].

A. Chinedu (✉)
Department of Physics and Astronomy, University of Nigeria, Nsukka, Nigeria
e-mail: Bedrock969@yahoo.com

N. Sundararajan et al. (eds.), *On Significant Applications of Geophysical Methods*,
Advances in Science, Technology & Innovation, https://doi.org/10.1007/978-3-030-01656-2_26

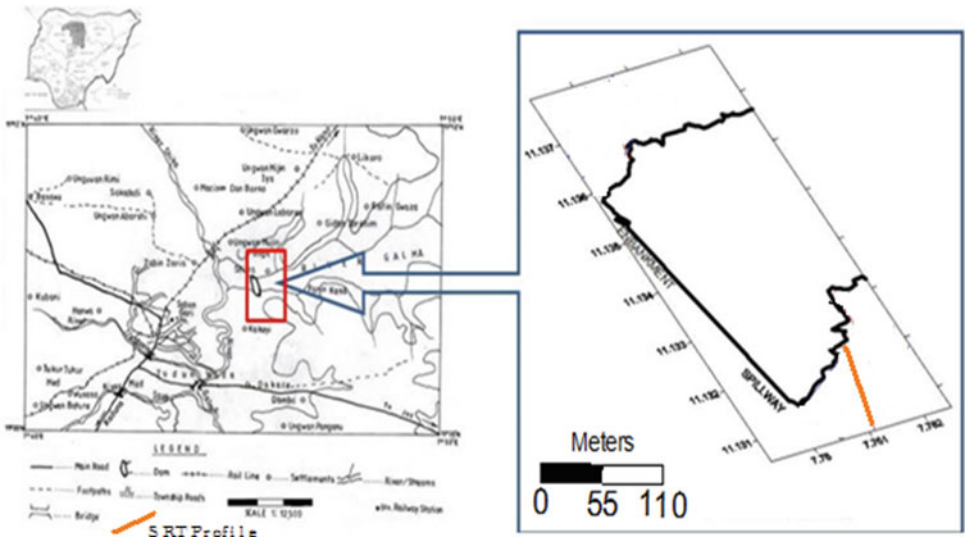

Fig. 1 Map showing the survey area with the profile line marked out in orange

Following this postulation, an in-line profile trending north–south direction was adopted (Fig. 1), with varying geometrical spreads and their respective geophone spacing of 5, 4, 3, and 2 m, (Table 1) for this study. This gave rise to having four (4) different take-out profiles within the main single profile and identified in this study as M_1, M_2, M_3 and M_4 respectively.

This direction of profile was adopted based on the reports of Chinedu and Osazuwa [4]. It is perpendicular to the dam axis. Having the same center of spread, each refraction investigation was conducted with 10 Hz vertical geophones connected to a 24-channel seismograph. Seismic energy was created by vertically striking a fortified rubber ground plate with an 89 N (20 lb) sledgehammer, thus producing compressional P-wave first arrivals.

3 Results

In this study, the results of the SRT inversion with their ray path and travel time curves confirm that all the P-wave arrivals originate from the main refractor.

Since these investigational profiles (M_1, M_2, M_3 and M_4) were run on the same profile (Table 1), it is very important to note that some of the features of interest in the tomograms may have been enhanced thus enlarging or thwarting the shape of the subsequent models. Due to the reduction of the geophones separation, most of the sub-surface features (Fig. 2) detected shifted according to the emplacement of the geophones. Convincingly, all layers were detected. However, the seismic refraction results were correlated with available borehole logs. More profiles will be shown in the main paper.

4 Discussion

Correlating the interpreted data with the borehole log, the overburden is dominantly Lateritic or clayey alluvium. The velocities range between 818 and 2419 m/s in M_3 and M_4. The obtained relative range of velocities of 1026–2717 m/s at the depth between 7 and 21 m confirms that the area contains granite pebbles with saturated clay in the weathered basement, while the fresh basement with higher velocity regimes lies below 20 and 30 m. The interpretation of data from M_2 revealed a lateritic outcrop under the geophones between 30 and 35 m, while other profile spreads detected the undulation at varying points due to different geophone spacing. This shows that the adopted technique using first arrivals is one possible way to derive a velocity model of the near surface under these conditions.

Table 1 Lengths of spread and geophone spacing for each traverse

Spreads with common center	Lengths of spread (m)	Geophones spacing (m)	Average velocities (ms^{-1})	Depth of probe (m)
M_1	120	5	1916	17
M_2	96	4	2359	16
M_3	72	3	1493	10
M_4	48	2	1505	2

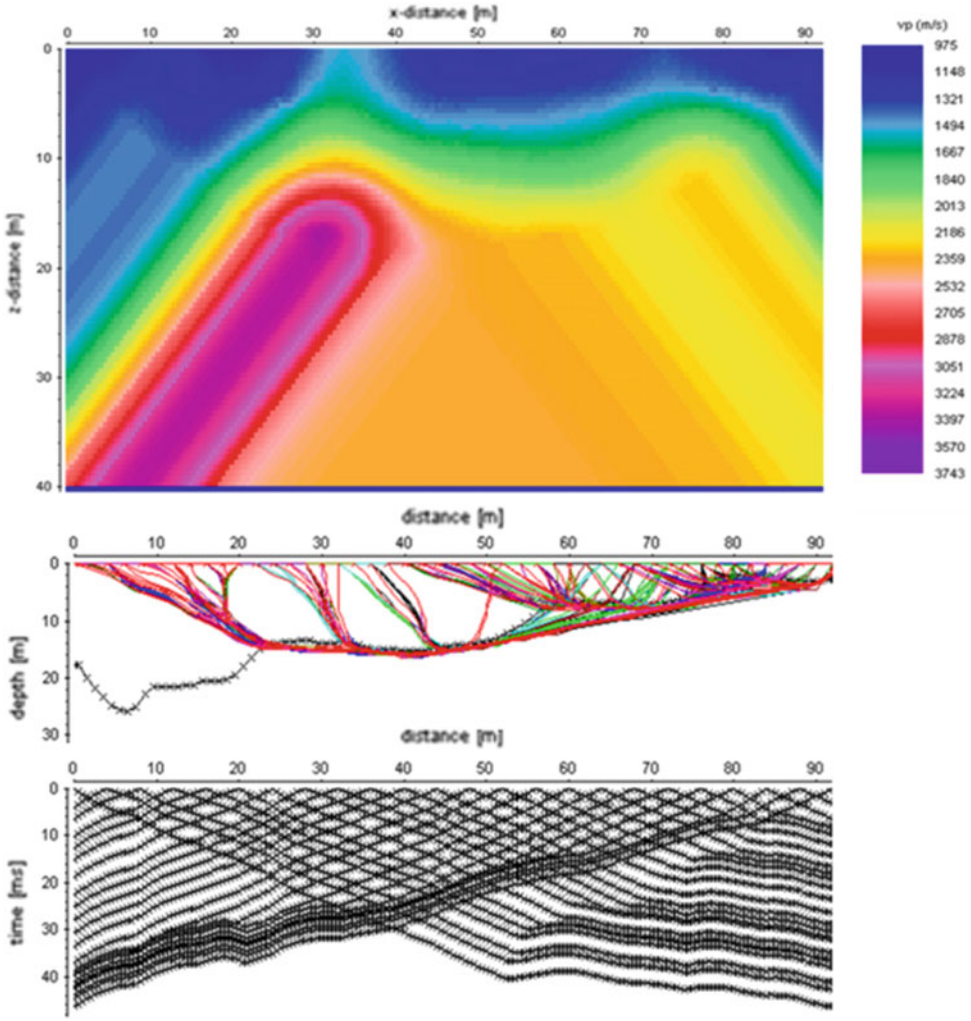

Fig. 2 Travel-time tomography section for profile M_2

5 Conclusion

This study has convincingly established that the area of study is of highly irregular subsurface, with substantial velocity variations within the overburden, weathered basement and refractor layers. It further confirms the existence of loose grounds and other forms of low velocity zones within the area in all the subsurface layers following the recovered range of average velocities in the overburden and the weathered basement respectively.

References

1. ICOLD (International Commission on Large Dams): World Register of Dams. Version updates 1998–2009. ICOLD, Paris. www.icold-cigb.net (2009)
2. Indiana Dam Safety Inspection Manual: Dam management and maintenance (Part 2). Division of Water, Department of Natural Resources, Indianapolis, Indiana (2007a)
3. Indiana Dam Safety Inspection Manual: Dam safety inspections (Part 3). Division of Water, Department of Natural Resources, Indianapolis, Indiana (2007b)
4. Chinedu, A.D., Osazuwa, I.B.: Generalized reciprocal method applied in processing seismic refraction data from the basement terrain of Zaria, North-Western Nigeria. Niger. J. Phys. **20**(2), 377–385 (2008)
5. Osazuwa, I.B., Chinedu, A.D.: Seismic refraction tomography imaging of high permeability zones beneath an earthen dam, in Zaria area, Nigeria. J. Appl. Geophys. **66**, 44–58 (2008)
6. Sumanovac, F., Weisser, M.: Evaluation of resistivity and seismic method for hydrogeological mapping in Karst terrains. J. Appl. Geophys. **47**, 13–28 (2001)

Part V

Integrated Geoscience Applications in the Exploration of Subsurface Resources

Contribution of Tomographic Imaging in the Study of the Tabellout Dam Site, Jijel (Northeast Algeria)

Mustapha Tekkouk, Riad Benzaid, Juan Martinez, and Chahra Yellas

Abstract

Whatever the nature and the location of dams, the problem of waterproofness of plates on the one hand and the continuous water leaks on the other hand, have always been one of the most important concerns of the designers. The geological studies and particularly the fracturing of the site of dam of Tabellout do not seem to have been well conducted. Indeed, the waterproofness risks to be compromised. In view of our statement on the spot of the fracturing of the way of being completed and the under surface one which will be deduced from the tomographic images, the geological study of the site of the dam were clearly valued. The present work was meant to draw attention to and raise awareness of the likely risks of water leaks that can jeopardize the global restraints.

Keywords

Fracturing • Seismic imaging • Electric imaging • Tabellout dam

1 Introduction

The village is situated in the surroundings of Texenna, in the Southeast of the city of Jijel, in the entrance of the steep gorges of Djebels Tabellout-Fortassa, on the course of the Wadi Djendjen where the construction of the compacted concrete dam rolled from Tabellout took place. From its appearance, and with regard to its geomorphological, and geological characteristics, the studied site here risks to create severe problems because of the fracturing of places. We intended from the topographic, geological, seismic tomography, electric imaging data and from the field measurements to establish a current situation of the fracturing of the dam site which was the main focus of our work.

2 Geology of Tabellout Site

The area highlighted in our study is a range of mountains belonging to the highlands of Texenna situated in the South-East of Jijel city (Northeast Algeria). Following the correlation between field observations and the information collected from the bibliography [1–3], Fig. 1 shows the various geological formations of the dam site. Besides the gypsy trias which appears in the right bank, the other geological formations which will be in direct contact with the water of the lake are represented in Fig. 2.

3 The Dam Site Fracturing

Figure 3 highlights the fracturing related mainly to the link Europe–Africa. Indeed, we have:

- The faults of carriage NW–SE (C1, C2) and faults of the same direction.
- The faults of direction NE–SW parallel to the big staggering dexter fault (GFD).
- The faults of direction NW–SE.

The geometry of the discontinuities, their extensions and the interconnection between them led to predict a very complex hydrodynamic situation at the level of the plate and the surrounding mountains and a overhanging over the future stretch of water.

M. Tekkouk (✉) · R. Benzaid · C. Yellas
Laboratoire de Génie Géologique (LGG), Université Mohammed Seddik Benyahia - Jijel, BP. 98 18000 Ouled Aissa, Jijel, Algeria
e-mail: tekkouk@yahoo.com

J. Martinez
Laboratoire de Génie Civil et Génie Mécanique (L.G.C.G.M.), INSA de Rennes, Rennes, France

N. Sundararajan et al. (eds.), *On Significant Applications of Geophysical Methods*,
Advances in Science, Technology & Innovation, https://doi.org/10.1007/978-3-030-01656-2_27

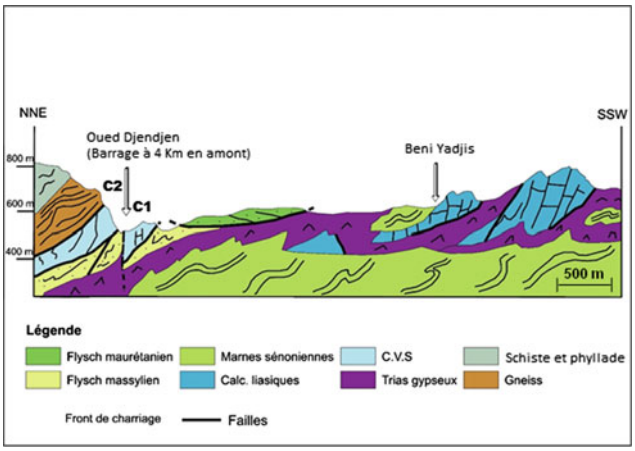

Fig. 1 Interpretative geological section of the Tabellout site

Fig. 2 The geological map of the study area

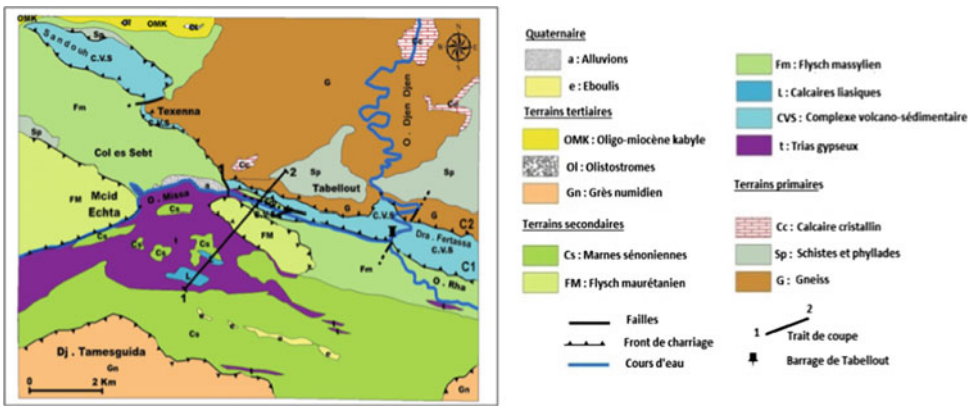

Fig. 3 Fracturing of the dam site

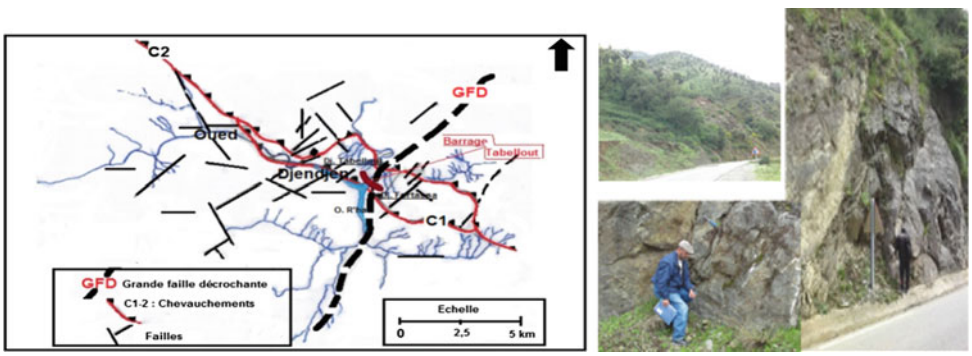

4 Geophysical Prospection

4.1 Equipment Used

Equipment used during the various campaigns are given in Fig. 4.

The seismic tomography and the electric imaging used here [5, 6] seemed perfectly adapted to the study of the fracturing and the risks of potential flights (leaks) which can turn out to be a serious threat to the lake of the dam.

4.2 At the Supports

Among the 24 profiles of seismic survey refraction (SR) of a total length of 3060 m, two (SR) were chosen as the present work. They are represented in Fig. 5a. The tomographic

Fig. 4 Seismographs

(a) Geode Geometricsn **(b)** Summit X Stream Pro (DMT) **(c)** résistivimètre Saris.

Fig. 5 **a** Setting-up of the seismic profiles, **b** tomographic images of dam supports [4, 5]

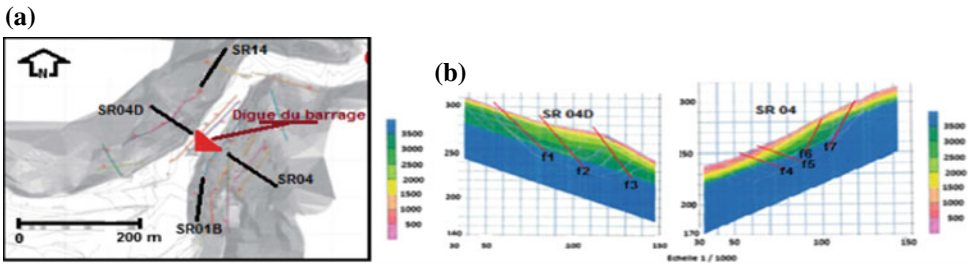

images show breaking lines (Fi) corresponding to oblique faults (Fig. 5b).

4.3 At the Plate

A geophysical study of 17 seismic profiles (PS) was conducted by a geophysical engineering consultancy [6] at the site of the viaduct of Tabellout (at present under construction).

4.3.1 Seismic Imaging

In the present work we displayed two seismic profiles (PS11 and PS14) among the 17 profiles made on the site (Fig. 6).

From the tomographic images presented in Fig. 5, we can remark that the major part of the network of faults of underground is filled with water infiltrated from the river and with alluvium.

4.3.2 Electric Imaging

Out of a total of 18 profiles of electric imaging achieved on the studied site [6], the electric profile 15 (PE15) was chosen for the present work and it is represented in Fig. 6. The tomographic image clearly let appear the fracturing of flyschs albo-aptiens. The breaking lines (Fi) corresponding to oblique faults (Fig. 7).

As it was checked by seismic survey refraction, the electric prospecting brought a more considerable support to the initial study made on the surface. Indeed it confirmed the state of fracturing of the dam site basement and clearly showed evidence that the waterproofness of the dam plate was vulnerable and that water leaks by infiltrations can actually well take place.

5 Conclusion

The geophysical methods applied to the site of the dam of Tabellout have come to complete our first work on the fracturing made during our various visits to the sites. Indeed, the geometry of the discontinuities, their extensions, their in-depth repercussions and the interconnections between them led to predict a very complex hydrodynamic situation at the dam site and the surrounding banks. Once

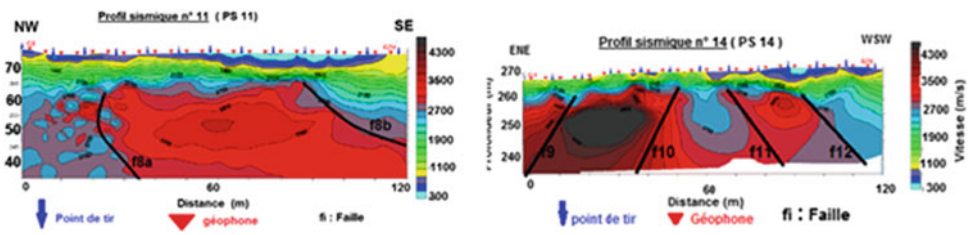

Fig. 6 Tomographic images of the basement of the viaduct crossing the plate of the dam [6]

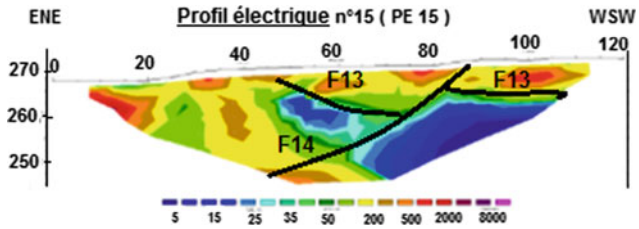

Fig. 7 Tomographic image of the dam plate

the impoundment is launched, the connection to the various scales of the different fault networks will give zones of high permeability which will be the preferred seats of future flow paths. Infiltrations or water leaks may appear which may be detrimental to the waterproofness of the dam foundation.

References

1. Bouillin, J.P., Kornprobst, J., Raoult, J.F.: Données préliminaires sur le complexe volcano-sédimentaire de Rekkada Metlétine (ex Texenna) en Petite Kabylie (Algérie). Bull. Soc. Géol. Fr. **XIX**(7), 805–813, fig. 2 (1977)
2. Bouillin, J.P.: Le "bassin maghrébin": une ancienne limite entre l'Europe et l'Afrique à l'Ouest des Alpes. Bull. Soc. Géol. Fr. (8), t. II.n°4, 547–558 (1986)
3. Durand Delga, M.: Note sur la structure géologique des environs de Texenna (Petite Kabylie- Algérie). Bull. Soc. Géol. Fr. **XIX**(5), 271–278 (1969)
4. RAZEL-CMC: Rapport géotechnique- Barrage de Tabellout, Jijel, Algérie (2010)
5. RBR: Etude géophysique par sismique réfraction sur le site de construction du barrage de Tabellout dans la région de Jijel, Algérie. Rapport final. RBR géophysics - SEA Consulting S.r.l. (2010)
6. Rapport de l'étude géophysique du Viaduc de Tabellout. Bureau d'engineering, études et équipements en géosciences "GeoExplo", 56 p, Alger, Oct 2015

Integrated Studies to Elucidate the Subsurface Structures and Groundwater at Moghra Oasis, Northwestern Desert, Egypt

Maha Abdelazeem, Sultan Araffa, Zenhom Salem, Mohamed Fathy, and Maha Saleh

Abstract

About 150 thousand Acres were restricted around Moghra Lake, north Western Desert of Egypt, and were irrigated mainly from groundwater. Geophysical and geological studies were integrated to assess the groundwater quality of the Miocene Moghra aquifer in the studied area. Stratigraphically, the Moghra Lake is cut into the clastic-dominated sediments of the Lower Miocene Moghra Formation. Subsurface petrophysical logs and surface facies analysis of sedimentary facies successions were treated separately and then integrated to investigate the sedimentary environments and stratigraphical sequence in the Moghra Formation. A land magnetic survey was conducted with 2 km station spacing to reveal the governing structures and the expected depth to basement. The reduced to pole map was subjected to various special filters to detect magnetic contacts in the area that may affect the flow of the water aquifer. Moreover, the results of four VES stations of AB/2 ranging from 1 to 500 m were implemented to delineate the upper surface of the aquifer. The chemical analyses of 20 water samples were used to investigate the groundwater suitability for irrigation purposes on the basis of standard guidelines and showed moderate suitability values.

Keywords

Moghra Lake • Land magnetic survey • Groundwater quality

1 Introduction

The Egyptian government is now very much interested in developing the northern part of the western desert both in agriculture and tourist aspects. One of the most promising areas is the area around Moghra Oasis located at the north-eastern corner of Qattara Depression was suggested for the purpose. Moghra Oasis is characterized by the presence of a large brackish water lake, which is around 4 km^2 in the area and surrounded by different desert plants and sand dunes.

2 Geologic Setting of Moghra Lake Area

The Moghra Formation includes the lowest and the oldest exposed rocks around Moghra Lake. It forms the floor of the depression and the basal part of the northern escarp. The base of the Moghra Formation is unexposed, but inferred to be at conformable contact with shales of the Oligocene Dabaa Formation and overlain by limestones of the middle-upper Miocene Marmarica Formation [1].

3 Methodology

The litho-facies, exposed in the northern part of the area, were studied in details. The magnetic data were processed to infer the faults affecting the aquifer. A total of twenty representative groundwater samples were analyzed to verify their suitability for irrigated agriculture. Moreover, eight VES's were measured to determine the top and borders of the aquifer and shallow structure [2]. Only four of them were inside our area.

M. Abdelazeem (✉) · S. Araffa
National Research Institute of Astronomy and Geophysics (NRIAG), Helwan, Cairo, Egypt
e-mail: maazeem03@hotmail.com

Z. Salem · M. Fathy
Geology Department, Faculty of Science, Tanta University, Tanta, Egypt

M. Saleh
Academy of Scientific Research and Technology, 101 El-Kasr El-Einy Street, Giza, Egypt

N. Sundararajan et al. (eds.), *On Significant Applications of Geophysical Methods*,
Advances in Science, Technology & Innovation, https://doi.org/10.1007/978-3-030-01656-2_28

4 Results

4.1 Stratigraphic Results

Repeatedly stacked cyclic deposits from channel-fill and flat-laminated lithofacies formed the surface and subsurface of Moghra aquifer. Highly vertical and lateral variations in the sedimentary facies of different environments caused the heterogeneity characters of the Moghra aquifer. Moghra Basin consists of sand bodies with thin shale breaks and intercalation of sand and shale bodies, in addition to sandy-limestone on the upper part of the studied borehole.

4.2 Results of Land Magnetic Data

The interpretation of the present land magnetic data (Fig. 1) was aided by evaluating the curvature of special functions of the field that peaked over magnetized sources such as contacts and faults [2]. The analysis of RTP using Tilt depth method and theta map helped greatly to define the edges of the vertical magnetized contacts/faults affecting the area. This is given in Fig. 1a, b, where solid lines indicate contacts and colored circles indicate depth to sources (vertical magnetized contact/faults). Deep sources (small circles) indicate possible thick sedimentary section, while larger circles indicate shallower sources i.e. corresponding to thin sedimentary section. The Maximum depth calculated was 3.2 km.

4.3 Geoelectric Results

The results of the manual interpretation were used as initial models for the second technique for quantitative interpretation of geo-electric data. The second quantitative technique was the analytical computer software IPI2WIN program (2008). The actual resistivity and thicknesses were computed for VES stations to construct geo-electric cross-section representing the subsurface (Fig. 2).

The resistivity values for the four geo-electric units reflect the variation of successive lithological units where the clay unit exhibited low resistivity values ranging from 39 to 130 Ω m, while the sandstone reflected high resistivity values ranging from 441 to 4590 Ω m.

4.4 Water Quality Results

Evaluation of water quality is a complex process involving numerous parameters capable of causing various stresses on the overall water quality. Water quality index (IWQ) is used to assess the suitability of ground water for irrigation purposes. The overall IWQ index was calculated using a linear combination of five hazard parameters where the electrical conductivity parameter was used to represent the salinity and the infiltration hazards. SAR, boron and chloride were incorporated to represent the specific ion toxicity.

The resistivity values of groundwater aquifer reflect the quality of the water in the area. The low resistivity at the center of the resistivity profile (Fig. 2) indicates the bad quality of the water, while the higher resistivity values at the eastern and western sides of the profile prove better water quality.

5 Discussion and Conclusion

Detailed investigations of different surface and subsurface stratigraphic sections showed the presence of repeatedly stacked cyclic deposits from channel-fill and flat-laminated lithofacies and the highly vertical and lateral variations in the sedimentary facies of different environments caused the heterogeneity characters of the Moghra aquifer. The geo-electric investigation showed that there are 3–5 layers in this area with resistivity values of range (3.48–4590 Ω m) and of thickness ranges (0.08–82.2 m). The resistivity of such unit ranges between 3.5 and 53 Ω m (Fig. 2).

In conclusion, the interpretation of land magnetic data revealed a structurally controlled aquifer. The system of faults runs in NE_SW, NW-SE and NS (Fig. 1). Most of the groundwater samples were characterized by recent marine and deep meteoric water origins. It was finally concluded that the quality of groundwater is moderately suitable for irrigation.

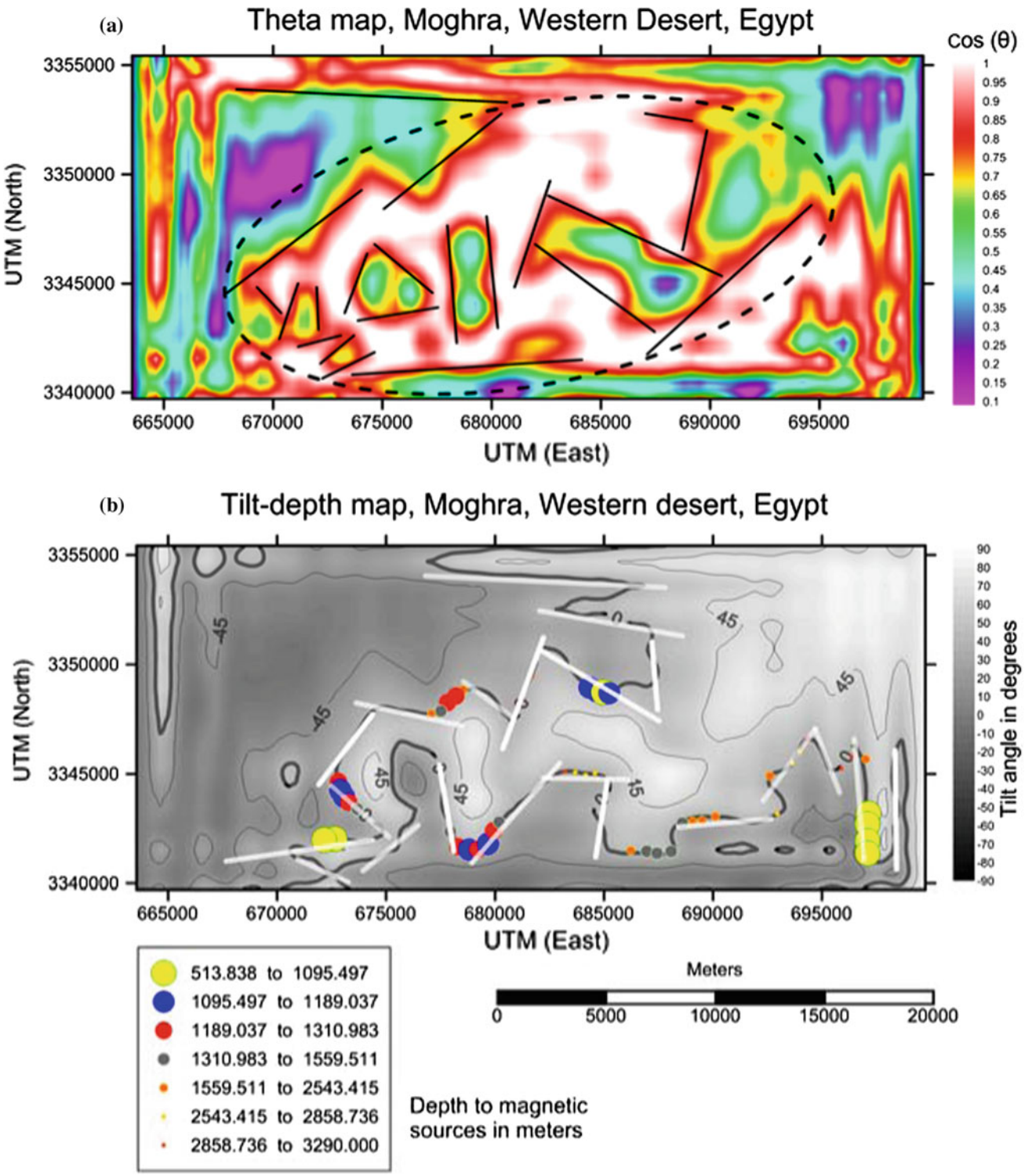

Fig. 1 Edge detection and source depth estimation using the theta map (**a**) and the tilt depth map (**b**) as calculated from reduced to pole (RTP) magnetic anomaly map. Solid lines indicate magnetic contacts/faults and colored circles indicate depth to sources

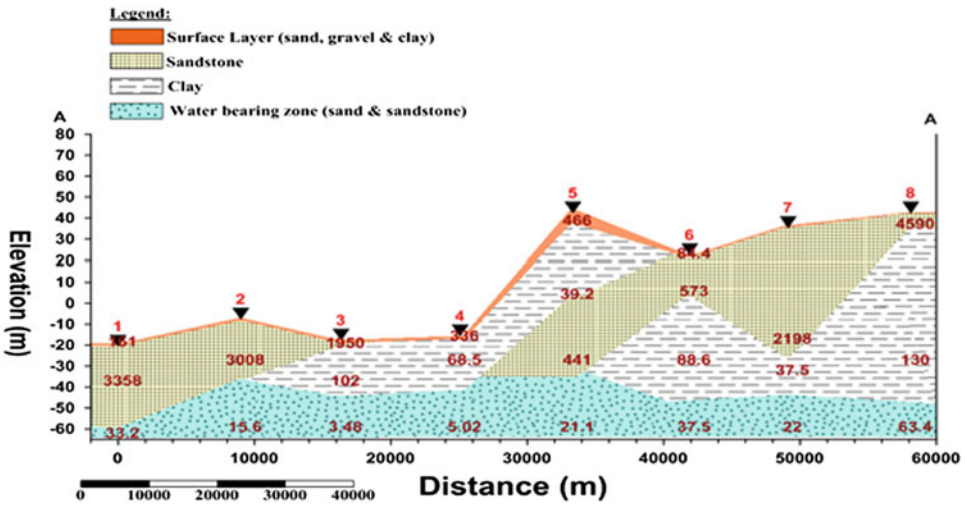

Fig. 2 Quantitative interpretation of VES stations

Acknowledgements This work is extracted from a project financially supported by the Science and Technology Development Fund (STDF), Egypt, Project ID:15239.

References

1. Said, R.: The Geology of Egypt, 370 p. Elsevier, Amsterdam (1962)
2. Abdelazeem, M.: Implementation of the Geosciences to Construct the New Desert Urban, Site Management, and Distribute Resources; Pilot area: Moghra Oasis, Qattara Depression, project financed by STDF, P ID: 15239, unpublished internal report 3 (2018)

The Way to a Clearer Seismic Image: An Integrated Approach in South Tunisia Ghadames Basin

Noura Saidi Ayari, Dorsaf Kebaier, Ferid Adouani, Mohamed Mnasri, Francis Chevalier, Jozsef Orosz, Alexandre Egreteau, and Sandor Bezdan

Abstract

In order to unlock the remaining exploration/appraisal potential within South Tunisia Ghadames Basin, OMV adopted an integrated approach focused on the enhancement of the seismic image. One of the crucial reservoir imaging challenges is the attenuation of the interbed multiple energy which is hampering the seismic image at both shallow and deep targets. The approach focused on optimizing a seismic data acquisition design as well as applying advanced/customized processing workflows. The QC of the final product with the synthetic well trace showed that the method adopted so far is the most efficient way to clean the seismic dataset from multiples.

Keywords

Ghadames basin • Interbed multiple attenuation • Seismic imaging • Seismic acquisition design • Processing workflow

1 Introduction

After more than 50 years of exploration activities, the Ghadames Basin in South Tunisia still offers attractive opportunities for finding hydrocarbons. Improving the seismic image at different reservoir levels is the key to unlock the remaining exploration/appraisal potential within the basin.

N. Saidi Ayari (✉) · D. Kebaier · F. Adouani · M. Mnasri · F. Chevalier
OMV—Österreichische Mineralöl Verwaltung Tunesien (Austrian Mineral Oil Administration Tunisia), Les Berges du Lac, 1053 Tunis, Tunisia
e-mail: noura.ayari@omv.com

J. Orosz · A. Egreteau · S. Bezdan
OMV—Österreichische Mineralöl Verwaltung (Austrian Mineral Oil Administration), Trabrennstraße 6, 81020 Vienna, Austria

The focus is still on exploring for structural traps, but stratigraphic traps and unconventional hydrocarbons might offer attractive opportunities for the future. Targeting this upside potential as well as the proven reservoirs requires the cleaning of the seismic dataset from the contamination of the multiples. With this perspective, a combination of optimized seismic field acquisition parameters and specific processing workflows was adopted to solve one of the crucial reservoir imaging challenges in this desert area: the strong multiple contamination.

2 Geological Settings

Four proven plays are present in the Ghadames Basin: the Triassic, Devonian, Silurian and Ordovician. All reservoirs correspond to clastic sediments, deposited under continental to marine influence. Their thickness does not exceed a few tens of meters, and they often correspond to thin bedded layers like the Silurian Acacus Fm. World-class source rocks are present in Silurian and Devonian series.

With the exception of the giant El Borma Triassic field, most hydrocarbon accumulations in the Tunisian Ghadames Basin have been found in small and low relief subtle traps corresponding to 4-way- to 3-way closures. Some indications of stratigraphic contribution are suspected especially when the cumulative production exceeds the computed resources for a given field.

In such context, successful exploration mostly depends on the ability to integrate all available data and perform a detailed seismic interpretation.

3 Major Issue

After years of success in exploring different plays in the Ghadames Basin, the remaining potential can only be unlocked by integrating the available information from seismic and well studies, and by highlighting the details of

N. Sundararajan et al. (eds.), *On Significant Applications of Geophysical Methods*, Advances in Science, Technology & Innovation, https://doi.org/10.1007/978-3-030-01656-2_29

the geology. The relationship between the structural evolution of the basin and the complex depositional environments succession should be understood in order to get access to any kind of subtle traps, and possibly find new ways of exploring the area.

With this perspective, an enhancement of the seismic image deemed necessary. The combination of optimized seismic field acquisition parameters and specific processing workflows has become essential to solve one of the crucial reservoir imaging challenges in this desert area: the strong multiple interference. These multiples conceal several primary reflections within different target levels.

The application of conventional multiple elimination techniques often fails to solve this issue due to the similarity of the primary and multiple velocities, the resemblance of their frequency spectra and the little dip discrimination (nearly flat geological dips: 1°–3°maximum).

From regional log analyses, internal multiples arise from two main generators: one in the first hundred meters in the Cretaceous layers with a vertical velocity inversion, and a second one deeper in cyclical high velocity carbonate/evaporite sections of Jurassic-Triassic (Figs. 1 and 2).

These generators are interfaces between subsurface layers presenting a high impedance contrast, thus producing high-energy events. These events, coupled with high velocity character of the generators (short travel time), will result in a high-reflection strength multiples starting at a short time shift from the primaries.

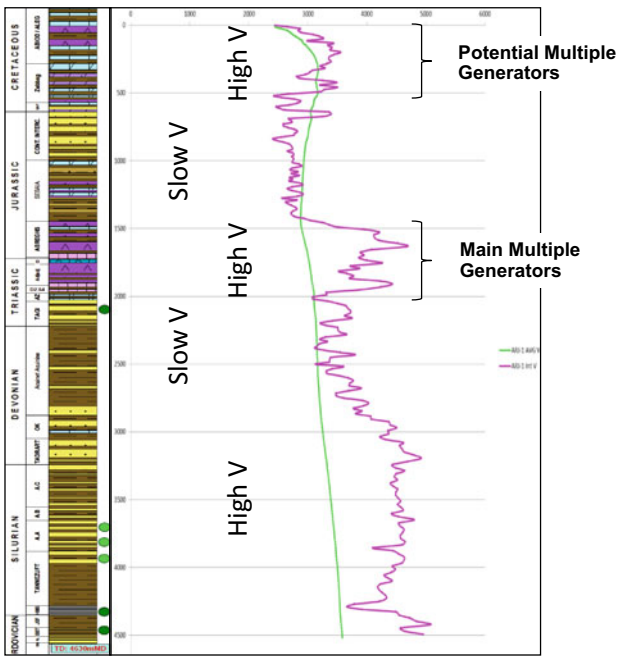

Fig. 1 Regional P-wave log showing two potential multiples generators

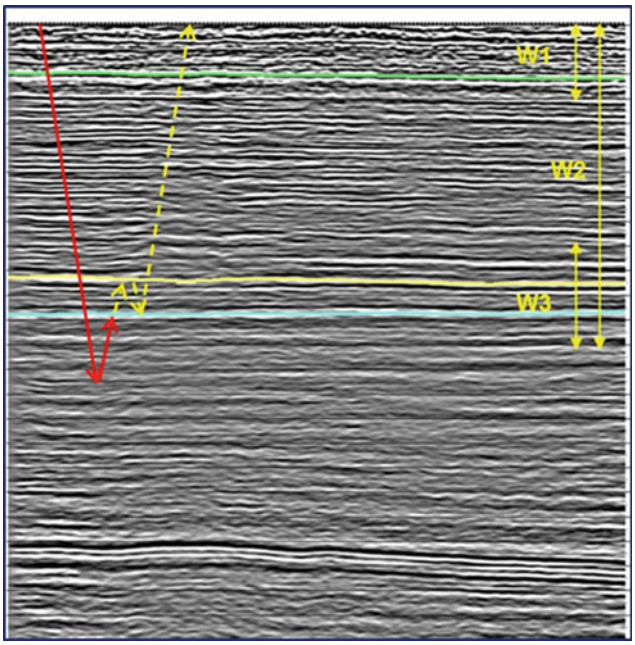

Fig. 2 Example of modelled inter-bed multiple generated in W3

4 Approach and Results

The approach adopted started with an optimization of the seismic acquisition design in order to increase the efficiency of the multiple suppression techniques. In 2016, OMV has run a feasibility study over the Jenein Sud permit in South Tunisia Ghadames Basin. A Kinematic modelling for primaries and multiples was performed together with a comparison between synthetic and vintage field data. This led to a better optimization of the offset range compared to previous 3D acquisitions (maximum offset up to 6 km instead of 4.5 km) (Fig. 3).

The second phase is during the processing where the multiples are modelled based on the wave field extrapolation ([1–4]). Three different windows are used to generate three independent multiple models which were then adapted and subtracted from the input. Each time sub-window (W1, W2 and W3) defines an area of down-going and up-going reflections where the multiples are generated.

Windows W1 (Cretaceous layers) and W3 (Jurassic-Triassic layers) correspond to the high periodicity multiples and the second window (W2) to the low periodicity multiples (Fig. 4).

The QC of the multiple attenuation process is performed through a comparison of pre-stack gathers before and after multiple attenuation and the validation is mainly done with detailed seismic to well tie based on post-stack inversed seismic cubes.

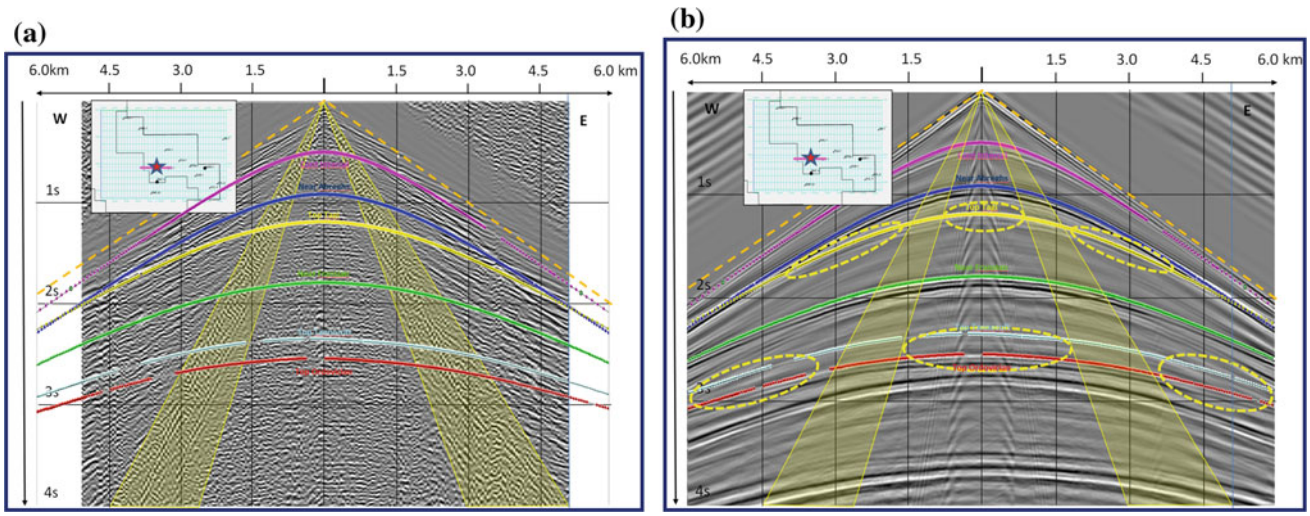

Fig. 3 Comparison between vintage field data (**a**) and synthetic data (**b**)

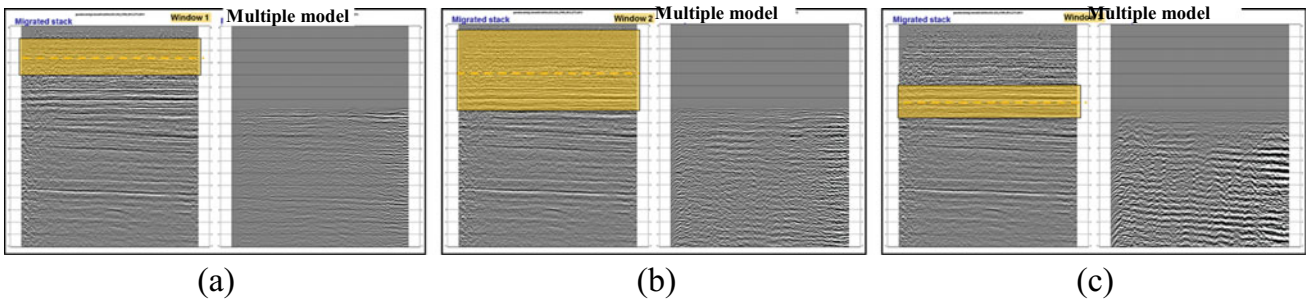

Fig. 4 Multiple models from W1 (**a**), W2 (**b**) and W3 (**c**)

The 2016 post stack inverted seismic data reveals less high contrast of impedance due to the attenuation of the multiples (Fig. 5). The comparison of a multiple free synthetic AI log and an inverted seismic trace extracted along the well path after multiple-attenuation shows better correlation than the one before multiple attenuation.

5 Conclusion

The approach of integrating all available data from the seismic acquisition until the interpretation phase seems to be one of the most efficient ways to enhance the seismic data

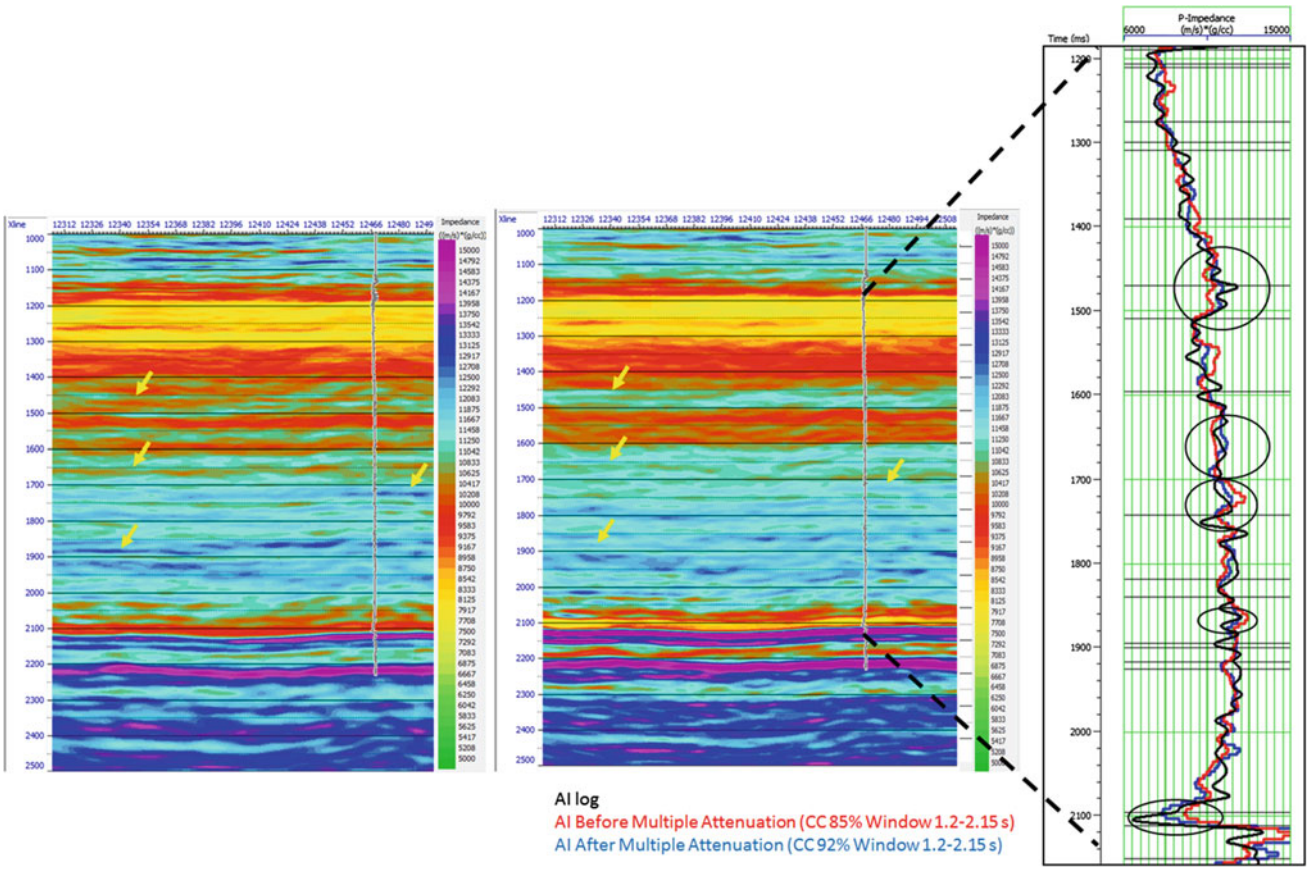

Fig. 5 Post-stack inverted seismic section before (**a**) and after (**b**) multiple attenuation. Traces extracted along the well are presented: AI synthetic log (black), AI before multiple attenuation (red) and AI after multiple attenuation (blue)

quality. This is especially because we are targeting thin-bed stacked reservoir levels with low continuity and often at the limit of the seismic resolution. The clearer seismic image obtained after multiple attenuation gives hope for advanced seismic processing/interpretation and for more success in exploring and appraising hydrocarbon resources in South Tunisia.

References

1. Berkhout, A.J., Verschuur, D.J.: Removal of internal multiples. In: 69th SEG Annual International Meeting, SEG Expanded Abstracts, pp. 1334–1337 (1999)
2. Jakubowicz, H.: Wave equation prediction and removal of interbed multiples. In: 68th SEG Annual International Meeting, SEG Expanded Abstracts, pp. 1527–1530 (1998)
3. Pica, A., Delmas, L.: Wave equation based internal multiples modeling in 3D. In: 78th SEG Annual International Meeting, SEG Expanded Abstracts, pp. 2476–2480 (2008)
4. Retailleau, M.G., Benjamin N., Pica, A., Bendjaballah, M., Plasterie, P., Leroy, S., Delmas, L., Hugonnet, P., Khalil, A., Gulunay, N., Smidth, R., Shorter, J.: Advanced 3D land internal multiple modeling and subtraction, a WAZ Oman case study. In: 74th EAGE Conference & Exhibition, Expanded Abstracts, Y014 (2012)

Geophysical Modeling of Contact Area Between Outer and Inner Western Carpathians (Slovakia)

Vladimír Bezák, Ján Vozár, Josef Pek, Radek Klanica, Miroslav Bielik, and Dušan Majcin

Abstract

The contact zone between the Outer and Inner Western Carpathians was investigated. The combination of different geophysical modeling (mainly magnetotelluric, gravimetric, and seismic) brings a new perspective to the understanding of deep crustal structures of this contact zone. The Klippen Belt is surface representation of this contact zone. According to geophysical modeling, the Klippen Belt is a narrow and shallow structure. In higher depths, the contact zone is represented by the Carpathian Conductivity Zone, which is deep shear zone between the European Platform and Inner Carpathian block. The shear zone origin is connected with transpressional movement of the Carpathian block towards the Northeast to the European Platform. The strike–slip shearing resulted in a flower structure in the contact zone.

Keywords

Contact zone of the Outer and Inner Western Carpathians • Geophysical modeling

1 Introduction

The Western Carpathians (WCp) are spreading predominantly on the territory of Slovakia. They belong to the young orogenetic mountain ranges of Europe and Asia, whose final formation occurred in the Neogene. They are tectonically divided into Outer (OWCp) and Inner (IWCp)—e.g. The Tectonic map of Slovak Republic [1]. OWCp are formed by Flysch Belt (FB) that emerged during the Neoalpine gradual oblique collision of the IWCp block with the European platform (EP) and the closure of the flysch basin. This collision is manifested in the overthrust of flysch sediments over EP and in various deep structures. In this contribution we presented examples of integrated geophysical modeling from transects in western and central part of Slovakia across the contact zone between OWCp and IWCp. The magnetotelluric modeling in combination with the seismic and gravity models exhibited sensitivity to show tectonic structures of this contact.

2 Geological Setting and Methods

The recent division of the Western Carpathians is based on the Neoalpine tectonic processes, which resulted in accretion of flysch nappes of the OWCp as a consequence of the oblique collision of the IWCp block with the EP (Fig. 1). Thus, the OWCp are represented by FB, which extends in an arch around the IWCp block and continues to the Eastern Carpathians. FB is formed by deep-sea sediments, which settled in the North Penninic basin. This basin was relatively wide, situated between EP and the southern microplates derived from the African continent. During Africa movement to the North, these microplates were gradually pressed into the oceanic space. During oblique collision, the North Penninic flysch basin was closed by transpressional movement of different tectonic blocks. Neoalpine faults are mostly of strike-slip character, that document "strike-slip type" of final stage of Western Carpathian Neoalpine orogeny, which ended by "basin and ranges" type of structure in the IWCp block connected with a volcanic activity. The vast majority of the North Penninic Basin was subducted and some of the sediments overthrusted in the form of nappes over EP (Fig. 1). The narrow KB is the dividing element between OWCp and IWCp. The IWCp block has a complex

V. Bezák (✉) · J. Vozár · M. Bielik · D. Majcin
Earth Science Institute of the Slovak Academy of Sciences, Dúbravská Cesta 9, 840 05 Bratislava, Slovakia
e-mail: geofbezv@savba.sk

J. Pek · R. Klanica
The Institute of Geophysics of the Czech Academy of Sciences, Praha 4, Czech Republic

M. Bielik
Faculty of Natural Sciences, Comenius University, Bratislava, Slovakia

N. Sundararajan et al. (eds.), *On Significant Applications of Geophysical Methods*, Advances in Science, Technology & Innovation, https://doi.org/10.1007/978-3-030-01656-2_30

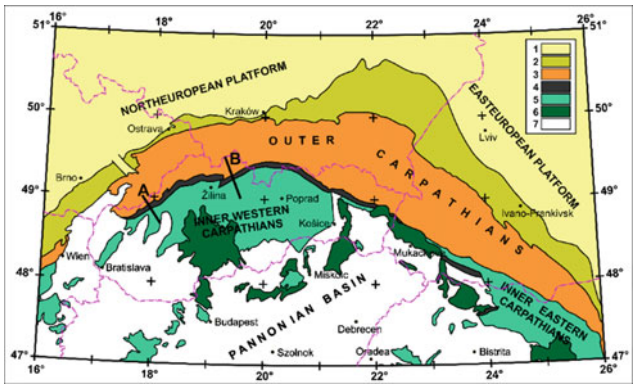

Fig. 1 Position of the MT profiles A, B in the OWCp and IWCp border in the northern part of the Carpathian-Pannonian region. Structure description: 1—European platform, 2—Foredeep units, 3—Outer Carpathian Flysch Belt, 4—Klippen Belt, 5—Inner Carpathian units, 6—Neogene vulcanites on the surface, 7—Neogene sediments

composition, which is a result of a long-term development from the Paleozoic to the Neogene. This block contains the fragments of previous orogeny—crystalline complexes from Hercynian orogeny, mostly Mesozoic formations of Paleoalpine orogeny and post-nappes Tertiary complexes.

For the investigation of deeper structures at the interface between OWCp and IWCp we used the geophysical data from the two sections in the western (A) and central (B) part of WCp collected during CELEBRATION 2000 and THERMES projects. We put together magnetotelluric (MT), seismic profiles and gravimetric models with thermal information gathered from the area and created integrated geophysical models of the structures of this zone.

3 Interpretation of Geophysical Models

For the interpretation of contact zone between OWCp and IWCp we used MT models along with the profile MT-15 [2] (section A) and profile 2T [3] (section B), shown in Fig. 2. Section B also uses the seismic data from the section 2T, with a comparison of gravity models. In both sections, the KB position is interpreted as a relatively shallow structure, which emerged as a result of the movement of IWCp along EP. It is probably just an accompanying transpressional structure, which can also be observed further south (red dashed lines in the presented figures). In our opinion, the deep and significant geoelectrical structure, named Carpathian Conductivity Zone (CCZ) [4], is the main tectonic zone along which this movement occurred. This conductive anomaly is presented along the contact zone between IWCp and OWCp in depths of about 10–20 km and we interpreted it as a main shear zone in the European Platform and Carpathian block border. The occurrence of steep shear-zones (mainly of strike-slip character) revealed in the geo-electrical profiles, as high conductive zones is typical features for Neoalpine tectonic development of the whole IWCp block. These kinds of transpressional movements are typical flower structures, which can be interpreted in the A section, and partly in the B section. These flower structures include the elements of FB, KB and IWCp units (Tatricum units and Inner Carpathian Paleogene complexes). In the mid-crustal depth, the Tatricum and the hypothetical Pienninic crust (PC) segment [5] are separated from the EP by the CCZ. Between EP and IWCp block was identified the shift of the Moho interface (thicker crust of EP), which was previously determined by seismic measurements [6]. This change of Moho was also interpreted in the gravimetric sections (e.g. Bielik et al. [7]). From geothermal measurements, it can be concluded that some inner parts of the OWCp in the eastern part have sufficiently interesting thermal conditions (heat flow density, temperature distributions with depth) for utilization of the geothermal energy (e.g. Majcin et al. [8]).

4 Conclusion

The subject of our research was a contact area between the Outer and Inner Western Carpathians and its manifestation in geophysical modeling. Our models are important in enabling of understanding the geodynamical and thermal processes during the collision of Carpathian orogen with the European platform and the following development of Outer Carpathian flysch belt. The interpretation of MT data from investigated area suggested a resistive European platform below conductive flysch sediments. The boundary between

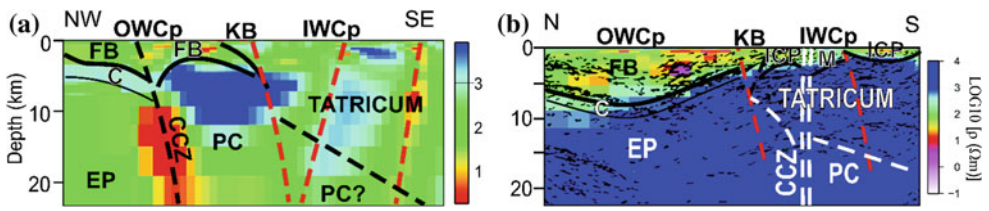

Fig. 2 Geological interpretation of the MT profiles A (left) and B (right). Seismic data in the profile B from Tomek [3]. Explanations: OWCp—Outer Western Carpathians, KB—Klippen belt, IWCp—Inner Western Carpathians, FB—Flysch belt, ICP—Inner Carpathian Paleogene, M—Mesozoic complexes, EP—European platform, C—platform cover, CCZ—Carpathian conductivity zone, PC—Pienninic crust

Inner and Outer Carpathians represented by the Klippen Belt on the surface was changed to the Carpathian conductive zone in higher depths.

Acknowledgements We are grateful for the partial support of the work by the APVV agency by means of projects APVV-16-0482 and 16-0146, and the Slovak Grant Agency VEGA by means of projects 2/0042/15 and 2/0091/15.

References

1. Bezák, V., Broska, I., Ivanička, J., Reichwalder, P., Vozár, J., Polák, M., Havrila, M., Mello, J., Biely, A., Plašienka, D., Potfaj, M., Konečný, V., Lexa, J., Kaličiak, M., Žec, B., Vass, D., Elečko, M., Janočko, J., Pereszlényi, M., Marko, M., Maglay, J., Pristaš, J.: Tectonic map of the Slovak republic 1: 500 000. Geol. Inst. D. Štúr, Bratislava (2004)
2. Bezák, V., Pek, J., Vozár, J., Bielik, M., Vozár, J.: Geoelectrical and geological structure of the crust in Western Slovakia. Stud. Geophys. Geod. **58**, 473–488 (2014)
3. Tomek, Č.: Deep crustal structure beneath the central and inner West Carpathians. Tectonophysics **226**, 417–431 (1993)
4. Hvoždara, M., Vozár, J.: Laboratory and geophysical implications for explanation of the nature of the Carpathian conductivity anomaly. Acta Geophys. Polonica **52**(4), 497–508 (2004)
5. Janik T., Grad M., Guterch A., Vozár J., Bielik M., Vozárová A., Hegedüs E., Kovács C.A., Kovács I., Keller G.R.: CELEBRATION 2000 working group: crustal structure of the Western Carpathians and Pannonian Basin: seismic models from CELEBRATION 2000 data and geological implications. J. Geodyn. **52**, 97–113 (2011)
6. Hrubcová, P., Środa, P., Grad, M., Geissler, W.H., Guterch, A., Vozár, J., Hegedüs, E.: From the Variscan to the Alpine Orogeny: crustal structure of the Bohemian Massif and the Western Carpathians in the light of the SUDETES 2003 seismic data. Geophys. J. Int. **183**, 611–633 (2010)
7. Bielik, M.: Continental convergence in the Carpathian region by density modelling. Geol. Carpath. **46**, 3–12 (1995)
8. Majcin, D., Bilcık, D., Kutas, R.I., Hlavnova, P., Bezak, V., Kucharic, L.: Regional and local phenomena influencing the thermal state in the Flysch belt of the northeastern part of Slovakia Contrib. Geophys. Geod. **44**(4), 271–292 (2014)

Geothermal Resources Database in Saudi Arabia (GRDiSA)

Essam Aboud, Atef Qaddha, Faisal Alqahtani, and Hussein Harbi

Abstract

Geothermal energy is a renewable and friendly environment energy source. This type of energy is required in a world where unclean and harmful energy sources, such as oil, coal, and others, have been in use for ages. Some nations use this clean/renewable energy in daily life and others are still looking for and trying to ways to benefit from these resources. Since Saudi Arabia has many geothermal energy sources such as volcanoes and hot spots along the Red Sea coast, some researchers have been looking for this type of energy since more than five decades. In this research, we tried to collect the previous studies and available data to be used in a new database format. This database would assist decision-makers in drawing up a road map to explore and assess geothermal energy. Accordingly, geological, geophysical, and geochemical data were collected in a digital form to build the first Geothermal Resource Database in Saudi Arabia (GRDiSA) in order to map the geothermal potentiality in the kingdom.

Keywords

Geothermal exploration • Volcanoes • Hot spot • Saudi arabia

E. Aboud (✉) · A. Qaddha · F. Alqahtani · H. Harbi
Geohazards Research Center, King Abdulaziz University, Jeddah, 21589, Saudi Arabia
e-mail: eaboudeshish@kau.edu.sa

E. Aboud
National Research Institute of Astronomy and Geophysics (NRIAG), Cairo, Egypt

F. Alqahtani · H. Harbi
Faculty of Earth Sciences, King Abdulaziz University, Jeddah, 21589, Saudi Arabia

1 Introduction

Geothermal Energy (GE) is a renewable energy source that is stored underneath the earth's surface. International community classified the GE as renewable because it is continuously restored by the upwards flow of heat from the earth's interior. The earth's heat reserves are immense. EPRI [1978] estimated the stored thermal energy down to 3 km within continental crust to be roughly 43 × 106 EJ. This is considerably greater than the world's total energy consumption (560 EJ in 2012).

Various renewable energy sources exist in Saudi Arabia, a huge area for solar energy, Red Sea coast line (>1500 km) where marine energy can be explored, volcanic fields and hot spots along the Red Sea coast for geothermal energy (Fig. 1). Accordingly, the Saudi government has initiated long term project called "**N**ational **R**enewable **E**nergy **P**rogram, **NREP**". This project is supported by the **N**ational **T**ransformation **P**rogram (**NTP**) and 2030 vision. The **NREP** will be phased and rolled out way to ensure that the Kingdom benefits from renewable energy resources. The main target of the **NREP** project is to increase the share of renewable energy in the total energy mix, targeting the generation of 3.45 GW by 2020 (approximately 4% of the current) and 9.5 GW (approximately 10%) by the 2030 vision.

Saudi Arabia has rich geothermal energy resources, as mentioned above. However, the geothermal energy studies started five decades ago or even earlier but studies are still on academic shelves and no geothermal power plant has been installed yet. Some direct-use low-grade geothermal applications have already been installed in the last five years. Some refreshment and swimming pools have already been constructed in the Bani Malik-Jizan area, southern Saudi Arabia.

The current research work documented/overviewed the previous studies in geothermal energy within the Kingdom where the available data would be digitized and imported

N. Sundararajan et al. (eds.), *On Significant Applications of Geophysical Methods*,
Advances in Science, Technology & Innovation, https://doi.org/10.1007/978-3-030-01656-2_31

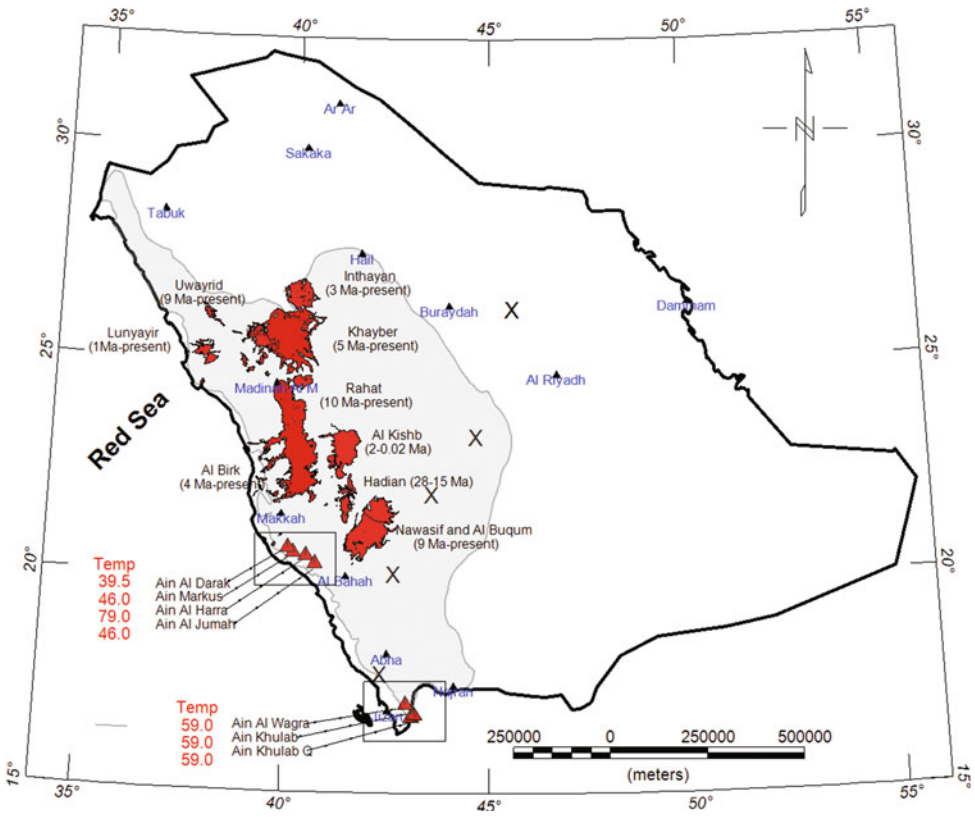

Fig. 1 Geothermal features in Saudi Arabia. Red polygons are volcanic fields, northern black rectangle is Al-Laith hot spring and southern rectangle is Jizan hot spring. X denotes measured heat flow from Mooney et al. [1]

into a database containing most if not all geothermal studies. This would be a simple data base using GIS technology.

2 Materials

Based on the previous data collection, we can divide the most interesting areas into four; Rahat Volcanic Field (RVF), Khayber Volcanic Field (KVF), Jizan region (JZN), and Al-Lith area (LTH). Each of these areas has some dataset type such as geophysical and geochemical and all have geological studies. Table (1) explains the available datasets in each area.

3 Results

Mapping the geothermal resources has become an important factor for renewable energy exploration. Building a geo-database for this purpose is a big challenge where most of the data should be stored in analog forms. The use of GIS technology in converting such kind of data into digital forms helped very much to create such data in one environment. Figure (2) shows the available database that contributed to geothermal exploration. It would help when geothermal project was planned in the potential sites. Basement contour lines from Konert et. al. [7] and Grainger [8] are displayed on the

Table 1 The available datasets for each area of interest; KVF = Khayber, RVF = Rahat, JZN = Jizan, LTH = Al-lith area, CDP = Curie Depth Point

	Grav/Mag	Seismic	EM	Temp.	CDP (km)	Geo-chemistry
KVF	√		177 AMT		35	
RVF	√		65 MT		32	√
JZN		√		√	19	√
LTH		√		√		
	Zahrani et al. [2]	Aref et. al. [3]	Demange [4], Aboud et al. [5]	Aref et. al. [3]	Aboud et al. [6]	Aref et. al. [3]

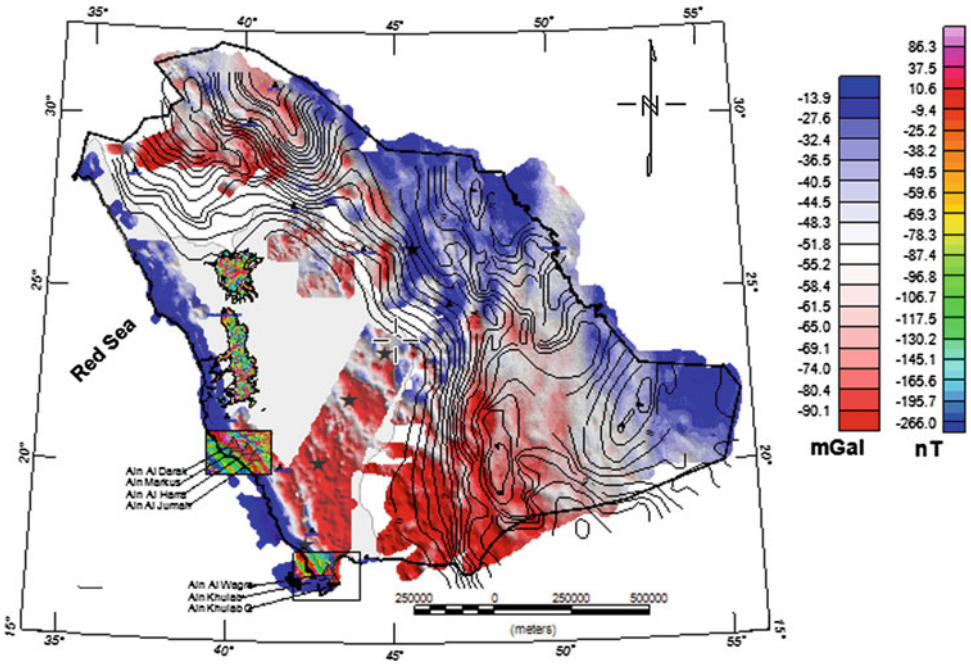

Fig. 2 Geoscience data for geothermal sites in the kingdom of Saudi Arabia

eastern portion of the Arabian shield where depth to the basement reaches 8 km toward the east. Aeromagnetic data [2] for Rahat volcanic field, Khayber volcanic filed, Al-lith area and Jizan area were extracted from Arabian shield aeromagnetic surveys to be available for further studies for geothermal exploration. Aboud el al. [6] used this aeromagnetic data and estimated the Curie Depth Point (CDP) for geothermal reconnaissance. Gravity data [9] for various places (Red Sea shore, eastern side of the Arabian Shield) were displayed too. Borehole temperate measurements at various depths (black filed starts) from Mooney et al. [1] was also added to the map. Additionally, geochemical data from the hot spots [3] can be used for re-evaluating the geothermal sites. Till writing this work, we are still looking for any other geoscience data which may help in geothermal exploration (e.g. logs, temperature gradient, resistivity maps, … etc).

4 Conclusion

Collecting various geoscience datasets for geothermal exploration in the Kingdom of Saudi Arabia helped for planning an exploration strategy for the 2030 Kingdom vision. From the current datasets, it can be recommended that Khayber volcanic field be recommended for further studies in large scale exploration. On the other hand, Al-lith area is recommended for small scale exploration. These recommendations are justified by the fact that the Curie depth points at these locations are shallow as 20 km.

References

1. Mooney, W.D., Gettings, M.E., Blank, H.R., Healy, J.H.: Saudi Arabian seismicrefraction profile: a travel time interpretation of crustal and upper mantle structure. Tectonophysics **111**, 173–246 (1985)
2. Zahrani, H.M., Stewart, I.C.F., Johnson, P.R., Basahel, M.H.: Aeromagnetic anomaly Maps of Central and Western Saudi Arabia: Saudi Geological Survey, Open-File Report SGS-OF-2002-8 (2003)
3. Aref, L., Nassir, A., Dornadula, C., Abdulaziz, A., Shafiqur, R., Michele, P.: Geothermal energy resources of Saudi Arabia: country update. In: Proceedings World Geothermal Congress. Melbourne, Australia (2015)
4. Demange, J.: Exploration for high enthalapy geothermal resources at harrat khayber. Retrieved from Jeddah, Saudi Arabia. SGS Open-File-Report (1982)
5. Aboud, E., Wameyo, P., Alqahtani. F., Moufti M.R.: Imaging subsurface northern Rahat Volcanic Field, Madinah city, Saudi Arabia, using Magnetotelluric study. J. Appl. Geophys. **159**, 564–572 (2018)
6. Aboud, E., Alotaibi, A.M., Saudi, R.: Relationship between Curie isotherm surface and Moho discontinuity in the Arabian shield, Saudi Arabia. J. Asian Earth Sci. **128**, 42–53 (2016)
7. Konert, G., Afifi, A.M., Al-Hajri, S.A., Droste, H.J.: Paleozoic stratigraphy and hydrocarbon habitat of the Arabian Plate. Geo Arabia **6**(3), 407–442 (2001)
8. Grainger, D.: The geologic evolution of Saudi Arabia—geonotes 1–16 and geologic excursion 1–6, p. 264. Saudi Geological Survey, Jeddah (2007)
9. El Difrawy, M.A., Runge, M.G., Moufti, M.R., Cronin, S.J., Bebbington, M.: A first hazard analysis of the quaternary Harrat Al-Madinah volcanic field, Saudi Arabia. J. Volcanol. Geoth. Res. **267**, 39–46 (2013)

Non-listed references

10. Al-Mahmoud, M.J.: Pressure and thermal regimes and systems in the sedimentary sequences of central and eastern Saudi Arabia. Arab. J. Geosci. **8**, 6249 (2015). https://doi.org/10.1007/s12517-014-1619-0
11. Roure, F., Amin, A.A., Khomsi, S., Al Garni, M.A.M.: Lithosphere dynamics and sedimentary basins of the arabian plate and surrounding areas (2017)

Hydrogeochemical and Geophysical Studies on the Shallow Groundwater Aquifer at New Galala City, Northern Galala Plateau, Egypt

Maha Abdelazeem, Mohamed Fathy, Zenhom Salem, and Mohamed Khalifa

Abstract

Galala is a new promising city developed by the Egyptian government in the Eastern Desert above the Northern Galala Plateau, western side of Gulf of Suez. The main aim of the present study is to help decision makers in planning the new city by delineating the subsurface lineaments/faults to avoid future disasters of roads, urban areas and infrastructure. Furthermore, the thickness and facies type of the sedimentary cover was determined in order to study the shallow groundwater aquifer, which is essential to start a new urban area. Such targets have been fulfilled by geologic field studies, detailed magnetic profiles and aeromagnetic data. The chemical analyses of several water samples were used to investigate groundwater suitability for different purposes on the basis of standard guidelines. The samples were generally characterized by recent marine and deep meteoric water origins.

Keywords

New Galala city • Aeromagnetic map • Ground water aquifer

1 Introduction

The New Galala City is being constructed above the Northern Galala plateau that is bounded from the North by Wadi Ghweiba and from the South by Wadi Araba (Fig. 1). In the present study, the integration of all the results of the aeromagnetic, geological and hydrogeological data analyses are carried out in the study area in order to reveal the different structural elements that might affect the mega future infrastructure in the area and give a clear view on the situation of the groundwater aquifer and water quality to assist future development planes in Galala City and surroundings.

2 Geomorphological and Geological Setting

The Gulf of Suez region can be considered as a morpho-tectonic depression extending between two series of elevated blocks which owe their origins to the complicated pattern of faults affecting both sides of the Gulf area. The regional geomorphic works, referred to in the present work, are numerous, e.g. [1]. The area under consideration can be geomorphologically subdivided into the following units: Watershed areas (high tablelands), Water collectors (hydrographic basins), and Coastal plain.

The lithological succession beneath the new city consists of Phanerozoic sedimentary rocks, which non-conformably overlies the Precambrian basement complex (Fig. 1). The sedimentary succession subdivided into clastic-dominated (Nubian sandstone) and carbonate-dominated (carbonate plateau) facies. The Nubian sandstone (Paleozoic–Lower Cretaceous age) exposes at the southern part of the city up to Wadi Araba, which represents the shallow groundwater aquifer. The Upper Cretaceous–Eocene carbonate-dominated facies constitute the basal platform of the New Galala City. The surface geological setting is mainly related to the Gulf of Suez general tectonic, whereas, the subsurface geology is further investigated using available Aeromagnetic analysis and a series of land magnetic profiles covering the study area. The results of such analyses are given in the next section.

M. Abdelazeem (✉) · M. Khalifa
National Research Institute of Astronomy and Geophysics (NRIAG), Helwan, Cairo, Egypt
e-mail: maazeem03@hotmail.com

M. Fathy · Z. Salem
Geology Department, Faculty of Science, Tanta University, Tanta, Egypt

N. Sundararajan et al. (eds.), *On Significant Applications of Geophysical Methods*,
Advances in Science, Technology & Innovation, https://doi.org/10.1007/978-3-030-01656-2_32

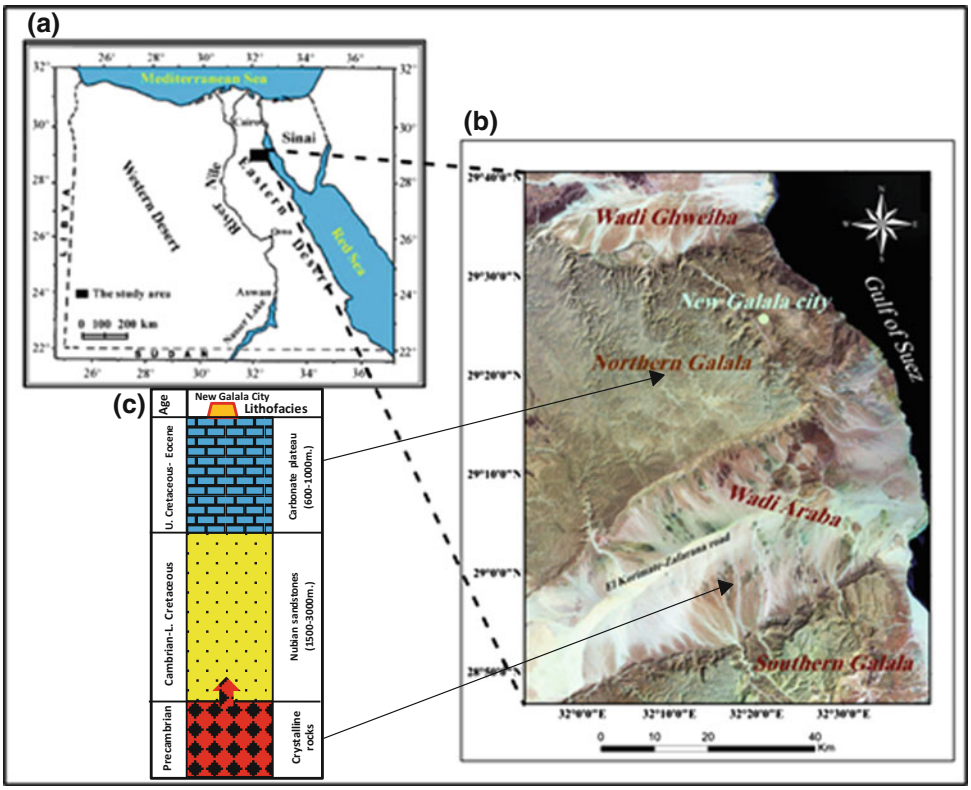

Fig. 1 **a** Location map of the study area, **b** landsat image shows the location of the New Galala City, **c** lithological succession beneath the New Galala City

3 Geophysical and Geochemical Results

3.1 Aeromagnetic Data Analysis

The aeromagnetic map covers the study area prepared by a digitized map of scale 1:50,000. It represents a part of the aeromagnetic survey of Eastern desert, compiled and carried out by CONOCO [2]. Depth to basement was estimated to delineate the thickness of sedimentary cover by different methods (Table 1). Depths can be obtained from the analytic signal, either from the width of the anomalies [5] or based on the ratio of the analytic signal to its higher derivatives if the source type is assumed [3, 7]. In our case we used the first choice. However, the correct estimation of the true depth is obtained only in case when the source corresponds to the chosen model [6]. The SPI method was used to calculate the depth to regional source or basement, which is not dependent on the inclination or declination. 3D-Euler deconvolution was used in calculating the depths to different sources. The structural index was determined automatically. Then, using the tilt angle map, depths to contacts was half the distance between contour of −45° and +45°. Finally, in power spectrum methods we applied a band pass filter with a narrow bandwidth to a data sequence and used the filter output power divided by the filter bandwidth as a measure of the spectral content of the input data. From the estimated power spectrum, the depth can be estimated.

The results from the digital filters analysis showed that the high thickness of sedimentary covers is mainly concentrated in the central zone in wadi Araba. Figure 2 shows depth solutions presented as colored clusters resulting from the application of Tilt depth method as posted on the RTP map. Blue circles are depth to magnetic sources >5000 m whereas pale green circles represent depths <500 m.

3.2 Geochemical Properties of the Shallow Aquifer

Thirteen groundwater samples were collected from water wells and springs tapping the shallow aquifer. The pH values of groundwater mostly reflect slightly acidic to alkaline condition. The total dissolved solids (TDS) range from 1025.0 to 50,233.0 mg/L. Sodium represents the dominant cation in the analyzed groundwater samples. It varies between 180.0 and 16,800.0 mg/L, with an average value of 1832.3 mg/L. Potassium is the least dominant cation; ranging from about 3.0 to 54.0 mg/L, with an average value of about 9.3 mg/L.

Table 1 Results of depth to basement analysis

Method	Depth to basement
Analytic signal	3500 m (Depth to top)
Source parameter imaging (SPI)	3500 m (Max. depth)
Standard 3D-Euler deconvolution	3400 m (Average depth)
The tilt angle derivative	4000 m (Max. depth)
Power spectrum	4000 m (Average depth)

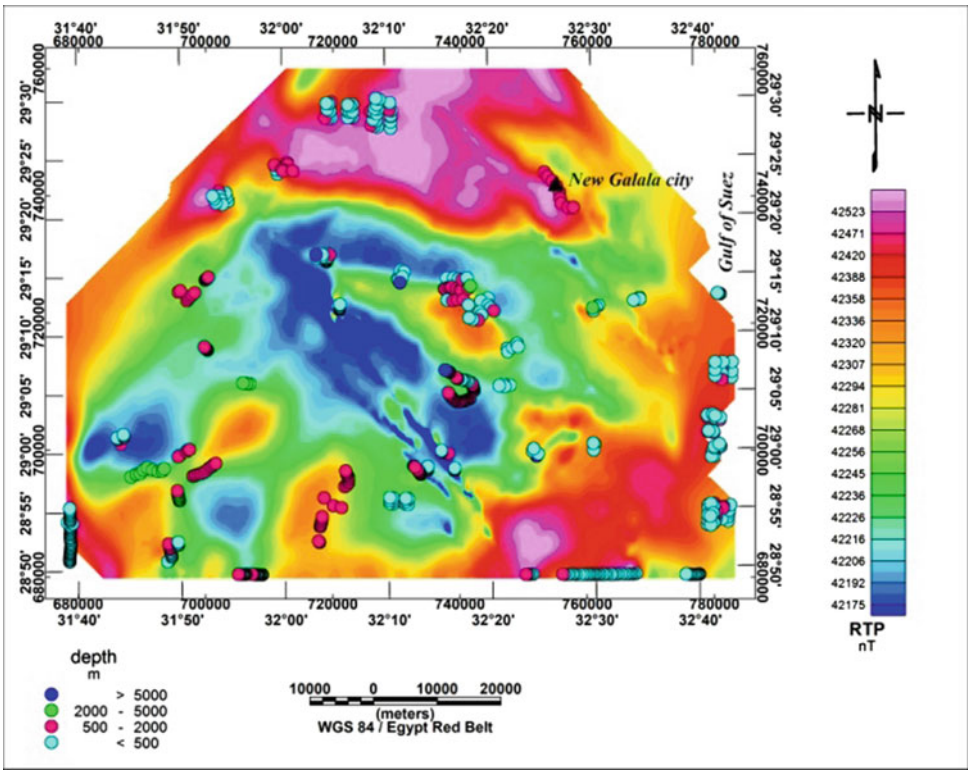

Fig. 2 Tilt depth solutions. Wadi Araba, Egypt

3.3 Classification of Groundwater

Piper plot [4] was used to evaluate the hydro-chemical facies of the groundwater and its trends of salinity evolution. The distribution of the samples pointed on Piper diagram revealed that all groundwater samples are of Na–Cl groundwater type. The distribution of all plotted groundwater samples revealed that evaporation and rock dominance type are the main hydro-geochemical processes affecting the groundwater chemistry. Most of the groundwater samples were characterized by recent marine and deep meteoric origins.

4 Discussion

The area of Wadi Araba, on the western bank of Gulf of Suez, comprises two very distinctive plateaus, The Northern and Southern Galala, the main interest of the future development planes was mainly focused on the development of this area. Although the geophysical and geological work has not completely covered the target region yet, but the present study revealed the type of the groundwater in the area and its chemical characteristics that should be considered in planting water treatment stations. Moreover, the deduced structural trends from the analysis of the magnetic data should be considered when designing the infrastructure layout in Galala city.

5 Conclusion

Detailed geological and land geophysical studies have been carried out to reveal the tectonic trends and elements that affect Northern Galala plateau near Galala City. Moreover, the available Aeromagnetic data was used together with a detailed ground water quality study from 13 samples distributed around the study area. The results showed that

evaporation process and rock dominance types are the main constituent. Most of the groundwater samples are characterized by recent marine and deep meteoric water origin.

References

1. Abu El Ezz, M.S.: Landforms of Egypt. The American Univ. Cairo press (translated by Fayid, Y.A.) (1971)
2. CONOCO: "Geological Map of Egypt" Scale 1:500,000. General Petrol. Corp., Cairo, Egypt (1989)
3. Hsu, S.K., Sibuet, J.C., Shyu, C.T.: High-resolution detection of geologic boundaries from potential anomalies: an enhanced analytic signal technique. Geophysics **61**, 373–386 (1996)
4. Piper, A.M.: A graphic procedure in the geochemical interpretation of water analysis. J. Am. Geophys. Union Trans. **25**, 914–923 (1944)
5. Roest, W.R., Verhoef, J., Pilkington, M.: Magnetic interpretation using 3-D analytic signal. Geophysics **57**, 116–125 (1992)
6. Salem, A.: Interpretation of magnetic data using analytic signal derivatives. Geophys. Prospect. **53**, 75–82 (2005)
7. Thurston, J.B., Smith, R.S.: Automatic conversion of magnetic data to depth, dip, susceptibility contrast using the SPI (tm) method. Geophysics **62**, 807–813 (1997)

Geophysical and Geochemical Exploration of the Gold Bearing Placer Deposits in the Southern Blue Nile (Sudan)

Mohamed A. Mohamed-Ali and Samia A. Ibrahim

Abstract

The Blue Nile River meander in the Southeastern Sudan consists of a dendritic drainage pattern that drains a basin bordered by regional Horst and Graben structures developed in Ingassana hills. It is assumed that the drainage system in the study area host gold-rich placer deposits, while it drains gold-bearing rocks. Satellite processed images were used to identify the main features regionally associated with the Quaternary deposits. Using Electrical Resistivity Tomography (ERT) survey for mineral exploration is feasible in the current study because the ground conditions of the study area are favorable for carrying out the geophysical survey. Interpretation of ERT data collected in the dry and the semi-dry areas of the streambeds in the study area were helpful for the characterization of sub-channel structures and defining the thickness of the gold-bearing deposits. The geochemical analysis of 110 placer gold samples taken from the superficial deposits and residual soils using an auger drilling machine shows promising results and indicates the existence of gold-rich placer deposits with recognized tonnages. The thickness of these deposits estimated by ERT and verified by drilling ranging between 3 and 9 m. These thicknesses have been used to calculate the placer deposit tonnages of 253,125 and 1,269,570 tons for the island locality and khor area with gold reserve of 0.76 and 3.94 tons respectively.

Keywords

ERT • Geochemical • Blue Nile Sudan • Placer deposit • Gold-bearing

M. A. Mohamed-Ali (✉)
Faculty of Earth Sciences and Mining, University of Dongola, Wadi Halfa, Sudan
e-mail: mohdabdwahab@yahoo.com

S. A. Ibrahim
Department of Geology, Faculty of Science, University of Khartoum, Khartoum, Sudan

1 Introduction

The study area (Fig. 1) is situated in the southern part of the Blue Nile State, Sudan. It includes the main course of Blue Nile and its main tributaries up to the Sudanese-Ethiopian border. The area is accessible along the eastern and western sides of the Southern Blue Nile via a gravel road connecting the study area to the Khartoum-Ed Damazin Highway.

The highlands are characterized by a steep escarpment on their southwestern margin rising to more than 1005 m above average sea level (Fig. 2b), whereas to the east they form a plateau that diminishes in elevation gradually towards the Nile valley. The drainage pattern (Fig. 2d) is typically dendritic by nature with pronounced northeast-southwest trend.

The Ingessana hills in the southern Blue Nile of Sudan are part of the southern sector of the ophiolithic belt of the Arab-Nubian Shield with mid-neoproterozoic age. They are part of the southern sector of the NE–SW trending ophiolithic belt, of the Arab-Nubian Shield with mid-neoproterozoic age and they are made up by ultramafic rocks such as dunites and hartzburgites intruding the metagabros outcropping in the central parts and creating the western-north-western semicircular ultramafic complex [1, 4, 5]. The whole mountain is consisting of igneous basement rocks (Granites, Gabbros …etc.) as high mountains and hills cut by dense drainage patterns having width between a few meters to more than 100 m. The gold mineralization is mainly hosted on border of Felsic dyke and Quartz veins. Placers can be found virtually in any area where gold bearing hard rock exist. The gold is released by weathering to be carried down by gravity and hydraulic action to some favorable point of deposition and are classified depending upon provenance and sorting in depositional environments.

The meandering of the Blue Nile River is expected to host gold-rich placer deposits, while it drains gold-bearing rocks. Quartz vein rubble is present in abundance in several areas along the river section. It is evident that it makes a

N. Sundararajan et al. (eds.), *On Significant Applications of Geophysical Methods*,
Advances in Science, Technology & Innovation, https://doi.org/10.1007/978-3-030-01656-2_33

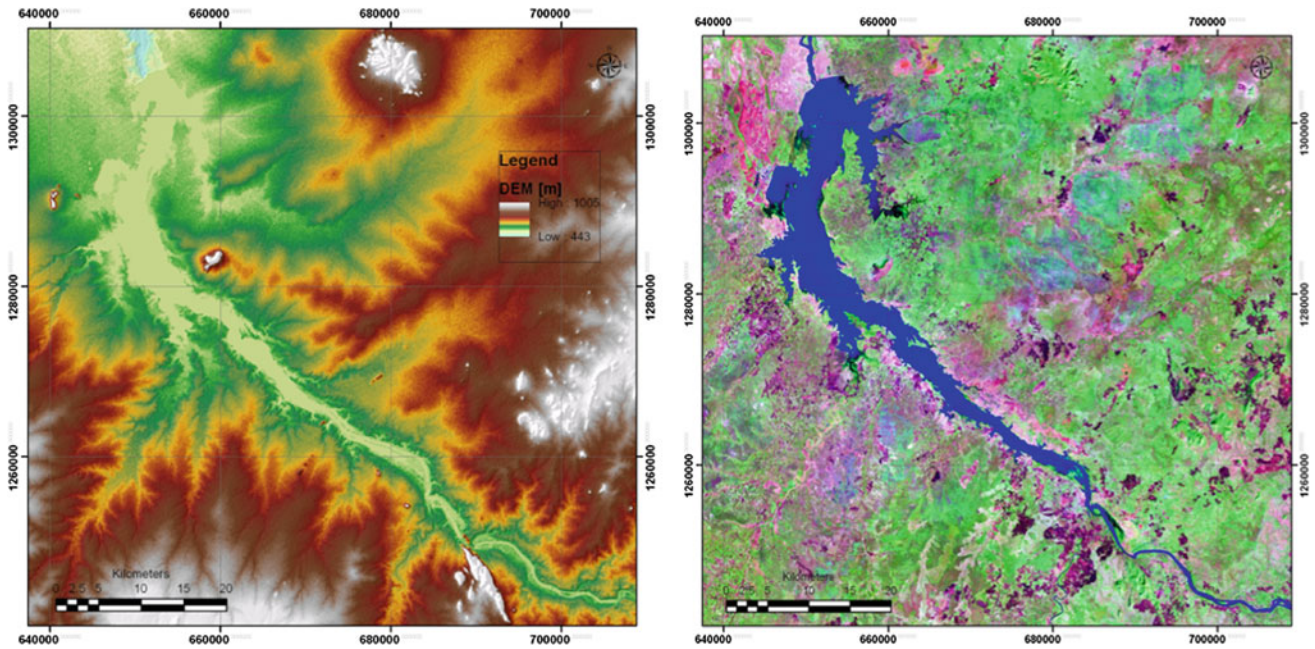

Fig. 1 The study area and its physiographic features, Left: topographical map expressed by the Digital Elevation Model (DEM), Right: Landsat7 ETM+ color composite images, linear stretched bands 7, 4 and 1 in R, G, B, respectively

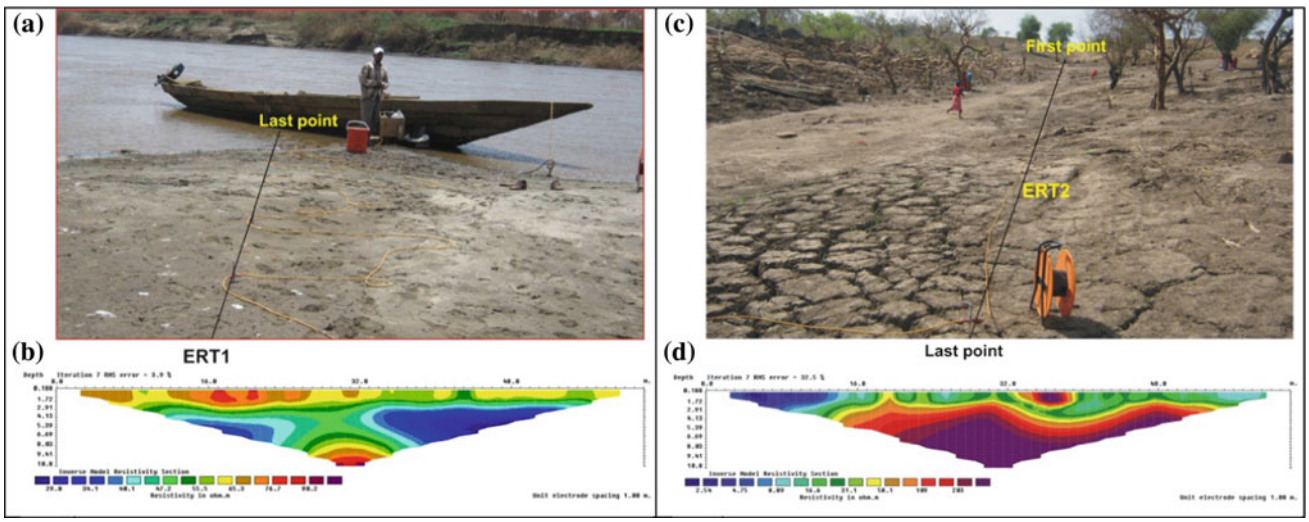

Fig. 2 Field conditions and results of ERT profiles, **a** ERT01 location and site view, **b** ERT01 Inversion result of ERT1, **c** ERT02 location and site view, **d** inversion result of ERT02

major component in alluvium of the streambed. The placer deposits consist of quartz gravel, cobbles and rare boulders.

The objectives of the current study were to define the depths to bedrock of the investigated sites, and accordingly to define thickness of the gold-rich placer deposits overlying overburden and to integrate these results with geochemical analysis for estimating the ore tonnage and gold reserve.

2 Electrical Resistivity Tomography Survey

Electrical resistivity tomography (ERT) is a geophysical technique used to measure the electrical resistivity of subsurface material in two dimensional, horizontally and with depth [3]. ERT data were processed with the Res2Dinv

software [2], which enables the visualization of the inversion results as electrical resistivity in pseudo- and real sections. The 2-D model used by the inversion code consists of a large number of rectangular blocks. The depth of the bottom row of the blocks is set to be approximately equal to the median depth of investigation of the data points with the largest electrode spacing.

2.1 ERT Fieldwork

A detailed geophysical survey employing ERT was carried out to delineate the placer deposits tonnage in the target zones in the study area and accordingly facilitate the positionining of exploratory drill holes for verification of results. A multi-electrode system (Tigre32, Allied-UK) was used in the current study to measure resistivities. 11 ERT were carried out based on ground conditions and characteristics of the targets drainage associated deposits. The Wenner electrode configuration and sometimes dipole-dipole array with electrode spacing 2 and 5 m were used for data collection in the field. The total length of ERT01 was 64 m and it was carried out using Wenner array in an island within the main course of the Blue Nile (see Fig. 2a). ERT02 is an example of profiles been carried out in the area of confluence of wadi with the Blue Nile (see Fig. 2c). It has a total length of about 155 m and Wenner array was chosen with electrode spacing of 5 m.

2.2 ERT Results and Interpretation

ERT01:

Figure 2b shows the inversion results of ERT01. It shows sandy layer of loose placer deposits up to a depth of 3 m, the variation of resistivities (different colours in the section) laterally are associated with deposits of different conditions. The second layer extends from 3 m up to the fresh bedrock at depth of 9 m. The relatively lower resistivity of this layer is associated with silt clay component in an aqueous phase. The full depth 9 m is recognized as target zone for estimation of placer tonnage and gold reserve.

ERT02:

The geo-electric section of ERT02 (Fig. 2d) shows a depth of 3 m up to the bedrock, this fresh bedrock shows a higher resistivity and trends to decrease upward gradually through a weathered basement and then superficial wadi deposits, which are the targeted gold rich bearing deposits. The resistivity of these deposits are variable based on soil conditions e.g. clay content (less than 3 Ω m) and sand lenses (up to 300 Ω m). Thickness of 3 m is considered appropriate average for estimation of reserve across the profile.

3 Geochemical Survey

110 streambed samples were collected for geochemical analysis from the khors and wadis expected to feed the Blue Nile reservoir with placer gold. The location of the samples either bottom of the khor or the place where the sand bars in the meandering are located (The space between samples ranges between 0.5 and 1 km). The total length of the sampled lithological column was mainly controlled by the depth to the bedrock, which varies from place to place and ranging from 2 up to 3 m. The samples were taken at each 0.5 m with depth using Auger machine.

The samples were analyzed chemically in the laboratory of Geological Research Authority of Sudan (GRAS) using volumetric chemical method, where concentration of gold was evaluated in ppm.

Examples of geochemical analysis results are shown for some locations along ERT01 and ERT02, and details about number of samples. Table 1 shows a summary for sample information and gold concentration results. The 4 samples taken from area of ERT01 show minimum of about 1.71 ppm, maximum of about 4.26 ppm and an average of about 3 ppm. The 12 samples taken from area of ERT02 show minimum of about 1.11 ppm, maximum of about 5.54 ppm and an average of about 3.1 ppm. These findings were also used for calculation of ore tonnage and gold reserve.

4 Discussion of Results

2D ERT sections revealed the existence of different subsurface layers and soil condition, and the classification of the subsurface material is dependent on the values of their electrical conductivity.

It was found that resistivity of placer deposits may raise up to 300 Ω m when the deposits are dry or decrease to less than 10 Ω m. The depths to the bedrock ranged between 3 and 9 m. The thicknesses revealed by ERT results and verified drilling were used afterward for estimation of placer deposit tonnage and integrated with gold concentration (3 ppm) for estimation of gold reserve.

For the estimation of placer deposit tonnage and gold reserve, we first calculated the ore volume using: (1) thickness revealed by ERT and verified by drilling, and (2) the surface area of the target zone, which was estimated using

Table 1 Summary for the analyzed sample information and gold concentration results

Sample location	No. of sample	Gold concentration (ppm)		
		Minimum	Maximum	Gold (g/ton)
Island (Area of ERT01)	4	1.71	4.26	3
Khor (Area of ERT02)	12	1.11	5.54	3.078

Table 2 Estimation of placer deposit tonnage and gold reserve of the localities in the study area

Code name	Area (m^2)	Thickness (m)	Volume (m^3)	Density (g/cm^3)	Placer tonnage (tons)	Grade (ppm)	Gold reserve (tons)
Dry-Loc1	11,250	3	101,250	2.5	253,125	3	0.76
Dry-Loc2	169,276	9	507,828	2.5	1,269,570	3.1	3.94

polygons tracing procedure in Google Earth. The volume was multiplied by density (2.5 g/cm^3) for yielding the ore tonnage, and finally multiplied by gold concentration average for yielding the gold reserve.

The above procedure was used for estimating tonnage and reserve at two selected locations in the study area, namely; Island (Area of ERT01 and Khor Confluence (Area of ERT02). Table 2 shows detail of parameters used for estimation tonnage and reserve. It has been found that the placer deposit tonnage are 253,125 and 1,269,570 tons for the island locality and khor area with gold reserve of 0.76 and 3.94 tons respectively.

5 Conclusion

The results presented in the current study proved that Electrical Resistivity Tomography is one of the reliable methods to investigate placer deposits for earth material type and thickness.

The current study reports on work undertaken for exploration of the gold bearing placer deposits in the Southern Blue Nile, Sudan, it assessed the status and potential for placer deposit resources and the associated gold reserves.

In the unexplored areas it might be favorable to use ERT first to detect the depth to bedrock as well as potentially placer bearing features such as; paleochannels, and clay layers. Then it can be checked at least by drilling test for calibration.

Thickness revealed by ERT can be valuably integrated with geochemical analysis results for estimation of ore tonnage and gold reserve.

The current results are promising and encourage further advanced exploration and development of the study area.

Acknowledgements We would like to express our deepest thanks and gratitude to Eng. Elhadi Abaker, Direcor General of Dallow Company for Trade and Constructing for granting us a permission to publish results of its investment project in Blue Nile State, thanks and appreciation for Dr Khalid M. Kheiralla for satellite image interpretation and geological background review. Sincere thanks to El Modather Mohamed Al-Amin (Mining Engineer), Abdelhalim Abou (Mining Geologist), Musaab Hussein (Hydrogeologist) and Zohaer Sowar (Mining engine er) for hardwork during the fieldwork time and analysis of results afterward.

References

1. Adli, A.M.: Sudan Industrial Minerals and Rocks, pp. 76–86. Centre for Strategic Studies, Khartoum (1998)
2. Loke, M.H., Barker, R.D.: Rapid least-square inversion of apparent resistivity pseudo-sections by a quasi-Newton method. Geophys. Prospect. **44**, 131–152 (1996)
3. Loke, M.H.: Electrical imaging surveys for environmental and engineering studies. A practical guide to 2-D and 3-D surveys (2000)
4. Mohamed-Ali, M.A., Simos, J., Kheiralla, K.M.: Chromite exploration using electrical resistivity tomography in Ingessana Hill, Blue Nile State, Sudan. Int. J. Ind. Electron. Electr. Eng. (IJIEEE) **5**(12), 68–74 (2018)
5. Seifelnassr, A., Tamam, T.: Flotation behavior of Sudanese chromite ores. J. Eng. Sci. **39**(3), 649–661 (2011)

Part VI
Hydrocarbon and Petrophysical Studies

Halokinetic Activities and Structural Style in the Jeffara Basin (Tunisia): Implication for Hydrocarbon Prospectivity

Asma Draoui, Benen Sarsar, and Sofiene Haddad

Abstract

The Jeffara Basin, located offshore central Tunisia, covers an area of about 20,000 km^2. It is a hydrocarbon productive area situated between the two main productive basins of Tunisia: the Ghadames and the Pelagian Provinces. The present work aimed to reconstruct the main tectonic styles and phases by means of seismic, well logs and geological data, for better understanding their role in hydrocarbon trapping and exploration. The interpreted key seismic lines showed a lateral variation of structural style in the Jeffara basin. They depicted that after the major upper Triassic-early Jurassic rifting phase, the NE–SW extension process continue during the upper Jurassic and lower Cretaceous. This tectonic phase was dominated by NW–SE to E–W normal faults disclosing the early stage of the halokinetic activity. From the Santonian period, the Jeffara basin was influenced by regional wrench, with disconnected major E–W oriented right lateral strike slip faults. The reactivation of these deep faults caused numerous structural elements toward Jeffara basin. Indeed, the halokinetic activity in the southern part of the Jeffara basin discloses different salt structures: pillows, domes and salt walls, which affect the surrounding strata differently. The detected salt bodies at different stages of growth enabled the prediction of subtle facies controlled hydrocarbon traps.

Keywords

Jeffara basin • Tectonic events • Salt structures
Halokinetic activity • Hydrocarbon prospectivity

1 Introduction

Ductile salt materials have proven to be effective in oil and gas trapping [1]. Impervious evaporites can move and deform to generate seal in hydrocarbon traps [1]. Many petroleum systems and hydrocarbon traps described worldwide were discovered beneath subsalt structures such as those in the Gulf of Mexico, Suez, Mahogany, Enchilada, Gemini, and North Sea, Gulf of Lion [5–7]. Since these discoveries, subsalt features have become one of the main targets for petroleum exploration. Along the passive margin of the African Paleo-Mediterranean Sea, salt structures are well extended. In southern Pelagian platform precisely in Jeffara basin, these structures occur along a NW–SE-trending domain defining the "Salt sub-basin" [3–9]. A good knowledge of these structures geometry and evolution is required for prospection programs which rise the Hydrocarbon prospectivity of the study area. The present study focused on the southern part of the Jeffara basin. Based on 2D seismic interpretation combined with geological structural analyses, it aimed at inferring an accurate picture of the subsurface geology, in view of geometrical types of salt deposits and their evolution mechanisms.

2 Geodynamic Evolution

The Jeffara Basin belongs to the southern part of the Pelagian Platform. It was considered as a subsiding basin since the Mesozoic and is characterized by major NW–SE trending fault [3–9]. The successive tectonic phases have contributed to the structural distribution as well as the geodynamic evolution of the Jeffara basin since the Late Hercynian phase. This latter is followed by the Neo-Tethysian rifting event causing a major E–W and NW–SE trending faults during Late Triassic-Santonian stages [9]. The Austrian and Santonian compressive events have contributed to the genesis of the major faults trending and the

A. Draoui (✉) · B. Sarsar · S. Haddad
ETAP, 54, Av Mohamed V, 1002 Tunis, Tunisia
e-mail: asma.draoui@etap.com.tn

N. Sundararajan et al. (eds.), *On Significant Applications of Geophysical Methods*,
Advances in Science, Technology & Innovation, https://doi.org/10.1007/978-3-030-01656-2_34

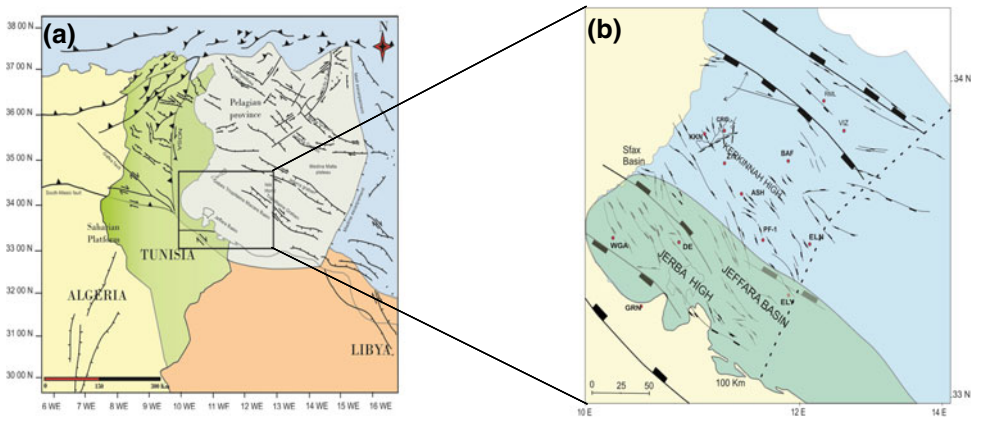

Fig. 1 **a** Combined structural map of Tunisia. **b** Zoom in of the structural map of the Jeffara Basin (Sarsar. B 2014, ETAP)

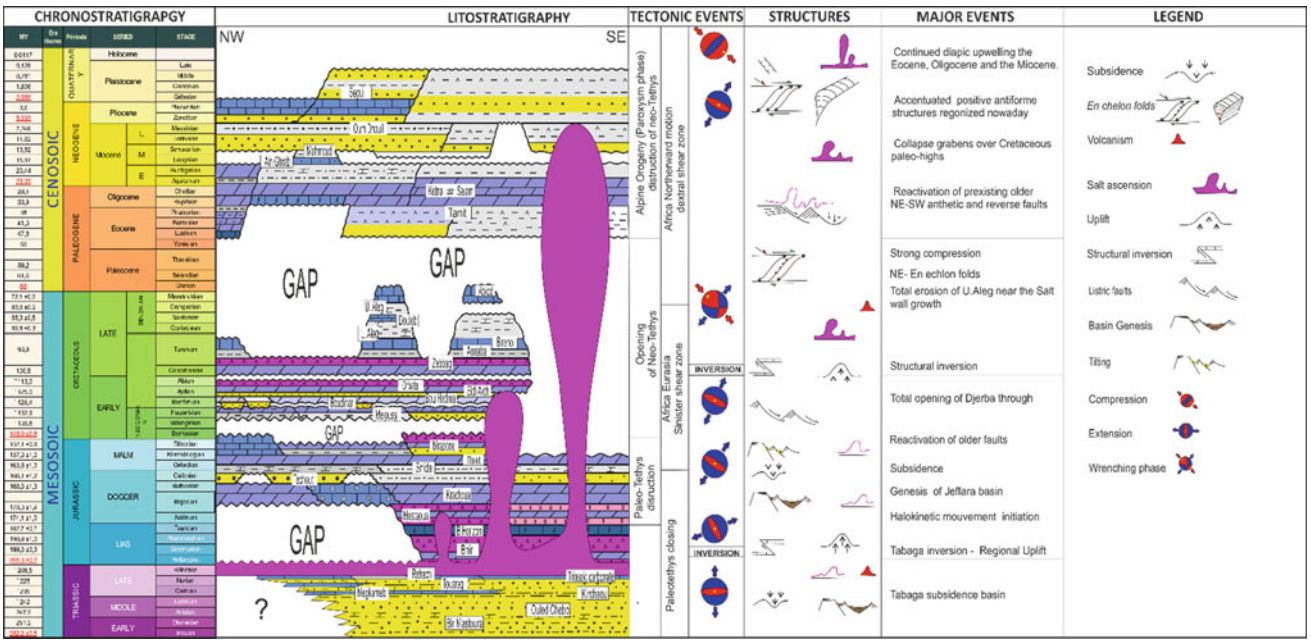

Fig. 2 Tectono-lithostratigraphic chart of the Jeffara Basin [2]

beginning of the salt movement. The Late Villafranchian compressive phases reactivated the existing structures [3–9] (Fig. 1 a, b).

The drilled wells in the region cross a lithostratigraphic column ranging from the Triassic Formation to the Plio-Quaternary (Fig. 2). It is not worthy to note that the tectonic event as well as the halokinetic salt activities are the main causes of the identified hiatus and gaps within the area.

3 Methodology

Seismic interpretation in southern Jeffara basin was achieved with three surveys: M82, M84, and PV09. The seismic quality is generally medium to good for the interpreted horizon. This quality was decreasing with depth, in the contact with diapirs, and locally near fault zones.

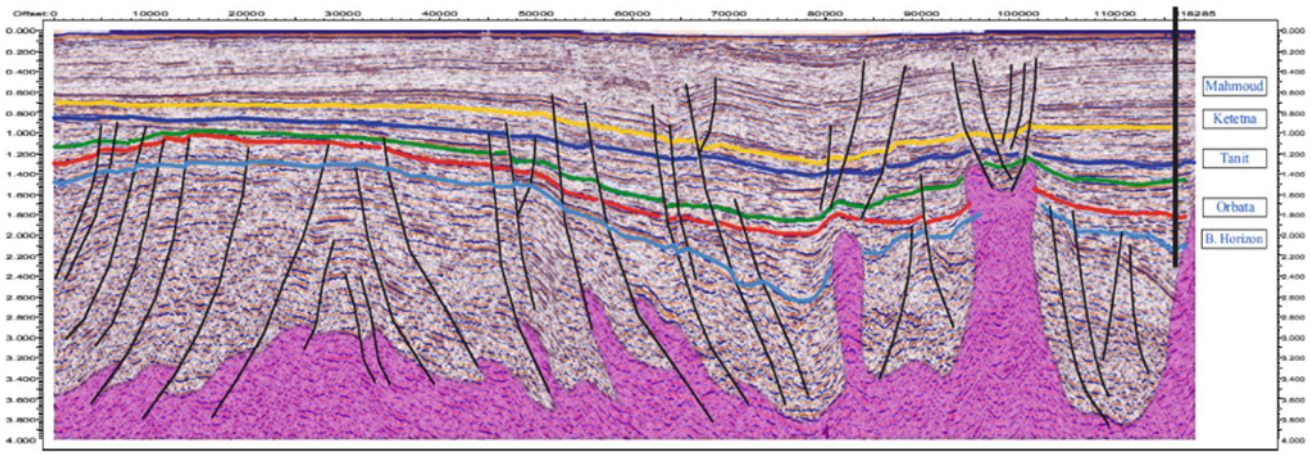

Fig. 3 Regional interpreted seismic profile showing halokinetic activity within the Jeffara Basin

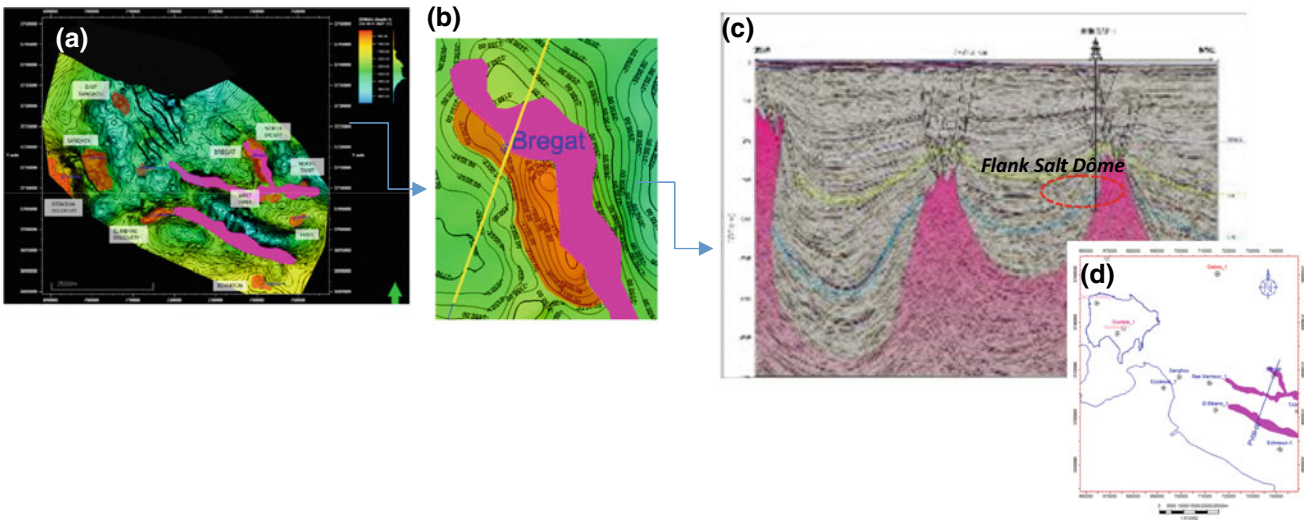

Fig. 4 **a** Zebbag Isobath map. **b** Bregat prospect. **c** Cross seismic section showing Bregat prospect. **d** Cross-section position

Generally, reflectors presented a good lateral continuity. Few shift problems exist between some seismic lines of different surveys. The shift was adjusted by using composite lines.

The calibration is performed using six wells: Tanit-1, Echemoun-1, Ras Marmour-1, Bregat-1, El Bibane-1, Sanghou-1.

4 Results

The study area is one of the most attractive petroleum potential in southern gulf of Gabes. The existence of productive oil fields (Ezzaouia, El Biban and Robbana), and the presence of the proven Callovian Source rock which is expected to be mature in this domain can be an asset to explore in this area.

Regional seismic profiles interpretation shows the evolution of salt from planar beds to nearly vertical structures that had contributed to the geodynamic evolution of Jeffara, where three stages model of dome growth were also identified: pillows, diapirs, and salt walls (Fig. 3). Indeed, each stage had distinctive effects on depositional facies, lithostratigraphy and thickness of surrounding sediments.

The seismic interpretation led to the identification of many good traps (leads and prospects) in vicinity of the salt complexes trending NW-SE and NNW-SSE (Fig. 4a).

5 Discussion

Halokinetic activity in the southern part of the Jeffara basin disclosed different salt structures, which affect the depositional facies, lithostratigraphy, and thickness of surrounding

strata. The least understood aspects of the Basin's geologic history reveal that the detected salt bodies at different stages of growth allow predicting subtle facies controlled hydrocarbon traps.

6 Conclusion

The study area is one of the most attractive petroleum potentials in southern gulf of Gabes. Our structural analyses integrated with seismic interpretation provided the identification of eight prospects which belong to the area.

References

1. Alsop, G.L., Archer, S.G., Hartley, A.J., Grant, N.T., Hodgkinson, R.: Salt Tectonics, Sediments and Prospectivity. Geological Society, London (2012)
2. Haddad, S., Sarsar, B., Asma, D., Salmouna, L.: Structural styles, salt tectonics and implications for hydrocarbon prospectivity in the Jeffara basin, Tunisia. AAPG, Salt Tectonics in Alpine Folded Belts —Spain, Granada (2018)
3. Khouni, R., Arfaoui, M.S., Dridi, S., Zargouni, F.: Polyphasic evolution of the Jeffara basin in southern Tunisia, influence of halokinesis on the passive margin structuration in the Mezosoic and the Cenozoic. Arab. J. Geosci. **11**(4), 11–68
4. Sarsar, B.: Chronology and structural evolution of Kerkena Island, Pelagian Platform, Tunisia. Rapport Interne, ETAP (2014)
5. Seni, S.J., Jackson, M.P.A.: Evolution of salt structures. East Texas Diapir Province, PART 1: sedimentary record of Halokinesis. AAPG Bull. **67**(8), 1245–1274 (1983)
6. Talbot, C.J.: Spreading of salt structures in the Gulf of Mexico. Tectonophysics **228**, 151–166 (1993)
7. Talbot, C.J., Pohjola, V.: Sub-aerial salt extrusions in Iran as analogues of ice sheets, streams and glaciers. Earth Sci. Rev. **97**, 155–183 (2009)
8. Touati, M.A., Rodgers, M.R.: Structural study of southern golf of Gabes, Zarzis/Gabes-Djerba-Ben Gardane Permits. Rapport interne, ETAP (1990)
9. Touati, M.A., Rodgers, M.R.: Tectono-stratigraphic history of the southern gulf of Gabes and the hydrocarbon habitats. In: Proceedings of the 6th Tunisian Petroleum Exploration and Production Conference, pp. 343–370 (1998)

Gas Hydrates Potential of Makran Area, Offshore Pakistan

Aamir Ali, Ihsan ul Haq, and Matee Ullah

Abstract

Gas hydrates are part of the unconventional energy resources called the gas clathrates. The present work focused on the assessment of gas hydrates potential of Makran area, Offshore, Pakistan. The presence of a clear bottom simulating reflector (BSR) is primary indicator for the occurrence of gas hydrates and generally referred to as base of gas hydrates stability zone. The gas hydrates zone in the study area was identified by the application of seismic attributes (sweetness, relative acoustic impedance and normalized apparent polarity) using major characteristics of BSR i.e. amplitude blanking, adopting the shape of seafloor, cross cutting the sedimentary structures and opposite polarity to seafloor. A low velocity layer was also interpreted beneath the hydrates layer due to the existence of free gas. Rock physics modelling for the two different geometrical distribution of hydrates was also applied to obtain effective elastic properties. The results of rock physics modelling showed that the hydrates as part of sediments have higher elastic properties compared to hydrates in pore spaces, and these properties were controlled by saturation of gas hydrates. Using the effective elastic properties, amplitude versus offset (AVO) forward modelling (Exact Zoeppritz + ray tracing) for different scenarios was performed to characterize the presence of BSR more efficiently.

Keywords

Gas hydrates • Unconventional resources • Bottom simulated reflection • Rock physics • AVO

1 Introduction

The ever-increasing demand for energy consumption requires a deep insight and search for all possible ways to fulfill it. There are numerous ways from which energy can be obtained. Currently, the natural gas and oil are amongst the most important sources of energy and are continuously exploited from both conventional and unconventional resources. Amongst these, the occurrence of methane gas in the form of gas hydrates (GH) is a prominent unconventional natural gas resource [1]. The existence of GH is limited to certain favorable thermobaric conditions. Generally, they are formed at continental margins or under permafrost covers. The worldwide estimated resources of GH are 2.1×10^{16} standard m^3 in the ocean sediments. The total offshore sources are twice the total energy of all other sources. The onshore resources of GH which are deposited under the permafrost layer are estimated to be about 7.4×10^{14} m^3 [2].

Geophysical exploration is one of the essential tools for the assessment of GH reservoirs by allowing us to image the GH containing deposits [3]. Most common geophysical techniques for detecting the GH and underlying free gas zone (FGZ) is the seismic reflection method [3]. In marine sediments, GH is identified by the presence of Bottom Simulating Reflector (BSR). BSR is referred as the base of GH system [3].

Response of reservoir properties as function of GH saturation can be achieved using several rock physics approaches, such as effective-medium modelling and three-phase Biot theory [4]. Changes in elastic properties across the BSR have promoted the scientific community to use amplitude versus offset (AVO) as an important tool to characterize GH. In marine environments, AVO analysis has traditionally been focused on estimating GH and FGZ related properties [5].

The objective of this paper is to evaluate the gas hydrates potential of the Makran area, offshore, Pakistan. The area is characterized by a well-known subduction zone between Eurasian and Arabian plates. The area hosts rocks of

A. Ali (✉) · I. ul Haq · M. Ullah
Quaid-i-Azam University, Islamabad, 45320, Pakistan
e-mail: aakgeo82@qau.edu.pk

N. Sundararajan et al. (eds.), *On Significant Applications of Geophysical Methods*,
Advances in Science, Technology & Innovation, https://doi.org/10.1007/978-3-030-01656-2_35

Paleocene–Pleistocene age including the Makran mud volcanoes [6]. The GH reserves in the areas have not been quantitatively estimated yet, but the BSR and underlying FGZ was observed in the offshore area of Makran at about 400 m beneath the seafloor in the single channel seismic profile acquired for testing purpose [7].

2 Data and Approach

The current research included two dimensional (2D) multi-channel seismic reflection data acquired by the Pak-German cruise (SONNE cruise SO-122; [7]). Different seismic attributes like sweetness, relative acoustic impedance and normalized apparent polarity were applied on seismic data to identify the characteristics of BSR using the approaches of [8]. Rock physics modelling for the two different geometrical distributions of GH were performed using Hill's approach detailed in [9]. The effective elastic properties were then used to perform AVO modelling (exact Zoeppritz solution for computation of reflection coefficients and ray tracing algorithm) on different scenarios [10, 11] to identify the formation of BSR and GH system classes.

3 Results

3.1 Seismic Interpretation

On multi-channel seismic reflection data BSR is the primary indicator of GH. A clear indication of BSR can be observed on seismic section presented in Fig. 1a, where a continuous reflector adopting the trend of seafloor with negative polarity marks the base of gas hydrate saturated zone. The results were further confirmed using seismic attributes like sweetness, relative acoustic impedance attribute and normalized apparent polarity. The choice of these attributes depends on the major characteristics of BSR as it exhibits high amplitude (sweetness), high relative acoustic impedance contrast, and negative polarity, respectively. The application of relative acoustic impedance (RAI) is shown in Fig. 1b.

3.2 Rock Physics Modelling for Gas Hydrates

Rock physics modelling provides the link between seismic and BSR properties. The results were obtained for two types of geometrical models of GH i.e. Model-A which considers that GH is present in the pore spaces, while Model-B considers that GH are part of the load bearing sediments. The predicted results of P- and S-wave velocities (*Vp* and *Vs*) as a function of GH saturation for different porosities in Model-B are presented in Fig. 2. The velocities show an increasing trend as a function of GH saturation.

3.3 AVO Modelling for Gas Hydrates

AVO forward modelling can help in quantitative assessment of BSR in the presence of varying GH saturation and free gas concentration. The reflection coefficient series was generated for both geometric models discussed in Sect. 3.2 considering different GH saturations. Model-B exhibits slightly negative AVO intercept and large gradient with the increase in concentration of GH as compared to Model-A (Fig. 3—Left). The corresponding synthetic AVO seismic data (forward modelling) is also presented for Model-B (Fig. 3—Right).

4 Discussion

As the BSR and the associated amplitude blanking are referred as the GH stability zone [5], therefore the seismic section was scanned for these spots of interest (Fig. 1a). The RAI attribute confirms the amplitude blanking above and below the BSR and a very low RAI free gas zone (GH zone; Fig. 1b). GH present in pore spaces only changes the fluid modulus, but when they are distributed within host rock, they alter the effective properties of rock. Our results show that the existence of GH causes an increase in saturated bulk modulus of unconsolidated sediments, which results in the form of higher seismic velocities (Fig. 2). AVO cross-plots and their synthetic modelling shows higher saturations of GH are responsible for more negative intercept and larger gradient of reflection amplitudes. Increasing free gas saturation below the BSR results in negative intercepts and larger AVO gradients than the water saturated sediments (Fig. 3).

5 Conclusion

In this study, the applications of seismic attributes, rock physics and AVO modelling were investigated for the characterization of GH zones at Makran area, offshore, Pakistan. Our seismic interpretation and attribute analysis confirmed the presence of BSR. Rock physics modelling showed large

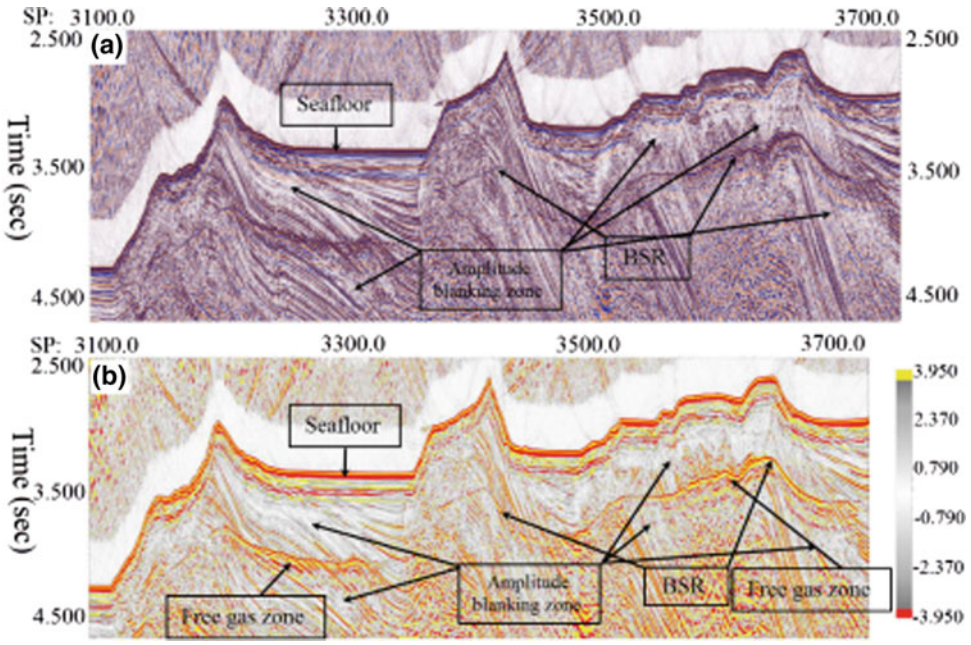

Fig. 1 Seismic section confirming the presence of BSR and free gas zone **a** seismic amplitude time section, **b** Relative acoustic impedance attribute time section

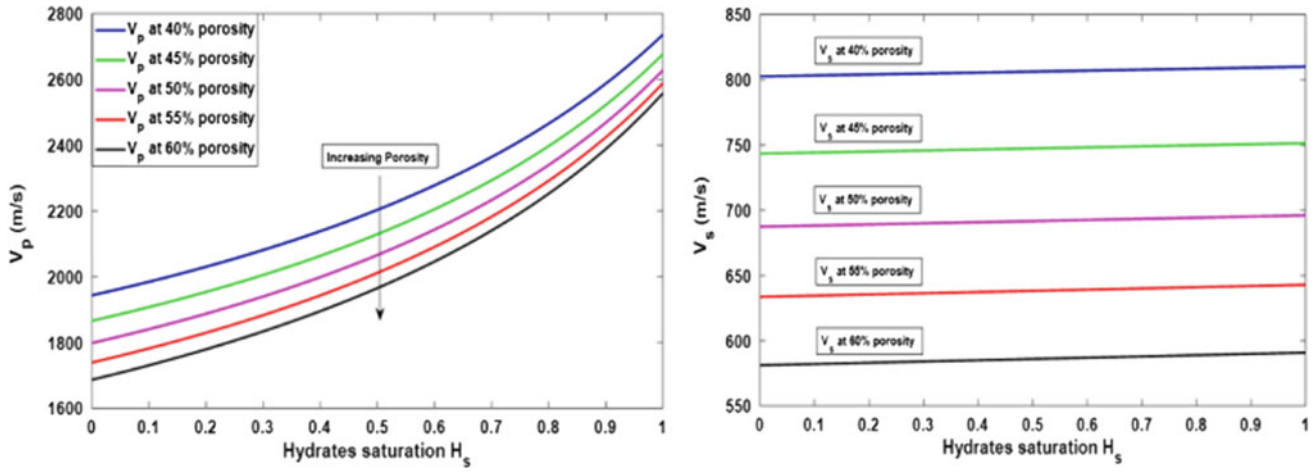

Fig. 2 *Vp* and *Vs* as a function of GH saturation for different porosities for Model-B

differences in elastic properties of GH and associating FGZ. The elastic properties increased in hydrates layer and abruptly decreased in underlying free gas region. AVO modelling showed that, higher saturations of GH are responsible for more negative intercept and larger gradient of reflection amplitudes. The presence of BSR is more pronounced when free gas is present. Furthermore, our AVO forward modelling results suggested that if GH were part of pore fluid then our area would have a potential of at least 50% GH with fully saturated sediments and if it were disseminated within the rock unit then the area under study would have a potential of at least 10% GH saturated sediments.

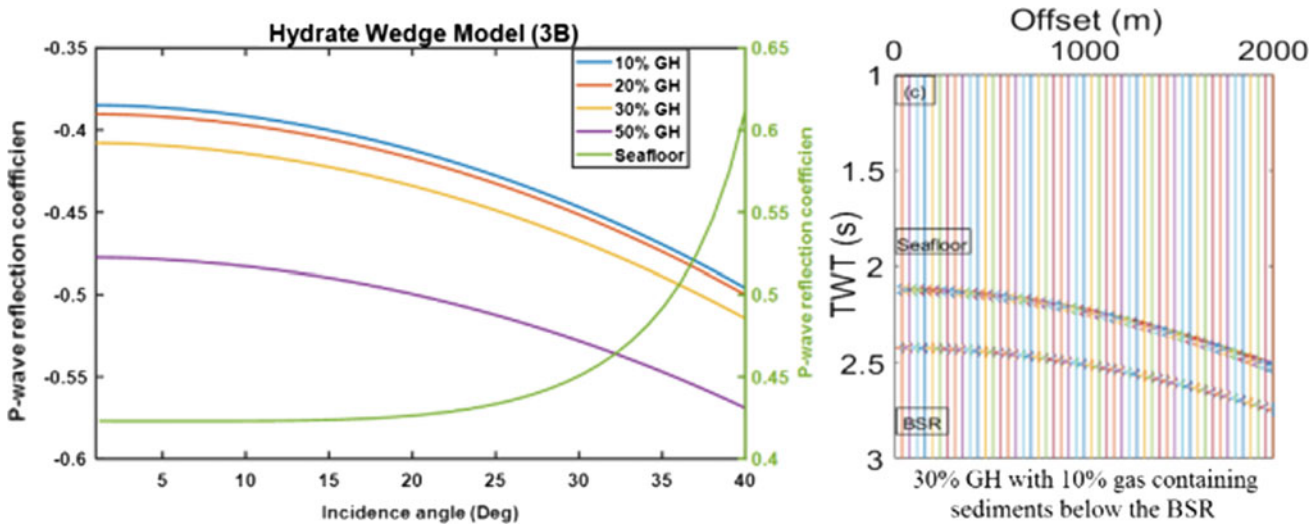

Fig. 3 Computed reflection coefficient for Model-B (left) and corresponding synthetic seismic data (right)

References

1. Johnson, H., Dore, A.G.: Unconventional oil and gas resources and the geological storage of carbon dioxide: overview. In: Geological Society, London, Petroleum Geology Conference series, vol. 7, issue 1, pp. 1061–1063. Geological Society of London (2010)
2. Aregbe, A.G.: Gas hydrate—properties, formation and benefits. Open J. Yangtze Oil Gas **2**(01), 27 (2017)
3. Riedel, M., Willoughby, E.C., Chopra, S. (eds.): Geophysical Characterization of Gas Hydrates. Society of Exploration Geophysicists (2010)
4. Chand, S., Minshull, T.A., Gei, D., Carcione, J.M.: Elastic velocity models for gas-hydrate-bearing sediments—a comparison. Geophys. J. Int. **159**(2), 573–590 (2004)
5. Chen, M.A.P., Riedel, M., Dosso, S.E.: Seismic AVO for gas-hydrate-related reflections. In: Geophysical Characterization of Gas Hydrates, pp. 73–93. Society of Exploration Geophysicists (2010)
6. Kadri, I.B.: Petroleum Geology of Pakistan. Pakistan Petroleum Limited (1995)
7. Roeser, H.A., Adams, J., Bargeloh, H.O., Block, M., Damm, V., Dohmann, H., Reichert, C., et al.: The Makran Accretionary Wedges off Pakistan: Tectonic Evolution and Fluid Migration-Part 1. SONNE Cruise SO-122 (7 Aug–6 Sept 1997). Operational Report and Preliminary Results: Published by BGR, Germany, 111 (1997)
8. Koson, S., Chenrai, P., Choowong, M.: Seismic attributes and their applications in seismic geomorphology. Bull. Earth Sci. Thai. **6**(1), 1–9 (2014)
9. Mavko, G., Mukerji, T., Dvorkin, J.: The Rock Physics Handbook: Tools for Seismic Analysis of Porous Media. Cambridge University press (2009)
10. Katzman, R., Holbrook, W.S., Paull, C.K.: Combined vertical-incidence and wide-angle seismic study of a gas hydrate zone, Blake Ridge. J. Geophys. Res. Solid Earth **99**(B9), 17975–17995 (1994)
11. Krebes, E.S.: Seismic forward modelling. CSEG Rec. **30**, 28–39 (2004)

A Model of Pore Pressure and Effective Stress Changes During Hydrocarbon Depletion by Slowness Integrated Data Analysis

Kurniawan Adha, Wan Ismail Wan Yusoff, and Luluan Almanna Lubis

Abstract

This paper focus on the use of slowness data analysis to identify and characterize the pore pressure and effective stress changes during oil field production, since the pore pressure estimation plays an important role in oil and gas industry. Pore pressure estimation is included in substantial prerequisite before taking a major step to start drilling, production or recovering a well. Moreover, the precise pore pressure estimation will determine the safety, profits and success in both production and recovery. To accomplish the objective of this study, the methodology consists of several broad stages. It dealt with field mapping to create stratigraphy model, coring/sampling, velocity measurement with saturations and pressures (i.e. pore and confining) variations, velocity analysis for constructing the empirical equation of pressure, saturation and pore pressure relationship in each facies, pore pressure and effective stress changes estimation model from interval velocity and transit time analysis. The pore pressure and effective stress changes model was established for characterizing the changes in pore pressure and effective stress due to hydrocarbon production. Variation in fluid saturation was considered to hydrocarbon production scenarios. During the reservoir production, the fluid flows out leading to a reduction in pore pressure. This reduction produced slowing seismic velocities and inversely to effective stress. The characterization of pore pressure and effective stress changes due to changes in fluids saturation linked to velocity anomalies can be useful in monitoring hydrocarbon production.

Keywords

Pore pressure • Effective stress • Hydrocarbon production • Overpressure mechanism • Velocity

1 Introduction

This study focus on the characteristics of pore pressure and effective stress changes during hydrocarbon depletion by integrating the slowness data analysis as the changes of factor from variances reservoir properties. Samples from outcrop inside the Miri formation were used in this analysis for representing the hydrocarbon reservoir [1–6].

Based on overpressure mechanism analysis in West Baram Delta, two overpressure mechanisms were characterized. Disequilibrium compaction or undercompaction could be identified in all wells whilst fluid expansion mechanism could not be determined in onshore area and area near proximal delta. According to this condition, this study was limited to pore pressure changes due to hydrocarbon production in disequilibrium compaction mechanism [7, 5, 8].

Characterize and investigate the pore pressure and effective stress changes through laboratory analysis with respect to the variance of overburden pressure, fluid saturation and temperature. Samples for variance porosity and permeability was used in laboratory analysis as sand reservoir representation and variance fluids saturation as hydrocarbon production representation was the main objective in this study.

2 Methodology

The model was developed using the response of velocity from variance of parameters including fluid saturation, confining pressure and pore pressure temperature, where the temperature data came from well data analysis. In normal pressure and disequilibrium compaction condition,

K. Adha (✉) · W. I. W. Yusoff · L. A. Lubis
Universiti Teknologi PETRONAS, Seri Iskandar, Malaysia
e-mail: kurniawanadhaa@gmail.com

W. I. W. Yusoff
e-mail: wanismail_wanyusoff@utp.edu.com.my

L. A. Lubis
e-mail: luluan.lubis@utp.edu.com.my

N. Sundararajan et al. (eds.), *On Significant Applications of Geophysical Methods*,
Advances in Science, Technology & Innovation, https://doi.org/10.1007/978-3-030-01656-2_36

temperature data were collected and plotted against confining pressure for determining the linear trend. The relationships between pressure and temperature were used in the laboratory analysis. The effective stress was determined using velocity analysis modified by Eaton equation and pore pressure was determined by direct calculation; (Overburden pressures minus effective stress) [6].

3 Pore Pressure, Effective Stress and Temperature Characterization and Models

This model was developed based on the response of velocity data to variance of pore pressure, fluids saturation and confining pressure. Several findings were obtained, such as (Fig. 1): (1) When the compaction confining pressure increased, the velocities tend to increase due to the increasing effective stress. (2) The decrease of pore pressure was caused by the reduction of fluid saturation as the function of hydrocarbon production and would lead to decrease P-wave velocities. (3) The decreasing saturation would reduce the pore pressure and tend to increase the effective stress and P-wave velocities.

This was an enhanced model from the previous one as it elaborated all the parameters to characterize the pore pressure and effective stress changes due to hydrocarbon production. Temperature and P-wave velocities response were applied to develop the model. Based on the model, the conclusion was determined, which means that during the compaction, the overburden pressure increased due to compaction and led temperature and effective stress to increase. This condition developed the high P-wave velocities. Another condition, due to hydrocarbon production the pore pressure was depleted due to loss of fluids inside the formation. The depletion of pore pressure tend stress to increase to cause the effective stress to increase and produce high P-wave velocities.

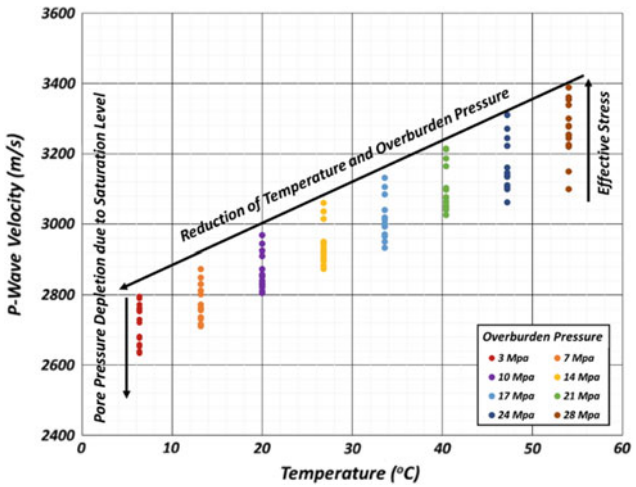

Fig. 1 The model of pore pressure and effective stress changes with saturation and temperature. Based on this model, increasing the confining pressure would lead to increase the effective stress and temperature and reducing of pore pressure due to hydrocarbon production that would lead to produce high velocities

4 Conclusion

Generally, the model was well-determined and established for characterizing the pore pressure and effective stress changes due to hydrocarbon production. In basic definition, the pore pressure was affected by hydrocarbon production. Variance of fluid saturation defined the hydrocarbon production scenarios. During the production, the fluid inside the formation pushes out leading to make the reduction of the pore pressure. This reduction produced low velocities and contradicted the effective stress. Unfortunately, this model was limited to disequilibrium compaction only, because of the lack of direct temperature data and the difficulty to map the temperature behavior in fluid expansion mechanism.

Consider the models the pore pressure changes can be analyzed and predicted for development of oil field purposes. Considering the changes of pore pressure, the accuracy of pore pressure prediction is very influential to safety and economic drilling with respect to the reservoir condition (normal pressure or overpressure zone). Determining overpressure zone is necessary for the petroleum industry because drilling into overpressure zone can be very risky and hazardous, hence fluids from this zone can escape rapidly. Specifically, an accurate determination of pore pressure has useful purposes for assisting drilling engineers in planning mud program and casing design in anticipated high overpressure zone and preventing a variety of drilling hazards, i.e. wellbore collapse, loss of circulation, stuck pipe and other possibilities.

In addition, the characterization of pore pressure and effective stress changes are due to the close relationship between hydrocarbon production and velocities anomalies that can be used in rock physic studies. The rock physics is the bridge between geophysics and geology. In fact, this area tried to quantify the seismic values based on its reservoir properties. Additionally, this model can be used for predicting 4D seismic after production and AVO analysis for a better hydrocarbon prediction. Since this model provides the variances of velocities response due to saturation, pore pressure, overburden pressure and temperature, it can be used to predict the next target and distinguish the reservoir variation due to its complexity

Acknowledgements The authors express their gratitude to Universiti Teknologi Petronas (UTP) for providing laboratory facilities and financial assistance to this study.

References

1. Singh, V., Yemez, I., Sotomayor, J.: Key factors affecting 3D reservoir interpretation and modelling outcomes: industry perspectives. Brit. J. Appl. Sci. Technol. **3**(3), 376–405 (2013)
2. Nweke, F., Dosunmu, A.: Analytical model to predict pore pressure in planning high pressure, high temperature (HPHT) wells in Niger Delta. Int. J. Eng. Sci. **2**(8), 50–62 (2013)
3. Swarbrick, R., Lahann, R., O'Connor, S., Hoskins, E.: Limitations of seismic pore pressure prediction—what is the alternative. In: 75th EAGE Conference & Exhibition Incorporating SPE EUROPEC (2013)
4. Zhang, J.J.: Effective stress, porosity, velocity and abnormal pore pressure prediction accounting for compaction disequilibrium and unloading. Mar. Petrol. Geol. **45**, 2–11 (2013)
5. Yussoff, W.I.W.: The study in Malaysia sedimentary basin. In: CCOP-ASCOP Workshop. Technical Paper 21 (1990)
6. Adha, K., et al.: Characteristics of pore pressure changes due to hydrocarbon production by velocity analysis approach. Presenting at the ICIPEG 2016: International Conference on Integrated Petroleum Engineering and Geoscience, 15–17 Aug 2016. Published on Springer 2017
7. Petroliam Nasional Berhad: The Petroleum Geology and Resources of Malaysia. International standard book number: 983-9738-10-0 (1999)
8. Tingay, M.R., Hillis, R.R., Swarbrick, R.E., Morley, C.K., Damit, A.R.: Origin of Overpressure and Pore-Pressure
9. Pandey, R.A.: Analysis of pore pressure—predrill tool in operation geology. Int. J. Adv. Earth Sci. Eng. **6**(1), 548–556 (2017)

Pre-drill Pore Pressure Estimation in Shale Gas Reservoirs Using Seismic Genetic Inversion: Application to Barnett Shale (USA)

Sid-Ali Ouadfeul and Leila Aliouane

Abstract

In this paper, a new formula of pore pressure derived from the Eathon's model was proposed, relating the acoustic impedance to the pore pressure. The acoustic impedance is obtained from the seismic inversion. The proposed process was applied for the estimation of the pore pressure in the Lower Barnett shale. The results demonstrate a lateral variation of the pore pressure and it can be used for well-bore stability and hydraulic fracture planning and simulation.

Keywords

Shale gas • Pore pressure • Eaton's model • Seismic • Inversion

1 Introduction

Pore pressure estimation is an important step in oil and gas exploration. Pore pressure maps and profiles are mandatory for well-bore stability, drilling and reservoir stimulation. Many models were proposed in literature to estimate the pore pressure. For example Zhang [9], reviewed the fracture gradient prediction methods, and proposed the minimum and maximum fracture pressures. Sayers et al. [6] published a paper about the Predrill pore pressure prediction using seismic data. Sayers et al. [8] published another paper about Well-constrained seismic estimation of pore pressure with uncertainty. Here, we suggest a method of pore pressure prediction from seismic data derived from the Eaton's model. Let us start by describing the proposed method.

S.-A. Ouadfeul (✉)
University of Khemis Miliana, Khemis Miliana, Algeria
e-mail: ouadfeul77@gmail.com

L. Aliouane
Laboratoire Physique de la Terre (LABOPHYT), Faculté des Hydrocarbure et de la Chimie, Université M'hamed Bougara de Boumerdes, Boumerdes, Algeria

2 Methods and Application to Barnett Shale

2.1 Geological Setting

The Barnett Shale was deposited over what is known in the present day as North Central Texas, during the late Mississippian Age with marine transgression caused by the closing of the Iapetus Ocean Basin. By the end of the Pennsylvanian the Ouachita Thrust belt began encroaching into the present day North Texas area. The thrust belt owes its existence to the subduction of the South American plate under the North American plate The Ouachita Thrust emergence created the foreland basin along the front of the thrust. Early studies of the basin attributed thermal maturation of the Barnett to burial history and the thermal regimes associated with depth of burial. Explorationists began to doubt this hypothesis as more data became available. Bowker [3] proposed a different model suggesting the maturation process was driven by displacement of hot fluids, from east to west, associated with the Ouachita Thrust [1].

2.2 Methods

The Eaton's model [2, 4] is usually used for the estimation of the pore pressure. Eaton's [4] method estimates the vertical component of the effective stress from the seismic velocity V by the flowing equation:

$$\sigma = \sigma_{Normal}\left(\frac{V}{V_{Normal}}\right)^{n}$$

σ_{Normal} and V_{Normal} are the vertical effective stress and seismic velocity expected if the sediment is normally pressured, and n is an exponent that describes the sensitivity of velocity to effective stress, n = 1.2.

N. Sundararajan et al. (eds.), *On Significant Applications of Geophysical Methods*,
Advances in Science, Technology & Innovation, https://doi.org/10.1007/978-3-030-01656-2_37

The pore pressure is then given by:

$$p = S_v - \left(S_v - p_{Normal)}\right) * \left(\frac{V}{V_{Normal}}\right)^n$$

To use Eaton's method, the deviation of the measured velocity from that of normally pressured sediments (V_{Normal}) with depth is given by:

$$V_{Normal} = V_0 + K * y$$

where V_0 and K are constants related to the formation, y is the depth.

A linear fit of the velocity of the P wave versus the depth of Barnett shale well-logs data provided the following values of V_0 and K

$$V_0 = 9656 \text{ ft/s}, \quad K = 0.89$$

If we suppose that Z is the acoustic impedance of the P wave, Z is the product of the velocity of the P wave and the density.

$$Z = \rho * V$$

Based on the Gardner's model [5] density is related to velocity by a power law:

$$\rho = a * V^b$$

where a and b are constants related to lithology. A linear fit of log density versus log velocity of the P wave of well-logs data of a horizontal well drilled in the Lower Barnett shale formation provides the following values:

$$a = 1.22, \quad b = 0.69$$

So, the acoustic impedance is related to the Velocity of the P wave V by:

$$Z = a * V^{b+1}$$

By consequence the velocity of the P wave is related to the acoustic impedance by:

$$V = \left(\frac{Z}{a}\right)^{\frac{1}{b+1}}$$

The Pore pressure of a normally pressured formation is given by:

$$p_{Normal} = y * Grad_{Pp}$$

where y is the depth and $Grad_{Pp}$ is the pore pressure gradient which is equal to 0.52 psi/ft in the Barnett shale after [3].

The vertical stress in a normally pressured formation at a depth y is given by:

$$S_v = \int_0^y \rho * g dy \tag{1}$$

where y is the depth, ρ is the density and g = 9.81 m/s^2 is the gravity field.

Including all these equations and parameters, the pore pressure can be derived from the acoustic impedance using the following equation:

$$p = S_v - \left(S_v - p_{Normal)}\right) * \left(\frac{\left(\frac{Z}{a}\right)^{\frac{1}{b+1}}}{(V_0 + K * y)}\right)^n \tag{2}$$

$$p = \int_0^y \rho * g dy - \left(\int_0^y \rho * g dy - y * Grad_{Pp}\right) * \left(\frac{\left(\frac{Z}{a}\right)^{\frac{1}{b+1}}}{(V_0 + K * y)}\right)^n \tag{3}$$

where n = 1.2 [4].

The Acoustic Impedance Z is obtained from the seismic genetic inversion using the Multilayer Perceptron neural network (Fig. 1).

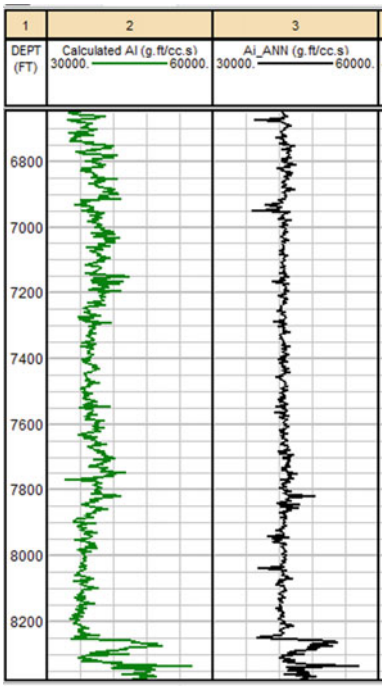

Fig. 1 A comparison between the calculated acoustic impedance (AI) using the density and the sonic logs for a borehole and the inverted AI near the same borehole

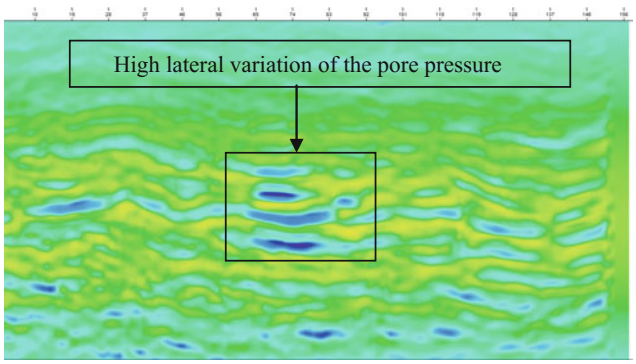

Fig. 2 Estimated pore pressure using the proposed method near the horizontal used for the seismic inversion in the Lower Barnett

3 Results

The obtained results of the application of the proposed technique to the data of the Lower Barnett shale formation confirm that the proposed model is able to provide good results (see Fig. 2). However we can observe that the estimated pore pressure does not have an exponential variation in some areas like the hydrostatic model. Also, some depth intervals have a high lateral variation of the pore pressure, which can be due to the natural fractures distribution and pore pressure. Consequently, the proposed model can be adequately used for shale gas reservoirs, geo-mechanic of the shale plays, wellbore stability and hydraulic fracking simulation and planning.

References

1. Aliouane, L., Ouadfeul, S.: Sweet spots discrimination in shale gas reservoirs using seismic and well-logs data. A case study from the Worth Basin in the Barnett Shale. Energy Procedia **59**, 22–27 (2014)
2. Bowers, G.I.: Pore pressure estimation from velocity data: accounting for pore pressure mechanisms besides undercompaction. SPE Drill. Complet. **10**, 89–95 (1995)
3. Bowker, K.A.: Barnett Shale gas production, Fort Worth Basin: issues and discussion. AAPG Bull. **91**(4), 523–533 (2007)
4. Eaton, B.A.: The equation for geopressure prediction form wells logs. In: SPE, 5544 (1975)
5. Gardner, G.H.F., Gardner, L.W., Gregory, A.R.: Formation velocity and density—the diagnostic basics for stratigraphic traps. Geophysics **39**, 770–780 (1974)
6. Sayers, C.M., Johnson, G.M., Denyer, G.: Predrill pore pressure prediction using seismic data. Geophysics **67**, 1286–1292 (2002)
7. Sayers, C.M., den Boer, L.D., Nagy, Z.R., Hooyman, P.J.: Well-constrained seismic estimation of pore pressure with uncertainty. Lead. Edge, pp. 1524–1526 (2006 Dec)
8. Zhang, J., Yin, S.X.: Fracture gradient prediction: an overview and an improved method. Pet. Sci. **14**(4), 720–730 (2017)

Petrophysical Characterization of Upper Permian Reservoir in Southern Tunisia

Thamer Balti, Imen Hamdi Nasr, and Mohamed Hédi Inoubli

Abstract

The Paleozoic series in southern Tunisia were affected by tectonic activities that generated reservoir structures. Petrophysical parameters show that Upper Permian carbonates have a poor reservoir quality due to diagenetic processes, the lack of hydrocarbon can be explained by the erosion of such Silurian, Devonian and Permian source rocks related to Caledonian and Hercynian orogenesis.

Keywords

Stratigraphic 3D model • Seismic data • Well log signatures • Upper Permian • Tebaga Formation • Carbonate reservoir

1 Introduction

During late Permian to Quaternary, the dynamic evolution of southern Tunisia has experienced several stages. Each stage was characterized by a specific structure, due to the paleogeographic evolution of the West Tethyan and Mediterranean margin [1–4]. The study area is favorable for oil exploration. Indeed, it is located in a Paleozoic basin where authors have reported the presence of reservoirs and source rocks from different ages (Silurian Tannazuft Formation–Devonian and Permian clay) expected to have expelled hydrocarbons [5].

T. Balti (✉) · I. H. Nasr · M. H. Inoubli
Research Unit of Applied Geophysics, University of Carthage, 7021 Jarzouna, Tunisia
e-mail: baltithamerst@gmail.com

T. Balti · I. H. Nasr
Faculty of Sciences of Bizerte, University of Carthage, 7021 Jarzouna, Tunisia

T. Balti · M. H. Inoubli
Faculty of Sciences of Tunis, University of Tunis El-Manar, 1060 Tunis, Tunisia

2 Materials and Methods

In this work, the structural and geodynamic study was achieved based on oil wells and seismic data to build a 3D model that presents the geometrical evolution and geological structures of the study area.

The petro-physical evaluation of the Permian reservoir was carried out using the logging data.

3 Results

3.1 Stratigraphic 3D Model

Stratigraphic 3D model study, that represents geometry evolution of crossed formations shows that the east side was affected by a set of E-W normal faults 'F1' affecting the Lower Permian series, Carboniferous and even Ordovician Sanrhar Formation. A second set of faults 'F2' with normal offset directed to the south has induced a collapse of the Murghabien Tebaga Formation. A third set of normal faults 'F3' with E-W direction was active at least from the lower Permian to the Upper Permian (Tebaga formation) and induced the collapse of blocks toward the north, this fault reactivated during the Triassic. The geometry of Permian displays a monoclinal structure.

The west side of the basin (Fig. 1) shows a graben structure as a result of NW-SE normal faults with offsets toward the SW and of E-W fault with offsets toward the north; these two faults sets were active from Upper Carboniferous to Murghabien.

NW-SE normal faults recognized across the northern part of the study area, induced the collapse of Permian and Carboniferous series toward the NE, it favors slimming of several layers to the West, of Triassic to lower Cretaceous series.

The southern part of the basin shows, a normal fault with westward offset affecting the Zoumit and Tiguentourine

N. Sundararajan et al. (eds.), *On Significant Applications of Geophysical Methods*,
Advances in Science, Technology & Innovation, https://doi.org/10.1007/978-3-030-01656-2_38

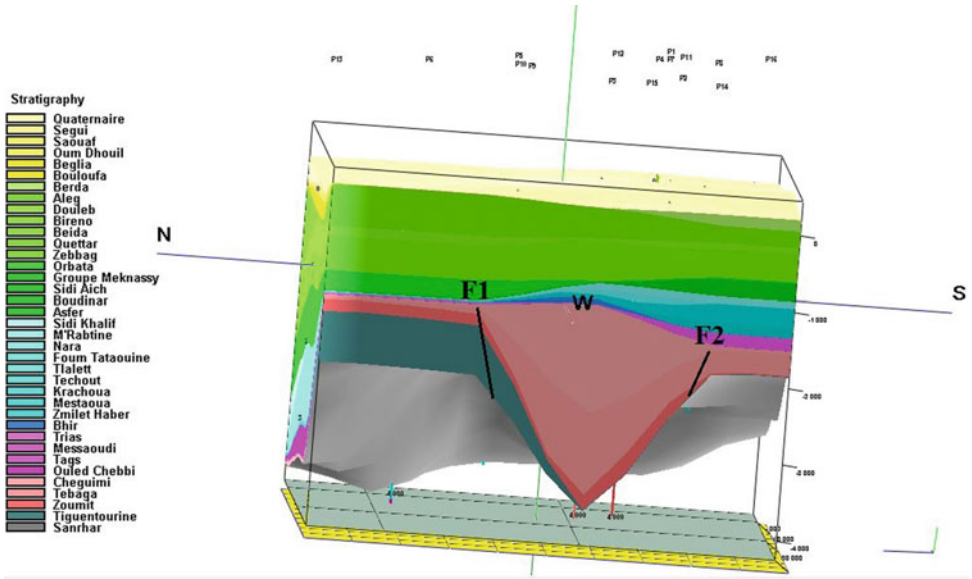

Fig. 1 West side of the 3D stratigraphic model

Formations. A second fault detected, with normal offset oriented NNE and NNW-SSE, affects the Tebaga Formation. A third fault probably affected the southern side of the basin, during the Triassic induced with an offset oriented toward the WNW.

3.2 Petrophysical Characterization

Interpretation of well log signatures (5 wells) allowed for a division of the Tebaga Formation into four distinct units TM1, TM2, TM3 and TM4. The TM1 units characterized by high values of GR and sonic, while TM2 and TM3 had the lowest values of GR (Fig.2) and sonic, TM4 is made up of clay and marls. The petro-physical parameters evaluation of the studied wells show that TM2 unit was characterized by low porosity between 11 and 13%, low clay content resulting in a clay volume which does not exceed 25% and a very low permeability (Fig. 2).

TM3 unit is characterized in the majority of the wells by a very low clay content that does not exceed 14%, with a porosity ranging from 12 to 15% and permeability between

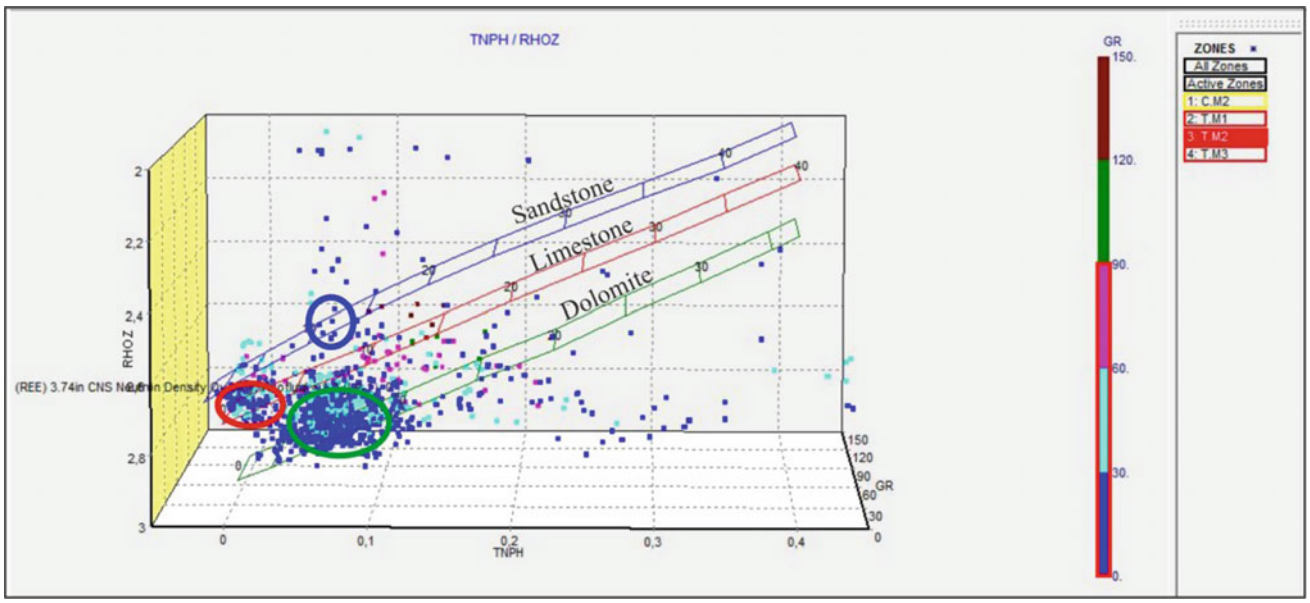

Fig. 2 TM2 lithology

0.08 and 1 MD, which shows medium reservoir quality. ‘SW values between 80 and 100%. Getting closer to the Baguel permit, the western part of study area shows that TM3 unit is characterized by good porosity, which reaches 20% with a net pay of 36.73 m, and water saturation does not exceed 30% showing hydrocarbon index.

4 Discussion

The 3D model shows the presence of normal Synsedimentary faults to the Upper Permian related to a NE-SW extension [3]. The tectonic activity that affected the Permian carbonate series generated tilted blocks and faulted anticlines forming traps structures [6].

Tectono-sedimentary analysis showed the existence of a system of synsedimentary normal faults, trending from N150 to N180 related to a N045 extension (Fig.3) (southern part of the 3D model).

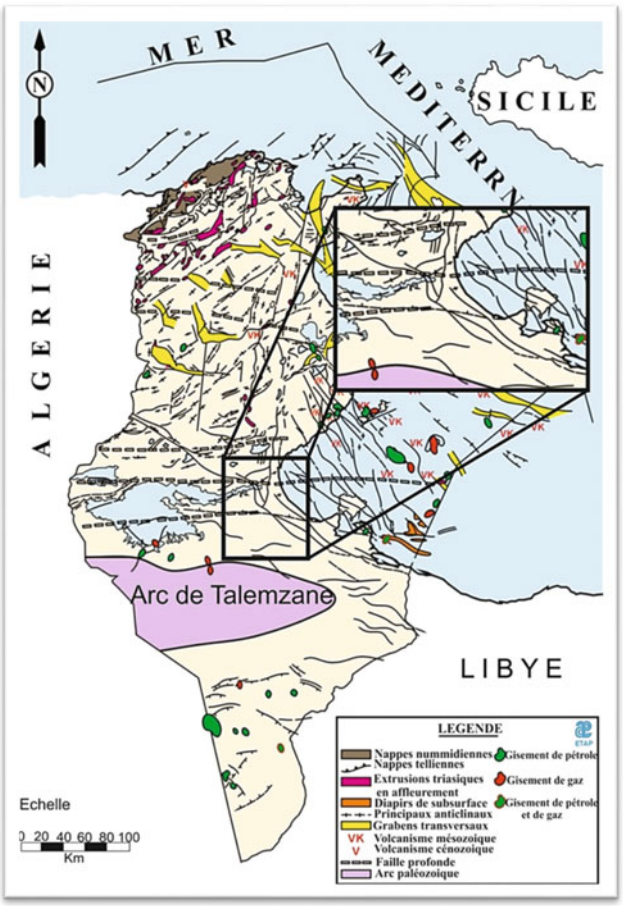

Fig. 3 Structural setting

The petro-physical parameters show a poor reservoir quality, low porosity and permeability values related to the diagenetic processes which affect the carbonate reservoirs of the Upper Permian (Tebaga Formation).

The absence of hydrocarbon can be explained by the erosion of Silurian and Devonian source rocks caused by Caledonian and Hercynian orogenesis.

5 Conclusion

A 3D Stratigraphic model and seismic data showed that Upper Permian carbonates (Tebaga Formation) were affected by normal faults with NW-SE, E-W and N-S directions, linked to a NE-SW extension (N045). This extensional tectonic activity generated tilted blocks, faulted anticlines and horst forming trap structures.

Petrophysical parameters of the Permian carbonate reservoirs show poor qualities for such reservoirs, which displayed, however, aquifer characteristics of these carbonate deposit. Lack of hydrocarbons demonstrate that the Paleozoic oil system was not efficient in the majority of studied blocks. This absence may be due to the effect of the Hercynian and Caledonian orogenesis, which caused the erosion of several source rocks in southern Tunisia (Silurian, Devonian and Permian source rocks).

References

1. Ben Ayed, N.: Evolution tectonique de l’avant-pays de la chaine alpine de Tunisie du début, du Mésozoïque à l’actuel. Ph.D. thesis, Paris Sud, Orsay; 286 p (1986)
2. Bouaziz, S: La déformation dans la plate-forme du sud Tunisien (Dahar et Jeffara): approche multiscalaire pluridisciplinaire. Ph.D. thesis Univ., Tunis ll, FST, 120 (1986)
3. Bouaziz, S.: Etude de la tectonique cassante dans la plate-forme et l’Atlas saharien (Tunisie méridionale): évolution des paléochamps de contraintes et implications géodynamiques. Thèse es Sciences; Univll, 485 (1995)
4. Touati, M.A., Rodgers, M.R.: Tectono-stratigraphic history of the southern Gulf of Gabes and the hydrocarbon habitats. In: Proceeding of the Sixth Tunisian Petroleum Exploration and Production Conference, May 1998, pp. 343–370 (1998)
5. Ben Ferjani, A., Burollet, P.F., Mejri, F: Petroleum Geology of Tunisia. E.T.A.P., 164 p (1990)
6. Ben Ayed, N., Khessibi, M.: Sur l’évolution géodynamique de la Jeffara Tunisienne au cours du Mésozoïque. Notes. Serv. Géol. Tunisie **47**, 41–54(1983)

Part VII

Earthquake Seismology and Seismic Hazard Assessment

Influence of Himalayan Topography on Earthquake Strong Ground Motions

Anjali C. Dhabu and S. T. G. Raghukanth

Abstract

The present paper analyzes the effect of Himalayan topography on the characteristics of ground motions due to large earthquake events. A spectral finite element model is developed to simulate ground motions for two past Himalayan earthquakes viz. 2005 Chamoli earthquake and 2011 Sikkim-Nepal border earthquake. The simulations are carried out twice; in the first set of ground motion simulations, Himalayan topography is considered while a flat terrain is considered in the second set. It is observed that the recorded displacements and velocities for the two earthquakes show a good comparison with the simulations carried out considering Himalayan topography as compared to results for flat terrain. This observation affirms that ground motions on mountains are higher compared to those on flat terrains. Also, as the Himalayan region is a complicated cluster of several ridges and valleys, there is a need to define amplification factors specifically for this Himalayan region.

Keywords

Earthquake ground motion • Himalayan topography • Amplification

1 Introduction

The Himalayan region of the Indian subcontinent has witnessed a number of great earthquakes in the past. Increasing population and migration have multiplied the number of residents in the cities located in the Himalayas over the last few decades. One great earthquake in this region in the near future can cost thousands of lives and huge economic losses. Proper design of structures resistant to earthquakes is therefore very important in this region. The earthquake resistant design forces are estimated from peak ground motions which are characterized by the earthquake source, the medium of wave propagation and topography of the region. The topography, ridge or valley, of a region can amplify or weaken the earthquake ground motions depending upon the type and gradient of the topography and its location with respect to the source [1]. Analytical and numerical studies are available in literature which provide amplification ratios for ground displacements [2, 3]. However, these amplification ratios are not generalized and are specific to particular types of topographies subjected to P-SV or SH wave propagation. The Himalayan topography is too undulating and cannot be characterized as a single ridge or valley profile. Also, in a real earthquake, the topographic region will be subjected to a combination of P-SV and SH waves. Therefore, there is a need to estimate expected amplification ratios for both displacement and velocity to obtain design forces for the Himalayas. As an initial step to this work, in the present paper, a finite element model is developed in SPECFEM [4] such that it accounts for the topography and the material properties of the region. In SPECFEM, the region under consideration is first discritized into non-overlapping hexahedral elements, the functions of which are represented by High degree Lagrange interpolant. The control points needed to define polynomial of order n is $(n+1)^3$ Gauss–Lobatto–Legendre (GLL) points per element. Thereafter, each of these elements are mapped to a reference cube using Jacobian matrix ensuring non-singularity particularly for boundary elements. The stability of numerical simulation is ensured by Courant–Friedrichs–Lewy condition, according to which, the maximum time step should always be less than the time taken by the wave to travel through the smallest element. Finally, the equation of motion for all the elements is assembled to form the global equation of motion as:

$$\mathbf{M}\ddot{u} + \mathbf{C}\dot{u} + \mathbf{K}u = \mathbf{F} \tag{1}$$

A. C. Dhabu (✉) · S. T. G. Raghukanth
Civil Engineering Department, Indian Institute of Technology, Madras, India
e-mail: anjalidhabu@gmail.com

N. Sundararajan et al. (eds.), *On Significant Applications of Geophysical Methods*,
Advances in Science, Technology & Innovation, https://doi.org/10.1007/978-3-030-01656-2_39

where **M** is the global mass matrix, **C** is the global damping or absorbing boundary matrix, **K** is the global stiffness matrix, **F** represents the force or the source term and u is displacement. The method uses the Newmark β integration method to march forward in time. The detailed description of the method can be found in literature [4]. In the present work, SPECFEM3D Cartesian package, a collection of FORTRAN subroutines, is used to simulate ground motions. The simulations are performed using parallel programming based on message-passing interface (MPI) in Rocks6.1 (Emerald Boa) Cluster with AMD opteron (TM) processor installed with Centos6.3 operating system. The present paper develops a model in SPECFEM 3D to simulate ground motions for two past earthquakes viz 2005 Chamoli earthquake and 2011 Sikkim-Nepal border earthquake. The next section discusses the parameters of developed model and obtained results in detail.

2 Ground Motion Simulations for Past Earthquakes

Ground motions are simulated for two past earthquakes viz. 2005 Chamoli earthquake with moment magnitude, M_w 5.2 and 2011 Sikkim-Nepal border earthquake with M_w 6.8. These two earthquakes were chosen due to the fact that recorded ground motion data is available in the surrounding region of the respective epicenters. Also, the recording stations for both the earthquakes are located at different altitudes which ensure that the effect of adjoining topography is captured in the recorded ground motions. Ground motions were simulated for two cases for each of the two earthquakes. In the first case the undulating Himalayan topography of the adjoining region is taken into consideration while in the second case the topography is not considered i.e. the adjoining region is modeled as a flat terrain. These two cases are considered in order to compare the ground motions simulated in the case of flat terrain model with that of model incorporating an undulating topography.

The epicenter of 2005 Chamoli earthquake is located at 30.9°N, 79.3°E at a focal depth of 25.7 km. According to PESMOS data, the strike angle for the fault plane is 117°, the dip angle is 67° and the rake angle is 92°. As the earthquake is of moderate magnitude, point source is considered to simulate ground motions. The epicenter of 2011 Sikkim-Nepal border earthquake is located at 27.73°N and 88.15°E at a focal depth of 50.5 km. The strike, dip and rake angle for the earthquake are 217°, 70° and 10° respectively. The source parameters for both earthquakes are summarized in Table 1. The material properties for Himalayas are deliberated as per Table 2.

The broad band seismometer network established by Department of Earthquake engineering, IIT Roorkee recorded ground motions in 8 stations for the Chamoli earthquake and at 13 stations for 2011 Sikkim-Nepal border earthquake. Ground motions are simulated at all these stations for both the cases for the two earthquakes under consideration. The simulated ground motions for both cases are compared with the recorded data. For the purpose of brevity, the comparisons of simulated and recorded velocity for 2005 Chamoli earthquake are shown for 3 stations in Fig. 1. The three stations Champawat, Roorkee and Rudraprayag are located at an elevation of 1621, 253 and 638 m from the mean sea level. The figure depicts comparison between recorded ground motions with that of ground motions simulated considering topographic profile. It is interesting to observe that the recorded data matches well with simulated ground motions considering Himalayan topography. However, slight differences in the magnitude and frequency can be attributed to the material properties and source parameters.

Table 1 Source parameters for 2005 Chamoli and 2011 Sikkim-Nepal border earthquake

Source parameters	2005 Chamoli earthquake	2011 Sikkim-Nepal border earthquake
Moment magnitude, Mw	5.2	6.9
Latitude (°)	30.9	27.73
Longitude (°)	79.3	88.155
Depth (km)	25.7	50.5
Strike angle (°)	117	217
Dip angle (°)	67	70
Rake angle (°)	92	10
Dimensions of fault (L × W) (km)	Point source is considered	43 × 28

Table 2 Material properties in the Himalayan region [5]

Depth (km)	V_p (km/s)	V_s (km/s)	Density (gm/cm^3)	Q_p	Q_s
0–0.4	3.5	2.00	1.8	50	25
0.4–1.0	5.0	2.86	2.40	80	50
1.0–15.0	5.2	2.97	2.6	4000	2000
15.0–30.0	6.0	3.43	2.90	4000	2000
>30.0	8.33	4.83	3.30	1000	500

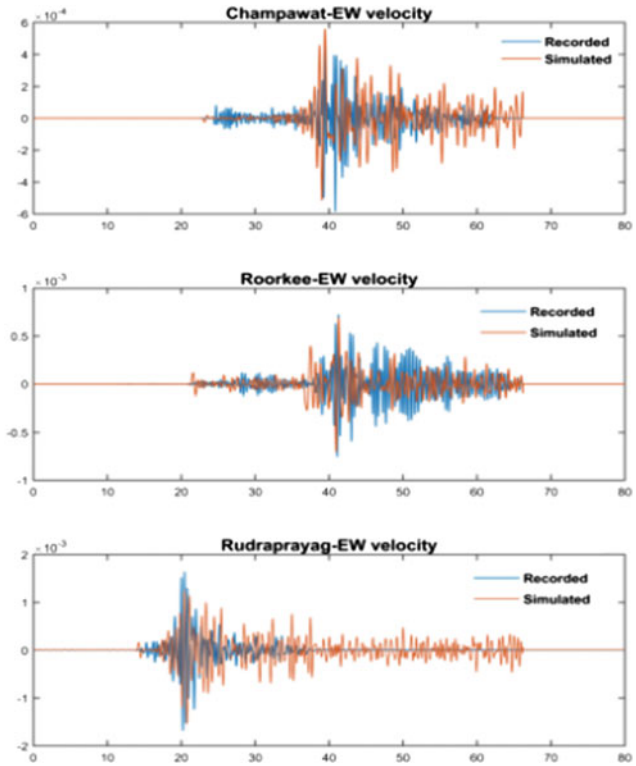

Fig. 1 Comparison of recorded and simulated ground motions for 2005 Chamoli earthquake

3 Conclusion

The paper analyzes the effect of Himalayan topography on earthquake ground motions. A spectral finite element model is developed taking into consideration the undulating topography and material properties of the Himalayas. The developed model is used to simulate ground motions for two past earthquakes viz. 2005 Chamoli earthquake and 2011 Sikkim-Nepal border earthquake. The simulated ground motions show good comparison with the recorded data. Also, it is observed that, the peak ground motions would be under-estimated if topography is ignored in the model. The present work will be extended to obtain amplification factors for a large hypothetical earthquake in Himalayas considering topography effect.

References

1. Dhabu, A., Dhanya, J., Raghukanth, S.T.G.: Effect of topography on earthquake ground motions. Recent Advances in Structural Engineering, vol. 2 (2018). ISBN: 978-981-13-0364-7
2. Bouchon, M., Barker, J.S.: Seismic response of a hill: the example of Tarzana, California. Bull. Seismol. Soc. Am. **86**(1A), 66–72 (1996)
3. Bouchon, M.: Effect of topography on surface motion. Bull. Seismol. Soc. Am. **63**(2), 615–632 (1973)
4. Komatitsch, D., Tromp, J.: Introduction to the spectral element method for three-dimensional seismic wave propagation. Geophys. J. Int. **139**(3), 806–822 (1999)
5. Yu, G., Khattri, K.N., Anderson, J.G., Brune, J.N., Zeng, Y.: Strong ground motion from the Uttarkashi, Himalaya, India, earthquake: comparison of observations with synthetics using the composite source model. Bull. Seismol. Soc. Am. **85**(1), 31–50 (1995)

The 13th-August-1822 Aleppo Earthquake: Implications for the Seismic Hazard Assessment at the Antakia Triple Junction

Ryad Darawcheh, Mohamad Khir Abdul-wahed, and Adnan Hasan

Abstract

The analysis of historical sources of macroseismic data based on different written languages, original and near contemporary sources for the 13th August 1822 earthquake that hit the *Pachalic* of Aleppo in northwestern Syria, the region that includes three regional active faults, reveals the following results: (1) the main event which occurred on 13th August 1822, caused heavy destruction with more than 10,000 lost lives in Aleppo city, and numerous towns and villages were destroyed; (2) the St. Simeon fault with 140 km long was suggested to be the causative fault of the event; (3) the earthquake parameters along with peak ground acceleration in the citadel of Aleppo were assessed according to the macroseismic data. The focal mechanism of the earthquake was estimated to be a strike-slip movement on that fault according to field investigations and the historical documents.

Keywords

Aleppo • Earthquake of 1822 • Sources of information • Syria

1 Introduction

Studying the historical earthquakes is one of the valuable investigations for understanding the active tectonics in the context of seismo-tectonic hazard assessment. This work deals with one of the most destructive earthquakes that hit Aleppo city and its surroundings in the 19th century. The earthquake of 1822, which was studied here, is one of the main events representing the seismic behavior of the Dead Sea fault system (DSFS) in the eastern Mediterranean region.

2 Materials and Methods

Numerous contemporary and near-contemporary historical sources have been used for studying the 1822 earthquake. They were written in Arabic, English, French and Ottoman. The sources include: (1) British and French consular correspondences from cities of Aleppo and Latakia [1]; (2) Local histories written by Aleppians [2–4]; (3) Ottoman historians [5]; (4) Letters written by visitors and accounts left by travelers [6–10]; (5) European Bulletins and Journals from both 19th and 20th centuries [11]; (6) Original manuscripts [12, 13]. We also used the work of Ambraseys [14], who documented many details of this earthquake using the consular archives available in Paris, London and India. For processing the historical documents, we used the methodology described by the International Atomic Energy Agency [15]. Regarding the assessing the peak ground acceleration (PGA), we used the extended stochastic method (EXSIM) proposed by Atkinson and Assatourians [16].

We believe the above-mentioned historical sources are sufficient to allow us to introduce the effects of the earthquake of 1822, then to define the possible causative fault and assess its seismic parameters along with the PGA.

3 Results and Discussion

The earthquake happened on the night of Tuesday 13th August 1822 (25 *Dhu'l Qa'da* 1237 *Hijra* Calendar), three hours after the sunset, during the Ottoman occupation. It was a tremendous event. Aleppo city, with about 200,000 inhabitants and nearly 40,000 houses, was at the heart of this earthquake. In a few seconds, it was transformed into ruins. This event instantly buried thousands of the inhabitants under these ruins. It was followed by a strong shock after

R. Darawcheh (✉) · M. K. Abdul-wahed · A. Hasan
Department of Geology, Atomic Energy Commission of Syria, P.O. Box 6091 Damascus, Syria
e-mail: rdarawcheh@aec.org.sy

N. Sundararajan et al. (eds.), *On Significant Applications of Geophysical Methods*,
Advances in Science, Technology & Innovation, https://doi.org/10.1007/978-3-030-01656-2_40

half an hour. A part of the tall city' wall collapsed on the people. The earthquake caused the fall of most of the minarets and tall buildings. Numerous schools and khans were damaged. Most of the damage was concentrated in Aqaba quarter and al-Attarin market inside the old city. Numerous mosques were severely damaged including the Great Mosque. The Citadel of Aleppo was totally damaged. The Maronite church of St. Elias was also damaged from the outside. The main synagogue was destroyed. The city was exposed to thieves and bandits. In fact, all forms public life in the city stopped. In addition, an immense quantity of valuable goods of all kinds from Persia and India were destroyed. In that night, there were violent shocks happening at short intervals, which cannot be described. The survivors rushed from their houses and settled in the orchards which extended along the Quwaiq river. Based on these above data, the seismic intensity can be assessed as X–XI after the EMS-98 [17].

Other towns and villages in the *Pashalic* of Aleppo were destroyed or damaged. Antakia with about 9000–10,000 inhabitant, and located 90 km west of Aleppo, was strongly damaged by this earthquake leaving most of it in ruins, and causing terrible loss of life. The coastal town of Latakia, located 145 km southwest of Aleppo with a population of about 4000–6000 at that time, suffered from the earthquake. Half of the town was destroyed and many houses were damaged. Also, some families migrated the city and settled in other nearby regions and towns. The fortress that was located along the coast, the big mosque, the custom and the Grand Khan located in the old seaport were among the structures that were damaged. Figure 1 shows most of the affected localities due to the earthquake.

Since the earthquake was of large size, a large number of aftershocks that followed and lasted for more than three months.

Based on the above-mentioned macroseismic data, we estimated the earthquake magnitude to be *Ms* 7.3, its proposed epicenter is located at the coordinate 36.19°N, 36.74°E and its focal depth is about 15 km. Also, the possible causative fault of the earthquake is St. Simeon fault (SSF) which represents one of the braided faults along the northern DSFS. According to field investigation and the results of Karakhanian et al. [18], the focal mechanism of the main shock could be assessed to be a strike-slip one (Fig. 1). The PGA in the citadel of Aleppo was estimated to be 0.5 g using the extended stochastic method. Regarding the instrumental seismicity, low-magnitude events were recorded along the SSF during the period 1995–2012 [19]. Therefore, SSF could be activated in the form of a large earthquake.

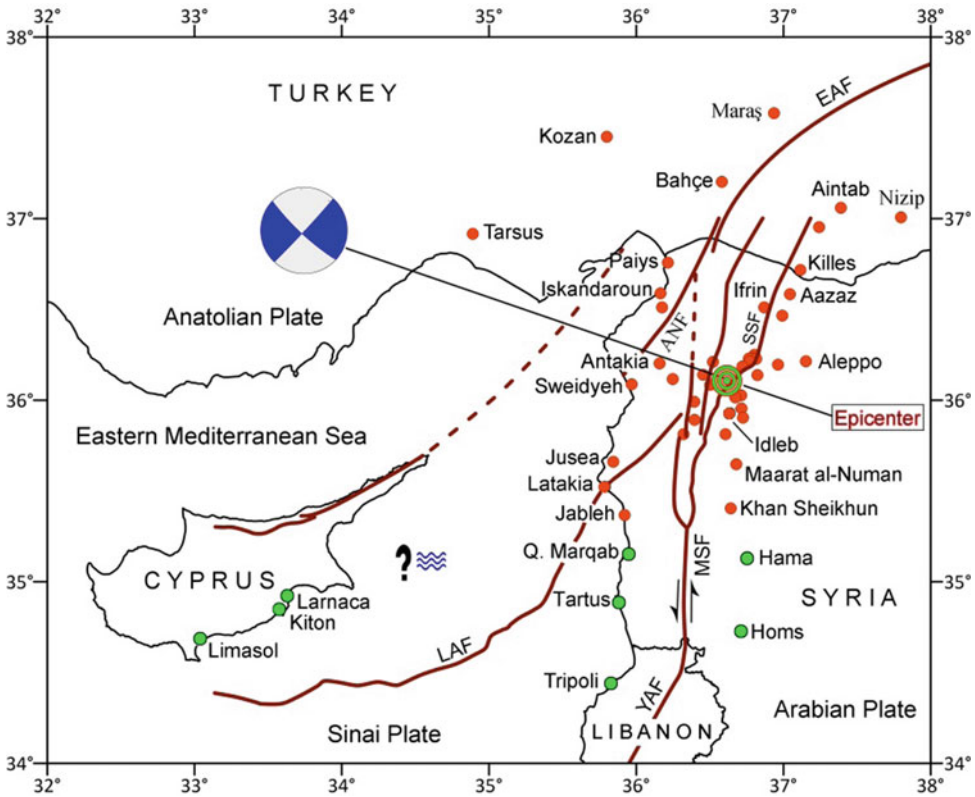

Fig. 1 A map showing distribution of the damaged and felt localities. Red circle is the most destructive locality and the green one represents the felt localities. Note the proposed epicenter of the earthquake, and the fault plane solution assessed. *Abbreviations* ANF: Antakia fault; LAF: Latakia fault; MSF: Mesyaf fault; SSF: St. Simeon fault; YAF: Yammouneh fault

4 Conclusion

This work shows that the earthquake of 13th August 1822 represents one of the largest seismic events along the northern DSFS. It destroyed several cities, towns and villages in north–west Syria, and chiefly Aleppo city. The northern DSFS was a site of several well-documented large (Ms ∼ 7.0) historical earthquakes such as those that occurred in 1157 AD., 1170, 1408, 1822 and finally 1872. We believe that earthquake hazards are genuine in the northwestern Syria. This implies that the results of studying these earthquakes must be used in the seismic hazard assessment on the regional scale for mitigating the risk in the area.

References

1. Guys, C.: Notice sur le tremblement de terre qui a bouleversé la Haute-Syrie en août 1822. Bulletin de la Société de Géographie. pp. 301–305. Tome Premier, Paris (1822)
2. Al-Ghazzi, K.: Nahr al-Dhahab fi Tarikh Halab (The River of gold in the history of Aleppo). (In Arabic), Part 3. pp. 329–334. Aleppo (1926)
3. Al-Tabbakh, M.R.: I'lam al-Nubala bi Tarikh Halab al-Shahba (Informing the nobles on the History of Aleppo). Part 3. pp. 400–410. Aleppo (1925)
4. Taoutel, F.: Watha'iq Ta'rikhiyyat an Halap: Akhbar al-mawarinah wa mailayhim min 1606 ila yawmina (Les documents Marounites et leurs annexes depuis 1606 jusqu'á nos jours). Al-Matb'ah al-Kathulikiyah, Beyrouth (1958)
5. Paşa, A.C.: Tarih-i Cevdet (History of Cevdet). Matbaa-y Amire, Istanbul (1874)
6. Conder, J.: The Modern Traveller: Syria and Asia Minor, vol. 1, pp. 299–305. James Duncan, London (1824)
7. Michaud, J.F, Boujoulat., J.J.F.: Correspondence D'Orient (1830–1831). Tome VIII. Gregoir-Wouters et Ce, Bruxelles (1841)
8. Neale, FA.: Evenings at Antioch; with sketches of a Syrian life. xxvi, xxvii. Eyre and Williams, London (1854)
9. Purdy, J.: The New Sailing Directory for the Strait of Gibraltar and the Western Division of the Mediterranean Sea. R.H. Laurie, London (1832)
10. Wolff, J.: Travels and Adventures of Rev. Joseph Wolff. Cambridge University Press, New York (1824)
11. Regnault, A.L.: Lettre de M. Le consul du Roi, saint-jean d'Acre, adresée à M. Jomard, Chiti (Chypre), 5 October 1822. Bulletin de la Société de Géographie. pp. 215–216. Tome Premier, Paris. (1822)
12. Galles, R.: Une lettre inédite sur le tremblement de terre à Alep en 1822 par M. Dercher. Bulletin de la Sociéité Archéologique du Morbihan, p. 10 (1885)
13. Salmon, O.: Alep dans la Littérarule de voyage européenne pendant la période ottomane (1516–1918). Tome III. pp. 1801–1918 (2011)
14. Ambraseys, N.N.: Temporary seismic quiescence: SE Turkey. Geophys. J. **96**, 311–331 (1989)
15. International Atomic Energy Agency: Methodology and procedures for compilation of historical earthquakes data. IAEA-TECDOC-434, Vienna (1987)
16. Atkinson, G.M., Assatourians, K.: Implementation and validation of EXSIM (A Stochastic Finite-Fault Ground-Motion Simulation Algorithm) on the SCEC broadband platform. Seismol. Res. Lett. **86**(1), 48–60 (2015)
17. Grünthal, G. (ed.): European macroseismic scale 1998 (EMS-98). Cahiers du Centre Européen de Géodynamique et de Séismologie, p. 99. Luxembourg (1998)
18. Karakhanian, A.S., Trifonov, V.G., Ivanova, T.P., Avagian, A., Rukieh, M., Minini, H., Dodonov, A.D., Bachmanov, D.M.: Seismic deformation in the St. Simeon monasteries (Qal'at Sima'n), northwestern Syria. Tectonophysics **453**, 122–147 (2008)
19. Abdul-wahed, M.K., Asfahani, J.: The recent instrumental seismicity of Syria and its implications. Geofísica Int. **57**(2), 121–138 (2018)

Recent Instrumental Earthquake Activity Along the Damascus Fault (Syria)

Mohamad Khir Abdul-Wahed

Abstract

In this study, the results of earthquake data processing, recorded essentially by the Syrian National Seismological Network (SNSN), were analyzed, and a special earthquakes catalogue for Damascus fault covering the period 1995–2012 was established. During the study period of approximately 17 years, it was observed that the seismic activity of this fault is characterized by low-magnitude events. It was therefore deduced that Damascus fault is actually in a quiescence state in contrast with other faults segments of the Dead Sea Faults System such as Yammoneh and Aqapa segments. Such a seismic quiescence along the Damascus fault implies that a large earthquake is overdue. The Gutenberg-Richter relationship, deduced from the established catalogue, inferred that the b-value is about 0.93 using the least-squares technique. This value, close to 1.0, can be accepted regarding the reported values in the literature. Extrapolation of Gutenberg-Richter relationship reveals long return periods of large earthquakes.

Keywords

Damascus fault • Instrumental earthquake • Gutenberg-Richter relationship • Syria

1 Introduction

Previous studies in Syria have revealed that the crustal deformation is ongoing along four tectonic zones: Palmyra Fold Belt (PFB), the Abd-el-Aziz-Sinjar, the Euphrates Fault System, and the DSFS [1, 2]. Numerous destructive earthquakes have occurred along these zones in the history [3]. Consequently, this study was an attempt to identify the seismic activity of one important fault, Damascus fault, passing beside Damascus, the most populated city in Syria.

2 Damascus Fault

Damascus fault (Fig. 1) is a conspicuous structure in the SW end of the PFB; it is a reverse fault, where the centre of Damascus is located in its footwall and the adjoining Jebel Qassioun mountain is forming its hanging-wall (e.g. [4]). A study of the rates of crustal shortening on the PFB revealed the possibility that Damascus fault has significant slip rates [5].

3 Regional Seismicity

Syria has been affected by many large historical earthquakes [3]. However, the actual instrumental seismic activity is passing through a quiescent status, which is supported by the low level magnitude of recorded events during the period 1995–2012 [6, 7]. The Syrian National Seismological Network (SNSN) has been operational since 1995 and allowed to record about 1600 local events during the period (1995–2012) along and around Damascus fault (Fig. 2). A noteworthy seismic activity has been observed along the north-eastern of Damascus fault, thus, this region can be regarded as potential seismic source area "southern part of the PFB".

4 Data and Method

Special earthquakes catalogue for Damascus fault covering the period from 1995 to 2012 was compiled by using essentially the data of the published SNSN bulletins. A total of 1600 earthquake events were recorded along and around Damascus fault during the period of 17 years. Magnitudes

M. K. Abdul-Wahed (✉)
Department of Geology, Atomic Energy Commission, Damascus, Syria
e-mail: mabdulwahed@aec.org.sy

N. Sundararajan et al. (eds.), *On Significant Applications of Geophysical Methods*,
Advances in Science, Technology & Innovation, https://doi.org/10.1007/978-3-030-01656-2_41

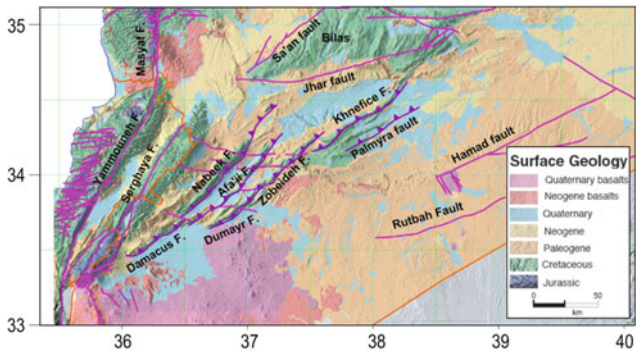

Fig. 1 Simplified geological map of Damascus region showing the main reverse faults (F.: fault) (modified from [2])

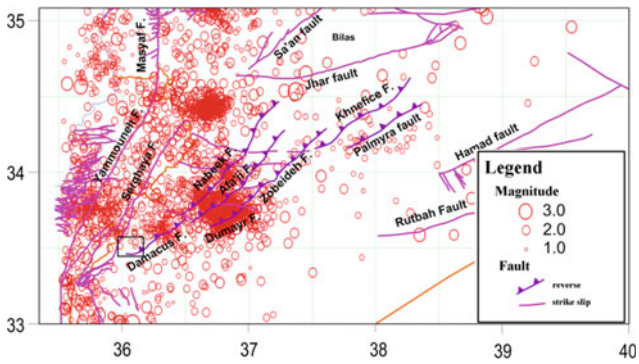

Fig. 2 Epicenters map showing the instrumental seismic activity recorded in Damascus region during the period 1995–2012

are calculated from the coda wave duration via the following formula [8]:

$$M_C = -3.0 + 2.6 * log(T) + 0.001 * D \qquad (1)$$

where D is the epicentral distance (in km) and T is the coda duration (in s).

The majority of these events are micro-earthquakes (Mc < 3.0). A quantitative idea about magnitude and frequency of events produced by the fault could be obtained by adopting the Gutenberg and Richter relation (G-R relation). This empirical relation is widely used in the studies of active faults and their earthquake activity. This empirical relation is given as:

$$logN = a - bM \qquad (2)$$

where N is the number of events of magnitude equal or greater than M per unit time, and a and b are empirical constants for a region, where **a** value is an indication of the level of seismic activity and **b** value is the rate of occurrence within a given magnitude range. It describes the relative abundance of large to smaller earthquakes.

5 Results

In this study, the empirical G-R relation, was evaluated using Seisan software (Seisan 10.3, 2014). Figure 3 shows the obtained forms of G-R relation. The results are shown in Table 1, where SD is the standard deviation of estimator, COR is the regression coefficient, and RMS is the root-mean-square error of estimate. The obtained results show a b-value to be 0.93 according to the least squares techniques. This value, close to 1.0, can be accepted regarding the reported values in the literature.The low standard deviation (SD = 0.12), the high regression coefficient (COR = 0.99), and the very low residual (RMS = 0.09) indicate that the return periods can be calculated by extrapolating the obtained G-R relation to larger earthquakes. The return periods for highest magnitude events than the catalogue are inferred from an extrapolation of curves fit to the log-linear distribution. A return period for an event of

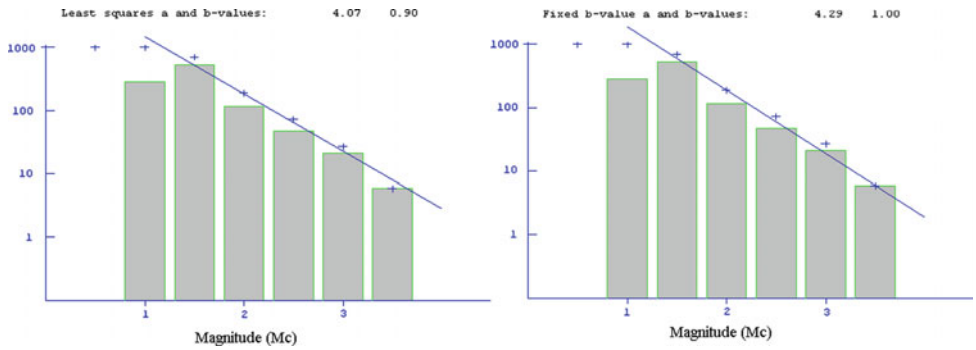

Fig. 3 Histograms showing comparison between the two used techniques

Table 1 a and b values calculated by using two techniques and two steps of magnitudes

Nb events	Mc min	Mc max	Mc step	Least-squares				Fixed b value		
				a	b	COR	RMS	a	b	SD
1007	1.0	4.0	0.1	4.17	0.93	0.99	0.09	4.33	1.0	0.12
1007	1.0	4.0	0.5	4.07	0.90	0.99	0.09	4.29	1.0	0.15

magnitude 6.5 is extrapolated to be 2700 years, which can be qualified as long return period.

6 Conclusion

The established catalogue for Damascus fault covering the period 1995–2012 reveals the earthquake activity produces low magnitude events and passes through a relative status of quiescence in contrast with other fault segments of Dead Sea Faults System such as Yammoneh and Aqapa segments. Such a seismic quiescence along the Damascus fault implies that a large earthquake is overdue. The empirical G-R relation shows a b-value of 0.93 and the extrapolation of this relation reveals long return periods of large earthquakes.

References

1. Barazangi, M., Seber, D., Chaimov, T., Best, J., Sawaf, T.: Tectonic evolution of the northern Arabian plate in western Syria. In: Boschi, E., Mantovani, E., Morelli, A. (eds.) Recent Evolution and Seismicity of the Mediterranean Region, pp. 117–140. Kluwer Academic Publishers (1993)
2. Brew, G., Lupa, J., Barazangi, M., Sawaf, T., Al-Imam, A., Zaza, T.: Structure and tectonic development of the Ghab basin and in Dead Sea fault system Syria. J. Geol. Soc. Lond. **158**, 665–674 (2001)
3. Sbeinati, M.R., Darawcheh, R., Mouty, M.: The historical earthquakes of Syria: an analysis of large and moderate earthquakes from 1365 B.C. to 1900 AD. Ann. Geofis. **48**(3), 347–435 (2005)
4. Sharkov, E.V., et al.: Geochronology of Late Cenozoic basalts in western Syria. Petrology **2**(4), 385–394. Russian original: Petrologiya **2**(4), 439–448 (1994)
5. Romieh, A., et al.: Active crustal shortening in NE Syria revealed by deformed terraces of the River Euphrates. Terra Nova **21**, 427–437 (2009)
6. Abdul-Wahed, M.K., Asfahani, J., Al-Tahan, I.: A combined methodology of multiplet and composite focal mechanism techniques for the identification of the seismological active zones in Syria. Acta. Geophys. **59**(5), 967–992 (2011)
7. Abdul-Wahed, M.K., Al-Tahan, I.: Preliminary outlining of the seismological active zones in Syria. Ann. Geophys. **53**(4), 1–9 (2010)
8. SNSN Bulletins: General Establishment of Geology and Mineral Resources, Syria. SNSN: Syrian National Seismological Network (1995–2012)

Physically-Based Ground Motion Prediction and Validation: A Case Study of Mid-Sized Marmara Sea Earthquakes

Aydın Mert

Abstract

Computation of realistic time histories for different locations around Marmara region can be helpful for engineering design, retrofitting the existing structures, hazard and risk management studies and developing new seismic codes and standards. This paper had two main purposes. The first one was to simulate five moderate earthquakes (Mw ≈ 5.0) recorded in the Marmara region. We synthesized ground motion for the full wave train on three components, and applied a 'physics based' solution of earthquake rupture. For each earthquake, we synthesized seismograms using 500 different rupture scenarios that were generated by Monte Carlo selection of parameters within the range. The second purpose was to validate synthetic seismogram with real seismogram. To develop credibility of a synthetic seismogram in engineering point of view, we followed the methodology of Anderson (13th World Conference on Earthquake Engineering, 2003 [1]). Because this methodology produces source and site specific synthetic ground motion time histories and goodness-of-fit scores of obtained synthetics was between 'good' to 'excellent' range based on Anderson's score. We concluded that it can be used to produce ground motion that has not previously been recorded during catastrophic earthquakes.

Keywords

Earthquake simulation • Marmara region Empirical Green's Functions • Validate synthetic seismogram • Physics based solution

1 Introduction

After the adoption of performance-based design approach with the Earthquake resistant design of engineering structures, accurate estimation of strong motion time histories are essential and one of the most well studied areas in engineering seismology and earthquake engineering. Computing realistic time histories for different locations around Marmara region can be helpful for engineering design, retrofitting the existing structures, hazard and risk management studies and developing new seismic codes and standards. Synthesized seismograms for five main events that occurred at different parts of the North Anatolian Fault Zone (NAFZ) in the vicinity of the Marmara Sea are generated by using quasi-dynamic models of earthquake rupture. Figure 1 describes the epicenters of all main events and aftershocks that were used as a Green's function in this study.

2 Materials and Methods

In this paper, the Green's function simulation methodology together with physically based rupture parameters proposed by [2] was used to develop realistic synthetic strong ground motions for specific sites from specific faults. By 'physically based' we refer to ground motion synthesized with quasi-dynamic rupture models [3] derived from physics and an understanding of earthquake process as described by [2, 4]. Theoretical background and formulation were summarized by [2, 4–7].

To generate randomly varying independent rupture parameters and include as much as possible rupture scenarios, we used 500 different rupture scenarios that were generated by Monte Carlo selection of parameters within the range. **The calculated moments** change between $0.303 \pm 0.062 \times 10^{24}$ and $0.356 \pm 0.082 \times 10^{24}$ dyn-cm, corresponding moment magnitude is $M_w = 5.0$ for the main events. **Hypocenter** locations of the simulated events were

A. Mert (✉)
Bogazici University, Çengelkoy 34684 Istanbul, Turkey
e-mail: mertay@boun.edu.tr

N. Sundararajan et al. (eds.), *On Significant Applications of Geophysical Methods*,
Advances in Science, Technology & Innovation, https://doi.org/10.1007/978-3-030-01656-2_42

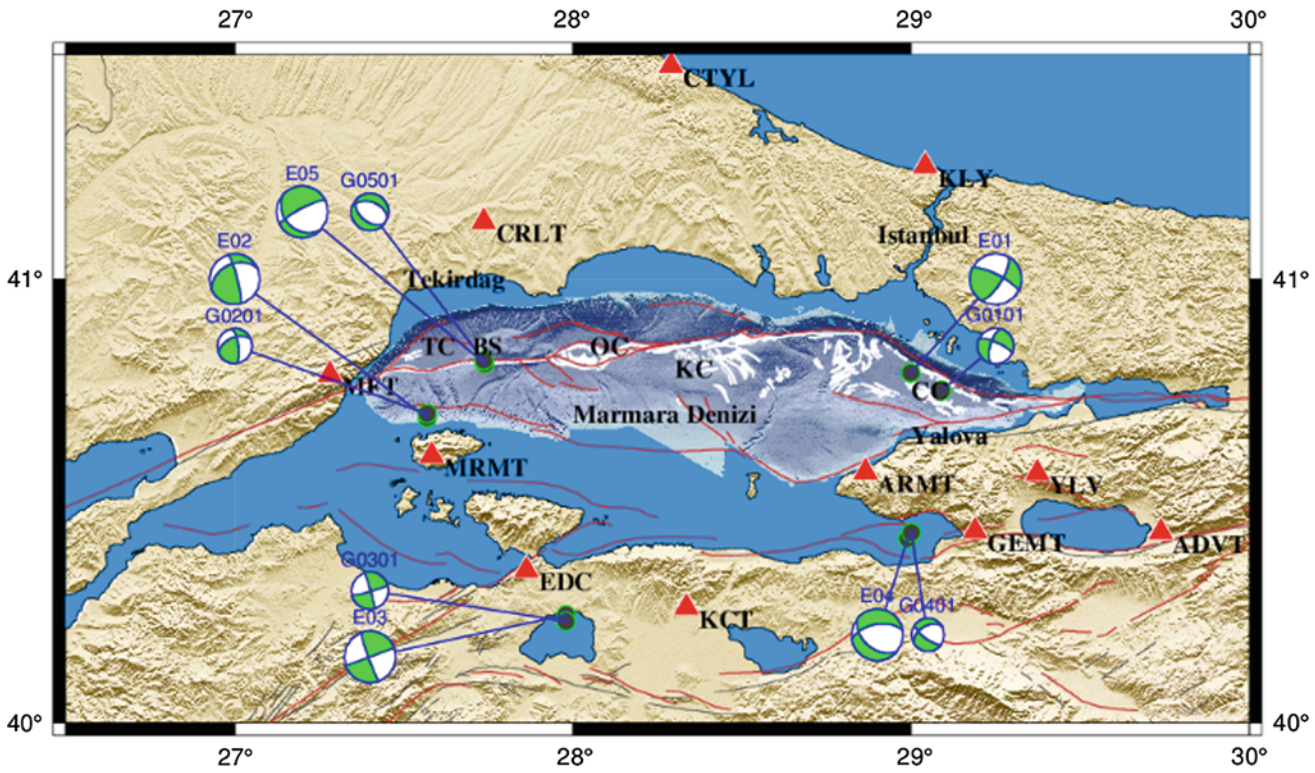

Fig. 1 Five simulated main earthquakes (large green beach balls, E01–E05) and aftershocks used as an EGF (small green beach balls) with earthquake recording network composed of broadband seismometers (red triangles)

changed randomly along the hazard area. **Rupture velocity** varies from 0.75 to 1.0 times shear wave velocity. **Healing velocity** varies from 0.8 to 1.0 times the rupture velocity for all of the different earthquake scenarios. **Roughness** is simulated as the elements resisting rupture and then breaking. **Stress drop** is a dependent variable derived from the Kostrov slip function.

To validate the simulation algorithm and develop credibility of synthetic seismogram in engineering, we followed the methodology presented by [1]. This methodology proposes a similarity score based on averages of the quality of fit measuring ground motion characteristics. Namely, the synthetics are confronted to real data by comparing the values obtained on ten representative ground motion criteria; Peak Ground Acceleration (PGA), Peak Ground Velocity (PGV), Peak Ground Displacement (PGD), Fourier Amplitude Spectrum (FAS), Response Spectrum (RS), Arias Duration (AD), Arias Intensity (AI), Energy Duration (ED), Energy Integral (EI) and Cross Correlation (CC). In order to compute the goodness-of-fit (GOF), each criterion was compared on a scale from 0 to 10, with 10 giving perfect agreement. Anderson finds that 40–60 represent a 'fair' fit, 60–80 a 'good' fit, and 80–100 an 'excellent' fit.

3 Results

We calculated and compared PGA, PGV, PGD for all synthetic seismograms obtained from the computed scenarios and recorded earthquakes. Figure 2 shows the comparison of the results for five different stations obtained from Kus Lake earthquake (E03). Similarities between recorded and simulated waveforms were investigated in terms of different parameters such as; First arrivals of P waves, time differences between S and P wave arrivals, recording duration etc. In Fig. 2, the blue solid line was for recorded earthquake and red solid line was best fitted simulation result.

We estimated the quality of the fit between synthesized seismograms from each scenario earthquake and observed records. We tested whether the simulated seismograms that match the recorded waveforms and if good or excellent fits to seismograms are due to source models. If so, we accept that this scenario is close to what happened in reality during

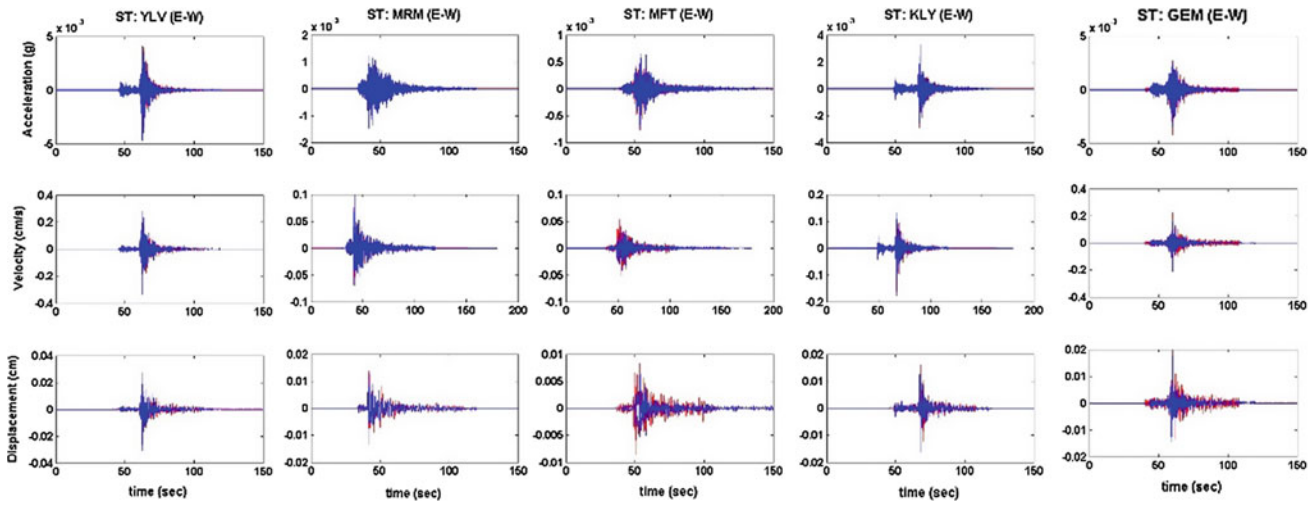

Fig. 2 Comparison of real and simulated time domain parameters of Kus Lake earthquake (E03) at five different stations

Table 1 Anderson scores that were obtained for the best scenario earthquake

EQ ID	Best scenario	Anderson score
E01	SC 11	6.8468
E02	SC 165	7.2739
E03	SC 181	8.2164
E04	SC 497	6.4332
E05	SC 252	6.1128

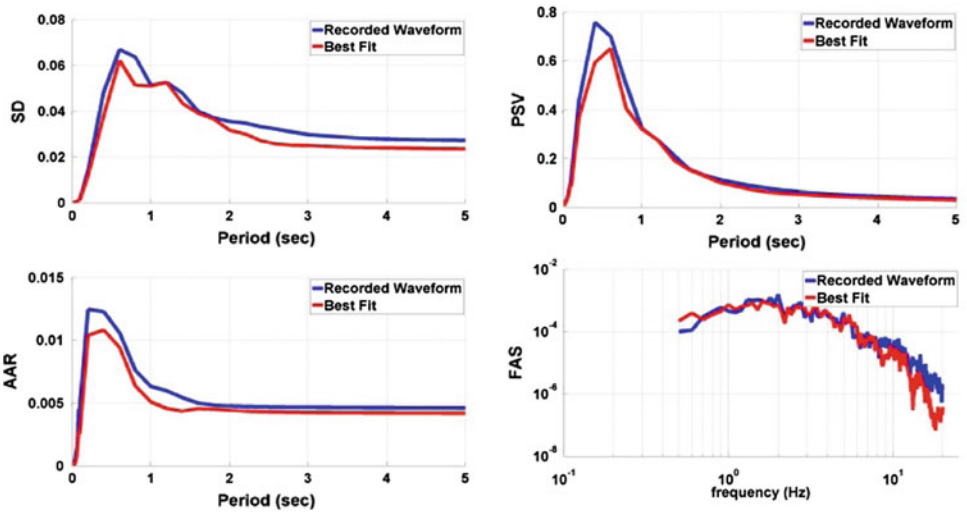

Fig. 3 Comparison of real and simulated spectral parameters for Kus Lake earthquake (event E03) based on best fitted (Sc. 181) scenario (YLV station)

the earthquake or represents an earthquake rupture process. Table 1 shows Anderson scores that were obtained by the best scenario between five hundred different earthquake scenarios. Figure 3 shows comparison of results (freq domain parameters; SD, PSV, AAR, FAS) only for Yalova (YLV) station obtained from Kus Lake earthquake that has the best Anderson score (8.2164) among all five simulated earthquakes.

4 Discussion

Simulation of high frequency ground motion is still a difficult problem in seismology due to its random nature. Probably the most important restriction for that kind of simulation algorithm is related to the calculation of source and propagation path characteristics. Using the small magnitude earthquake as an EGF together with appropriate source function to simulate high frequency ground motion is the most promising idea to cope with this problem.

5 Conclusion

Modeling exact waveforms was not perfect for all of the stations. However, a good match to observed seismograms was obtained. This methodology produces source and site specific synthetic ground motion time histories with goodness-of-fit scores in the 'good' to 'excellent' range (6.1128–8.2164) based on Anderson's score. This means the methodology can be used to produce ground motion that has not previously been recorded during catastrophic earthquakes in the region or some very active seismic area to develop or improve seismic codes and standards.

References

1. Anderson, J.G.: Quantitative measure of the goodness of fit of synthetic accelerograms. In: 13th World Conference on Earthquake Engineering, Vancouver, B.C., Canada, August 1–6, 2004, Paper N.243 (2003)
2. Hutchings, L., Ioannidou, E., Kalogeras, I., Voulgaris, N., Savy, J., Foxall, W., Scognamiglio, L., Stavrakakis, G.: A physically-based strong ground-motion prediction methodology; application to PSHA and the 1999 M = 6.0 Athens Earthquake. Geophys. J. Int. **168**, 569–680 (2007)
3. Boatwright, J.L.: Quasi-dynamic models of simple earthquake: an application to an aftershock of the 1975 Oroville, California earthquake. Bull. seism. Soc. Am. **71**, 69–94 (1981)
4. Scognamiglio, L., Hutchings, L.: A test of physically based strong ground motion prediction methodology with the 26 September 1997, Mw = 6.0 Colfiorito (Umbria-Marche sequence), Italy earthquake. Tectonophysics **476**, 145–158 (2009)
5. Hutchings, L.: Kinematic earthquake models and synthesized ground motion using empirical green's functions. Bull. Seismol. Soc. Am. **84**, 1028–1050 (1994)
6. Hutchings, L.: "Prediction" of strong ground motion for the 1989 Loma Prieta Earthquake using Empirical Green's Functions. Bull. Seismol. Soc. Am. **81**, 88–121 (1991)
7. Hutchings, L., Wu, F.: Empirical Green's Functions from small earthquakes: a waveform study of locally recorded aftershocks of the San Fernando Earthquake. J. Geophys. Res. **95**, 1187–1214 (1990)

Comparison Between Non-linear and Stochastic Methods for Dynamic SSI Problems

Mohamed Elhebib Guellil, Zamila Harichane, and Arkan Çelebi

Abstract

Soil-structure interaction (SSI) effect plays important roles on the seismic behaviour of structure. The soil exhibits spatial heterogeneities and in many cases is imperfectly known. In addition, during an earthquake, the non-linearity of the soil affects the dynamic response of structure and soils. The most important material properties with which to characterize the dynamic behaviour of soils are the shear modulus (G) and damping (ξ). For these two reasons, a comparative study between the non-linear and stochastic methods using Monte Carlo simulation for the soil parameters (G and ξ, respectively) on impedance functions and response of the coupled system. Our results show that the impedance functions and response of coupled system are greatly affected by the non-linear method related to the stochastic method.

Keywords

Cone model • Non-linear method • Stochastic method • Impedance functions • Structure response

1 Introduction

During an earthquake, the soil properties below and around the foundation have an important effect on the dynamic behaviour of structures [1, 2]. However, this soil exhibits spatial heterogeneities resulting from its deposition history and in many cases is imperfectly known, and a large error might appear during the identification of the parameters of the soil model, as it has been perturbated during construction. For this reason, the dynamic soil-structure interaction problem should be cast into a stochastic form [2–4].

For an earthquake, the strain would invariably be larger than measured during test, even for a moderate earthquake when the strain range increases. Soils exhibit nonlinear, inelastic, stress-strain behaviour under cyclic loading conditions. Chawdhary [5] presents an iterative method that can determine the new values of G and ξ due to an earthquake. The shear modulus and damping are the most important material properties with which to characterize the dynamic behavior of soils [6].

The main objective of this paper is to compare the effects of the corrected values of G and ξ based on Chawdhary method, and the influence of the uncertainty of these two parameters by the use of a probability analysis based on the Monte Carlo simulation on the response of the structure (impedance functions and structure distortions).

2 Method

In this study the model, representing a shallow foundation, the inertial interaction only needs to be considered where the structure is modelled as a single-degree-of-freedom system (impedance functions). The details of the cone model can be found in the literature [7].

3 Results

Firstly, the impedance functions determined for a cylindrical foundation of radius r_0 on the surface of layered soil. The mean values are: $d/r_0 = 1$, $G1/G2 = 0.544$, $\rho_1/\rho_2 = 0.85$, Poisson's ratio $\nu_1 = \nu_2 = 0.25$ and the damping ratio $\xi_1 = \xi_2 = 5\%$. The coefficient of variation (CV) for each soil parameters (G, ξ) is assumed in the range of 10 and 20%. Then, using the Dasgupta method [6], the soil parameters

M. E. Guellil (✉) · Z. Harichane
Geometrical Laboratory, Civil Engineering Department, Hassiba Benbouali University, P.O.Box 78 02000 Ouled Fares, Chlef, Algeria
e-mail: m.guellil@univ-chlef.dz

A. Çelebi
Civil Engineering Department, Sakarya University, Sakarya, Turkey

N. Sundararajan et al. (eds.), *On Significant Applications of Geophysical Methods*, Advances in Science, Technology & Innovation, https://doi.org/10.1007/978-3-030-01656-2_43

(G_1, ξ_1) are corrected and subsequently: $G_1/G_2 = 0.309$ and $\xi_1 = 6.6\%$.

Secondly, the aim of this step is to observe the effects of uncertainties and non-linearity of soil parameters on the dynamic response of the coupled system.

3.1 Results of Impedance Functions

See Figs. 1 and 2.

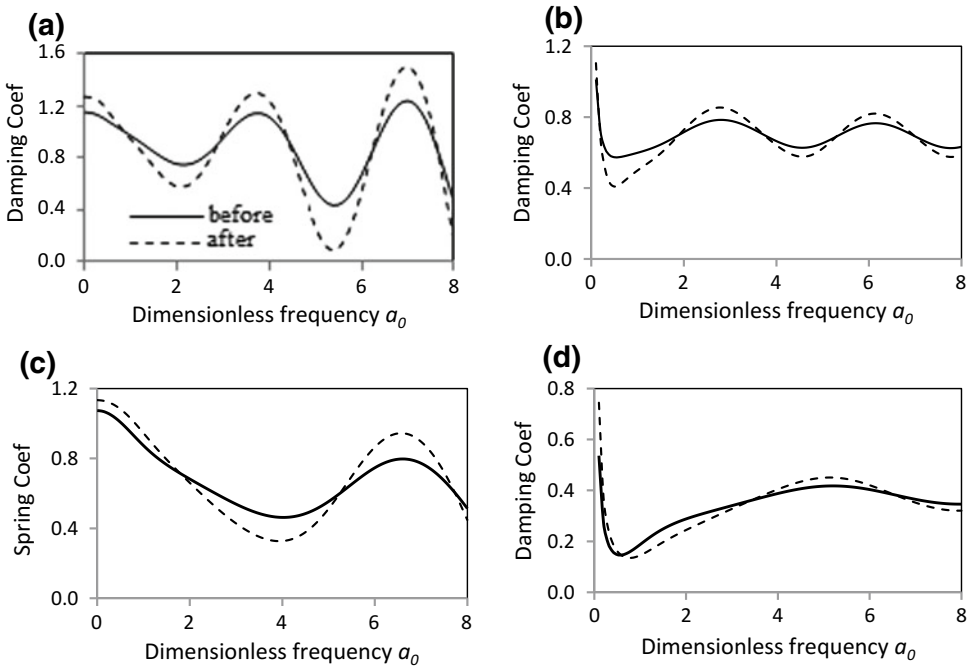

Fig. 1 Mean impedance function before and after corrected parameters: **a**, **b** Horizontal motions and **c**, **d** Rocking motion

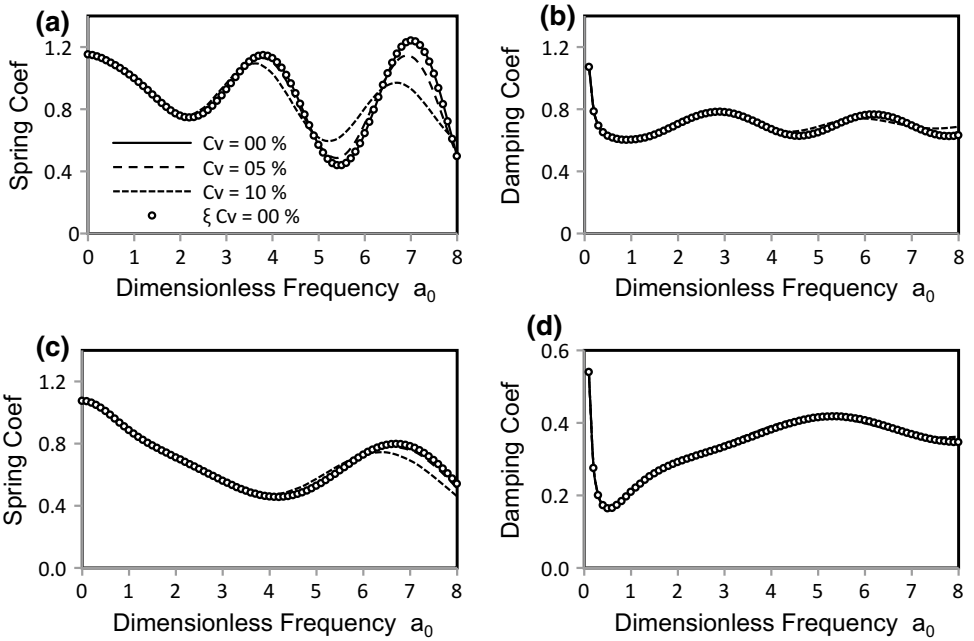

Fig. 2 Mean impedance function before and after stochastic analysis of soil parameters: **a**, **b** Horizontal motions and **c**, **d** Rocking motion

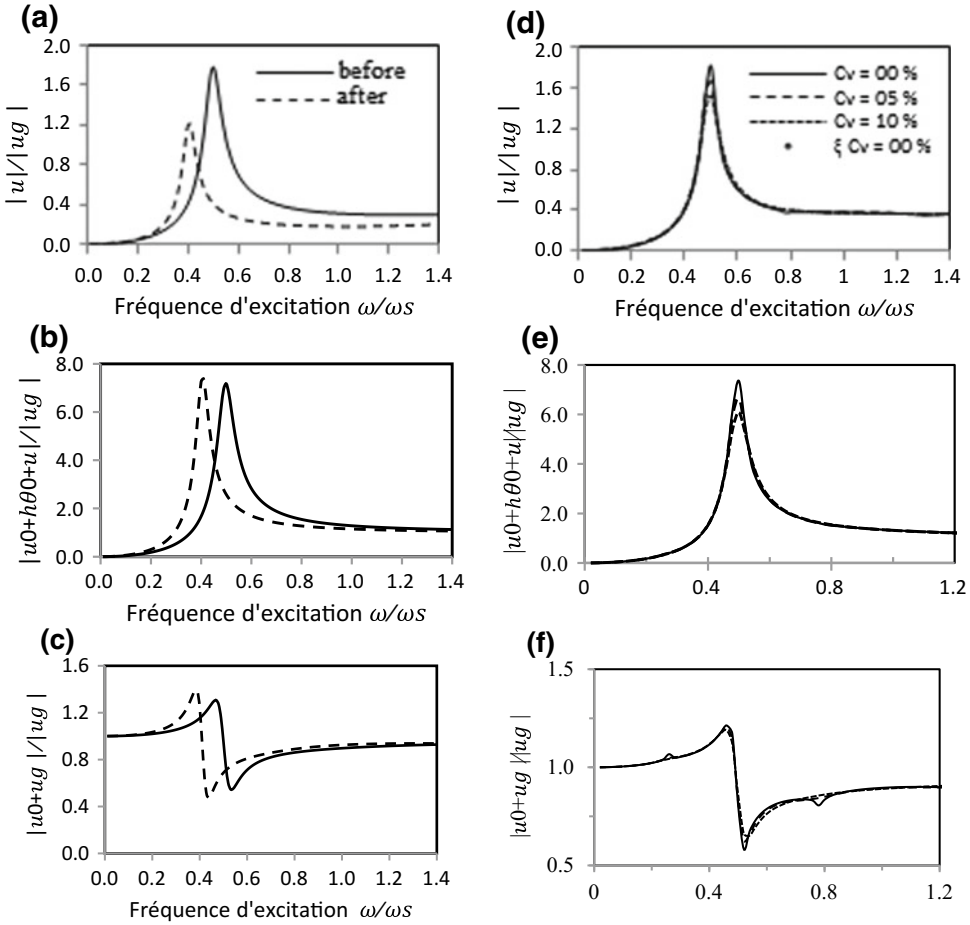

Fig. 3 Structure response: **a–c** for non-linear method and **d–f** for stochastic method

3.2 Structural Responses

From the comparison of Figs. 1 and 2, it appears that the correction effect of G and ξ due to the imposed seismic moment is very remarkable and greatly related to stochastic method on all frequencies. Figure 3 shows, that the structure has a displacement decrease of about 33%, while mass displacement and total displacement of the base relative to the free field increases by about 4 and 6%, respectively. For stochastic method, the displacements decrease when CV increases. This variation explains that the structure becomes more rigid and the soil is more flexible.

4 Conclusion

In this study, it is concluded that the parameters (G and ξ) have a large effect on the soil-structure interaction problem. Nonlinear behaviour was accounted for by the use of strain-dependent shear modulus and damping ratio. After correction, the displacements decreased with a remarkable shift of the frequency ratio for the three displacements. The stochastic spatial variability of the subsoil properties affects the structural response where the pick for the three displacements decrease only with a small value.

References

1. Jaya, K.P., Meher Prasad, A.: Embedded foundation in layered soil under dynamic excitations. Soil Dyn. Earthq. Eng. **22**, 485–498 (2012)
2. Guellil, M.E., Harichane, Z., Djilali Berkane, H., Sadouki, A.: Soil and structure uncertainty effects on the soil foundation structure dynamic response. Earthq. Struct. **12**(2), 153–163 (2017)
3. Harichane, Z., Guellil, M.E., Gadouri, H.: Benefits of probabilistic soil-foundation structure interaction analysis. Geotech. Earthq. Eng. **9**(1), 42–64 (2018)
4. Manthos, P., Stjn, F., Geert, D., Geert, L.: Analysis of stochastic dynamic soil structure interaction problems by means of coupled

finite elements-perfectly matched layers. In: VII European Congress on Computational Methods in Applied Sciences and Engineering, Greece, pp. 1–14 (2016)
5. Chowdhury, I., Dasgupta, S.P.: Dynamics of Structure and Foundation—A Unified Approach, Applications, 2nd edn. Taylor & Francis Group, London, UK (2009)
6. Jia, J.: Soil Dynamics and Foundation Modeling. Springer Nature, Norway (2018)
7. Wolf, J.P.: Foundation Vibration Analysis Using Simple Physical Models. Pearson Education, Prentice-Hall (1994)

Impact on the Dynamic Characteristics of Reinforced Concrete Buildings in Algiers Following Two Seismic Events

Yamina Ait-Meziane, Rania Souici, Nabila Guessoum, Djilali Bouziane, and Khadidja Abbes

Abstract

Most of the housing stock of the old cities in the north of Algeria is on masonry and reinforced concrete. These agglomerations are located in the coastal strip, which are precisely exposed to a high seismic hazard. As a reminder, the north of Algeria has been shaken by several major and moderate seismic events. In the case of Algiers, for the greatest part of the area the buildings were constructed during the 1871–1936 period, so bearing the traces of several earthquakes since no major reinforcement campaign was undertaken. This paper reported the analysis results of the impact of a seismic event by considering the fundamental period of the reinforced concrete buildings identified before and after the earthquake. A comparison between the obtained results with the site conditions were operated using a non-destructive technique, that of background noise.

Keywords

Building • Soil • Frequency • Earthquake Impact

1 Introduction

The urban centers of northern Algeria consists of masonry buildings and have been densified by reinforced concrete buildings during the 1920s. The first reinforced concrete buildings built in Algiers were inserted into the existing urban fabric for some and, into the periphery for others. The example of the district of Bab El Oued illustrates this state. In Fig. 1, the cities Consolation and Press were inserted inside the ancient urban fabric and the cities Taine and Eucalyptus on the outside. To absorb the demand for housing, these buildings were built on several levels, isolated block for some and several blocks separated by seals for others. Their design was achieved, like masonry buildings, to support vertical loads.

Seismic activity in the Mediterranean basin is concentrated in northern Africa, where oblique convergence between the African and European plates is accommodated and Algeria is one of the most seismic countries [1]. Old agglomerations are located along the coast, an area exposed to high seismic hazard. Mw = 6.8 [2, 3]. On August 1st, 2014 a moderate earthquake (Mw = 5.5) hit the Capital city of Algiers and its surroundings. Thus, most of the old housing stock experienced many major earthquakes [4]. Algiers is classified in zone III (high seismicity) according to the Algerian code (RPA 99/2003) [5]. The post seismic expertise carried out after the 21st May 2003 earthquake on reinforced concrete buildings located in Algiers concluded to a green classification.

This category corresponds on the macroseismic scale to a pathology that does not require repair or reinforcement of buildings. This level of diagnosis allows the immediate reoccupation of buildings.

The scope of this research is to present our contribution to improve the post seismic diagnostics of buildings to account for the dynamic structural parameters before and after a seismic event. The diagnosis has become quantitative and not qualitative.

The experimental frequencies obtained from buildings supplemented by the knowledge of the ground frequency must give us information on the probability of ground-structure resonance which aggravates the seismic behavior of buildings. Prevention to reduce the risk of damage would consist in proposing a solution to keep the frequency of the buildings from the ground frequency as far as possible.

Y. Ait-Meziane · N. Guessoum · D. Bouziane · K. Abbes
National Earthquake Engineering Research Center, CGS, Algiers, Algeria

R. Souici (✉)
FGC, LBE, University of Science & Technology Houari Boumediene (USTHB), Algiers, Algeria
e-mail: souicirania@gmail.com

N. Sundararajan et al. (eds.), *On Significant Applications of Geophysical Methods*,
Advances in Science, Technology & Innovation, https://doi.org/10.1007/978-3-030-01656-2_44

Fig. 1 View of Bab El Oued fabric

2 Measurements Methods

In earthquake engineering, the fundamental period is an important parameter in seismic design. It depends on the number of internal and external factors, such as building material, structural system building, design building, environment (seismic and soil conditions) and conditions used. The experimental testing investigations for existing buildings have been in use since 1936 [6].

Ambient background noise is of anthropoid and natural type. It generates shearing waves of the same type as those emitted by a seismic moment [7, 8]. The ambient methods have been used for several years as they are non destructive methods. Ambient vibration testing methods are based on recording and processing the response of structures to background excitations. The procedure was successfully used to identify the fundamental resonance frequencies of buildings [9, 10]. In the dynamic structural field the natural frequency/period is mostly used for the qualification of the global behavior of civil structuring. The decrease of natural frequency meant the dynamic quality of the building structure was modified; it was regarded as an indicator of structure damage.

The non destructive technique of ambient background noise, commonly used today to characterize the ground and/or buildings was used for assessment the seismic risk.

3 Results of in Site Full Scale Testing of the Selected Buildings

The buildings population taken as a sample in this research was chosen for their age, date of construction 1949–1954 [11] construction type of reinforced concrete, their regularity shape, their maintenance level and the site environment. All of them were used for housing and located in Algiers. The group of buildings is classified in the green category following fourth seismic events, El Asnam October 1980, Tipaza November 1989, Boumerdes May 2003 and Bologhine August 2014.

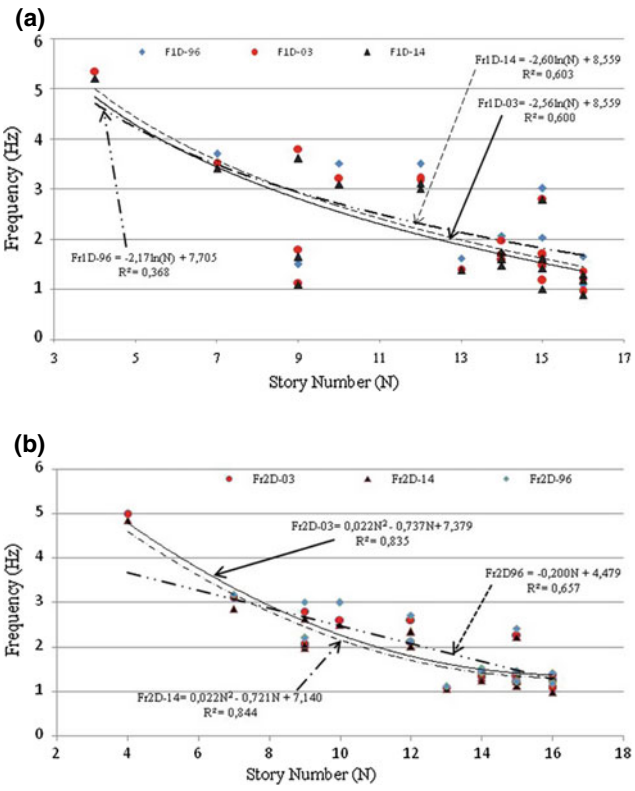

Fig. 2 **a** Variation frequency of the longitudinal buildings direction. **b** Variation frequency of the second direction buildings

The investigation conducted to identify the natural frequency in the two principal directions of each building was selected using the ambient background noise technique. This experimental work was conducted during three seasons, the first in 1996, the second in July 2003 after the Boumerdes seismic event [10] and the third in September 2014, after the Bologhine seismic event. The sample is composed of nineteen (19) buildings. So, we have used this opportunity to compare their natural frequency before after 2003 and 2014 (Fig. 2). The same technique and equipments were used during the three test sequences. The seismometers were installed using the same protocol in each building.

4 Discussion

The correlation of the number of levels with the experimental frequency value obtained for the three periods in the longitudinal direction, resulted in curves of the same type, (Log N), parallel with a coefficient of determination R^2 of 0.60 for the tests after 2003 after 2014. Compared to 1996 results, the coefficient of determination is 0.368. The same observation was obtained for the transverse direction.

5 Conclusion

The exploitation of the recordings of the two earthquakes recovered at the Hussein Dey (Algiers) station N = 508,609 and E = 4,066,027, gave pseudo-acceleration spectra with frequencies higher than 5 Hz, the peaks were observed to be in the range between (5 and 10) Hz for the EW direction and in the range of (4–9) Hz for the NS direction, for the earthquake of May 21st, 2003. For the 1st August, 2014 event, the pseudo-acceleration spectra was in the frequency range corresponding to (11–27) Hz for the EW direction, and in (8–22) Hz for the NS direction. The resonance frequency of the buildings composing the sample was less than 5 Hz. This was not included in the frequency range of the two seismic events, which explains the undamaged state of buildings.

References

1. Calais, E., DeMets, C., Nocquet, J.M.: Evidence for a post-3.16 Ma change in Nubia-Eurasia plate motion. Earth Planet Sci. Lett. **216**, 81–92 (2003). https://doi.org/10.1016/S0012-821X(03)00482-5
2. Earthquake Engineering Research Institute (EERI): The Boumerdes, Algeria earthquake of May, 21, 2003, Report, pp. 57. Learning from Earthquakes Program, Oakland, CA (2003)
3. Edwards, L.C.: Zemmouri, Algeria, Mw = 6.8 Earthquake of May 21, 2003. ASCE. Rapport (2004)
4. Benfedda, A., et al.: The August 1st, 2014 (Mw = 5.3) moderate earthquake: evidence for an active thrust fault in the Bay of Algiers (Algeria). Pure Appl. Geophys. (2017). https://doi.org/10.1007/s00024-017-1481-6
5. Algerian Earthquake Resistant Regulation «R P A 99/Version 2003»
6. Trifunac, M.D.: Comparisons between ambient and forced vibration experiments. Earthq. Eng. Struct. Dyn. **1**, 133–150 (1972)
7. Grunthal, G.: European macroseismic scale EMS-98, Cahier du Centre Européen de Géodynamique et de Séismologie, vol. 15, Luxembourg (1998)
8. Bonnefoy, S.C.: Nature du bruit de fond sismique: implications pour les études des effets de site», Thèse de Doctorat, LGIT, Grenoble (2004)
9. Dunand, F.: Pertinence du bruit de fond sismique pour la caractérisation dynamique et l'aide au diagnostic sismique», Thèse de Doctorat, UJF Grenoble (2005)
10. Ait-Meziane, Y., et al.: Vunerability of the existing buildings: empirical evaluation and experimental measurement. Nat. Hazards (2011). https://doi.org/10.1007/s11069-011-9986-2
11. Breil J.: Données statistiques sur les immeubles et les logements: Résultats statistiques du dénombrement de la population effectué le 31 octobre 1954, Service de statistique générale, Délégation générale du gouvernement en Algérie (1954)

Reassessing the Rupture Process of the 2003 Boumerdes-Zemmouri Earthquake (Mw 6.8, Northern Algeria) Using Teleseismic, Strong Motion, InSAR, GPS, and Coastal Uplift Data

Hamoud Beldjoudi, Bertrand Delouis, and Abdelkrim Yelles-Chaouche

Abstract

In this work we determined the coseismic slip distribution of the Boumerdes-Zemmouri earthquake (Mw 6.8, 2003) by inverting the most comprehensive data set, teleseismic seismograms, strong motion seismograms, Coastal uplift, Global positioning system and Interferometric Synthetic Aperturs Radar. We suggested a model of coseismic slip distribution on two segments; the first segment oriented N70° and the second segment located to the west of the first one and oriented N100°. The two fault segments exhibit some overlap in the Boumerdes area. The resulting slip maps do not overlap. The slip distribution shows two slip patches on the N70 segment containing the hypocenter. The eastern patch is shallower, located between 0 and 9 km deep, with a maximum slip of 230 cm. The western patch on this same segment is deeper, between 4 and 12 km depth, and slip reaches 270 cm at its center. The N100 segment also displays two slip patches, a small one in the East of the segment located between the depths of 4 and 8 km and a larger one in the western part of the segment, located between 0 and 10 km. In both patches of the N100 segment, the maximum slip lies between 110 and 140 cm.

Keywords

Waveform modeling • Rupture process • Boumerdes • Zemmouri • Coastal uplift • Geodetic data • Seismological data

1 Introduction

The Boumerdes-Zemmouri earthquake occurred ~50 km East of Algiers on May 21, 2003, at 19h44 (UTC). It is the second strong earthquake that struck northern Algeria, after the El Asnam earthquake (Ms = 7.3) on 10th October 1980. The Boumerdes-Zemmouri event was the subject of many studies, among which several focused on the seismic source [1–5], or on the aftershock sequence [6–8]. The 2003 rupture developed below the coastal area, partly under the sea, and Déverchère et al. [9] described active structures offshore which might have been activated during the 2003 earthquake.

Regarding the analysis of the rupture process of the 2003 earthquake, different kinds of observations and measurements have been inverted jointly, notably different combinations of purely static displacement data among Global Positioning System (GPS), Synthetic Aperture Radar Interferograms (InSAR) and Coastal Uplift (CU), in Yelles et al. [1], Meghraoui et al. [2] and Belabbès et al. [5]. Two studies combined seismological and static displacement data; Delouis et al. [3] and Semmane et al. [4]. However all the available kinds of data were never inverted altogether. In particular, Strong-Motion (SM), Teleseismic seismograms (TELE) and InSAR data were never combined.

2 Common Characteristics of Fault Models and Inversion Procedure

The rupture of the Boumerdes earthquake was modeled using the kinematic fault approach of Delouis et al. [10]. It allows for multiple segments of rupture, each defined by its dimension, strike and dip angles, discretized by a regular mesh of point sources to model seismological data, and by a mesh of rectangular subfault dislocations to model geodetic data. Each point source is defined by a local source time function (local STF) representing the seismic moment rate,

H. Beldjoudi (✉) · A. Yelles-Chaouche
CRAAG, BP 63, Route de l'Observatoire, Bouzaréah, Alger, Algeria
e-mail: h.beldjoudi@craag.dz

B. Delouis
Geoazur, 250 Rue Albert Einstein, 06560 Valbonne, France

N. Sundararajan et al. (eds.), *On Significant Applications of Geophysical Methods*,
Advances in Science, Technology & Innovation, https://doi.org/10.1007/978-3-030-01656-2_45

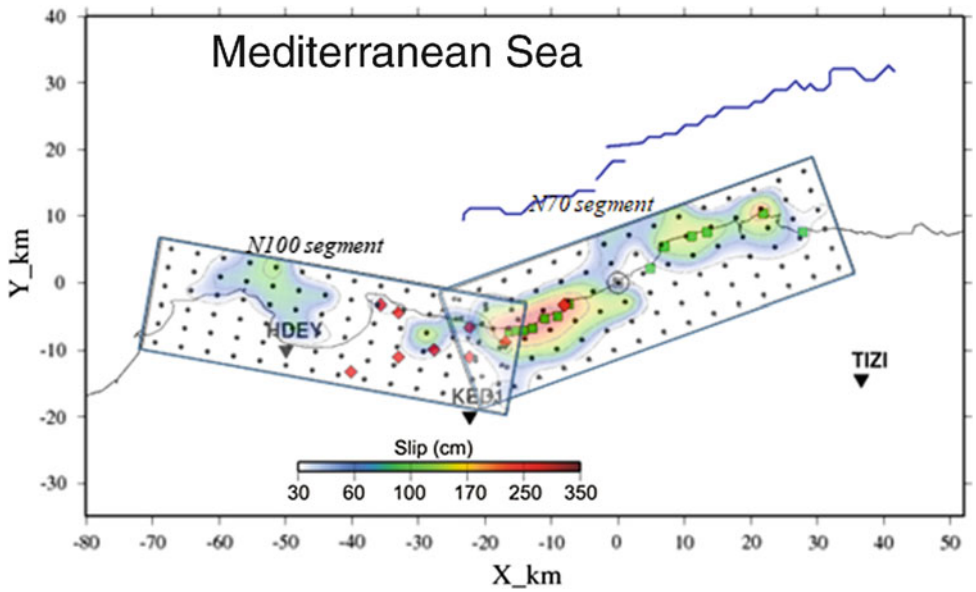

Fig. 1 Surface projection of the slip distribution obtained by joint inversion of all datasets with model 2 segments. Black dots correspond to the point sources at the center of the subfaults. Grey square within an open circle: subfault corresponding to the hypocenter; black line: coastline; blue lines: offshore escarpments B1 and B2 described in Déverchère et al. [9]; red diamonds: GPS stations; green squares: points where coastal uplift was measured [2]; black inverted triangles with names\strong motion stations. Y axis is oriented towards the north

the slip direction (rake angle), and the rupture onset time. Each local STF is represented by three isosceles triangular functions, of width 3s, mutually overlapping. One of the point sources coincides with the earthquake hypocenter. The parameters to be inverted, for each point source (i.e. subfault), are the rupture onset time, the rake angle, and the amplitudes of the three triangular functions. We included seven additional parameters, corresponding to the allowed shifts of the seven fringe groups of the InSAR data. Simplest models would incorporate a single rupture plane (or fault segment), while the more complex ones would include several rupture planes (fault segments) with possibly different dimensions, strikes and dips.

3 Fault Models and Results

In all fault models, we considered the position of hypocenter as fixed. The epicenter was relocated on the coastline at 36.83°N and 3.65°E by Bounif et al. [6]. The hypocentral depth is the same as in Delouis et al. [3], i.e. 6.5 km. It is well constrained by the teleseismic data. In all cases, the rake was allowed to vary between +80° and +110°, except for the N100 segment (see below) where rake is in between +75° and +105°. We did not show the slip vectors on the slip maps since they do not vary much. Rupture timing can vary according to a minimum and maximum rupture velocity, respectively Vrmin = 1.6 km/s and Vrmax = 3.5 km/s. For a given subfault, the rupture velocity considered here is the distance to the hypocenter divided by the rupture onset time.

3.1 Two Segment Models with a Change in Strike

In order to invert jointly purely geodetic data (SAR, GPS, and CU), Belabbès et al. [5] proposed a rupture plane which curves are in its western part. Their slip model trends NE–SW (∼N60°) between Dellys and Boumerdes, and change to WNW–ESE (∼N100°) between Boumerdes and Cap Matifou. It is remarkable that the trend of the coastline changes in the same way near Boumerdes, so that their model follows approximately the curve of the coastline. In this section, we tested such a change in strike of the rupture plane, investigating in particular its effect on the modelling of the seismological data which were not included in Belabbès et al. [5]. We decomposed the model in two segments (see Fig. 1), the first one trending N70° (*N70 segment*), identical to our previous model 1seg, and the second one trending N100° (*N100 segment*). We tested different positions for the *N100 segment*, moving it in the inland direction or locating it more offshore, with a dip angle of 40°, 45°, or 50°. These tests were carried out with joint inversions of the whole dataset (TELE, SM, GPS, SAR, CU). The slip distribution shows two slip patches on the *N70*

segment containing the hypocenter. The eastern patch is shallower, located between 0 and 9 km in depth, with a maximum slip of 230 cm. The western patch on this same segment is deeper, between 4 and 12 km, and the slip reaches 270 cm at its center. *The N100 segment* displays also two slip patches, a small one in the East of the segment located between 4 and 8 km and a larger one in the western part of the segment, located between 0 and 10 km. Maximum slip lies between 110 and 140 cm in both patches of the *N100 segment*.

4 Discussion-Conclusion

We started by using a simple model with uniform geometry (strike N70, dip 40), identical to the one used in Delouis et al. [3] except for the dip which was formerly 45°, but incorporating additional data, namely the InSAR (SAR) and strong motion (SM) data. This simple model provided a slip distribution similar to the one of Delouis et al. [3] but we identified some incompatibility among the more complete datasets, with a difficulty to model the records of the SM station HDEY and the GPS data. This led us to explore more complexity in the geometry of the rupture model. A change in strike of the rupture plane in the West was already proposed by Belabbès et al. [5] and the activation of shallow offshore ramp and flat faults was suggested by Déverchère et al. [9]. Based on these elements, we constructed two alternative models, named 2seg and 4seg, incorporating a second segment oriented N100° (2seg model). With the 2seg model, the apparent incompatibility among the datasets could be solved, with a slip distribution modelling correctly all the datasets, in particular the GPS and SM station HDEY which were problematic with the 1seg model. However, a new slip area appeared offshore Algiers, not identified in previous studies. We showed that this slip zone is required by the SM station HDEY only. We also emphasize that the other data (TELE, GPS, INSAR, CU), although globally little impacted by this slip zone, are compatible with this finding. For example, we observed that computed InSAR fringes are effectively nearly closing at, or just east of, Cap Matifou, as the observed ones do. Regarding coastal uplift, nothing was documented in the Algiers area. In order to assess whether this westernmost slip zone should have produced coastal uplift which should have been observed, we calculated the related vertical uplift along the coast near Algiers in Beldjoudi [11]. We found the predicted uplift to be equal or lower than 20 cm in the Algiers area, a value which may be effectively below the observational threshold.

References

1. Yelles, K., Lammali, K., Mahsas, A., Calais, E., Briole, P.: Coseismic deformation of the May 21st, 2003, Mw = 6.8 Boumerdes earthquake, Algeria, from GPS measurements. Geophys. Res. Lett. **31**, L13610 (2004). https://doi.org/10.1029/2004GL019884
2. Meghraoui, M., Maouche, S., Chemaa, B., Cakir, Z., Aoudia, A., Harbi, A., Alasset, P.J., Ayadi, A., Bouhadad, Y., Benhamouda, F.: Coastal uplift and thrust faulting associated with the Mw = 6.8 Zemmouri (Algeria) earthquake of 21 May, 2003. Geophys. Res. Lett. **31**, L19605 (2004). https://doi.org/10.1029/2004GL020466
3. Delouis, B., Vallée, M., Meghraoui, M., Calais, E., Maouche, S., Lammali, K., Mahsas, A., Briole, P., Benhamouda, F., Yelles, K.: Slip distribution of the 2003 Boumerdes-Zemmouri earthquake, Algeria, from teleseismic, GPS, and coastal uplift data. Geophys. Res. Lett. **31**, L18607 (2004). https://doi.org/10.1029/2004GL020687
4. Semmane, F., Campillo, M., Cotton, F.: Fault location and source process of the Boumerdes, Algeria, earthquake inferred from geodetic and strong motion data. Geophys. Res. Lett. **32**, L01305 (2005). https://doi.org/10.1029/2004GL021268
5. Belabbès, S., Wicks, C., Cakir, Z., Meghraoui, M.: Rupture parameters of the 2003 Zemmouri (Mw 6.8), Algeria, earthquake from joint inversion of interferometric synthetic aperture radar, coastal uplift, and GPS. J. Geophys. Res. **114**, B03406 (2009). https://doi.org/10.1029/2008JB005912
6. Bounif, A., Dorbath, C., Ayadi, A., Meghraoui, M., Beldjoudi, H., Laouami, N., Frogneux, M., Slimani, A., Alasset, P.J., Kharroubi, A., Ousadou, F., Chikh, M., Harbi, A., Larbes, S., Maouche, S.: The 21 May 2003 Zemmouri (Algeria) earthquake Mw = 6.8: relocation and aftershocks sequence analysis. Geophys. Res. Lett. **31**, L19606 (2004). https://doi.org/10.1029/2004GL020586
7. Ayadi, A., Dorbath, C., Ousadou, F., Maouche, S., Chikh, M., Bounif, M.A., Meghraoui, M.: Zemmouri earthquake rupture zone (Mw 6.8, Algeria): aftershocks sequence relocation and 3D velocity model. J. Geophys. Res. **113**, B09301 (2008). https://doi.org/10.1029/2007JB005257
8. Kherroubi, A., Yelles-Chaouche, A., Koulakov, I., Déverchère, J., Beldjoudi, H., Haned, A., Semmane, F., Aidi, C.: Full aftershock sequence of the Mw 6.9 2003 Boumerdes earthquake, Algeria: space-time distribution, local tomography and seismotectonic implications. Submitted to Pure Appl. Geophys. (2017)
9. Déverchère, J., Yelles, K., Domzig, A., Mercier de Lépinay, B., Bouillin, J.P., Gaullier, V., Bracène, R., Calais, E., Savoye, B., Kherroubi, A., Le Roy, P., Pauc, H., Dan, G.: Active thrust faulting offshore Boumerdes, Algeria, and its relations to the 2003 Mw 6.9 earthquake. Geophys. Res. Lett. **32**, L04311 (2005). https://doi.org/10.1029/2004gl021646
10. Delouis, B., Giardini, D., Lundgren, P., Salichon, J.: Joint inversion of InSAR, GPS, teleseismic and strong motion data for the spatial and temporal distribution of earthquake slip: application to the 1999 Izmit mainshock. Bull. Seismol. Soc. Am. **92**, 278–299 (2002)
11. Beldjoudi, H.: Modélisation de la source des séismes par inversion des données sismologiques et géodésiques: application aux séismes du Nord de l'Algérie. Sciences de la Terre. Université Côte d'Azur. Français. NNT: 2017AZUR4053 (2017)

Overview of Recent Seismic Activity in Northeastern Algeria

Issam Abacha and AbdelKarim Yelles-Chaouche

Abstract

This work was devoted to recent seismicity of Northeastern Algeria. It was achieved after the installation of the new Algerian seismological network. This study showed clearly that this region is the most active because almost 2/3 of seismic events occur there. Recently, several important events occurred in this region such as, the 2007 Mila crisis, the 2010 Beni-Ilmane earthquake sequence, the 2012–2013 Bejaia earthquake sequence, the 2015 Ain Azel earthquake and the 2017 earthquake sequence along North Constantine Fault (NCF). We determined the physical parameters of these events in order to understand their rupture processes. We also calculated the reorientation of the stress tensor in some regions. Finally, this work could be considered as the most representative contribution to the knowledge of seismic hazard of the North-East region of Algeria.

Keywords

Tellian Chain • Focal mechanism • Source parameters • Scaling la seismic sequence

1 Introduction

The earthquakes occurrence in Northern Algeria remains an important research topic for many reasons that are both scientific and societal due to their disastrous impacts on the socio-economic development of the country.

Through the development of the Algerian seismological network since 2000 [1], the first maps of reliable seismicity as well as the first hazard studies have appeared [2].

One of the important characteristics of Algeria seismicity is its concentration in the Eastern part of the country. Indeed, almost 2/3 of the Algerian seismic events occur in this region which remained poorly studied until recent time despite its lively seismic activity (Fig. 1). This region has witnessed many moderate seismic events in several parts during the last twenty years. Among these events, we can cite the 2000 Beni-Ouartilane earthquake of Md = 5.3, the 2006 Lalaam earthquake Md = 5.2 [3], the 2010 Beni-Ilmane earthquake sequence Md = 5.2 [4], the 2012–2013 Bejaia earthquake sequence [5], the 2015 Ain Azel earthquake [6] and the 2017 seismic sequence along the North Constantine Fault (NCF) [7]. Induced seismicity has also been detected for some events such as, the 2007 Mila seismic crisis [8], or seismic events around Grouz (2003–2007) and Beni-Haroun dams (2011–2012). In this study, we focused on all these main moderate events, presented their source parameters and the stress pattern in order to understand the rupture process in the studied area.

2 Methodology Analysis

The purpose of this research work is to study the main recent seismic events of northeastern Algeria. The seismic data were acquired through the Algerian seismic network and also during the several seismic surveys made after the occurrence of several moderate shocks. The first step was to locate precisely all these seismic events using several location and relocation programs with their focal mechanisms calculation. In the second step, we preformed statistical tests on the time intervals between successive earthquakes to better understand the physical correlation among the seismic events from the same cluster. In the last step we determined the source parameters and the scaling laws of these seismic parameters.

I. Abacha (✉) · A. Yelles-Chaouche
Centre de Recherche en Astronomie Astrophysique et Géophysique, CRAAG, BP 63, Bouzaréah, Algiers, Algeria
e-mail: i.abacha@craag.dz

N. Sundararajan et al. (eds.), *On Significant Applications of Geophysical Methods*,
Advances in Science, Technology & Innovation, https://doi.org/10.1007/978-3-030-01656-2_46

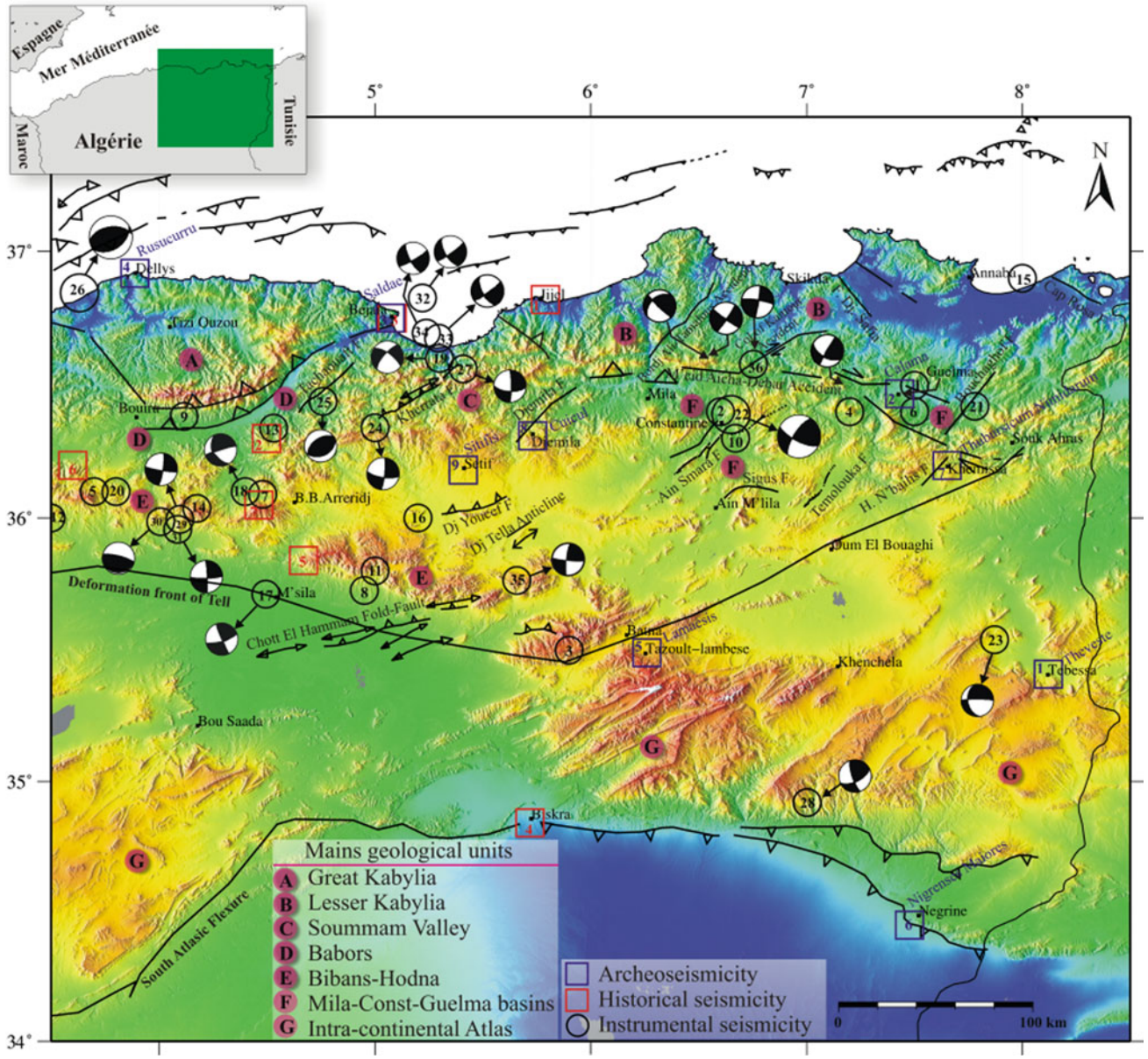

Fig. 1 The main geological units (capital letters); historical and instrumental earthquakes (M $\geq$ 4.7) with their focal solutions in our study area and the major active fault in the area

3 Results

In the following, we present the analysis of the main seismic events that occurred in our study area (Fig. 2).

4 Discussion

This study which covers a large part of the North Algerian territory allowed integrating these new results for understanding of the seismicity of the eastern region of Algeria.

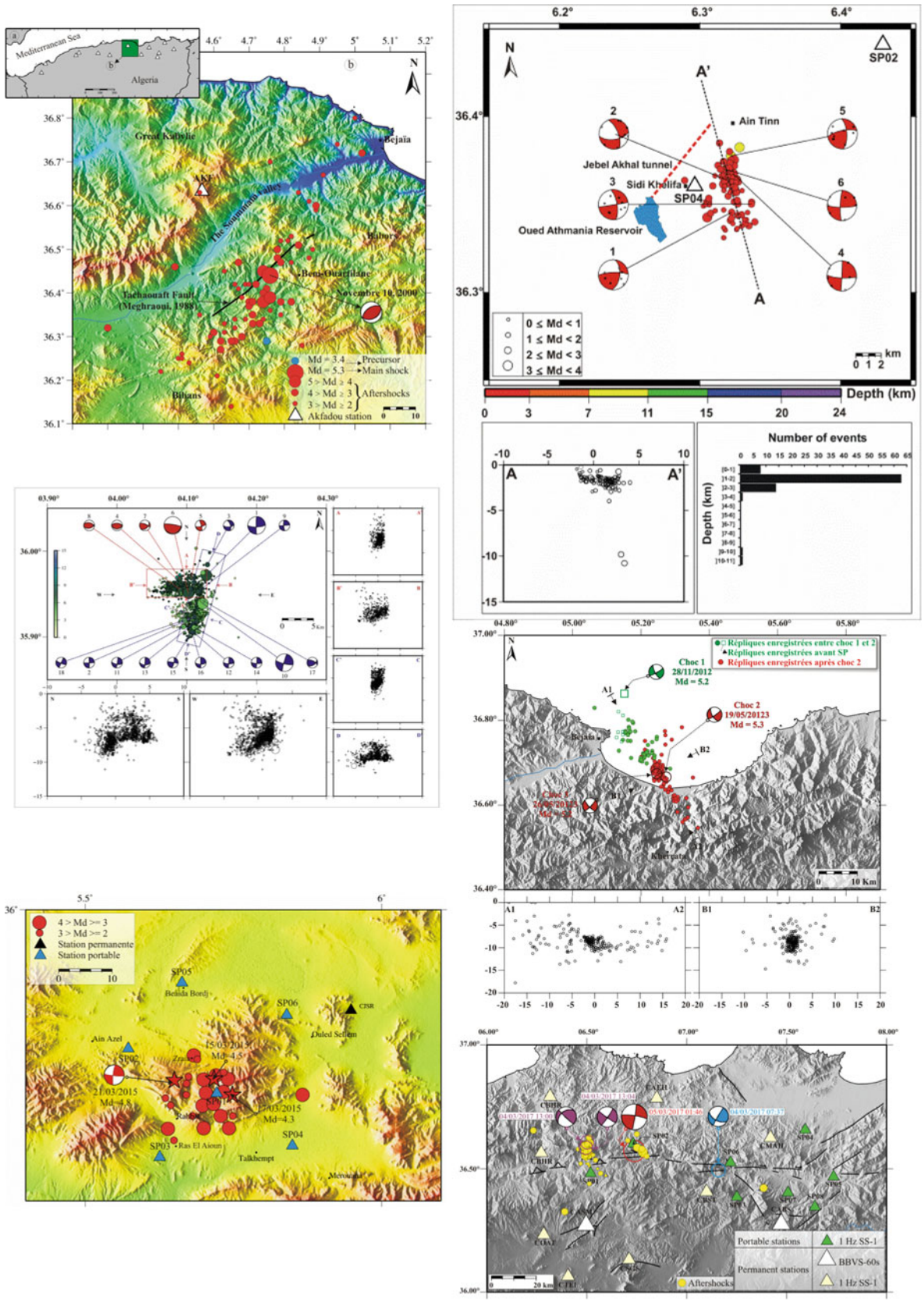

Fig. 2 Spatial distribution: (1) the 2000 Beni-Ouartilane earthquake (up left), (2) the 2007 Mila seismic crisis [2] (up right), (3) the 2010 Beni-Ilmane seismic sequence (middle left). (4) The 2012–2013 Bejaia seismic sequence (middle right). (5) The 2015 Ain Azel earthquake (bottom left) and the 2017 seismic sequence along NCF (bottom right)

Through this study, we tried to understand better the spatial distribution of the events, their rupture process to improve the previous seismic hazard models carried out. On the other hand, it is important to outline that several seismic sequences occurred with two or three main shocks of the same magnitude. This pattern suggests that the energy released in these events was split on at least two main faults may be avoided for a large earthquake.

5 Conclusion

This study allowed us to establish new seismic map for the northeastern region characterized by recent events which occurred there and to determine their source parameters. The main events which are in general superficial, happened along newly revealed active faults like the NCF or the Beni-Ouartilane fault system. The rupture process of these main events involves in general a segmented fault system with a repartition of the energy release. The determination of these new seismogenic zones remains an important contribution to the seismic hazard assessment of the Northeastern region of Algeria.

References

1. Yelles-Chaouche, A.K., Allili, T., Alili, A., Messemen, W., Beldjoudi, H., Semmane, F., Kherroubi, A., Djellit, H., Larbes, Y., Haned, S., Deramchi, A., Amrani, A., Chouiref, A., Chaoui, F., Khellaf, K., Nait Sidi Said, C.: The new Algerian Digital Seismic Network (ADSN): towards an earthquake early-warning system. Adv. Geosci. **36**, 31–38 (2013). https://doi.org/10.5194/adgeo-36-31
2. Hamdache, M., Peláez, J.A., Talbi, A., López Casado, C.: A unified catalog of main earthquakes for Northern Algeria from A.D. 856 to 2008. Seismol. Res. Lett. **81**, 732–739 (2010)
3. Beldjoudi, H., Guemache, M.A., Kherroubi, A., Semmane, F., Yelles-Chaouche, A.K., Djellit, H., Amrani, A., Haned, A.: The Laâlam (Béjaïa, North-East Algeria) moderate earthquake (Mw = 5.2) on March 20th, 2006. Pure Appl. Geophys. **166**(4), 623–640 (2009)
4. Yelles-Chaouche, A.K., Abacha, I., Semmane, F., Beldjoudi, H., Djellit, H.: The Beni-Ilmane (North-Central Algeria) earthquake sequence of May 2010. Pure Appl. Geophys. (2013). https://doi.org/10.1007/s00024-013-0709-3
5. Abacha, I., Yelles-Chaouche, A., Kherroubi, A., Boulahia, O.: Recent seismicity of the Babors region: case of the Bejaia (east Algeria) earthquake sequence of May 2013. In: 7ème colloque maghrébin de Géophysique appliquée tenu le 20 et 22 Février 2018 à Alger, Algérie (2018)
6. Chami, A., Yelles-Chaouche, A., Abacha, I., Benaissa, Z., Khelif, M.: Séquence sismique de la région d'Ain Azel (Sud de Sétif) Janvier-Mai 2015. Analyse Préliminaire. In: International Symposium on «Seismic Risk and Induced Effects in the Maghrebian Region», Sétif, 27–28 Oct 2015. Commemoration of the Constantine Earthquake (27/10/1985) (2015)
7. Abacha, I., Boulahia, O., Yelles-Chaouche, A., Bendjama, H.: Source parameters of the main seismic events in Northeastern Algeria. In: 2nd General Assembly of African Seismological Commission (AFSC2018), Al Hociema, Morocco, 23–27 Apr 2018
8. Semmane, F., Abacha, I., Yelles-Chaouche, A.K., Haned, A., Beldjoudi, H., Amrani, A.: The earthquake swarm of December 2007 in the Mila region of northeastern Algeria. Nat. Hazards (2012). https://doi.org/10.1007/s11069-012-0338-7

Induced Seismicity in Sidi Salem Dam, NW Tunisia

Sinda Gaieb and Najet Shimi

Abstract

The Sidi Salem reservoir was built in Beja, a semi-arid region in Northwestern Tunisia, for such purposes as the protection of the lower valley against floods, irrigation, water supply, and power generation. It is the biggest reservoir in Tunisia. It is a 73-m high, 814 Mm^3 water storage capacity compacted-earth dam. The seismic events in the studied area were monitored by a seismic network operated by the National Institute of Meteorology. The main aim of this study was to establish the correlation between water level in the reservoir and the induced seismicity. The first earthquake susceptible to be an induced event was found out in 1987 with magnitude of 5 after complete filling of the dam. Shortly afterwards, there was an increase in the number of seismic events, and many earthquakes were noted. It was suggested that this induced seismicity took place after the reservoir loading effect and also the postponed effect of the diffusion of pore pressure. The comparison between the seismic data and reservoir water level indicated that there was a correlation between the changes in the water level and the seismic activity.

Keywords

Sidi Salem reservoir • Seismic activity • Induced seismicity • Correlation • Water level

1 Introduction

The studies of induced seismicity by human activities are becoming more common because of its high probability to destroy constructions and to cause loss among humans. In addition to field studies, other factors playing an important role in RIS were identified. Ambient stress, the appearance of fractures, the subsurface properties of the reservoir rocks [1, 2] are all examples of these factors. Observational and theoretical models [2] highlighted that there are two impacts when a dam is filled with water. The first is due to the water load and it is manifested by the variation of the condition of local stress, which causes weaknesses and the second effect is the increase of pore pressure into the rocks and in fractures and faults in or under the reservoir. This effect is due to the pore pressure diffusion into fractures and it can also be due to the saturated rock compaction by water because of the over weight of the reservoir.

North Tunisia is one of the important seismic regions in the country. It is one of the most earthquake prone areas. The Sidi Salem reservoir was built in Beja, a semi-arid region in Northwestern Tunisia. The studied artificial lake is an embankment dam 73 m high and 814 Mm^3 volume. It was built for the protection of the lower valley against floods as well as other purposes like, water supply, irrigation, and power generation. The seismicity in the studied region is controlled by a seismic network operated by INM (National Institute of Meteorology). This dam is considered to have the potential of occurrence of reservoir induced seismicity with its structures. The construction of the dam was achieved in 1981. The first identified reservoir-induced events occurred in 1987 with magnitude of 5 after complete filling of the reservoir. The seismicity around the dam has become increasingly frequent since 2003.

2 Materials and Methods

The data of the dam water level were acquired from the monthly table of water volume and water level of the artificial lake achieved by the direction of dams (Ministry of Agriculture, Water Resources and Fisheries). The seismic events were collected from the INM (National Institute of Meteorology) seismic catalog (412-2011). The maps in this study were geo-referenced and digitized using ARCGIS 10.1

S. Gaieb (✉) · N. Shimi
Department of Geology, Faculty of Sciences of Tunis, El Manar University, 2092 Tunis, Tunisia
e-mail: sinda.gaieb@gmail.com

N. Sundararajan et al. (eds.), *On Significant Applications of Geophysical Methods*,
Advances in Science, Technology & Innovation, https://doi.org/10.1007/978-3-030-01656-2_47

software. The dam water level and seismic activity data were analyzed by MATLAB (matrix laboratory), a programming language used for numerical calculation purposes.

3 Results

3.1 Seismicity Around Sidi Salem Dam

The seismicity in the study area is monitored by the network of seismic stations of the INM (National Institute of Meteorology). The events used for this work were those that occurred over 1976–2010 period. This period was chosen because the network has become more refined since 1976 by the installation of an important number of seismic recording stations. The magnitude of all events used in this study was greater than 2. The seismicity around the artificial lake is far from being negligible (Fig. 1).

It is observed that after the filling of the reservoir, 30 seismic shocks occurred within a radius of 15 km around the dam. Among these, there were 5 seismic events very close to the dam. The last recorded earthquake in the chosen study period occurred in July 2009 with a 3.3 magnitude on the Richter scale and a depth of 5 km, 5 km away from the dam itself.

3.2 Seismicity and Water Level

Figure 2 shows the relationship between the seismicity and the water level in the dam since 1982. Seismicity seemed to be in relation with the complete filling of the reservoir even within a radius of 10 km of the dam. A seismic shock occurred mainly in 1987 with a magnitude of 5.0 after a complete filling of the reservoir (Total net input to Sidi Salem for the hydrological year 1986–1987 was more than 725 hm^3) with a water level 109 m exceeded in 4 months. Concerning the September 1991 earthquake of magnitude 3.3, the epicentre was located at the level of the Trajan Bridge at the Sidi Salem retaining tail, this event came after a particularly wet hydrological year 1990–1991 (Water level of the dam varied between 109.96 m in April 1991 and 108.24 m in August 1991). The frequency of seismicity has been increasingly important since 2003. For the record, the

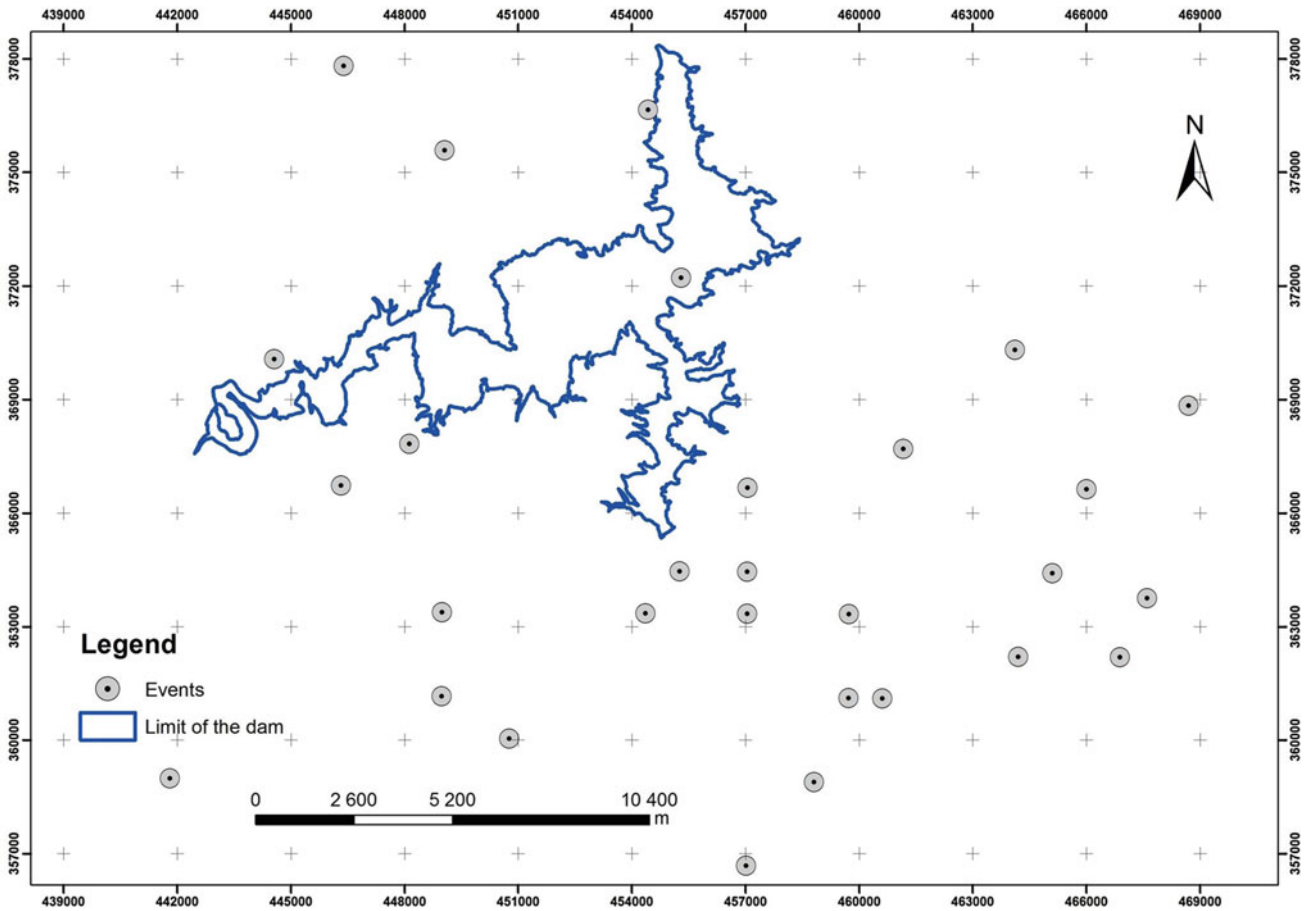

Fig. 1 Number of events after the impoundment of the dam (INM catalog)

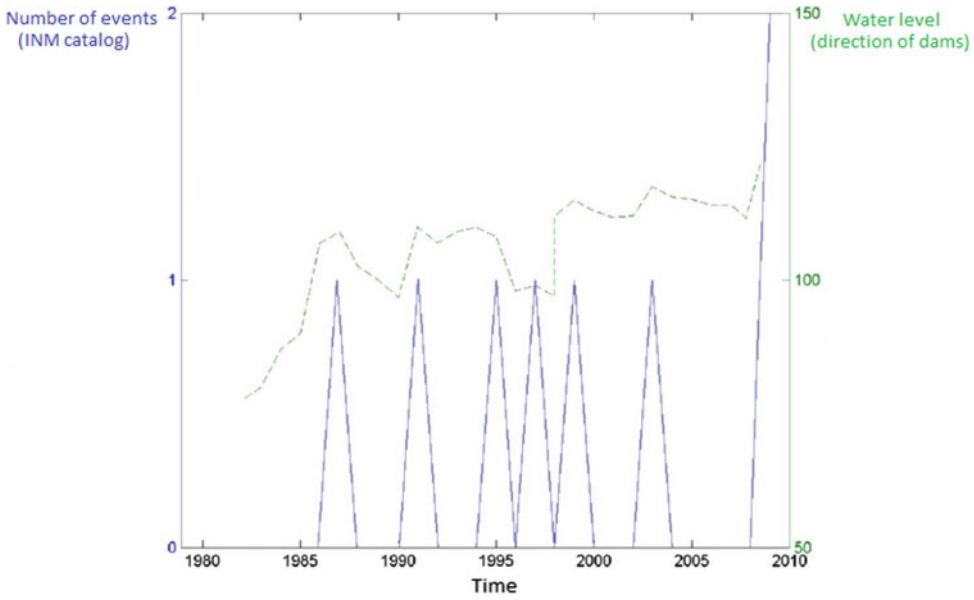

Fig. 2 Correlation between the number of events in a radius of 10 km around the dam (seismic catalog of INM) and the water level (monthly table of water level of the dam from the direction of dams)

normal water level of the dam reservoir (110 m) was elevated to 115 m in the autumn of 1999. This New rating was reached and exceeded several times in particular in January 2003 (117.51 m). The floods of this year have accumulated more than one billion cubic meters of water in Sidi Salem. The Mejerda experienced very strong floods in 2003 coupled with exceptional contributions after three consecutive years of drought. During that year, the reservoir of the Sidi Salem dam reached 117.51 m for the first time since the impoundment of the artificial lake, i.e. 2 m below the highest exceptional water level (119.5 m). In 2009, two seismic events occurred at 1 km of the dam with magnitude of 3.5. That year, the water level in the reservoir exceeded 117 m (Fig. 2).

4 Discussion

The Sidi Salem dam is located in Northwestern Tunisia. This reservoir is the center-piece of water mobilisation of northern Tunisia in an interconnected system ensuring the security and sustainability of the country's economic infrastructure. The magnitude of all the recorded events is more than 2. This is due to the absence of monitoring seismic stations in the vicinity of the reservoir despite its importance. The seismic data showed that the number of events increased after the impoundment of the reservoir.

The increase of the seismic activities at Sidi Salem reservoir for the chosen period seems to be associated to seasonal increase of the lake water level. The water level exceeded 109 m 3 months during 1987, the level of water was 109.96 in April 1991 after a wet hydrological year 1990–1991. Moreover, the normal water level of the reservoir fixed 110 m was elevated to 115 m in 1999, this new rating was reached and exceeded several times in 2003 (117, 5 m). The flood of that year accumulated more than one billion cubic meters of water after three years of drought. During these three years we showed that the seismicity has followed quiescent period. In 2003, the water level in the reservoir exceeded 117, 5 m for the first time. In 2009, the water level reached 117, 5 m, i.e. 2 m below the highest exceptional water level (119, 5 m). A clear correlation between seismicity around the reservoir and the water level in the dam is shown in Fig. 2.

5 Conclusion

The seismicity at Sidi Salem dam seems to be a good example of initial seismicity [2]; the earthquake that occurred in 1987 seems to be related to the first filling of the dam. An increase of seismic activity around the lake was noticed during the period from 1982 (date of the impoundment of the reservoir) until 2010. These seismic events occurred following the seasonal increase of the dam water level which reached its maximum level on many occasions. The magnitude of all the recorded events is more than 2 in the Richter scale. Unfortunately, despite the importance of the reservoir, there are no seismic monitoring stations in the vicinity of the dam which would allow us to determine the seismic activity below 2 in magnitude and microseismic activities.

Therefore it should be noted that it is necessary to install "Accelerographs" in the center of the body of the dam and at different points of the lake. These devices are necessary to obtain quantitative data (Accelerate of the ground). This will allow us to follow the micro-seismic activity around the dam and thus obtain enough amounts of data which will allow us to make a more detailed analysis concerning the seismicity induced by the Sidi Salem dam.

References

1. do Nascimento, A.F., Lunn, R.J., Cowie, P.A.: Modeling the heterogeneous hydraulic properties of faults using constraints from reservoir-induced seismicity. J. Geophys. Res. **110** (2005). https://doi.org/10.1029/2004jb003398
2. Talwani, P.: On the nature of reservoir-induced seismicity. Pure. Appl. Geophys. **150**, 473–492 (1997)

Recent Deformations of New Zealand GNSS Permanent Network Caused by 2016 Mw7.8 Kaikoura Earthquake

Bachir Gourine, Saddam Housseyn Allal, Hicham Dekkiche, and Kamel Hasni

Abstract

This paper deals with generation of post-seismic velocity and deformation fields of the GNSS network of New Zealand, due to the Kaikoura earthquake (Mw7.8), on November 13th, 2016. The PPP model was performed to estimate daily coordinates, during one year (November 2016–November 2017), of 138 stations of GeoNet with RTKLIB 2.4.2 software (University of Marine Sciences and Technology of Tokyo). The Deformation analysis software (Research Institute of Geodesy, Topography and Cartography, Czech Republic) was used for obtaining results in terms of displacements and deformations (strain tensors, total dilatation, and shears). This software, as a web application, uses Web Map Services (WMS) as its graphic representation of estimated results in GIS format. The results show clearly the post-seismic activity of New Zealand, particularly, near the epicenter and at frontier zone between South and North islands.

Keywords

Deformation analysis • Post-seismic activity
PPP • GNSS • Velocity field

1 Introduction

New Zealand is located at the border of the tectonic plates of Australia and the Pacific, where up to 15,000 earthquakes are recorded each year. The last great earthquake that shook the country was that of Kaikoura, November 13th, 2016, with a magnitude of M = 7.8, causing terrible damage to infrastructures and a tsunami on the southern coast of the country. It is considered as one of the most tectonically complex earthquakes of multi-segmented faults recorded in the last few years, this earthquake occurred as the result of shallow oblique-reverse faulting on or near the boundary between the Pacific and Australian Plates. More than a year after this disastrous earthquake and it is high time we studied the post-seismic movements of this region. The GNSS positioning technique was therefore used to estimate these movements. There are two modes of positioning which can be used for deformation monitoring: relative positioning and PPP (precise point positioning) [1, 2]. The PPP method can directly estimate the coordinates of geodetic point without any reference station, instead of the baseline vector calculation in case of relative positioning. This seems to be a great advantage during an earthquake because the reference points are also in motion. However, this technique requires mainly precise ephemeris and accurate clocks. PPP was demonstrated to be an efficient method for seismology and earthquake studies, such as [3–5]. The objective of this study was to perform a deformation analysis of the region surface using web application [6]. It consisted of generating the velocity and deformation (strain tensor, shear and dilation) fields from the displacements based on PPP GNSS stations of 138 points of GeoNet (Geological hazard Information for New Zealand) [7], during one year period from November 2016 to November 2017. Different results obtained from the adopted methodology are presented and discussed.

2 Methodology

2.1 Data Used and Processing Strategy

A set of 138 points from GeoNet [7] (permanent GNSS network of New Zealand/NZGD2000) forms the test network of our study.

The necessary data for the processing consists of observations archived in files of 24 h/30 s cadence, during one year (November 16th, 2016–November 30th, 2017), of precise ephemeris and accurate clocks of the IGS and auxiliary files. The treatment was carried out by RTKLIB 2.4.2 software [8]

B. Gourine (✉) · S. H. Allal · H. Dekkiche · K. Hasni
Department of Space Geodesy, Centre of Space Techniques, 31200 Arzew, Algeria
e-mail: bachirgourine@yahoo.com; bgourine@cts.asal.dz

N. Sundararajan et al. (eds.), *On Significant Applications of Geophysical Methods*,
Advances in Science, Technology & Innovation, https://doi.org/10.1007/978-3-030-01656-2_48

(University of Marine Sciences and Technology of Tokyo). The results obtained were time series of position (daily solutions) estimated by the PPP-static method and expressed in the topocentric coordinate system (NEU: Northing, Easting, Up) with their precisions. The station displacement components were derived from each coordinate time series.

2.2 Deformation Analysis

Assuming infinitesimal deformations and continuous, homogeneous and elastic media, the strain tensors of a geodetic network can be defined as follows: The 2D local displacement field around a given point $M(x, y)$, is simply the difference of coordinates of this point between two epochs, as:

$$U(x,y) = \begin{pmatrix} u(x,y) \\ v(x,y) \end{pmatrix} \tag{1}$$

This representation of deformation mainly suffers from dependence on a reference frame. In our case, the displacement vectors are absolutes even if they are derived from PPP method. The strain tensor $E(x, y)$ is defined as the gradient of the displacement field and is expressed by:

$$E(x,y) = \frac{\partial U(x,y)}{\partial X} = \begin{pmatrix} \frac{\partial u}{\partial x}(x,y) & \frac{\partial u}{\partial y}(x,y) \\ \frac{\partial v}{\partial x}(x,y) & \frac{\partial v}{\partial y}(x,y) \end{pmatrix} = \begin{pmatrix} e_{ux} & e_{uy} \\ e_{vx} & e_{vy} \end{pmatrix} \tag{2}$$

This matrix gathers most of the information of the displacement field behavior. However, its interpretation is not obvious. So, the decomposition of this matrix in invariant deformation primitives makes the representation of the deformation meaningful. In this study, the deformation parameters are [9]:

- Total dilatation:

$$\Delta = e_{ux} + e_{vy} \tag{3}$$

- Total shear:

$$\gamma = \sqrt{(e_{ux} - e_{vy})^2 + (e_{uy} + e_{vx})^2} \tag{4}$$

- Axis of maximum strain:

$$e1 = (\Delta + \gamma) \tag{5}$$

- Axis of minimum strain:

$$e2 = (\Delta - \gamma) \tag{6}$$

3 Results and Discussion

Figure 1 shows the velocity field obtained by interpolation of GNSS network displacement vectors on regular grid (0.5° × 0.5°). The displacements on measured points are

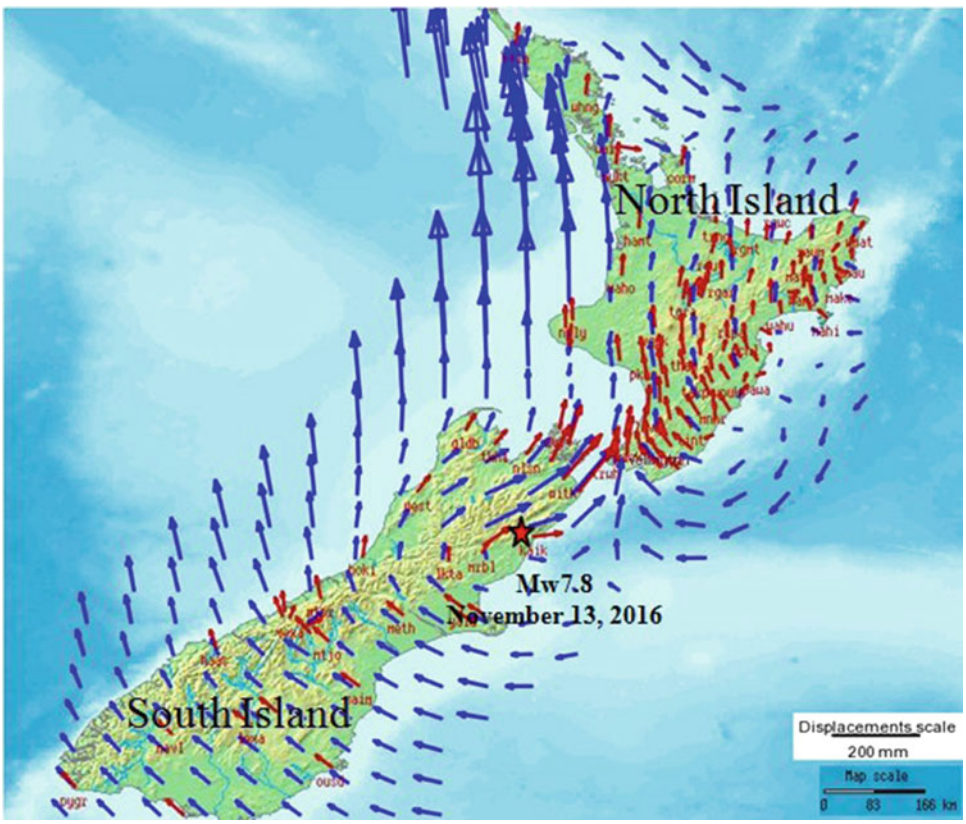

Fig. 1 Displacements and velocity field of New Zealand GNSS network

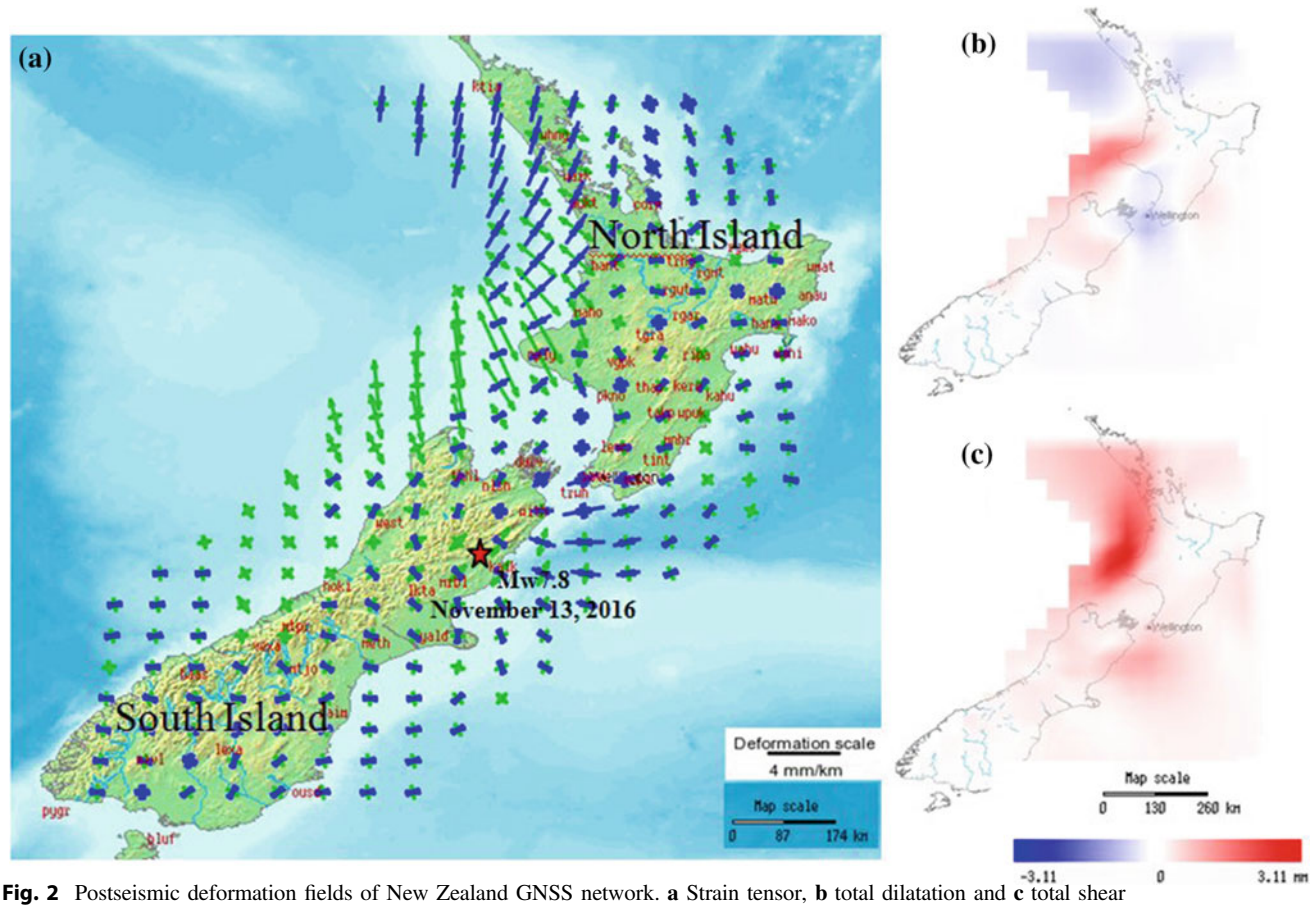

Fig. 2 Postseismic deformation fields of New Zealand GNSS network. **a** Strain tensor, **b** total dilatation and **c** total shear

displayed in red color and the interpolated ones in blue color where they are characterized by NW direction, at South Island of about of 44 mm/year, which are mainly caused by tectonic activity (alpine fault, oblique collisional regime). Indeed, this part of the region is far from the Kaikoura earthquake epicenter. The velocity field at the Northern South Island is of amplitude of 13 mm/year, in NE direction, which is in the same rupture orientation of the seism. This is due to the closeness to the location of the main shock. In the Northern Island, most of the directions of displacements are in the North showing a Hikurangi subduction system.

Figure 2 illustrates the deformations field of New Zealand GNSS network, in terms of strain tensors, total shear and total dilatation. It displays the axis of maximum and minimum strains. Over most of the region, the size of the deformations is minimal with an average of 0.5 mm/km/year. But at the frontier between both islands (South and North) the deformations are significant (4 mm/km in maximum) with important compression and dilatation where the highest value reach 3.11 mm/km. Also, significant shears are observed in that region.

4 Conclusion

The aim of this paper is to perform a deformation analysis of the New Zealand GNSS network after the Kaikoura Earthquake (M = 7.8) which occurred on November 13th, 2016. The PPP method was successfully used for post-seismic monitoring. The deformation analysis methodology is based on the estimation of displacements, generating velocity and deformation fields. It allowed an easy interpretation of the obtained results which showed a tectonic behavior of New Zealand region and post-seismic deformation, notably, near the epicenter zone.

References

1. Ge, M., Gendt, G., Rothacher, M., Shi, C., Liu, J.: Resolution of GPS carrier-phase ambiguities in precise point positioning (PPP) with daily observations. J. Geodesy **82**, 389–399 (2008)
2. Zumberge, J.F., Heftin, M.B., Jefferson, D.C., Watkins, M.M., Webb, F.H.: Precise point positioning for the efficient and robust

analysis of GPS data from large networks. J. Geophys. Res. **102**, 5005–5017 (1997)
3. Larson, K.M., Bodin, P., Gomberg, J.: Using 1-Hz GPS data to measure deformations caused by the Denali fault earthquake. Science **300**, 1421–1424 (2003). https://doi.org/10.1126/science.108
4. Wang, R., Parolai, S., Ge, M., Jin, M., Walter, T.R., Zschau, J.: The 2011 Mw 9.0 Tohoku earthquake: comparison of GPS and strong-motion data. Bull. Seismol. Soc. Am. **103**, 1336–1347 (2013)
5. Wu, Y., Wu, C.: Approximate recovery of coseismic deformation from Taiwan strong-motion records. J. Seismol. **11**, 159–170 (2007)
6. Deformation Analysis Homepage. http://www.vugtk.cz/~deformace
7. GeoNet Homepage. Geological Hazard Information Website for New Zealand. https://www.geonet.org.nz
8. Takasu, T.: User Manual of Software RTKLIB Ver. 2.4.2 (2013)
9. Talich, M.: Geometrical analysis of deformation measurement using continuum mechanics by web application. In: FIG Working Week Proceedings, pp. 1–13, Hong Kong, China (2007)

Contemporary Seismic Code of Russia and Other Countries of Former Soviet Union

Nadira Mavlyanova

Abstract

This paper reviews the seismic hazard issues on the territory of Russia and some other Former Soviet Union countries. The USSR included 15 states that had a unified political and economic system. In 1991, after the collapse of the USSR, 15 independent states were formed on the territory of the previously united country and thus new boundaries were formed, and the existing environmental problems have become cross-border. After the USSR eventually disintegrated, new building codes were introduced by each Republic (and the difference between the states is rather big). Some independently seismic hazard maps were developed, according to its individual specificities (which show considerable discrepancies along national borders), and they independently participated in several international projects on seismic risk assessment.

Keywords

Seismic zoning map • Seismic code • USSR Uzbekistan

1 Introduction

In Russia, as well as other CIS countries, research of seismic hazards has a long history (Commonwealth of Independent States). As an example, the instrumented seismology started in 1892, when 14 seismographs of Russian Geographical Society were settled in Tashkent city. In May 1901, Repsold-Zelner instruments were installed. Since the 13th July 1901, regular seismic observations have been recorded from fixed stations [1]. Seismic zoning maps were compiled for all the territory of the USSR several times.

N. Mavlyanova (✉)
Sergeev Institute of Environmental Geoscience of Russian Academy of Sciences, Ulansky Pereulok 13, Building 2, P.O. box 145 Moscow, 101000, Russia
e-mail: georisk2015@mail.ru

Subsequently, the Soviet Union included 15 states: Azerbaijan, Armenia, Belarus, Estonia, Georgia, Kazakhstan, Kyrgyzstan, Latvia, Lithuania, Moldova, Russia, Tajikistan, Turkmenistan, Ukraine, and Uzbekistan. All of them had unified political and economic system during 69 years (from 1922 to 1991). After the collapse of the USSR, on the territory of the previously united country, 15 independent states were formed, and new boundaries were formed respectively, and the existing environmental problems have become cross-borders. Recently, a feature of the post-Soviet model of cross-border cooperation is, on the one hand, cultural-historical proximity of the countries participating, and on the other hand economic and political differences that require from neighboring countries considerable effort. The development of an integration processes between the countries-participants of the former USSR has been a process with several stages and multiple projects. There are several international and regional organizations created on the post-Soviet territories: the Commonwealth of Independent States (CIS), the Eurasian economic Union (EEU), and Organization of collective security Treaty (CSTO). The geological features of this vast region determine the probability of occurrence of different existing natural disasters with catastrophic social and economic damage. The cross-border cooperation is essential to deal with seismic damage such as different risks of floods, landslides, pollution of surface and ground water because natural hazards can be a cause of destruction anywhere, despite the boundaries between states.

2 Contemporary Seismic Code and Seismic Zoning Map

The maps of seismic zoning for the territory of the USSR during its existence were compiled four times. The first map was made in 1937, then the following maps in 1957, 1968 and 1978. The last seismic zoning map in 1978 was a common standard for several years after USSR broke up. As

N. Sundararajan et al. (eds.), *On Significant Applications of Geophysical Methods*,
Advances in Science, Technology & Innovation, https://doi.org/10.1007/978-3-030-01656-2_49

far as before the disintegration of the USSR, a national seismic-zoning map and seismic code, was used by all the republics in the same way. After getting the status of independency, common standards and rules for assessment and mapping of seismic hazards were imposed along with appropriate anti-seismic design and construction guidance. It is worth noting here, that information was taken from hard lessons of past disastrous earthquakes, for example, at Spitak city (1988, Armenia), Zaisan city (1990, Kazakhstan), Racha-Djavsk city (1991 in Georgia), Susamir city (1992, Kyrgyzstan) and at Neftegorsk city (1995, Russia). These natural disasters underlined inadequacies in the seismic hazard zonation and revealed the seismic vulnerability of buildings common types.

For example the recent seismic zoning map in Russia compiled in 1997 and is modifying several times, now Russia has a General Seismic Zoning Map of 2014, and new seismic building design code also approved in 2014.

In Uzbekistan, all the design institutes use the new seismic code KMK 2.01.03-96 for the purposes of seismic resistant designs. "Norms and Regulations for Construction in Seismic Zones" was approved by the government in 1996. In Tajikistan the new seismic zoning map and seismic code was approved in 2007.

3 Seismic Code of Uzbekistan

This section shortly presented the seismic code of Uzbekistan which was one of the Former Soviet Union countries. The territory of the Uzbekistan Republic is located in a zone of high seismicity. Several cities such as the capital Tashkent with a population of 3 million people, famous ancient cities Samarkand and Bukhara and others have expected seismic intensity YIII and IX (MSK). The earthquakes on the territory of Uzbekistan are the most frequent and dangerous. There happened more than 10 violent and destructive earthquakes with M = 5.5–7.3 that took place the last 40 years [2].

A reduced version of the official seismic hazard map for the former Soviet Union, indicates that Tashkent can expect earthquakes with intensity VIII (by MSK scale). There are two reasons to believe that this map significantly underestimated the regions hazard. First, it does not take into account important parameters such as a local soil conditions, because soft soil can produce intensities of one or more MSK units greater than on nearby stiff soils. Second, all of the recent destructive earthquakes in the Former Soviet Union have been significantly larger than would be expected examining the map (even allowing for soft-soil conditions) [3].

In order to prevent seismic threat, all the design institutes use the seismic code "Norms and Regulations for Construction in Seismic Zones" [4] and "Town-planning, lay-out and building of urban and rural settlements", put into operation by the state Committee for architecture and construction in 1994 and 1996.

To decrease the seismic vulnerability of buildings, it is necessary to reduce the seismic loadings and increase the resistance to seismic influences. When developing projects and carrying out reconstruction works of existing buildings it is crucial to take into account the parameters of a seismological regime of the construction area: expected intensity of seismic effects; repeatability of earthquakes; spectral structure of seismic fluctuations of the basis.

The seismic code consists of 6 basic sections [4].

1. Principle position. In this part of the code, the main problems relate to the construction in areas with seismic intensity greater than VI. At specialized research institutes, the seismicity of the construction site should be determined on the basis of a map of seismic micro-zoning in areas with similar intensity of seismicity, according to a Table developed taking into account all soil conditions in the construction area. For example, the site seismicity can be reduced by 1 point from the initial seismicity if the construction site is located on rocky soil with a velocity of seismic waves of VP >3000 m/s and VS >1700 m/s. The seismicity of the construction site can be increased by 1 point from the initial seismicity if the construction site is located on loess soils with a porosity coefficient e > 0,8 or with the velocity of seismic waves against <300 m/s.
2. Calculations of seismic effects. Calculations of the designed structures and foundations of buildings for seismic areas are carried out taking into account the main and special combinations of loads and seismic effects.
3. Residential and public, industrial buildings and facilities. In this paragraph, we consider the different types of structures used in construction.
4. Underground facilities and utilities. This paragraph considers the requirements for the construction of underground facilities and utilities in seismic hazardous areas.
5. Reconstruction and strengthening of buildings. The requirements of this unit must be met when holding and increasing seismic resistance, including the restoration of damaged buildings by an earthquake and other natural hazards; strengthening due to changes in seismic resistance of the settlement or reconstruction of the object.
6. Features of production and quality control. In the manufacture of building materials and construction of buildings must comply with the degree of quality that ensures the operation of the object in the specified period of operation. The paragraph of this Code defines the requirements for the quality of building materials and

monitoring system in compliance with the rules of seismic construction. Ensuring compliance with the design rules is the responsibility of the General state expert Commission. Construction monitoring is carried out under the architectural supervision of design organizations, the technical service of builders, as well as the General architectural and construction Inspection of the State Committee for architecture and construction.

In Annex I, the intensity and return period of earthquakes with a probable intensity of more than VII shall be determined by a special table attached to this project code. This list includes 333 occupied points of Uzbekistan located in seismic areas.

4 Conclusion

For almost seventy years in the ex-USSR, all former Soviet Republics used common standards and rules for assessment and mapping of seismic hazards for anti-seismic design and construction. After the disintegration of the USSR in 1991 all these new independent countries introduced into practice their own building codes, which differed considerably from one country to another; they developed national maps of seismic hazards, which show considerable discrepancies along the national borders. The scientific collaborative links between the seismological and earthquake engineering institutions of the independent countries were broken or became inefficient. The development of a harmonized approach to seismic vulnerability classification of buildings is considered as one of the main goals of the cross-border collaboration, because currently the earthquake engineers in different countries use different building classifications based on the national building codes.

References

1. Mavlyanova, N., Denisov, I., Lipatov, V.: A review of central Asian trans-border issues associated with environmental problems and hazard mitigation. In: Environmental Security of the European Cross Border Energy Supply Infrastructure. Springer (2015)
2. GeoHazards International: Lessons for Central Asia from Armenia and Sakhalin. GeoHazards International, Stanford (1997)
3. Artikov, T., Ibragimov, R., Ibragimova, T., Mirzaev, M.: Synoptic forecast of the sites of the expected seismic activation for the next few years. In: Proceedings of International Conference on Actual Problems of Modern Seismology, pp. 191–198. Lesson Press, Tashkent, Uzbekistan (2017)
4. Seismic Code of Uzbekistan KMK 2.01.03-96: Norms and Regulations for Construction in Seismic Zones. Tashkent, Uzbekistan (1996)

Possible Tsunami Wave Heights in the Eastern Mediterranean Region from 1222 Paphos Earthquake

Ergin Ulutaş

Abstract

The aim of this study is the simulation and visualization of the initial and maximum tsunami wave heights along the Eastern Mediterranean coasts inferred from a largest earthquake in history in this region. The earthquake considered in the study is 11 May 1222 Paphos earthquakes. The study was conducted to explain what the potential tsunami consequences caused by similar earthquakes occurring in the Eastern Mediterranean region could be in the future. The methodology used for the calculation of tsunami wave heights from the earthquake included the determination of earthquake parameters, modeling of the initial wave height, simulation of the wave propagation and calculation of the maximum wave heights near coastal areas. The numerical models were performed by using nonlinear and dispersive long wave tsunami models with GEBCO30 bathymetry data for a 0.25 arc-min calculation grid scale. The simulated waves were particularly high on the south shore of the Cyprus Island. Although the magnitude of the earthquake could lead to higher wave tsunamis occurrence, Cyprus Island as a barrier for Turkish coasts offers protection against such tsunamis. The arrival times of tsunami waves according to the possible large earthquakes around south of Cyprus was also calculated.

Keywords

Tsunami waves • Eastern Mediterranean • Shallow water theory • Earthquake source parameters

1 Introduction

The Mediterranean region is seismically very active. Although the large-scale geodynamic regime is dominated by the 100 Myr long convergent motion between Africa and Eurasia, the regional-scale kinematics reveals a very complex pattern (Fig. 1). Some of the major earthquakes that triggered tsunamis are 21 July 365 Crete, 11 May 1222 Paphos, 8 August 1303 Crete, 3 May 1481 Rhodes, 28 December Messina and 21 May 2003 Algeria. The 1222 Cyprus earthquake occurred at about 06:15 UTC on 11 May. It had an estimated magnitude of 7.0–7.5 and triggered a tsunami that was recorded in Alexandria. The strongest shaking was felt in Nicosia, Limassol and Paphos [1]. Seismicity can be followed through the whole area, as it described a rather convoluted active belt (Fig. 1). With the increasing rate of economic development of coastal regions, there is also an increase in socio-economic consequence resulting from the hazardous action of tsunami waves generated from submarine seismic activity and other causes (e.g. [2]). For this reason, the results of this study could be used for evaluating the tsunami potential in the region, installing alarming facilities and preventing economic losses.

2 Methodology for Tsunami Generation and Source Modelling

Tsunamis are very large ocean or sea wave triggered by various large scale disturbances of the ocean floor such as submarine earthquakes, volcanic activities or landslides [1]. It is important to model the size of disturbances of the ocean floor for calculation and propagation of the tsunami waves. When an earthquake occurs beneath the sea, the water above the deformed area is displaced from its equilibrium position. Then, waves are formed as the displaced water mass, which acts under the influence of gravity, attempts to regain its equilibrium (e.g. [3]). The final amplitude of a tsunami wave

E. Ulutaş (✉)
Department of Geophysical Engineering, Kocaeli University, 41200 Kocaeli, Turkey
e-mail: ergin.ulutas@gmail.com

N. Sundararajan et al. (eds.), *On Significant Applications of Geophysical Methods*, Advances in Science, Technology & Innovation, https://doi.org/10.1007/978-3-030-01656-2_50

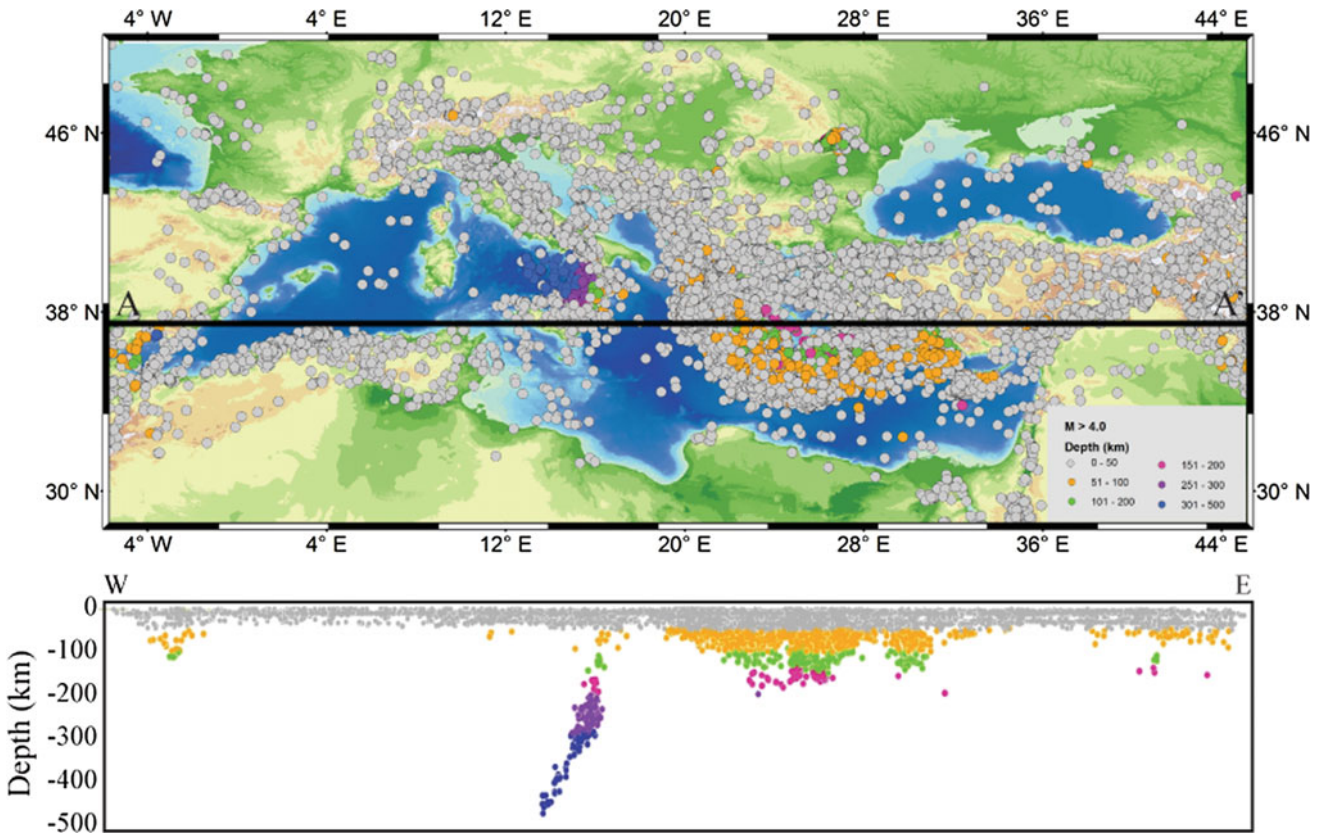

Fig. 1 **a** Location of epicenters and a profile (black line) and **b** depths of the earthquakes to be projected onto the profile for a cross-section view of A-A′. Earthquake depths are color-coded according to the depth scale in the lower right

at coasts is a combination of the amplitude of the tsunami on the high seas. In this study it was used as a common approach that the waves are formed as the displaced water mass and the deformation of the ocean floor is the initial condition of the tsunami modeling. Then, the approximation of non-linear long wave equations [4] was performed in geographical coordinates and adopted to simulate tsunami propagations with an initial displacement of the ocean bottom deformation due to faulting. For the tsunami simulations presented herein, a SWAN code [4] was used to solve incompressible shallow water equations with a finite difference scheme in time and space including Coriolis and frictional effects. The model used finite difference scheme in time which included Coriolis and frictional effects. In order to model the tsunami caused by May 11, 1222 (M_w: 7.5) Paphos earthquake, uniform slip distributions on a single rectangular fault were used. Initial tsunami heights were calculated by setting the fault geometry under the assumption of a uniform slip using a statical dislocation model (e.g. [5]). For the input values; the length (L) and Width (W) of the rectangular fault were inferred from moment magnitude using the scaling law [6].

$$\mathrm{Log\,L} = -2.42 + 0.58\mathrm{M} \tag{1}$$

and

$$\mathrm{Log\,W} = -1.61 + 0.41\mathrm{M} \tag{2}$$

where M is the moment magnitude, L is the subsurface rupture length (km) and W is the down dip rupture width (km). The slip amounts (S) of rectangular fault were inferred from the moment magnitude calculation equations:

$$\mathrm{M_0} = \mu\mathrm{SLW} \tag{3}$$

where μ is the rigidity of the earth crust, S is the amount of average slip motion (slip), M_0 is the scalar moment of an earthquake. The rigidity was assumed 30 GPa to calculate the seismic moment. Using the above mentioned equations, the fault plane was calculated in length and width with an average uniform slip on fault plane corresponding to the source parameters for a uniform model from the source parameters of Yolsal and Taymaz [1] based on the analyzing tele-seismic long-period P- and SH- and broad-band P waveforms (Table 1). The calculation times for the tsunami propagations for uniform slip model of 1222 Paphos earthquake is 4.0 h. The maps of maximum tsunami heights performed using a 0.25 min cell size in order to describe more reasonable tsunami heights for the Eastern

Table 1 Source parameters for the tsunami simulation from uniform slip model

M_w	7.5
Latitude of epicenter	34.7 N
Longitude of epicenter	32.6 E
Focal depth (km)	15.0
Strike/dip/rake	305/35/110
Average slip (m)	3.0
Fault length (km)	85
Fault width (km)	30

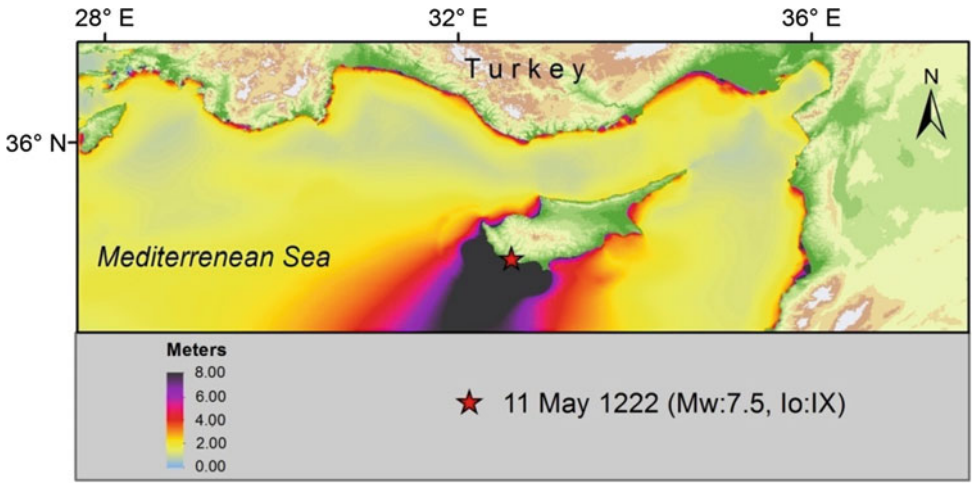

Fig. 2 Maximum simulated heights from uniform slip model with a cell size of 0.25 min of the 1222 Paphos earthquake. The red star depicts the possible epicenter location of the earthquake with M_w: 7.5

Mediterranean Region due to GEBCO30 bathymetrical data set (Fig. 2).

3 Results and Discussions

In this study, maximum tsunami heights for the historic 11 May 1222 Paphos earthquake was simulated. The scenario earthquake thought to be the same location of the Paphos earthquake is based on the reverse fault mechanism solutions, known as the worst case scenario earthquakes for tsunamis. This approach corresponds to the tectonic properties of the previous focal mechanism solutions calculated in the area of south Cyprus. Based on the tsunami simulations, the southern part of Cyprus shows the earliest arrival of tsunamis. The simulated highest tsunami heights were 3.12 m in Kouklia (Cyprus), 3.95 m in Yennadhi, Rodos (Greece), 1.52 m in Tarabulus (Lebanon), 0.37 m in Tartus (Syria), and 0.76 m in Selimiye (Turkey). Anamur town, a town in South of Turkey, was the earliest to be exposed to arrival times in Turkey from the earthquake. The results demonstrated that awareness of tsunami hazard should be spread in the Eastern Mediterranean region. The authorities should focus on analyzing the state of the tsunami risk communication strategies, and intend evacuation behavior along the coastal areas especially for tourist areas in the region to reduce possible loss of lives.

References

1. Yolsal, S., Taymaz, T.: Sensitivity analysis on relations between earthquake rupture parameters and far-field tsunami waves: case studies in the Eastern Mediterranean region. Turk. J. Earth Sci. **19**, 313–349 (2010)
2. Jaiswal, R.K., Singh, A.P., Rastogi, B.K.: Simulation of the Arabian Sea tsunami propagation generated due to 1945 Makran earthquake and its effect on the western coast of India. Nat. Hazards **48**, 245–258 (2009)
3. Ulutas, E.: Comparison of the seafloor displacement from uniform and non-uniform slip models on tsunami simulation of the 2011 Tohoku-Oki earthquake. J. Asian Earth Sci. **62**, 568–585 (2013). https://doi.org/10.1016/j.jseaes.2012.11.007
4. Mader, C.: Numerical Modeling of Water Waves. CRC Press (2004). ISBN 0-8493-2311-8
5. Okada, Y.: Surface deformation due to shear and tensile faults in a half-space. Bull. Seismol. Soc. Am. **75**, 1135–1154 (1985)
6. Wells, D.L., Coppersmith, K.J.: New empirical relationships among magnitude, rupture length, rupture width, rupture area, and surface displacement. Bull. Seismol. Soc. Am. **84**(4), 974–1002 (1994)

Faulting Style and b-Value: A Global Perspective

Emad Al-Heety and Losyan Al Esho

Abstract

The b-value in the frequency-magnitude relation provides significant information to understand seismicity, seismotectonics, and seismic hazard analysis. In this study, we investigated the relation between the b-value and faulting style on a global scale. The used data were extracted from the Global Centroid Moment Tensor (GCMT) catalog. The least square fit and maximum likelihood methods were used to calculate the b-value. The obtained results show that thrust, strike-slip and normal-faulting earthquakes, occur in regions of low, intermediate, and high b-values, respectively. Our results are in good agreement with the previous works, and we found that the study scale does not affect the hypothesis of a general relationship between faulting style and the b-values ($b_{normal} > b_{strike\text{-}slip} > b_{reverse}$).

Keywords

b-constant • Normal fault • Reverse fault • Strike-slip • Maximum likelihood

1 Introduction

The distribution of earthquake size follows the power law proposed by Gutenberg and Richter [1] in the form: $Log_{10}N = a - bM$, where N is the cumulative number of earthquakes with magnitude $\geq$M. The *a* and *b* constants describe the seismic activity and the event-size distribution, respectively. The possible relations between the b-value and geophysical parameters were investigated by many authors, such as, material heterogeneity [2], stress state [3], earthquake depth [4], heat flow [5], and with faulting style [6]. The potential relation between the b-value and faulting type was studied on local and regional scales, in California, Japan [6], Italy [7], and India [8]. These studies reported high b-values in normal faulting regions, and intermediate and low values in strike-slip and reverse faulting regions, respectively. The lack of studies at the global scale motivated us to carry out this work. The aim of this study was to investigate the potential relation between the b-values and the faulting type, particularly, pure normal, pure reverse and pure strike-slip faults.

2 Data and Methods

The source of the used data is the Global Centroid Moment Tensor catalog GCMT (http://www.Globalcmt.org/CMTsearch.html). The catalog covers the period from Jan. 1976 to Dec. 2005. We selected only the shallow (depth less than 70 km) pure normal, strike-slip and reverse faults events and excluded the oblique faults events. When selecting earthquakes, we took into account the uncertainties in estimating the rake of slip which represents ±5°. In this study, the fault plane solution of 2575 earthquakes of Mw equals or larger than 5 was used to investigate the relation between the b-value and the faulting type, Fig. 1 Calculating the magnitude of completeness (Mc) of the earthquake catalog was a necessary step for correctly estimating the values of *b* and *a* [9]. There are two methods to calculate the b-value: the Least Square Fit (LSF) and the Maximum Likelihood (ML). In the LSF-method, the log values of the cumulative number of earthquakes (Nc) are plotted against magnitude (Mw). In the ML method, the b-value is estimated using the following equation [10]:

E. Al-Heety (✉)
Department of Applied Geology, University of Anbar, Rammadi, Iraq
e-mail: emadsalah@unoanbar.edu.iq

L. A. Esho
Department of Geology, University of Mosul, Mosul, Iraq

N. Sundararajan et al. (eds.), *On Significant Applications of Geophysical Methods*,
Advances in Science, Technology & Innovation, https://doi.org/10.1007/978-3-030-01656-2_51

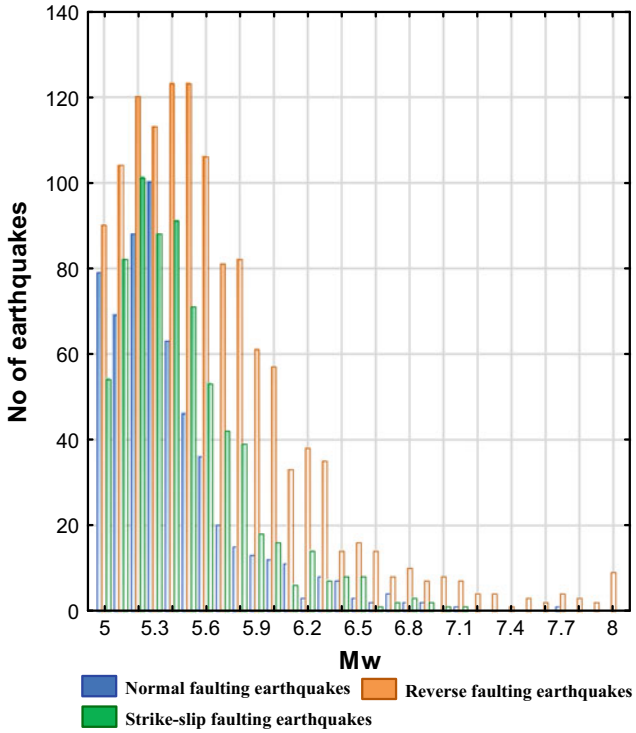

Fig. 1 Number of earthquakes as a function of magnitude

$$b = \frac{\mathrm{Log}_{10} e}{(M_{mean} - M_c)} \tag{1}$$

where M_{mean} is the mean magnitude of a sample of earthquakes with M > Mc, Mc is the magnitude of completeness and $\log_{10}e = 0.4343$. An uncertainty of the b-value is estimated by Aki [10]:

$$\delta_b = \frac{b}{\sqrt{N}} \tag{2}$$

where N is the number of earthquakes. In our study, we used both methods mentioned above to estimate the b-values for pure normal, reverse, and strike-slip faulting earthquakes.

3 Results

The magnitudes of completeness Mc are 5.1, 5.1 and 5.2 for reverse and normal events and strike-slip events, respectively. The b-values calculated by both methods are shown

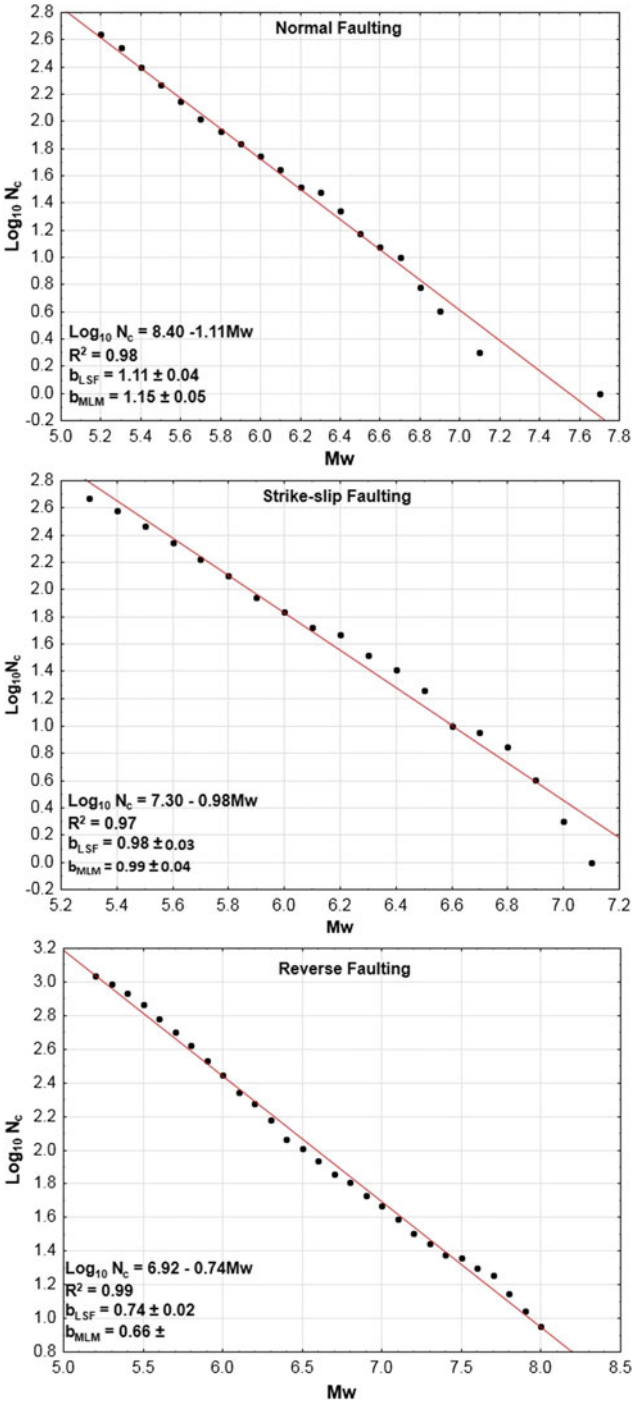

Fig. 2 Frequency-magnitude distribution of different faulting styles earthquakes. b_{LSF} value is calculated by least square fitting, b_{MLM} is calculated by maximum likelihood method

in Fig. 2.The main trend for the derived b-values for the three faulting styles is: $b_{\text{normal faulting}} > b_{\text{strike-slip faulting}} > b_{\text{reverse faulting}}$. Both calculation methods show the same trend.

4 Discussion

As far as we know, the present study is the first attempt to investigate the relation between b-values and faulting style for a global earthquake catalog. Previous studies investigated the potential relation between b-values and faulting style only on local and regional scales [6–8]. These studies showed that normal faulting events typically show higher b-values, while strike-slip and reverse events have intermediate and low b-values, respectively. Schorlemmer et al. [6] found that the b-value acts as a stress meter, and that it is inversely proportional to the differential stress. Recently, Wu et al. [11] investigated the relation between b-values and crustal stress in a young orogenic belt in Taiwan. They found that high b-values correlate with normal faulting, and intermediate and low b-values correlate with strike-slip and reverse faulting, respectively. In the Mexican subduction zone, normal faulting events occur in high b-value regions while reverse events occur in low b-value regions [4]. Our results are therefore consistent with the linear decrease of the stress state from normal to strike-slip to reverse [6, 7]. Scholz [12] found that b-values decrease linearly with the differential stress in the continental crust. The low b-values reflect high differential stress while high b-values indicate low differential stress.

5 Conclusion

Investigating the relation between different faulting types and b-values for a 30-years long global catalog of earthquakes reveals that reverse faulting is associated with low b-values, while normal and strike-slip faulting are associated with high and intermediate b-values, respectively. We thus found that the scale of the study, whether local, regional or global, does not affect the relation between the b-values and the faulting type. We note that these findings do not depend on the calculation method for estimating the b-values.

References

1. Gutenberg, B., Richter, C.: Frequency of earthquakes in California. Bull. Seismol. Soc. Am. **34**, 185–188 (1944)
2. Mogi, K.: Magnitude-frequency relation for elastic shocks accompanying fractures of various materials and some related problems in earthquakes. Bull. Earthq. Res. Inst. Univ. Tokyo **40**, 831–853 (1962)
3. Scholz, C.: The frequency—magnitude relation of microfracturing in rock and its relation to earthquakes. Bull. Seismol. Soc. Am. **58**, 339–415 (1968)
4. Rordríguez-Pérez, Q., Zuũiga, F.: Imaging b-value depth variations within the Cocos and Rivera plates at the Mexican subduction zone. Tectonophysics **734–735**, 33–43 (2018)
5. Kalyoncuoglu, U., Elitok, O., Dolmaz, M.: Tectonic implications of spatial variation of b-values and heat flow in the Aegean region. Mar. Geophys. Res. **34**, 59–78 (2013)
6. Schorlemmer, D., Wiemer, S., Wyss, M.: Variations in earthquake-size distribution across different stress regimes. Nature **437**, 539–542 (2005)
7. Gulia, L., Wiemer, S.: The influence of tectonic regimes on the earthquake size distribution: a case study for Italy. Geophys. Res. Lett. **37**(L110305) (2010). https://doi.org/10.1029/2010gl043066
8. Bora, D., Borah, K., Mahanta, R., Borgohain, J.: Seismic b-values and its correlation with seismic moment and Bouguer gravity anomaly over Indo-Burma ranges of northeast India: Tectonic implications. Tectonophysics **728–729**, 130–141 (2018)
9. Woessner, J., Wiemer, S.M.: Assessing of the quality of earthquakes catalogues: estimating the magnitude of copletenes and its uncertainty. Bull. Seismol. Soc. Amer. **95**, 684–698 (2005)
10. Aki, K.: Maximum likelihood estimate of b in the formula logN = a−bM and its confidence. Bull. Seismol. Soc. Am. **43**, 237–239 (1965)
11. Wu, Y., Chen, S., Huang, T., Huang, H., Chao, W., Koulakov, I.: Relationship between earthquake b-values and crustal stresses in a young orogenic belt. Geophys. Res. Lett. (2018). https://doi.org/10.1002/2017gl076694
12. Scholz, C.: On the stress dependence of the earthquake b value. Geophys. Res. Lett. **42**, 1399–1402 (2015). https://doi.org/10.1002/2014GL06286394

Seismic Hazard Assessment of Al Mashair Area, Makkah Al-Mukaramah (Saudi Arabia)

Kamal Abdelrahman, Abdullah M. Al-Amri, Naif A. Al-Otaibi, Mohammad Fnais, and Enayat Abdelmonem

Abstract

Makkah is one of the most important cities not only in Saudi Arabia but also for all Muslims all over the world. Recently, it has experienced strong earthquakes that caused panic due to the fact that it is mostly occupied by soft Quaternary deposits overlying basement rocks. The spatial variation of ground motion in Al Mashair area was estimated by generating synthetic ground motion considering the point source model coupled with site response analysis. The rock level peak ground acceleration time histories was simulated at 87 sites in Al Mashair area for maximum credible earthquake moment magnitude 5.0. The results are presented in the form of peak ground acceleration (PGA) at rock level. In addition, the ground surface acceleration assessed by horizontal to vertical spectral ratio technique based on microtremor measurements at 87 sites. The ground surface response spectral curves with 5% critical damping were calculated using shear wave velocity calculations from the MASW results and the earthquake time histories. Surface response spectral values were mapped using the GIS platform at 1.5, 3.0, 5.0, 8 and 10 Hz. The surface ground motion maps show that the hazard level ranges from low to moderate with spectral acceleration (SA) in the range from 13 to 124 cm/s^2.

Keywords

Seismic hazard • Al Mashair area • Makkah Saudi Arabia

1 Introduction

Makkah area experienced some of destructive earthquakes in recent times and through history. The most serious recorded earthquake had 7.2 magnitude and occurred in 1967 to the southwestern side of Jeddah city in the Red Sea axial trough. This earthquake affected Makkah and the adjacent area. The historical records of earthquakes in Makkah, the 12/4/1413H Al-Sharai'a earthquake, the 8/8/1426H non-tectonic seismic shock, and the location of the city less than 70 km from the seismically active Red Sea and its associated potentially active tectonic structures, all warrant a comprehensive seismic hazard, risk, and vulnerability assessments of Makkah. Accordingly, and due to the abovementioned, it is of utmost importance to assess the earthquake activities and its relation to the tectonic trends through Makkah area. These data will represent the input parameters for the seismic hazard assessment study of the area.

2 Soils and Rocks in Makkah City

Makkah is mostly situated over the Quaternary alluvial deposits of Wadi Ibrahim incised into the Precambrian rocks of the Arabian Shield. This is a typical situation for a significant soil amplification [1]. The importance of soil amplification effects to seismic hazard assessment of the city of Makkah can be illustrated by inspecting the geological setting of Makkah. More than 90% of the built-up area of the Makkah city is occupied by the Quaternary soft wadi alluvium sediments of sand and gravel, as well as talus deposits overlying the Precambrian basement [2]. Sonbul [3] reported weak alluvial deposits made up of sand and gravel reaching

K. Abdelrahman (✉) · A. M. Al-Amri
N. A. Al-Otaibi · M. Fnais
Department of Geology and Geophysics, King Saud University, Riyadh, Saudi Arabia
e-mail: khassanein@ksu.edu.sa

M. Fnais
Princess Nourah Bint Abdulrahman University, Riyadh, Saudi Arabia

K. Abdelrahman · E. Abdelmonem
Seismology Department, National Research Institute of Astronomy and Geophysics, Cairo, Egypt

N. Sundararajan et al. (eds.), *On Significant Applications of Geophysical Methods*,
Advances in Science, Technology & Innovation, https://doi.org/10.1007/978-3-030-01656-2_52

19 m in thickness. Further, in north-western Makkah, there are weak soil layers reaching thicknesses as high as 25 m. Moreover, the lithology information acquired from more than 60 boreholes drilled in Makkah city illustrates that the weak alluvial deposits can exceed 30 m in thickness.

3 Seismicity and Seismic Hazard Assessment

The recent earthquake activity of Makkah Al-Mukarramah was recently demonstrated by the event that occurred in September 28th, 1993, when the city was rocked by an earthquake shock located in Al Sharai'a, 30 km northeast of the Holy Mosque. The shock that was felt but not recorded was estimated to have exceeded a magnitude of 3.6. Since then, a series of small earthquakes have occasionally been felt in the Makkah region and recorded by one or more seismic station. Among these is the seismic swarm that occurred at Al Sharai'a in Oct. 3rd, 1993, with the largest felt event having a magnitude of 4.1 [4]. Another felt event with magnitude 3.6 was recorded near the same area in June 18th, 1994. Again, a seismic shock affecting Al Utaibiyya District of Makkah occurred on 8/8/1426H, when people were shocked by the roaring sound of a suspected very shallow focus earthquake, as might be indicated by the extremely localized effect it produced.

The synthetic ground motion model of Boore [5, 6] was used to determine rock level Peak Ground Acceleration (PGA) and generate a synthetic acceleration-time history [7] while ground surface acceleration was calculated based on the integration between bedrock PGA and local site response effects that resulted from shear wave velocity of MASW survey and amplification factors of microtremor measurements.

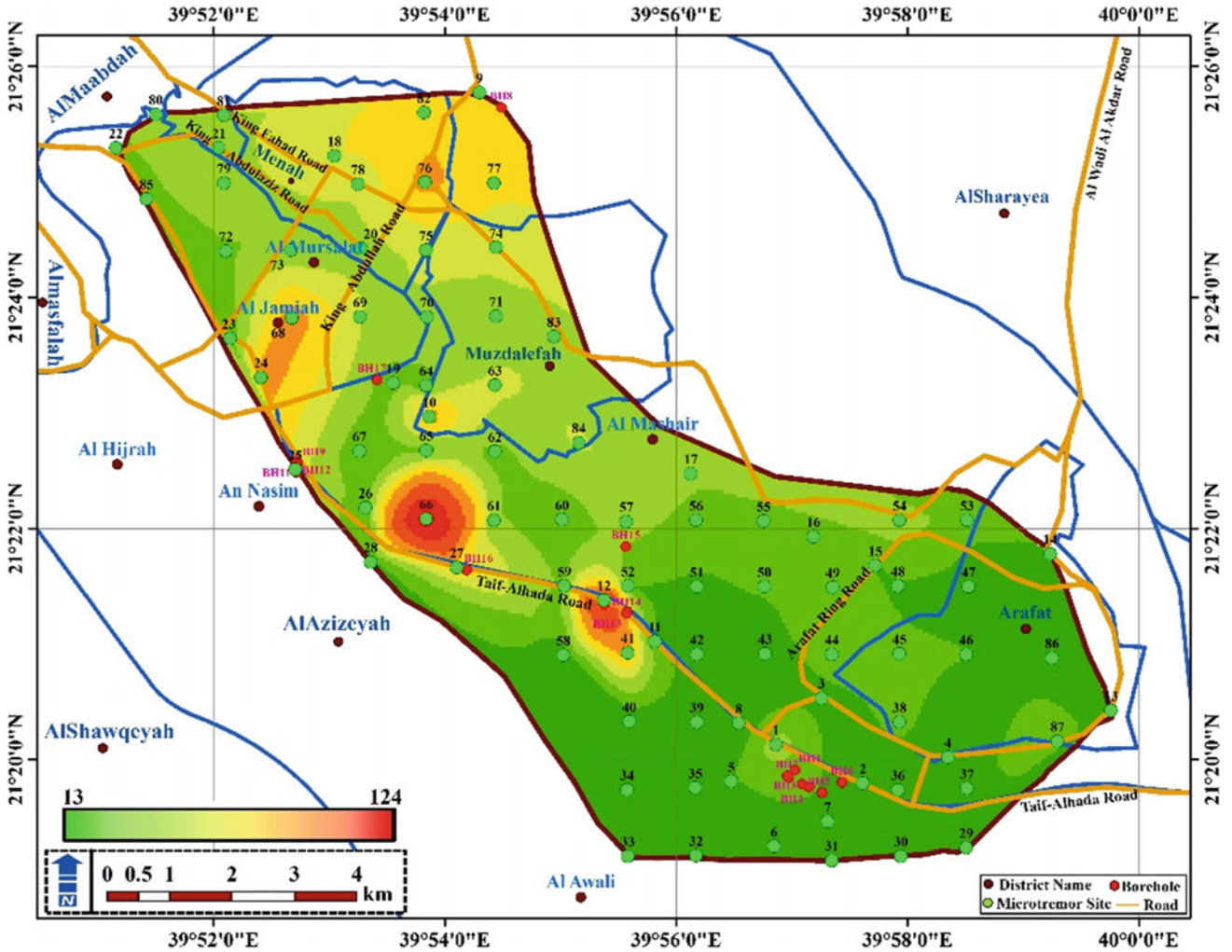

Fig. 1 Distribution of Pseudo-Spectral acceleration at ground surface of Makkah city

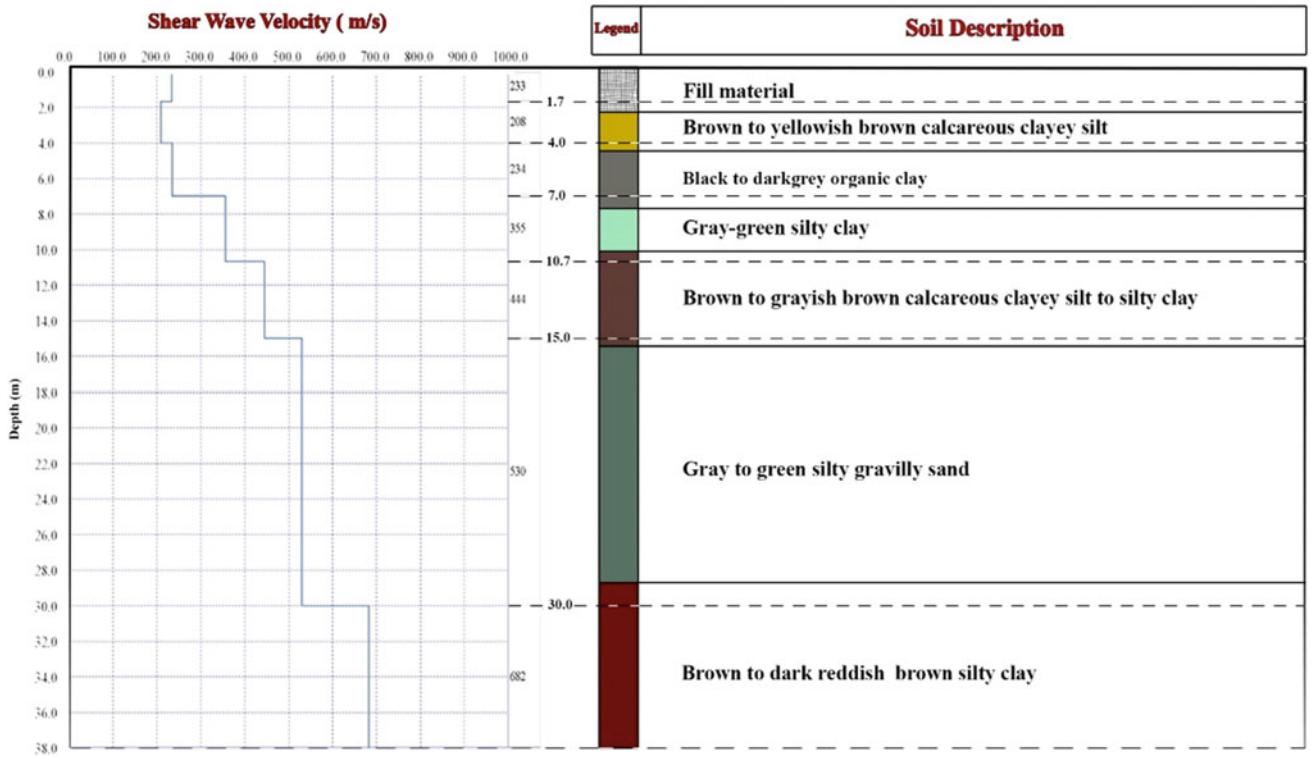

Fig. 2 Correlation between 1 D MASW model and borehole data in the central zone

4 Results and Conclusions

The earthquake amplitudes are usually represented by the peak ground acceleration; however, for structural designs and building codes the most widely used parameter is spectral acceleration and corresponding frequency/period. The Pseudo-Spectral acceleration (PSA) values were computed at 27 locations for 1.5, 3, 5, 8 and 10 Hz with 5% damping ratio using the GIS platform. The above frequencies from 1.5 to 10 Hz were selected because they represented the natural frequency range from tall buildings to single story buildings [8]. The maximum PSA have been computed and contoured using GIS platform (Fig. 1).

The highest PSA values at 1.5 and 3 Hz frequency cover the central and southwestern zones of the Al Mashair area while at 5 and 8 Hz, indicate that the central and southwestern zones have higher PSA and extend to the extreme north-eastern zone. These PSA expand from the central part to cover the whole area of the north-eastern part besides specific areas southwest of the district at 10 Hz. The highest PSA correlated well with areas of soft sediments and/or fill materials where the amplitude of peak acceleration was amplified (Fig. 2). The presence of higher PSA values reflects high seismic risk compared to the lower values. According to this map, PSA ranges from 13 to 124 cm/s^2 where the northern and southwestern parts having higher spectral acceleration than that of the rest of the area. These results will help civil engineers and decision makers for land-use planning of Makkah city.

References

1. Kawase, H.: Site effects on strong ground motions. In: Lee, W.H.K., Kanamori, H., Jennings, P.C., Kisslinger, C. (eds.) International Handbook of Earthquake and Engineering Seismology, Chapter 61, pp. 1013–1030. Academic Press (2003)
2. Solami, A.-A.M., and others.: Saudi Geological Survey (SGS), Geological map of the Greater Makkah area; 1: 50,000. In: Engineering Geological Mapping of the Greater Makkah Al Mukarramah Area. SGS-OF-2005-17 (2004)
3. Sonbul, A.A.R.: Engineering geology as applied to urban development of the north-western area of the Holy city of Makkah. M.Sc., Faculty of Earth Sciences, King Abdul-Aziz Univ. p. 138 (1995)
4. Al Furaih, A.A., Al Aswad, A.A., Kebeasy, R.M.: New aspects on estimating risk around the Makkah region, (abs. 2nd Ann. Mtg., Saudi Soc. of Earth Sci.), Oct. 25–27, p. 19 (1994)
5. Boore, D.M.: Stochastic simulation of high-frequency ground motions based on seismological models of the radiated spectra. Bull. Seism. Soc. Am. **73**, 1865–1894 (1983)

6. Boore, D.M.: Simulation of ground motion using the stochastic method. Pure. Appl. Geophys. **160**, 635–675 (2003)
7. Hwang, H., Huo, J.R.: Attenuation relations of ground motion for rock and soil sites in eastern United States. Soil Dynam. Earthquake Eng. **16**, 363–372 (1997)
8. Raju, G., Ramana, G.V., Hanumantha Rao, C.H., Thallak, S.G.: Site-specific ground response analysis. Curr. Sci. **87**(10), 1354–1362 (2004)

A Preliminary Seismic Hazard Modelling in Northern Algeria

Mohamed Hamdache, José A. Peláez, AbdelKarim Yelles-Chaouche, Ricardo Monteiro, Mario Marques, Miguel Castro, Hamoud Beldjoudi, and Abdel Aziz Kherroubi

Abstract

It is established that seismic hazard evaluation, especially by analyzing the most energetic seismicity and its spatial distribution, provide critical information on earthquake-prone areas and their seismic potential. Therefore, during the last few years many efforts have been developed to improve our knowledge in Seismology and seismo-tectonic fields, especially with regard to the mitigation of the impact of destructive events and seismic risk assessment of populated urban areas. In this context, the EU-funded project "*Improved Tools for Disaster Risk Mitigation in Algeria*" (ITERATE) aims at seismic risk mitigation in Algeria, leading to updates in the seismic design regulations. This work, as a stage of the whole project, addressed a number of proposed developments and considerations made towards a further improvement of the component of seismic risk related to the probabilistic quantification of seismic hazard. Furthermore, and for some specific sites, Oran and Blida, a detailed probabilistic seismic hazard analysis was carried out. The obtained results were presented in terms of different ground motion parameters, i.e., PGA, spectral acceleration for different oscillation periods and uniform hazard spectra for different return periods. Moreover, a seismic disaggregation for different oscillation periods was performed to derive the contribution of the different seismic scenarios.

Keywords

Peak ground acceleration • Spectral acceleration • Uniform hazard spectra • Disaggregation • Northern Algeria • ITERATE project

1 Introduction

The study focused on the seismic hazard estimation at the Oran and Blida cities, including all the contribution of the surrounding areas. The first step was based on a recent and new seismogenic source zone model for the Algeria-Morocco region, proposed by Peláez et al. [1]. The Seismogenic source zone model is considered as a key-step to perform any probabilistic seismic hazard study in a given region. As shown by Pelaez et al. [1], the zone model, including several seismogenic zones, delineated, by taking care of adjusting them to the boundaries of the tectonic domains, more attention was given to include both well-known tectonic structures as well as known seismicity. An extensive data set including information on the seismic activity distribution, on the geology and on the stress pattern, was used as basis of the proposed model for the studied region. In order to characterize each source zone of the model the predominant focal mechanism was computed using the stress field inversion approach. To this end, a focal mechanism catalog was specifically compiled for this work, and the most recent earthquake catalog was considered.

2 Earthquake Data File and Seismogenic Zone Model

The working earthquake data file needed to perform this study was obtained by aggregating and updating two unified catalogs for northern Morocco [2] and northern Algeria [3]. The final obtained file was a unified catalog in terms of the moment magnitude including, after a declustering process,

M. Hamdache (✉) · A. Yelles-Chaouche · H. Beldjoudi
A. A. Kherroubi
Dépt Etudes et Surveillance Sismique, CRAAG, BP 63, 16348 Bouzareah, Algeria
e-mail: m_hamdache@hotmail.com

J. A. Peláez
Department of Physics, University of Jaén, Jaén, Spain

R. Monteiro
University School of Advanced Studies IUSS Pavia, Pavia, Italy

M. Marques · M. Castro
Facultade de Engenharia, Universidade do Porto, FEUP, Porto, Portugal

N. Sundararajan et al. (eds.), *On Significant Applications of Geophysical Methods*,
Advances in Science, Technology & Innovation, https://doi.org/10.1007/978-3-030-01656-2_53

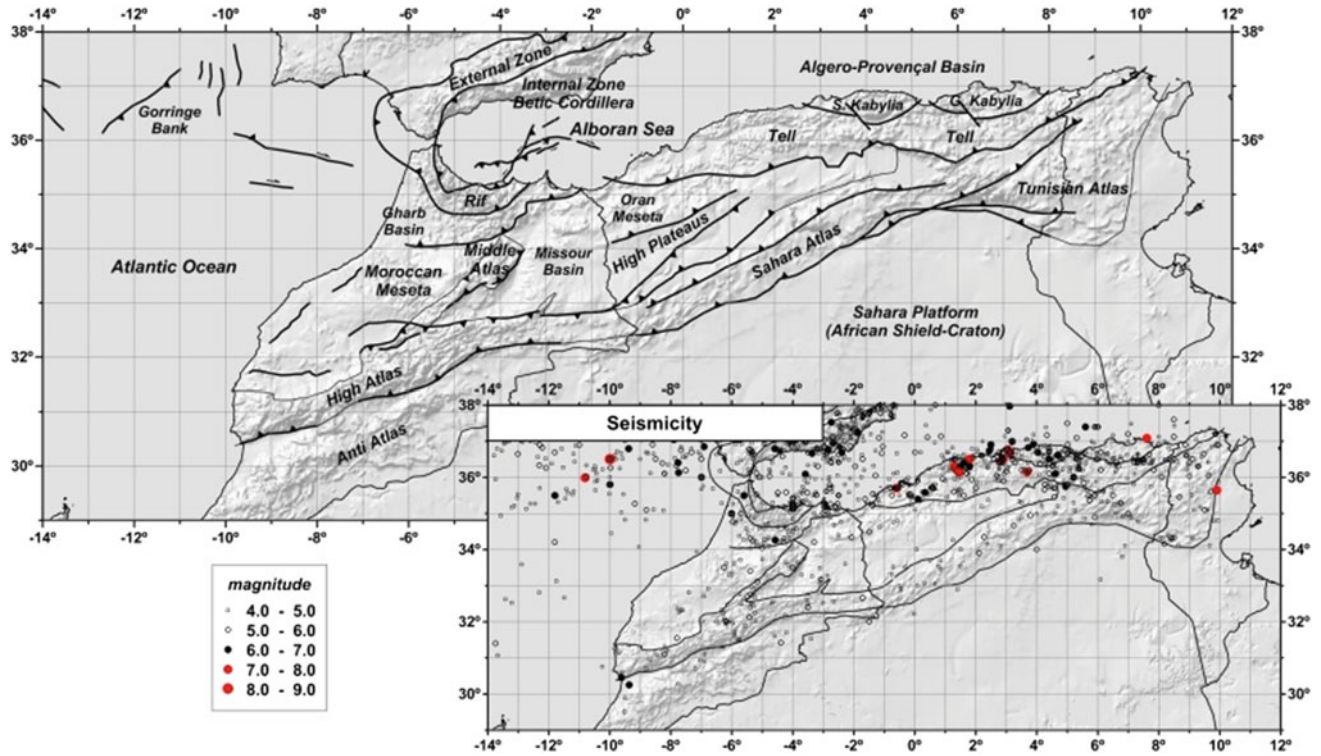

Fig. 1 The study area, including a tectonic sketch overview. Spatial distribution of earthquakes above magnitude M_W 4.0 is depicted

only Poissonian events. The compiled file was more appropriate, as shown by Pelaez et al. [1, 4] for seismic hazard and forecasting studies in the region.

In order to carry out the magnitude unification process, several empirical relationships between reported magnitudes were used, some of them were specifically developed for these two catalogs. The performed completeness analysis shows that the entire data file, as pointed out by Pelaez et al. [4] and Hamdache et al. [5] can be considered complete for magnitudes above M_W 6.0 since 1885, and for magnitudes above M_W 5.0 since 1900, with mean rates about 0.21 and 2.15 events by year, respectively. For engineering purposes, the used file included magnitudes above M_W 4.0, which were complete only during the last 15 years. The mean rate was estimated considering about 30 events per year [4]. The performed detailed analysis showed important characteristics of the compiled catalog obtained from previous works [2–5].

Figure 1 shows the tectonics and the spatial distributions of the main events.

3 Results

We used the approach designed by Kijko and Graham [6] and Kijko et al. [7] to derive the seismic hazard parameters for each zone (annual mean activity rate, *b*-value and maximum possible magnitude). The seismic hazard estimation needs an appropriate ground motion attenuation equation. To this end, we used two recent ones proposed by Abrahamson et al. [8], denoted ASK 2014 and by Campbell and Bozorgnia [9], denoted CB_2014 that took into account the uncertainty in the estimated parameters. Considering the two previous attenuation equations, a logic tree scheme was used. Figure 2 shows the seismic hazard curves obtained at

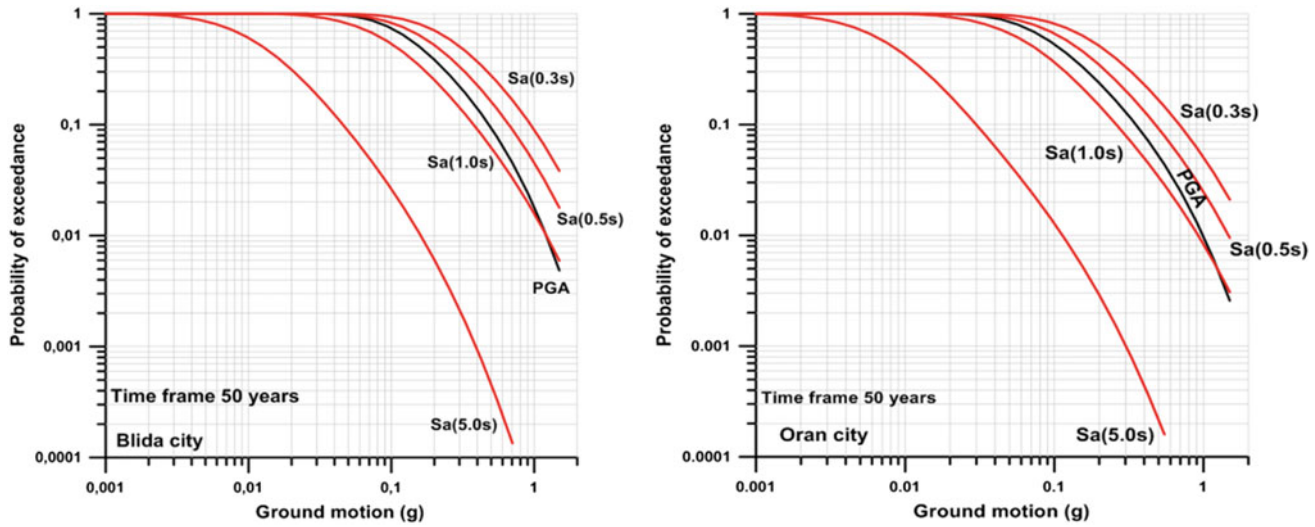

Fig. 2 Obtained PGA and SA curves at Blida and Oran

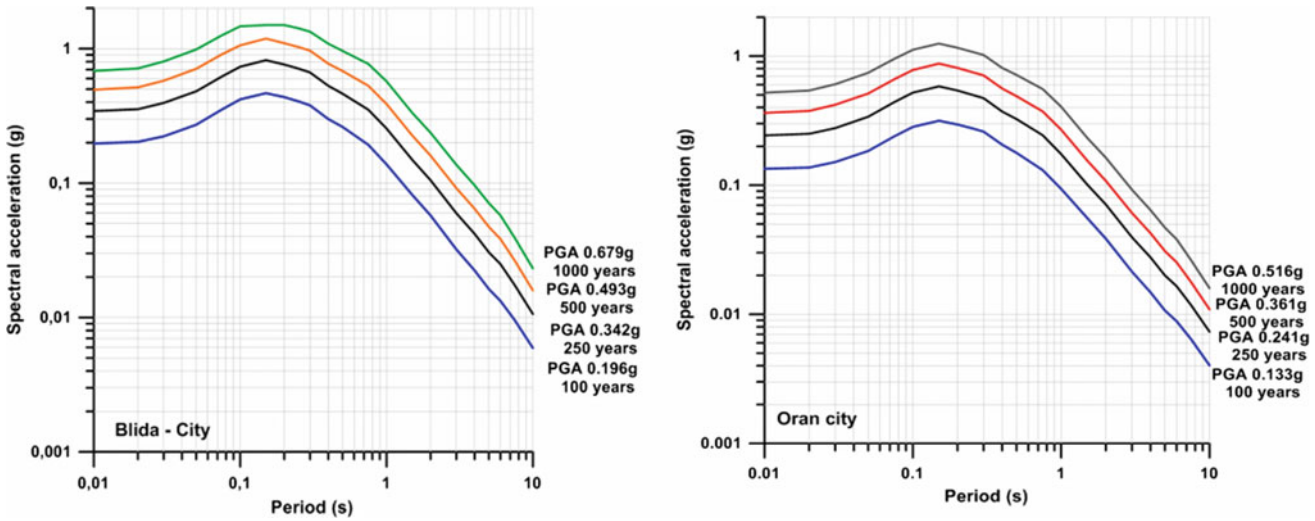

Fig. 3 Plots of UHS obtained at Blida and Oran for different return periods

Blida and Oran, for a return period of 475 years in terms of PGA and spectral acceleration (SA) for different oscillation periods.

The uniform hazard spectra (UHS) for different return periods are depicted in Fig. 3 for each studied city.

Moreover, the epsilon disaggregation of the seismic hazard results for a return period of 475 years was performed in terms of SA for different oscillation periods. Figure 4 displays these obtained results at the two cities for T = 0 s (PGA) and 0.25 s and epsilon values of 0 and 5.

4 Discussion and Conclusion

In this note we presented preliminary seismic hazard results obtained at Blida and Oran, using a recent seismic zone model for northern Algeria. Despite the fact that each zone source was characterized by the prevailing stress regime using the Delaux and Barth [10] method, the topic is still under research. Although the obtained results can be combined with an exposure model for each city to perform

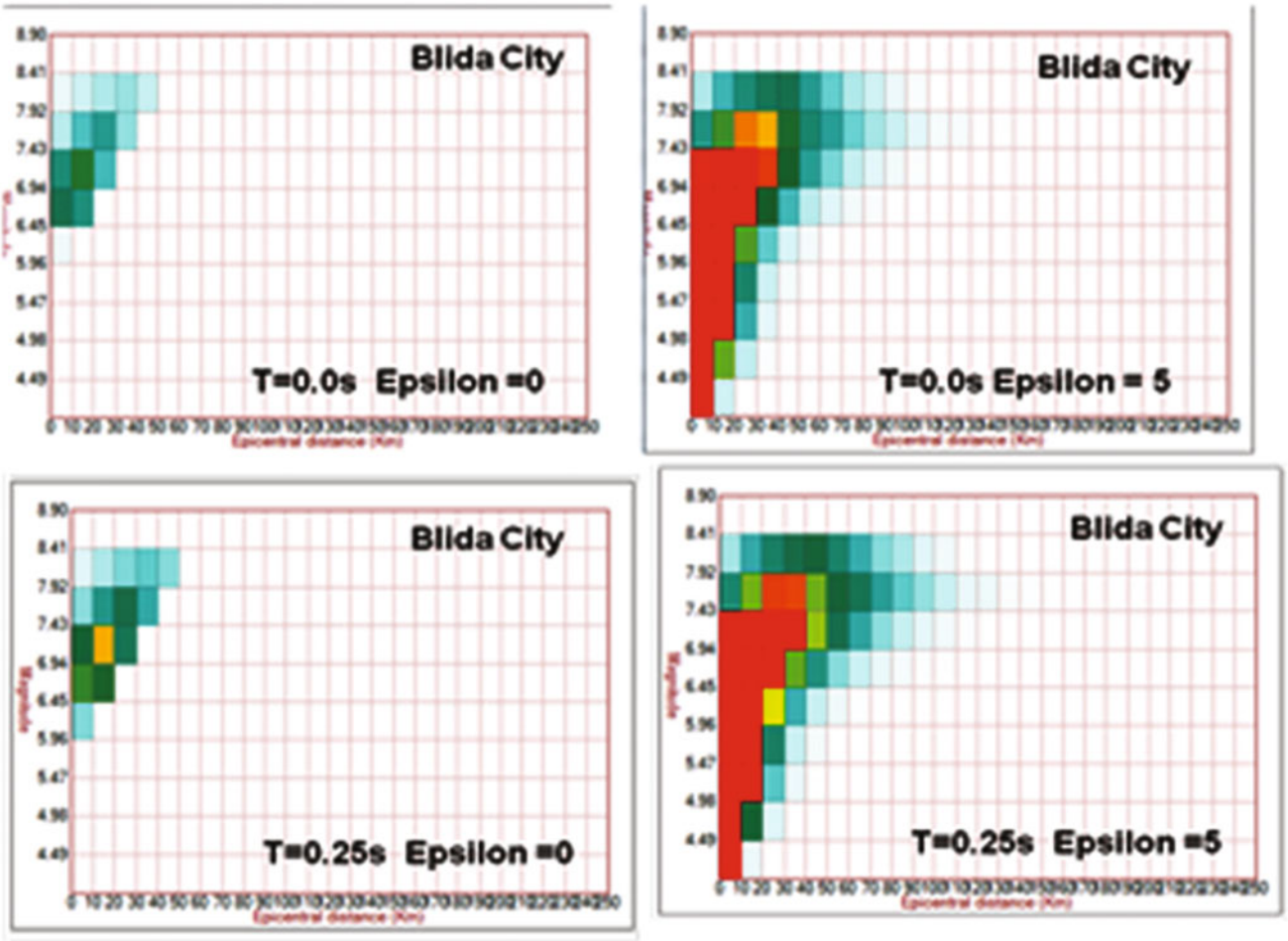

Fig. 4 Disaggregation of PSHA in terms of SA at 0.0 s (PGA) and 0.25 s for epsilon values equal to 0 and 5

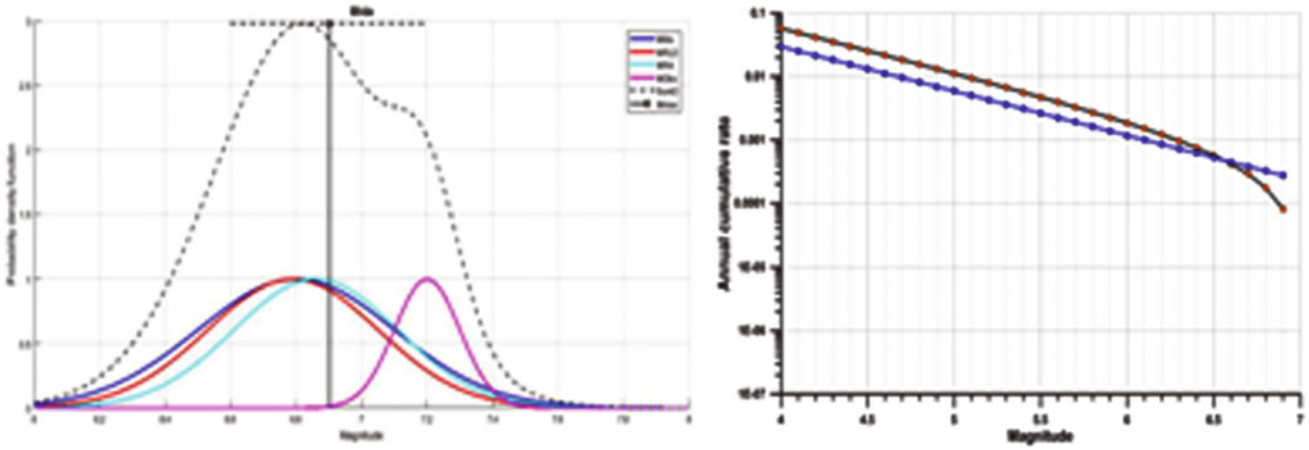

Fig. 5 Maximum magnitude and plot of the Gutenberg-Richter relationship (blue classical and red truncated) obtained using the fault parameters

seismic risk analysis, the identification of active faults close to each city, allowed us using Pace et al. [11] to turn the fault data as input for the seismic hazard model, completing and thus improving the used logic tree. Figure 5 displays the results obtained for a fault identified close to the city of Blida.

References

1. Peláez, J.A, Henares, J., Hamdache, M., Sanz de Galdeano, C.: A seismogenic zone model for seismic hazard studies in northwestern Africa. In: D'Amico, S., (ed.) Moment Tensor Solutions—A Useful Tool for Seismotectonic. Springer (2018)
2. Peláez, J.A., Chourak, M., Tadili, B.A., Brahim, L.A., Hamdache, M., López Casado, C., Martínez Solares, J.M.: A catalog of main Moroccan earthquakes from 1045 to 2005. Seismol. Res. Lett. **78**, 614–621 (2007)
3. Hamdache, M., Peláez, J.A., Talbi, A., López Casado, C.: A unified catalog of main earthquakes for northern Algeria from A.D. 856 to 2008. Seismol. Res. Lett. **81**, 732–739 (2010)
4. Peláez, J.A., Hamdache, M., Sanz de Galdeano, C., Sawires, R., García Hernández, M.T.: Forecasting moderate earthquakes in northern Algeria and Morocco. In: D'Amico, S. (ed.) Earthquakes and Their Impact on Society. Springer Natural Hazards, pp. 81–95. Springer (2016)
5. Hamdache, M., Peláez, J.A., Kijko, A., Smit, A.: Energetic and spatial characterization of seismicity in the Algeria-Morocco region. Nat. Hazards **86**, S237–S293 (2017)
6. Kijko, A., Graham, G.: Parametric-historic procedure for probabilistic seismic hazard analysis. Part I: estimation of maximum regional magnitude mmax. Pure Appl. Geophys. **152**(3), 413–442 (1998)
7. Kijko, A., Smit, A., Sellevoll, M.A.: Estimation of earthquake hazard parameters from incomplete data files. Part III. Incorporation of uncertainty of earthquake-occurrence model. Bull. Seismol. Soc. Am. **106** (2016)
8. Abrahamson, N.A., Silva, W.J., Kamai, R.: Summary of the ASK14 ground motion relation for active crustal regions. Earthq. Spectra **30**, 1025–1055 (2014)
9. Campbell, K.W., Bozorgnia, Y.: NGA-West2 ground motion model for the average horizontal components of PGA, PGV, and 5%-damped linear acceleration response spectra. Earthq. Spectra **30**, 1087–1115 (2014)
10. Delaux, D., Barth, A.: African stress pattern from formal inversion of focal mechanism data. Tectonophys. **482**, 105–128 (2010)
11. Pace, B., Visini, F., Peruzza, L.: Fish: matlab tools to turn fault data into seismic-hazard models. Seismol. Res. Lett. **87**(2A) (2016)

Evaluation of Liquefaction Potential for Two Sites Due to the 2016 Kumamoto Earthquake Sequence

Bashar Ismael and Domenico Lombardi

Abstract

Following the 2016 Kumamoto earthquake sequence, which struck the island of Kyushu in Japan, a reconnaissance mission was conducted in the affected region by the seismic events by the UK-based Earthquake Engineering Field Investigation Team (EEFIT). The sequence caused widespread liquefaction in the coastal areas of Kumamoto Prefecture, arguably due to the presence of saturated loose sand deposits. Liquefaction-induced failure was observed in several places including Akitsu River and Kamiezu Lake. Generally, signs of ejected sand, extensive ground settlement and localised ground lateral spreading were noted, which were apparently due to liquefaction. One purpose of this study is to present liquefaction-induced failure during the Kumamoto earthquake for the aforementioned visited regions. An assessment of liquefaction vulnerability for all investigated sites was also conducted using different approaches, namely Eurocode8 and Idriss and Boulanger. The computed factors of safety were compared to results from numerical analyses performed in the object-oriented software OpenSees. The results show that different methods yield similar factors of safety, which are consistent with the numerical results and field observations.

Keywords

The 2016 Kumamoto earthquake sequence • Liquefaction • OpenSees • Post-earthquake field survey

1 Introduction

A series of forceful earthquakes struck Japan starting on 14th April 2016 with 6.5 Japan local magnitude (6.2 Mw). The mainshock magnitude was 7.3 Japan local magnitude (7.1 Mw). The foreshock was generated from Hinagu fault located in the south-western region of Japan at approximately 11 km focal depth, while the main shock was initiated from the Futagawa fault not far from the Hinagu fault at 12 km focal depth. As a consequence of these earthquakes, extensive damage was recorded in several places including Akitsu River and Kamiezu Lake. The earthquakes caused significant losses of both people and infrastructure; the total number of fatalities was 69 [1] and the damage cost was approximately 24–46 billion dollars [2], excluding more than 3 billion US dollars insurance loss [3].

Generally, signs of ejected sand, extensive ground settlement and localised ground lateral spreading were noted, which were apparently due to liquefaction. This liquefaction also caused differential settlement and tilting of residential houses.

An assessment of liquefaction vulnerability for the investigated sites was conducted using different approaches, namely Eurocode8 [4] and Idriss and Boulanger [5]. Borehole data and SPT count numbers for the sites under investigation were obtained from the electronic national data hub for Japan organized by the Geospatial Institute of Japan. The blowcount number N_{SPT} obtained from the SPT test was normalised to a reference overburden stress of 100 kPa and the ratio of the impact energy to theoretical free-fall energy (0.6) was taken as equal to 1.2. The material that could be used for modelling liquefaction is called Pressure depend Multi Yield 02. The input parameters required by the constitutive law to conduct the Finite Element (FE) analysis were obtained from Yang et al. [6]. It is worth mentioning that when using the aforementioned materials, different parameters were required for different relative densities/void

B. Ismael (✉) · D. Lombardi
School of Mechanical, Aerospace and Civil Engineering, University of Manchester, Manchester, UK
e-mail: bashar.ismael@manchester.ac.uk

N. Sundararajan et al. (eds.), *On Significant Applications of Geophysical Methods*, Advances in Science, Technology & Innovation, https://doi.org/10.1007/978-3-030-01656-2_54

ratios because they were not formulated following the critical state soil mechanics framework.

The results confirmed that the sites under investigation are highly liquefiable with a factor of safety less than a unit. Additionally, the numerical results confirmed the high liquefiability of the above mentioned sites in which liquefaction was predicted to be triggered at some depth below the ground surface, based on the nature of deposit and the characteristics of the applied ground motion. The results show that different methods yield similar factors of safety, which are consistent with the numerical results and field observations.

2 Ground Motion

The ground motion characteristics were obtained from KiK-NET and K-NET operated by the National Research Institute for Earth Science and Disaster Resilience in Japan. The maximum ground motion recorded at KMMH16 station located in Mashiki town (32.7967°N, 130.8199°E) for the mainshock is presented in Fig. 1. Then, the response spectra at 5% damping ratio as recommended by most of the current codes such as Eurocode 8 [4] are presented in Fig. 2.

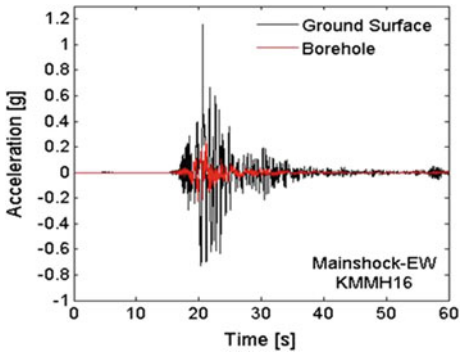

Fig. 1 Acceleration time-histories for the main shock

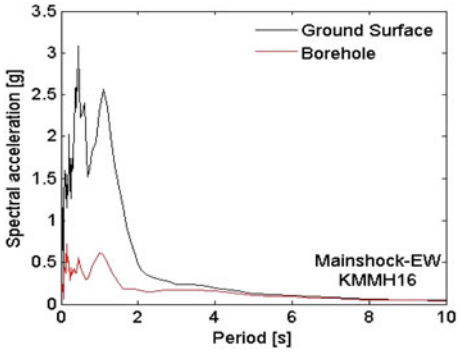

Fig. 2 Spectral acceleration for the main shock

3 Post-earthquake Field Survey (Analysis and Discussion)

As a consequence of the Kumamoto earthquake, liquefaction signs were observed as sand boiling, ground fractures, localised ground lateral spreading, differential settlement and tilting of residential houses. Typical liquefaction-visited spots were Akitsu River and Kamiezu Lake. The Akitsu River is an internal river in Mashiki town. Liquefaction was observed in roads alongside the river, where significant damage to the asphalt occurred. Liquefaction was apparent at different locations along the river and signs of ejected sand were observed. As shown in Fig. 3a, sand erupted from the edge of foundations and a footpath. Moreover, a tennis court was thoroughly liquefied, and tension cracks were also visible, as depicted in Fig. 3b.

Moving to Kamiezu Lake: extensive ground settlement with localised lateral displacement and cracking occurred on the lake's embankment in Kumamoto City (see Fig. 4). Usually, man-made riverbanks have shallow slopes downward towards the river, if there is no retaining structure put in place. When the sub-layer liquefies and the generated excess pore water pressure (EPWP) is prevented from escaping to the surface (capped by a low permeable/impermeable layer at the surface), the lateral movement occurs for the whole liquefied layer.

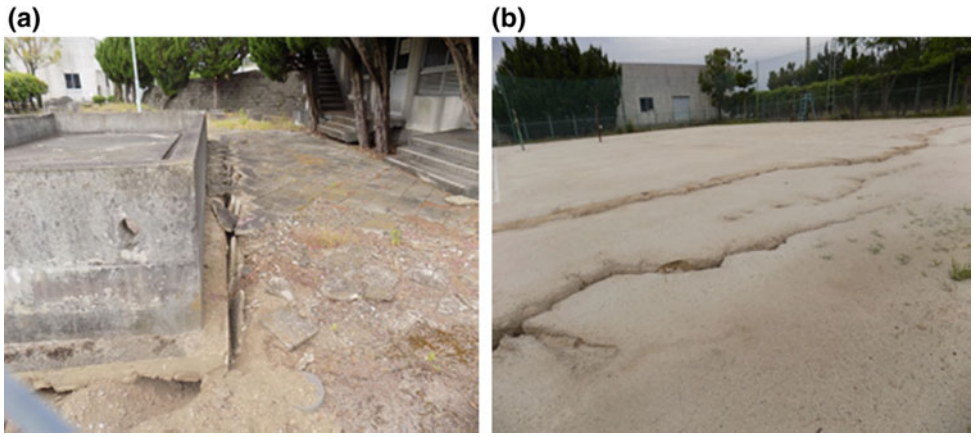

Fig. 3 Widespread of liquefaction at **a** bottom of a foundation and **b** Tennis court

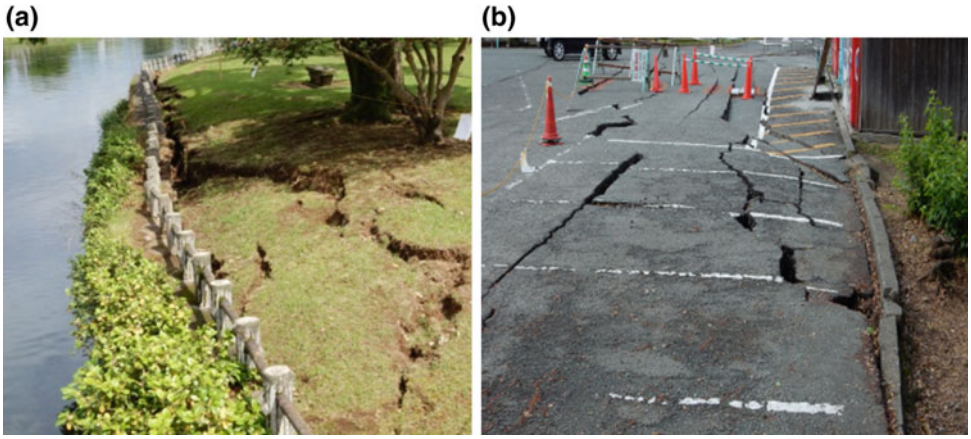

Fig. 4 Liquefaction-induced lateral displacement at Kamiezu Lake

The calculated factor of safety for Akitsu River at different depths is introduced in Fig. 5 together with the borehole log and the corresponding SPT count number. At Akitsu River, the factor of safety is below unity from 2 m below the ground surface up to 8 m. The two approaches show approximately a similar trend comparable with the numerical analysis performed in the object-oriented software framework OpenSees. The numerical analysis shows that full liquefaction (i.e. the ratio of the EPWP to the effective pressure $r_u \geq 0.8$) was mobilised for the total depth from 3.5 up to 5.5 m.

The factor of safety was found to be less than 1 up to 15 m depth at Kamiezu Lake, except for the surficial layer where the soil is made up of non-liquefiable organic soil and clay, as can be seen in Fig. 6. Kamiezu Lake shows that full liquefaction initiated in the confined zone below 3 m, Fig. 6. It is suggested that the surficial non-liquefiable layer with limited permeability prevented the dissipation of the generated EPWP leading the ground to spread laterally, as confirmed in the site investigation near the examined area.

4 Conclusion

An assessment of liquefaction vulnerability for the two visited sites was conducted using the EuroCode8 approach and Idriss and Boulanger method. The computed factors of safety were compared with the results from numerical analyses performed in the object-oriented

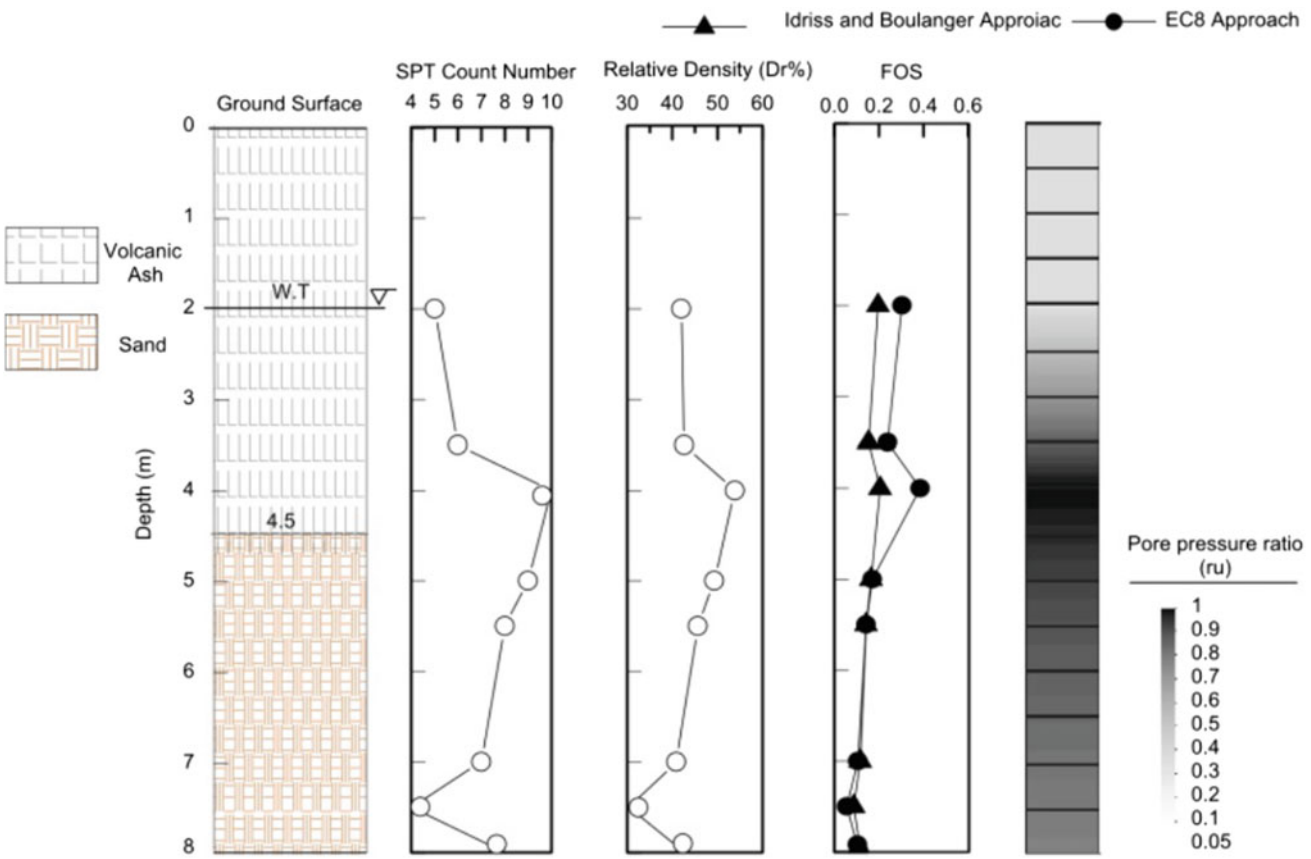

Fig. 5 Borehole log, SPT count number, relative density, liquefaction assessment using two approaches and r_u generated at Akitsu River as calculated by OpenSees software

software framework OpenSees. The results show that different methods yield similar factors of safety, which are consistent with the numerical results and field observations. It could be concluded that liquefaction is a complex phenomenon and the simplified approaches may be considered conservative because of the limitation to consider all factors that may affect liquefaction triggering for a specific site.

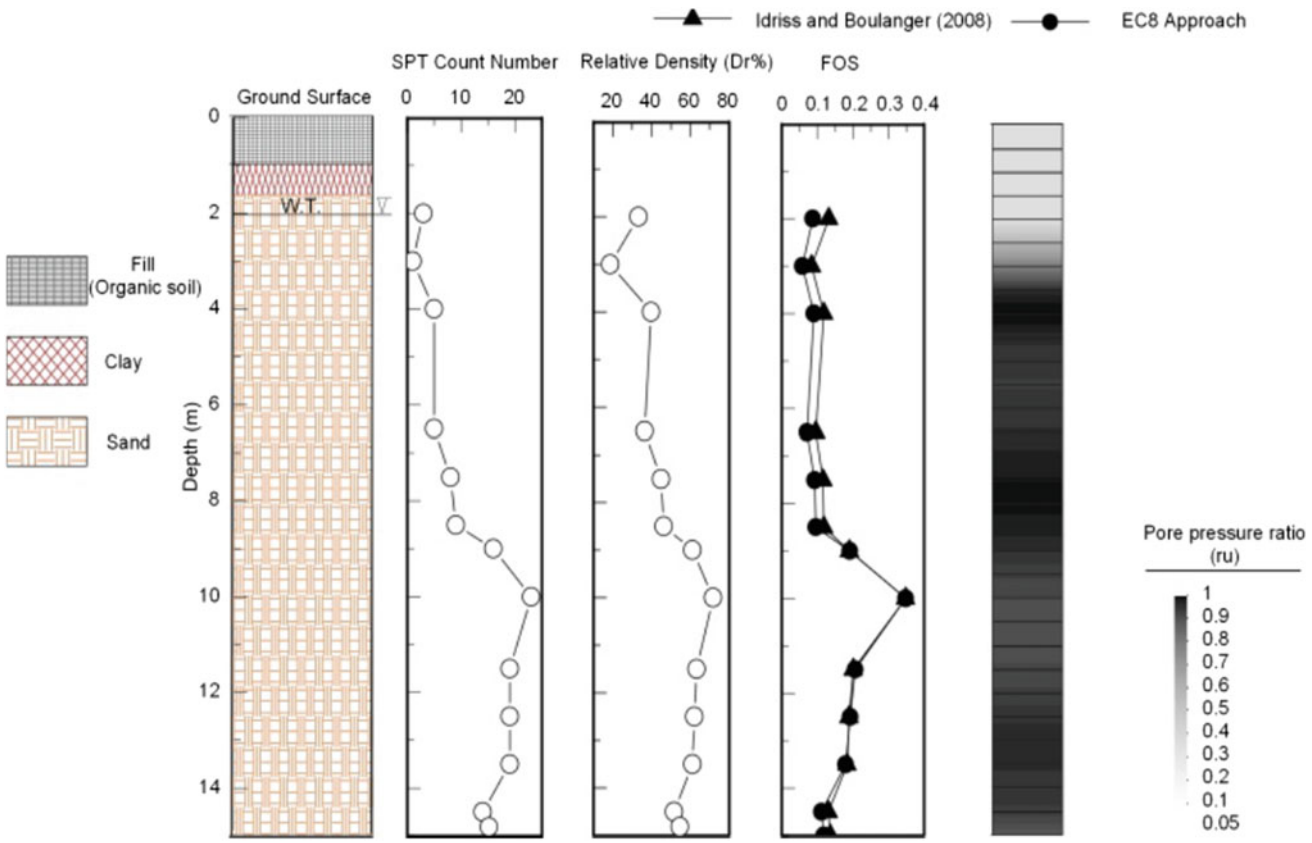

Fig. 6 Borehole log, SPT count number, relative density, liquefaction assessment using two approaches and r_u generated at Kamiezu Lake as calculated by OpenSees software

References

1. Bhattacharya, S., Hyodo, M., Nikitas, G., Ismael, B., Suzuki, H., Lombardi, D., Egami, S., Watanabe, G., Goda, K.: Geotechnical and infrastructural damage due to the 2016 Kumamoto earthquake sequence. Soil Dyn. Earthq. Eng. **104**, 390–394 (2018)
2. Goda, K., Campbell, G., Hulme, L., Ismael, B., Ke, L., Marsh, R., Sammonds, P., So, E., Okumura, Y., Kishi, N.: The 2016 Kumamoto earthquakes: cascading geological hazards and compounding risks. Front. Built Environ. **2**, 19 (2016)
3. GIS. General Insurance Association of Japan: Key Figures Related to Insurance Claims Due to the 2016 Kumamoto Earthquake as of June 13, 2016. Available at: http://www.sonpo.or.jp/en/news/2016/1606_03.html. Accessed 08 Dec 2016 (2016)
4. EC8, European Committe de Normalisation, C.B.: Eurocode 8: design of structures for earthquake resistance. Part 5: foundations, retaining structures and geotechnical aspects (1998)
5. Idriss, I., Boulanger, R.W.: Soil Liquefaction During Earthquakes. Earthquake Engineering Research Institute (2008)
6. Yang, Z., Lu, J., Elgamal, A.: OpenSees soil models and solid-fluid fully coupled elements. User's Manual. Ver, 1 (2008)

Part VIII
Tectonics

Active Tectonics in the Guelma Basin (Eastern Algeria)

Said Maouche, Nesrine Djaroun, Chakib Harouz, Noureddine Sahi, Kamel Amri, and Assia Harbi

Abstract

In the Guelma intra-mountainous basin, the neotectonic activity is concentrated around the NE-SW and E-W oriented folds and faults. The Djebel Debbagh fold structure and the Roknia fault, which are the northern and western borders of the basin respectively, shows witnesses of Quaternary tectonics. Southward, the Debbagh fold is limited by a typical east-west right lateral strike slip that was reactivated during the post-Miocene period and, which shows recent tectonic activity affecting the Pliocene deposits. Other structures, such as the Roknia fault (or Hammam Debbagh-Roknia fault), which is the western boundary of the Guelma basin is a normal fault with right lateral component that plays a role in the placement of travertine deposits. The tectonic stress inferred from field measurements shows NNW-SSE directions that are at the origin of the Guelma basin development in a pull-apart system. Field investigations and satellite image analysis show that the recent tectonic activity in the Hammam Debbagh zone is marked by deformations affecting recent Pliocene and Quaternary series.

Keywords

Guelma basin • Hammam Debbagh fault
Active tectonics • Earthquakes

1 Introduction

The Tell Atlas (Northern Algeria) is a fold and thrust fault system [1, 2] (Fig. 1). The recent tectonic activity of the Tell Atlas is at the origin of moderate seismicity and is related to the 4–5 mm/year convergent movement of the African plate towards the Eurasian plate with a NNW direction [3]. Several studies [2, 4] indicate that the post thrusting intermountains Neogene basins are characterized by reverse faulting in the western and central part of the Tell Atlas domain and strike slip mechanism in the eastern part. In this work, we focus on the characterization of active faults, which is critical for constraining the integration of tectonic parameters into the seismic hazard analysis. We used field observations and measurement to illuminate and identify the active tectonics markers and quantify this deformation particularly in the western border of the Guelma basin. This border is characterized by hydrothermal active spring. This part of the Tell Atlas is underlined by permanent low to moderate seismicity.

2 Materials and Methods

In this study an attempt was made to understand the active tectonics and neotectonics responsible for the seismic activity using multidisciplinary approaches. It consisted of a combination of geology (particularly tectonics and neotectonics), geomorphology (field observations and classical image processing), and seismicity distribution and focal mechanism solutions. We particularly focused on the Quaternary deposits (uplifted alluvial terraces) and organization of the hydrothermal structures underlying the Guelma basin and elaborate a structural scheme based on field measurements.

3 Results

Along the northern border of the Guelma basin, a clear fault scarp can be observed in several places. It is the case of a natural section showing the contact that corresponds to an EW trending and vertical strike slip (Fig. 2b). Strike, dip and pitch of slickensides that are well-preserved on the fault

S. Maouche (✉) · A. Harbi
CRAAG, BP 63, Bouzaréah, Algiers, Algeria
e-mail: said.maouche@gmail.com

N. Djaroun · C. Harouz · N. Sahi · K. Amri
FSTGAT, USTHB, Algiers, Algeria

N. Sundararajan et al. (eds.), *On Significant Applications of Geophysical Methods*,
Advances in Science, Technology & Innovation, https://doi.org/10.1007/978-3-030-01656-2_55

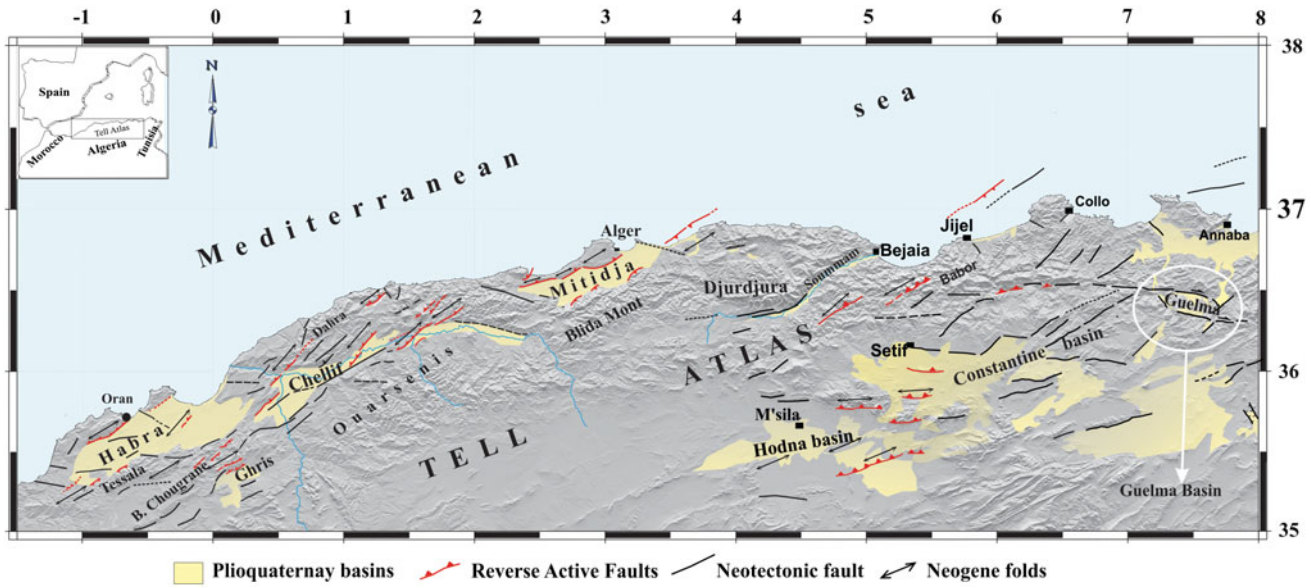

Fig. 1 Neotectonics and active tectonics in the Tell Atlas-Algeria (after Meghraoui et al. [2]; Harbi et al. [4]; Maouche [1])

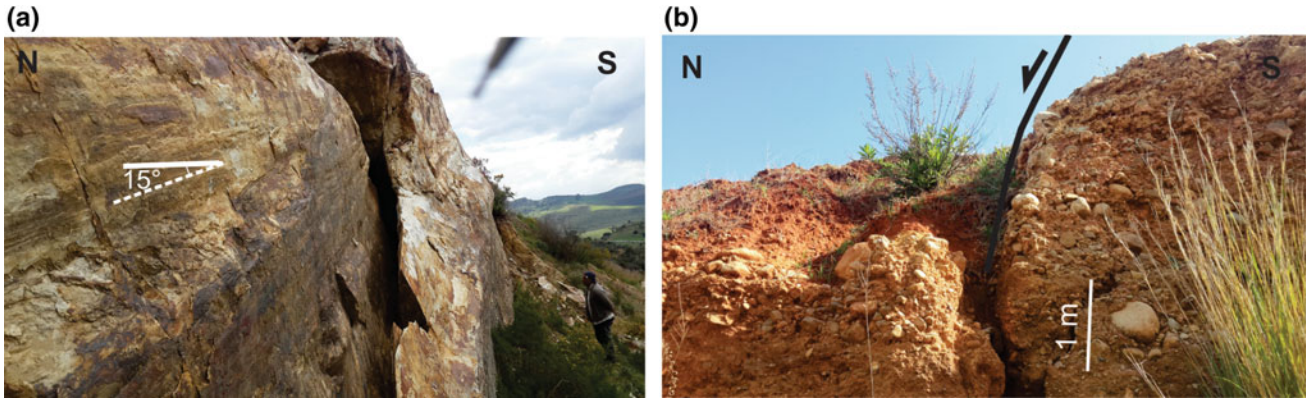

Fig. 2 Example of observed surface faulting, **a** normal fault observed in Hammam Debbagh area, **b** Djebel Debbagh strike slip fault showing right lateral displacement

plane, are N80°E, 85°S, and 10°W, respectively, and indicate a main strike slip consistent with the NW-SE compression.

We note the presence of a series of uplifted tilted alluvial terraces along the Bou Hamdane River in the Hammam Debbagh site. The hydrographic network individualizes at least three levels of alluvial elevated terraces located near the village. The dip value variations measured on terrace levels shows that the lower terrace close to the Bou Hamdane River is the youthful. The abundance of these alluvial deposits evidences the existence of strong streaming of the Bou Hamdane River during the Quaternary. The travertine accumulations are organized as spring orifices along fractures such as joints of faults and form elongated ridges. In this site, one of the ridges walls oriented N20°W, exceeds seven meters high and shows extensional fractures, which seem to be active during recent times (Quaternary). In one of the Roman quarry sites, we measured significant normal motion on a NNW-SSE fault. This recent tectonic motion is also observed outside the travertine field, particularly on faults affecting Pliocene deposits (Fig. 2a). The field observations and measurements reveal that a system of youthful travertine was deposited along a normal fault. From a tectonic point of view, this study highlighted the role of the

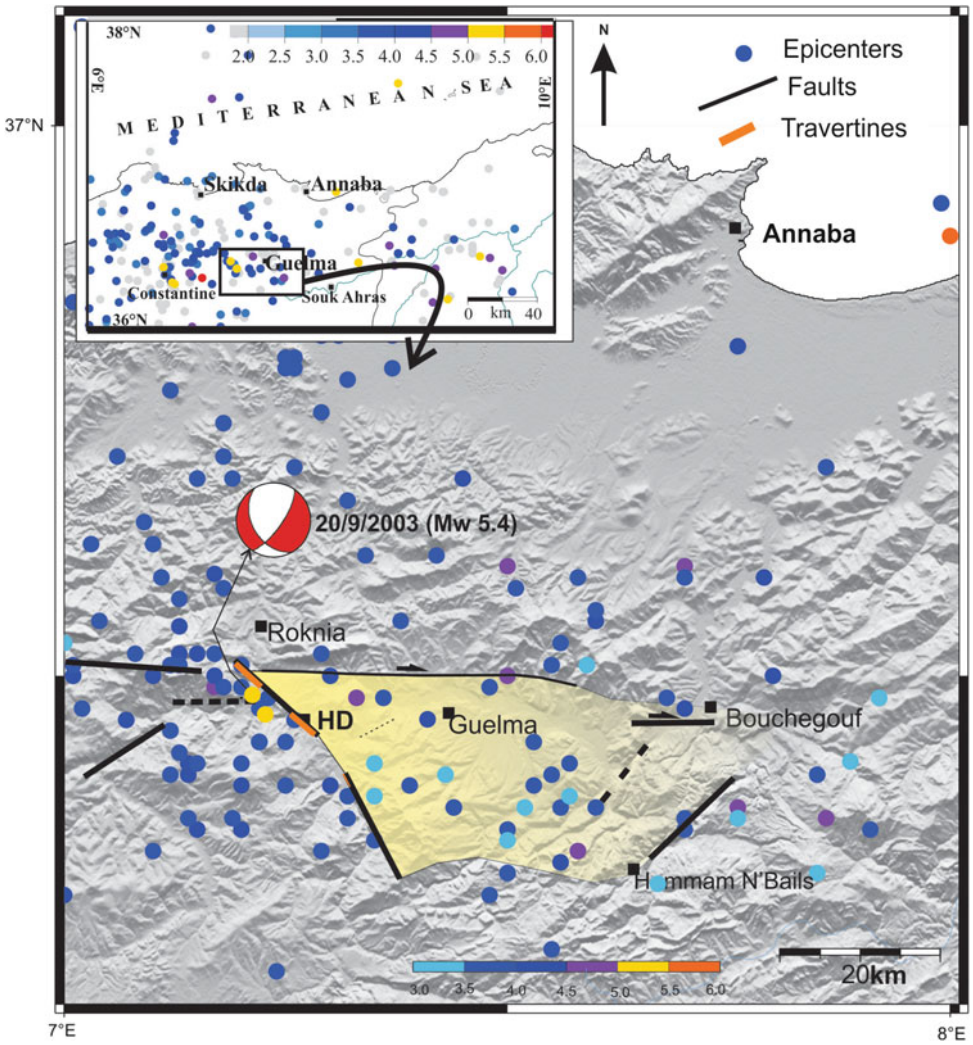

Fig. 3 The earthquake distribution in the Guelma basin and surroundings, yellow circles represent the two earthquakes that occurred in the region with the focal mechanism of the 20/09/2003, 5.4 Mw, Hammam Debbagh earthquake (modified from Maouche et al. [5]), inset: seismicity distribution in the northeastern Algeria (updated from Harbi et al. [6])

Hammam Debbagh active fault in the seismic potential framework of the Guelma basin in which earthquakes exhibit normal fault mechanisms. Figure 3 shows the local seismicity distribution and particularly the focal mechanism of the 2003 earthquake highlighting normal faulting nature.

4 Discussion

Local seismicity indicates the occurrence of small to moderate shallow seismic events that are distributed along faulted zones (i.e, Hammam Debbagh-Roknia fault and the E-W strike slip fault representing the northern border of the Guelma basin). The 2003 (5.4 Mw) earthquake which occurred in the western border of the Guelma basin seems to be linked to the Hammam Debbagh normal fault. No surface faulting was reported during this event but small slides were observed in the Hammam Debbagh site. This is consistent with field observations showing Quaternary tectonic activity and uplifted alluvial terraces located along the Bouhamdane river.

5 Conclusion

The present study provided new insights into the active tectonics within the western part of the Guelma basin. The tectonic activity is expressed by the existence of two major structures (1) the Debbagh E-W strike slip fault and (2) the NW-SE Hammam Debbagh-Roknia fault, which show vertical movement as indicated by juxtaposed alluvial terraces. The observed fault-plane orientations are coherent with those determined from focal mechanism and the geomorphic trends of the structures related to the hydrothermal sources.

References

1. Maouche, S.: Tectonique active et géodynamique le long de l'Atlas Tellien: Etude des soulèvements côtiers. PhD dissertation, (USTHB-FSGAT, Alger), p. 315 (2010)
2. Meghraoui, M., Morel, J.L., Andrieux, J., Dahmani, M.: Neotectonique de la chaîne Tello-Rifaine et de la Mer d'Alboran: une zone complexe de convergence continent- continent. Bull. Soc. Géol. Fr. **167**, 143–159 (1996)
3. Nocquet, J.M., Calais, E.: Geodetic measurements of crustal deformation in the western Mediterranean and Europe. Pure Appl. Geophys. **161**(3), 661–681 (2004)
4. Harbi, A., Maouche, S., Ayadi, A.: Neotectonics and associate seismicity in the eastern Tellian Atlas of Algeria. J. Seismolog. **3**(1), 95–104 (1999)
5. Maouche, S., Abtout, A., Merabet, N., Aïfa, T., Lamali, A., Bouyahyaoui, B., Boughchiche, S., Ayache, M.: Tectonic and hydrothermal activities in Debbagh, Guelma Basin (Algeria). J. Geol. Res. http://dx.doi.org/10.1155/2013/409475 (2013)
6. Harbi, A., Peresan, A., Panza, G.F.: Seismicity of eastern Algeria: a revised and extended earthquake catalogue. Nat. Hazards **54**(3), 725–747 (2010)

Active Inversion Tectonics from Algiers to Sicily

Alain Rabaute and Nicolas Chamot-Rooke

Abstract

Using an updated active faults map in the easternmost Western Mediterranean (Algeria to Calabria), plus constraints from geodesy (GPS horizontal motion) and seismology (focal mechanisms) input in a strain model, we discussed how the slow Africa-Eurasia motion (4 mm/year) is accommodated along this segment of the Mediterranean. The width of the inverted domains is variable, strain being concentrated into narrow belts in northern Algeria and north Sicily while it is distributed in Tunisia and over the Pelagian platform. The style of deformation further evolves from west to east, from pure thrusting in Algeria to distributed strike-slip in Tunisia to transtension in the Pelagian grabens. We suggest that the present-day deformation is best explained in terms of (1) accommodation of the obliquity following a strain partitioning process with dextral shear onland and en-échelon thrusts offshore northeastern Algeria, along the past trace of the STEP fault that opened the Miocene Algerian Basin, (2) thrusting offshore northern Sicily along the same STEP fault that opened the Tyrrhenian Basin in the Pliocene, (3) increasing thin-skin versus thick-skin in Tunisia as a result of inherited structures, (4) far field Ionian slab pull, strongly active at the Mio-Pliocene initiation of the Pelagian grabens and still remnant today.

Keywords

Africa/Eurasia kinematics • Active tectonics
Strain partitioning • Inverted margin • Slab pull

1 Introduction

Slow motion between Africa and Eurasia in the easternmost western Mediterranean is accommodated within belts of variable widths, from relatively narrow in central Algeria (50–100 km), to wide in Tunisia (>100 km). From western Algeria to Sicily the style of active deformation gradually evolves from pure thrust to a combination of strike-slip and thrust (eastern Algeria and Tunisia), and finally to extension in the Siculo-Tunisian Strait. Both widths and styles of deformation thus evolve from west to east, in relation with the complex geological history of the African margin, a patchwork of mountain building (Tell, Atlas), continental block collages (Kabylia), subduction, back-arc opening and closing. Based on a recent seismo-tectonic map of the area [1], we discussed the compatibility of the active tectonics with the known present-day regional plate kinematics and the recent geodynamics of the region.

2 Active Faults and Seismicity

The core of the work is the identification of active faults, with special attention to offshore areas, in particular Algerian Basin, Tyrrhenian Basin, Pelagian Sea and Ionian Sea. The mapping process included the analysis of seismicity, both instrumental and historical, using epicenter locations and focal mechanisms [2–4]. Various sources were homogenized to obtain a comprehensive catalogue of earthquakes in the 0–50 km depth range. Satellite images on land and seismic profiles offshore further helped in discriminating active faults. The Geographic Information System (GIS) database includes 94 fault segments with parameters and related bibliography.

A. Rabaute (✉)
Geosubsight, 119 Avenue de Stalingrad, 91120 Palaiseau, France
e-mail: alain.rabaute@geosubsight.com

A. Rabaute
Institut des Sciences de la Terre Paris, ISTeP UMR 7193, Sorbonne Université, CNRS-INSU, 75005 Paris, France

N. Chamot-Rooke
Laboratoire de Géologie, Ecole Normale Supérieure, PSL Research University, CNRS, UMR8538, 75005 Paris, France

N. Sundararajan et al. (eds.), *On Significant Applications of Geophysical Methods*,
Advances in Science, Technology & Innovation, https://doi.org/10.1007/978-3-030-01656-2_56

3 Strain Modeling Using Earthquakes and Geodetic Constraints

The map is complemented by a strain model based on the style of deformation documented by earthquakes together with GPS (Global Positioning System) constraints (Fig. 1). Haines and Holt methodology was used to derive a continuous crustal velocity field [5]. The model consists of a finite-element grid, with ~400 grid cells (0.5° by 0.5° in dimension) covering the Nubia-Eurasia plate boundary zone between longitudes 3°E (Algiers) and 18°E (Calabria). To avoid any a priori assumption on the location of the main deformation zones, all cells are allowed to deform, with the exception of bottom rows (Nubia) and top rows (Eurasia).

The model derives a continuous velocity field by fitting simultaneously observed geodetic velocities and style of deformation (i.e. principal strain axis direction). The continuous velocity gradient tensor field provides estimates of the strain rate tensor (second invariant, dilatational and shear components), rotation rate, interpolated velocities and rigid plate motions [5]. To put reliable constraints on the far-field velocity boundary condition, the motion of Nubia with respect to Eurasia was prescribed to a global geodetic solution [6].

4 Results

Faults map and strain modeling document various patterns of deformation, which are generally attributed to the complex geological history of this segment of the Mediterranean. The slow convergence (4 mm/year) is presently accommodated close to the North African margin, at the boundary with the Oligocene to mid-Miocene Algerian Basin and Miocene to Pliocene Tyrrhenian Basin. From Algeria to eastern Sicily, inversion tends to locate close the present-day coastline, which is also the trace of the STEP fault that accompanied the eastward escape of the Ionian slab—resting nowadays below the Tyrrhenian and Calabria—and the

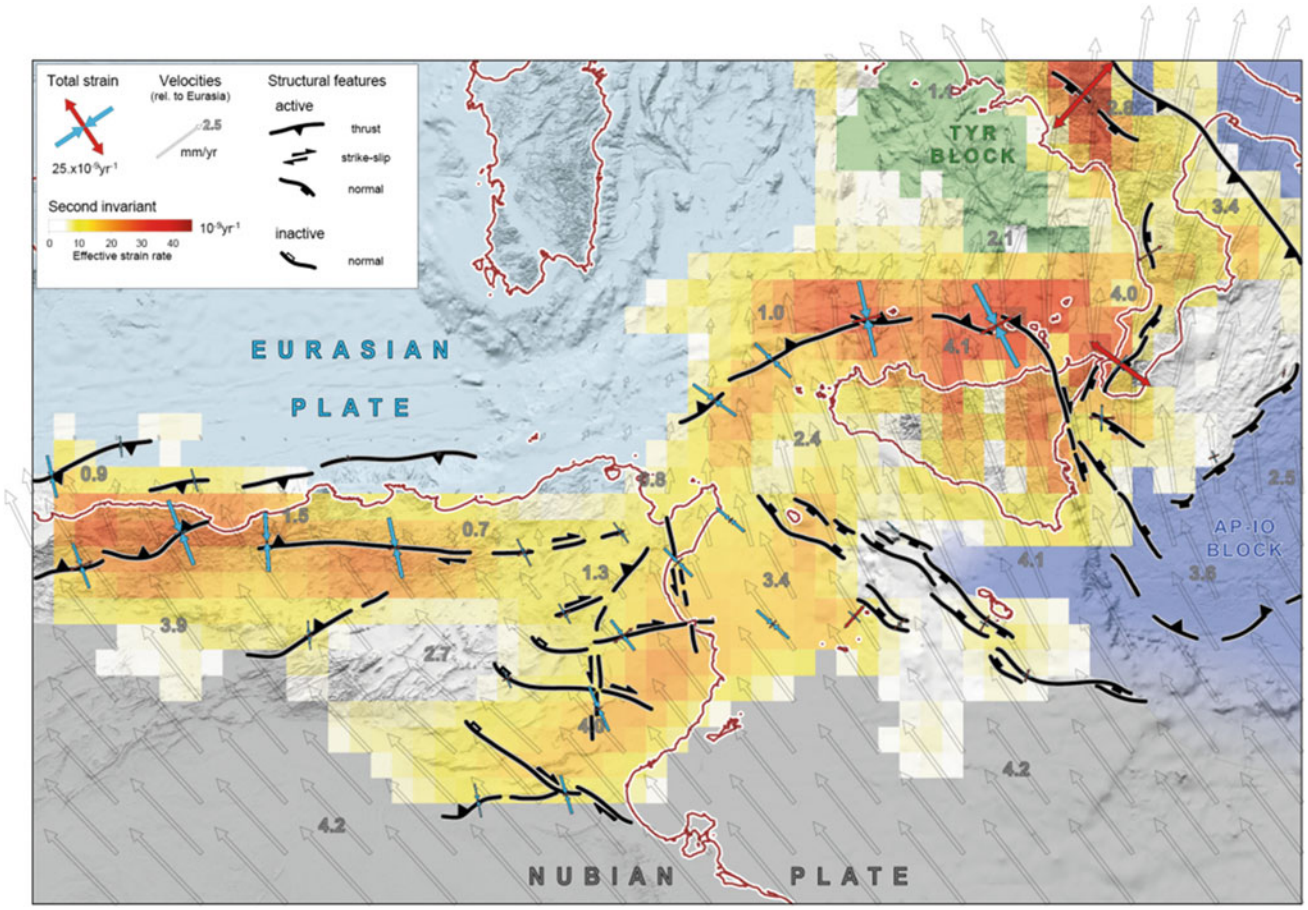

Fig. 1 Strain model based on the style of deformation documented by earthquakes together with GPS constraints. Modeled velocities were shown with respect to Eurasia, together with the effective strain rate (second invariant). Strain-rate axes were shown only in strategic locations. Areas not deforming were colored in green (Tyrrhenian block) and blue (Ionian plain). Structural features were simplified from mapped faults

successive Algerian and Tyrrhenian openings [7]. In both cases—i.e. northern Algeria and north Sicily—high strain is restricted to a rather narrow belt of thrusts, one of which being responsible for the Boumerdes-Zemmouri earthquake in 2003 [8].

The width of the inverted domain increases eastward with increasing thin-skinned versus thick-skinned deformation [9]. In northeastern Algeria strain is partitioned into strike-slip and reverse faults on land [10], and N80° en-échelon reverse faults offshore [11]. In Tunisia, convergence is accommodated within an area three to four times larger, from the Gafsa fault zone in the south to the northern coast. Obliquity of Africa–Eurasia motion is accommodated through a series of E–W trending right-lateral strike-slip faults (Gafsa, Kasserine, Sbiba-Cherichira faults). Conjugate left-lateral strike-slip faults are also active in eastern Tunisia, both onland and offshore (North-South axis, Hammamet-Monastir, Sidi Ali Ben Aoun faults).

Further east, the Pelagian grabens (Malta, Pantelleria and Linosa) that initiated in the upper Miocene [12] are presently transtensive. Focal mechanisms for the entire Pelagian platform indicate strike-slip [13], while GPS shows that the Pantelleria rift system still accommodates a small extensive component of motion between the Nubia plate and the Apulia-Ionian block [6].

5 Conclusion

The style of faulting observed from Algeria to Calabria is compatible with Africa-Eurasia kinematics but modulated by two effects: structural inheritance of the Atlasic and Alpine phases and a lateral slab pull imposed by the Ionian slab retreat. In northeastern Algeria, the obliquity of convergence is accommodated through a strain partitioning process, with dextral strike-slip on-land and en-échelon thrusts offshore located at pre-existing sharp boundaries. Strain is accommodated over a larger inverted domain in Tunisia in relation with increased thin-skinned deformation above Triassic salt. Convergence is taken along conjugate strike-slip faults, so that offshore thrusts die out and material is escaping eastward towards the "free" Pelagian side. Pelagian pull was probably stronger in Mio-Pliocene time with the initiation of the Pelagian and Tunisian grabens, retreat of the Ionian slab and last pulse of opening of the Tyrrhenian. Focal mechanisms indicate a progressive stress permutation, from pure thrusting in northern Algeria to strike-slip in Tunisia and finally transtension in the Pelagian grabens, compatible with a moderate but still active pull.

References

1. Rabaute, A., Chamot-Rooke, N.: Active Tectonics of the Africa-Eurasia Boundary from Algiers to Calabria, Map at 1:1500000 scale with GIS database. ISBN 978-2-9548197-0-9, Geosubsight, Paris (2014)
2. Boschi, E.: A "new generation" earthquake catalogue. Ann. Geofis. **43**(4), 1–12 (2000)
3. Guidoboni, E., Ferrari, G., Mariotti, D., Comastri, A., Tarabusi, G., Valensise, G.: CFTI4Med, Catalogue of Strong Earthquakes in Italy (461 B.C.-1997) and Mediterranean Area (760 B.C.-1500) INGV-SGA (2007)
4. Hamdache, M., Pelaez, J.A., Talbi, A., Casado, C.L.: A unified catalog of main earthquakes for northern Algeria from ad 856 to 2008. Seismol. Res. Lett. **81**(5), 732–739 (2010)
5. Haines, A.J., Holt, W.E.: A procedure for obtaining the complete horizontal motions within zones of distributed deformation from the inversion of strain-rate data. J. Geophys. Res. **98**(B7), 12057–12082 (1993)
6. Pérouse, E., Chamot-Rooke, N., Rabaute, A., Briole, P., Jouanne, F., Georgiev, I., Dimitrov, D.: Bridging onshore and offshore present-day kinematics of central and eastern Mediterranean: Implications for crustal dynamics and mantle flow. Geochem. Geophys. Geosyst. **13**(9), 1–25 (2012)
7. Govers, R., Wortel, M.J.R.: Lithosphere tearing at STEP faults: response to edges of subduction zones. Earth Planet. Sci. Lett. **236**, 505–523 (2005)
8. Deverchère, J., Yelles, K., Domzig, A., Mercier de Lépinay, B., Bouillin, J.-P., Gaullier, V., Bracène, R., Calais, E., Savoye, B., Kherroubi, A., Le Roy, P., Pauc, H., Dan, G.: Active thrust faulting offshore Boumerdes, Algeria, and its relations to the 2003 Mw 6.9 earthquake. Geophys. Res. Lett. **32**(4), 1–5 (2005)
9. Roure, F., Casero, P., Addoum, B.: Alpine inversion of the North African margin and delamination of its continental lithosphere. Tectonics **31**(3), 1–28 (2012)
10. Meghraoui, M., Pondrelli, S.: Active faulting and transpression tectonics along the plate boundary in North Africa. Ann. Geophys. **5**, 955–967 (2013)
11. Arab, M., Rabineau, M., Déverchère, J., Bracene, R., Belhaic, D., Roure, F., Marok, A., Bouyahiaoui, B., Granjeon, D., Andriessen, P., Sage, F.: Tectonostratigraphic evolution of the eastern Algerian margin and basin from seismic data and onshore-offshore correlation. Mar. Pet. Geol. **77**, 1355–1375 (2016)
12. Argnani, A.: Neogene Basins in the strait of sicily (Central Mediterranean): tectonic settings and geodynamic implications. In: Boschi, E., et al. (ed.) Recent Evolution and Seismicity of the Mediterranean Region, pp. 173–187. Springer, Netherlands (1993)
13. Soumaya, A., Ben Ayed, N., Delvaux, D., Ghanmi, M.: Spatial variation of present-day stress field and tectonic regime in Tunisia and surroundings from formal inversion of focal mechanisms: geodynamic implications for central Mediterranean. Tectonics **34** (6), 1154–1180 (2015)

Paleoseismological and Morphotectonical Characteristics of Active Faults in the Vicinity of Muğla Area (SW Turkey)

H. Serdar Akyüz, Erdem Kırkan, Mehran Basmenji, Ersen Aksoy, Aynur Dikbaş Akyüz, Gülsen Uçarkuş, Müge Yazıcı, Nurettin Yakupoğlu, and Cengiz Zabcı

Abstract

Turkey is seismically one of the most active regions of the world. The interaction of three major plates, Eurasia, Arabia and Africa, generates different neotectonic provinces in this region. The SW Anatolia, as part of the western extensional province, is mostly defined by E–W striking normal and NW–SE striking strike-slip and normal faults. We studied the morphotectonics and paleoseismological characteristics of these faults in order to have a better understanding on their seismic history and kinematic behavior. NW-striking Milas Fault is a right-lateral strike slip fault with a length of 50 km. Yatağan and Muğla faults are normal faults and they are almost parallel to the Milas Fault with 30 and 25 km length, respectively. The Gökova Fault is composed of E–W striking normal faults, which dip to the south and make the northern boundary of the Gökova Gulf. Geomorphic indices represent a weak signal for the tectonic activity of the Milas Fault, whereas the Yatağan Fault has a more intense impact on the geomorphology. Paleoseismological trench studies on both faults reveal that destructive earthquakes have occurred on Milas and Yatağan faults.

Keywords

Active fault • Earthquake • Paleoseismology • Morphometry • SW Turkey

1 Introduction

The Western Anatolia is seismically one of the most active regions on the earth under the effect of N–S extensional tectonic forces, which is generated by the westward extrusion of Anatolian plate along the North Anatolian and the East Anatolian transform faults (Fig. 1). This general tectonic behavior is represented by E–W trending horst-graben structures on land and gulfs on coastal area, printing significantly the regional morphology of western Turkey. Some active cross faults accompany this tectonic framework as well.

Muğla area is located in the southern part of the western Anatolia, where important active faults, named as Milas, Yatağan, Muğla and Gökova, trend within or close to large settlements (Fig. 2). Although there are some damaging earthquakes in the area documented in historical catalogues (e.g. [1, 5, 6]), we have limited information about the source faults. BC 411, 27 and AD 141, 465, 551, 1493, 1869, 1933 and 2017 (Gökova Fault Zone), AD 142 (Yatağan Fault?), AD 1631, 1896, 1941 (Milas Fault?), AD 1869 (Muğla Fault?) earthquakes might have occurred on active faults of Muğla region.

This study summarizes the general characteristics of these faults and morphometric and paleoseismological studies on Milas and Yatağan faults.

2 General Characteristics of Active Faults Around Muğla Area

Active faults in the vicinity of the Muğla area are mapped in the field, after some remote sensing studies in office such as google-earth, topo maps and aerial photo studies. Convenient trench sites were also defined during mapping. Kinematic indicators were observed and measured on some fault outcrops especially cutting Mesozoic marbles. Beside, characteristic morphological indicators for active faulting are observed in the field such as linear scarps, linear saddles,

H. S. Akyüz (✉) · E. Kırkan · M. Basmenji · A. D. Akyüz · G. Uçarkuş · M. Yazıcı · N. Yakupoğlu · C. Zabcı
Faculty of Mines, Department of Geological Engineering, İstanbul Technical University, İstanbul, Turkey
e-mail: akyuz@itu.edu.tr

E. Aksoy
Faculty of Engineering, Department of Geological Engineering, Muğla Sıtkı Koçman University, Muğla, Turkey

N. Sundararajan et al. (eds.), *On Significant Applications of Geophysical Methods*,
Advances in Science, Technology & Innovation, https://doi.org/10.1007/978-3-030-01656-2_57

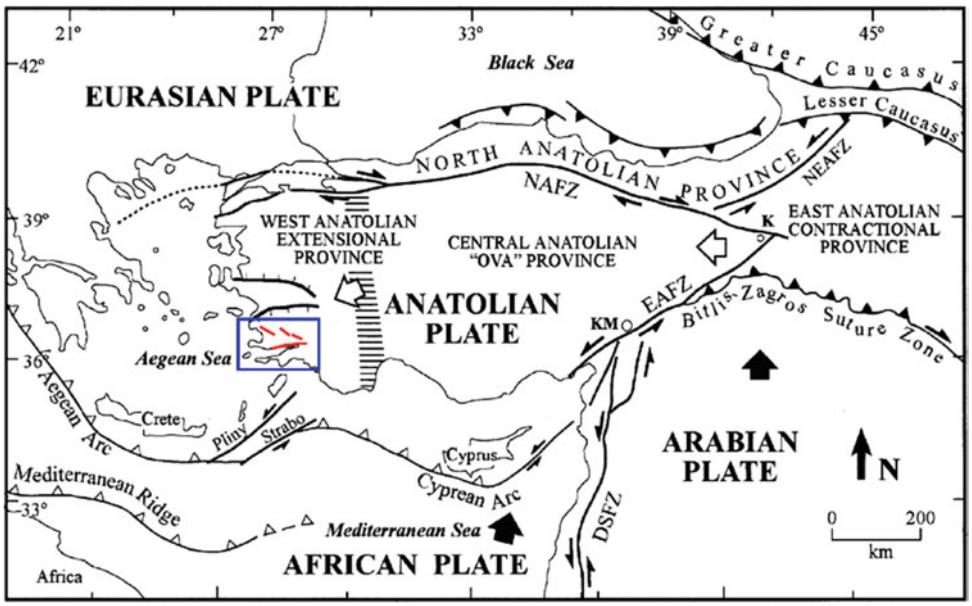

Fig. 1 Neotectonic framework of Turkey and surroundings [2, 3, 7]. Blue rectangle indicates project area

Fig. 2 Simplified active fault map of Muğla area, SW Turkey

triangular facets, linear mountain fronts, etc. The Milas Fault is a strike slip fault with the NW–SE orientation. It consists of two segments at the NW and SE parts of the Milas town that are named as Karakuyu and Beçin segments, respectively [4]. The 30 km-long Karakuyu Segment is separated from the 20 km-long Beçin Segment with a 3 km-wide right step around Milas. The Yatağan Fault is located between the Yatağan Town and west of the Muğla City with the NW-SE orientation throughout 30 km. It has clear outcrops which presents high-angled-normal faults dipping to NE. The Yatağan Fault is linked with the Muğla Fault to the west of the city. The Muğla Fault continues to SE with nearly similar orientation as Yatağan Fault, however its dip direction is SW, opposite of Yatağan Fault. The Muğla Fault has also clear surfaces especially on Mesozoic marbles, indicating pure normal slip. It is mainly composed of a number of

parallel fault sets throughout its 25 km length. The Gökova Fault is the most dangerous active fault among them, evidenced by historical and instrumental records. It consists of parallel fault sets with general E–W trend and southward dip and constitutes a stepped fault zone. This zone controls the morphology of the northern shore of the Gökova Bay along 60 km on land and then continues to the south of the Kos Island of Greece under the Aegean Sea.

3 Results

Trench studies have been carried out Milas and Yatağan faults to find out about the past large earthquakes. Three paleo-earthquakes are defined on three different trench locations on the Milas Fault while two trench studies on the Yatağan Fault revealed one (most probably last) event (Figs. 3 and 4) which was evidenced by fault branches cutting Holocene deposits. The dating analyses for the past earthquakes are still under laboratory processes. Dating results will lead to understand the seismic history of these faults.

In order to evaluate the effects of tectonic activity on the geomorphological evolution of the Milas and Yatağan faults, some basic geomorphic indices were analyzed. Hypsometric curves and integrals, mountain front sinuosity, valley width-height ratio indices revealed dominant tectonic activity which affected the morphological evolution on and around the Yatağan Fault while the traces of tectonic activity seem weaker on Milas Fault.

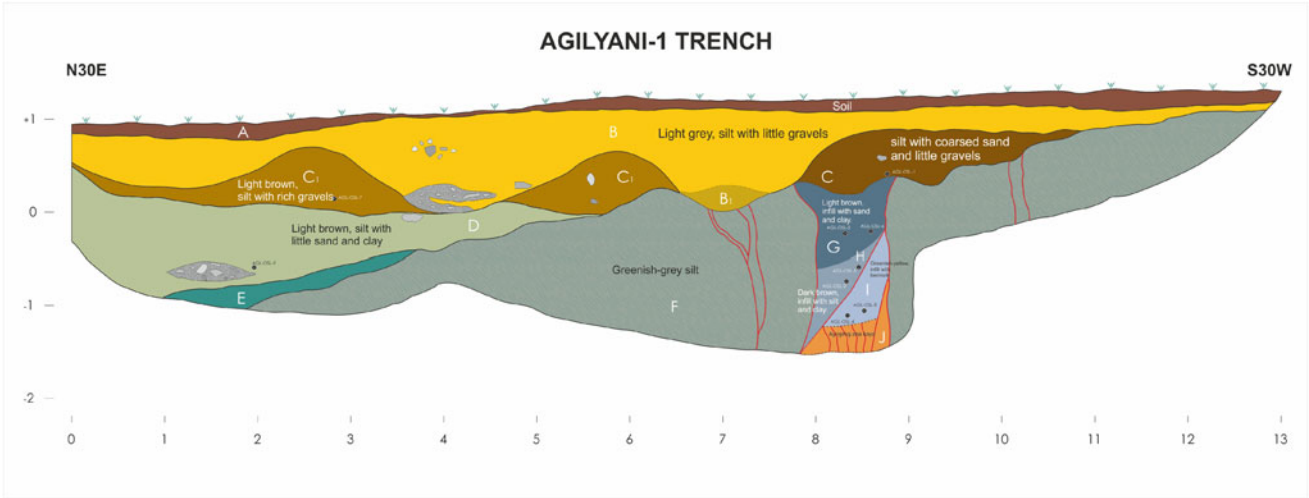

Fig. 3 An example of trench logs from the Milas Fault

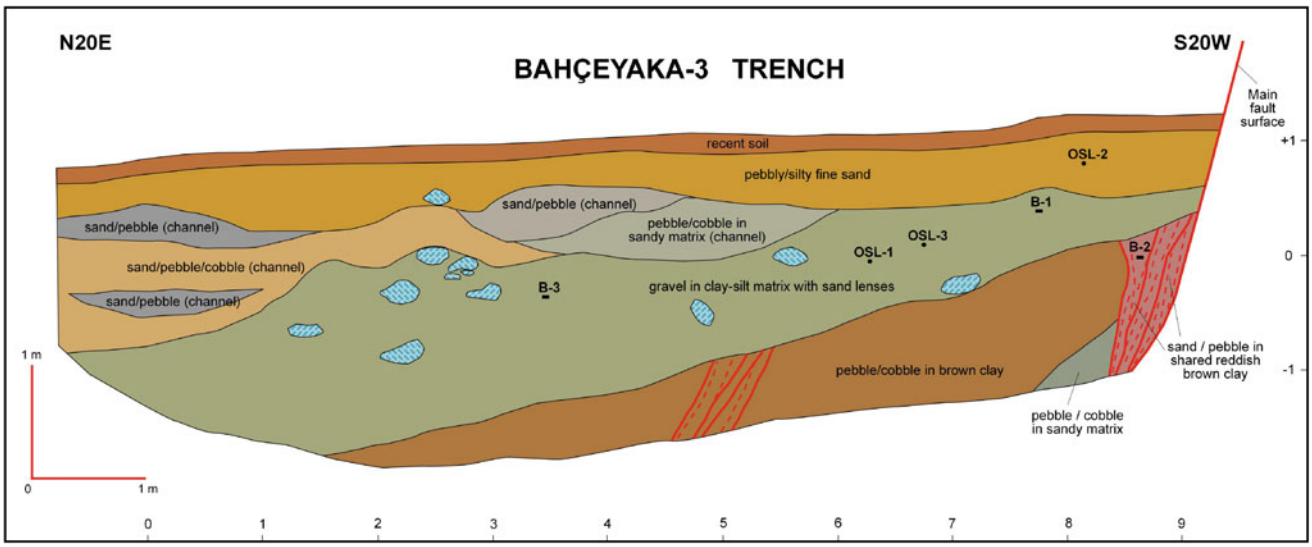

Fig. 4 An example of trench logs from the Yatağan Fault

Paleoseismic trench studies and morphometric analyses on Muğla and Gökova faults are currently in progress.

This study is a part of an ongoing project supported by The Scientific and Technological Research Council of Turkey (TUBITAK; Project No: 116Y179).

References

1. Ambraseys, N.N.: Earthquakes in the Mediterranean and Middle East: A Multidisciplinary Study of Seismicity Up to 1900. Cambridge University Press (2009)
2. Barka, A.A.: The North Anatolian Fault zone. Ann. Tectonicae **6**, 164–195 (1992)
3. Bozkurt, E.: Neotectonics of Turkey—a synthesis. Geodin. Acta **14**, 3–30 (2001)
4. Emre, Ö., Duman, T.Y., Özalp, S., Elmacı, H., Olgun, Ş., Şaroğlu, F.: Active Fault Map of Turkey with an Explanatory Text 1:1,250,000 scale. Special Publication Series 30, MTA, Ankara-Turkey (2013)
5. Guidoboni, E., Comastri, A.: Catalogue of earthquakes and tsunamis in the mediterranean area from the 11th to the 15th century. Istituto Nazionale di Geofisica e Vulcanologia, 1037 p. ISBN: 88-85213-10-3 (2005)
6. Guidoboni, E., Comastri, A., Triana, G.: Catalogue of Ancient Earthquakes in the Mediterranean Area Up to the 10th Century. Istituto Nazionale di Geofisica e Vulcanologia, 504 s. ISBN:88-85213-06-5 (1994)
7. Sengör, A.M.C., Görür, N., Saroglu, F.: Strike-slip faulting and related basin formation in zones of tectonic escape: Turkey as a case study. In: Biddle, K.T., Christie-Blick, N. (eds.) Strike-slip Faulting and Basin Formation, vol. 37, pp. 227–264. Society of Economic Paleontologists and Mineralogists. Special publication (1985)

The Western Makran Active Seismic Transects Preliminary Results

Mohammad Mokhtari, Christian Haberland, Trond Ryberg, Hassan Ali Babaei, Joern Lauterjun, and Michael Weber

Abstract

The Makran subduction zone is a result of the northward subduction of the Arabian plate beneath the Eurasian plate. It is located in a complicated tectonic setting. From seismicity point of view, the east and west Makran have two different characteristics; the latest being considered as seismically more active. But in general, the seismicity in the region compared to other subduction zones in the world and at the same time with respect to its low surrounding. These three active seismic crustal scale refraction/wide angle reflection data together with large explosions, the necessary data has been acquired. In this paper using the newly acquired seismic data, a better estimation of the plate geometry of the western part of the Makran subduction zone (Iran), the crustal structure and hence the seismo-genic and tsunami-genic potential of this region were discussed.

Keywords

Makran • Subduction • Active seismic • Velocity model • Wide angle

1 Introduction

The Makran subduction zone is a result of the northward subduction of the Arabian plate beneath the Eurasian plate. It is located in a complicated tectonic setting. Despite showing a relatively low seismicity, three earthquakes generating tsunamis in the Makran region have been reported [1, 2, 4].

Due to low seismicity access to seismic data for structural modeling and velocity analysis, we faced many challenges. In this respect in September 2017 three north-south oriented crustal-scale seismic refraction lines across onshore Markan have been acquired. Along each profile 315 autonomous seismic recorders were deployed and 9–10 artificial shots were fired. The distance between each shot point along each profile was approximately 20 km.

This work was intiated by discussing the data acquisition. Then, the data quality was reviewed and the first result based on travel time picking and tomographic modeling was elaborated. It is important to mention that these types of data were achieved and gathered for the first time in the region.

2 Experiment and the Data

In September 2017 three north-south oriented crustal-scale seismic refraction/wide angle reflection lines crossing the Makran accretionary wedge (on-shore) have been acquired (one after the other). Figure 1 shows the location of the profiles where shot pints and receiver position were super-imposed. Along each profile 315 autonomous seismic recorders (with vertical component 4.5 Hz geophones) were deployed and 9–10 artificial shots (explosions of up to 800 kg charge size at the depth of 30 m borehole) were fired. The distance between each shot point along each profile was approximately 20 km.

Figure 2 shows a shot gather of line 2, at shot point 3. The crustal phase Pg can be observed up to 130 km. Note the strong over-critical reflections (Px) at 80–140 km. The Y-axis is in reduced travel time (vred = 6 km/s). The only processing step applied to the data in the figure was the band pass filtering (2–10 Hz) and trace balancing. The first arrival times for further analysis of the P-waves were manually picked.

M. Mokhtari (✉) · H. A. Babaei
International Institute of Earthquake Engineering and Seismology, Tehran, Iran
e-mail: m_7_mokhtari@yahoo.com; mokhtari@iiees.ac.ir

C. Haberland · T. Ryberg · J. Lauterjun · M. Weber
GFZ German Research Centre for Geosciences, Potsdam, Germany

N. Sundararajan et al. (eds.), *On Significant Applications of Geophysical Methods*,
Advances in Science, Technology & Innovation, https://doi.org/10.1007/978-3-030-01656-2_58

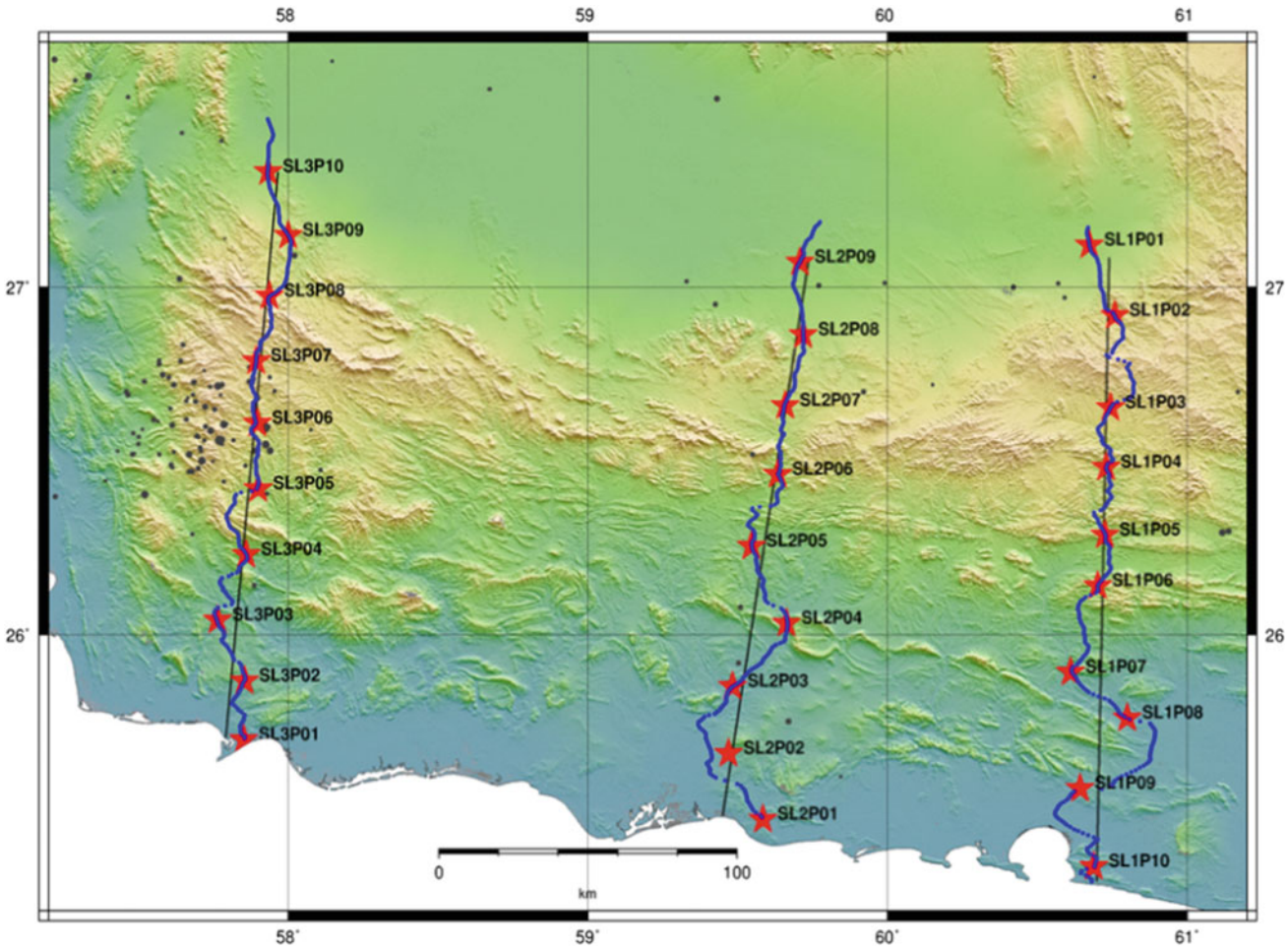

Fig. 1 Shows the location of the profiles onshore Makran

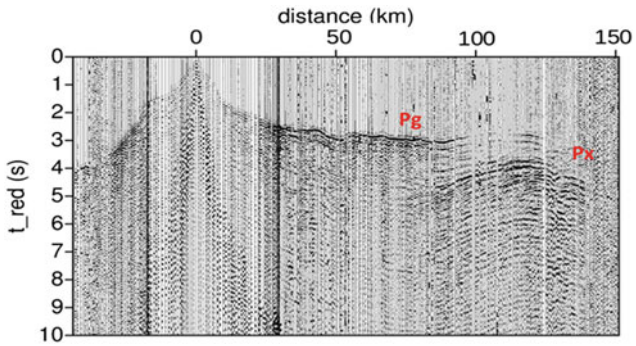

Fig. 2 Data example from line 2 shot 3

3 Results

The acquired data along all the profiles are of high quality with rather high signal-noise ratio. The picked first arrivals have been tomographically inverted [3] (Fig. 3). The model clearly shows the full crust and the upper mantle velocity structure. The strongest reflections indicate the crust-mantle boundary. It is important to mention that the results shown so far preliminary. The wide angle reflection data observed along all the profiles (indicated by Px in Fig. 2) need to be studied and possibly different analysis methodologies should be applied at a later stage. The data analysis is ongoing in joint cooperation between IIEES and GFZ and the final results will be used for the geological and geophysical modeling and defining the subduction dip angle and other parameter definitions.

4 Discussion

Due to the absence of deep seismic profiles and low seismicity, little is known about the accretionary wedge at depth or the lithospheric structure in the Makran region, especially in the west. The main aim of this study is therefore to

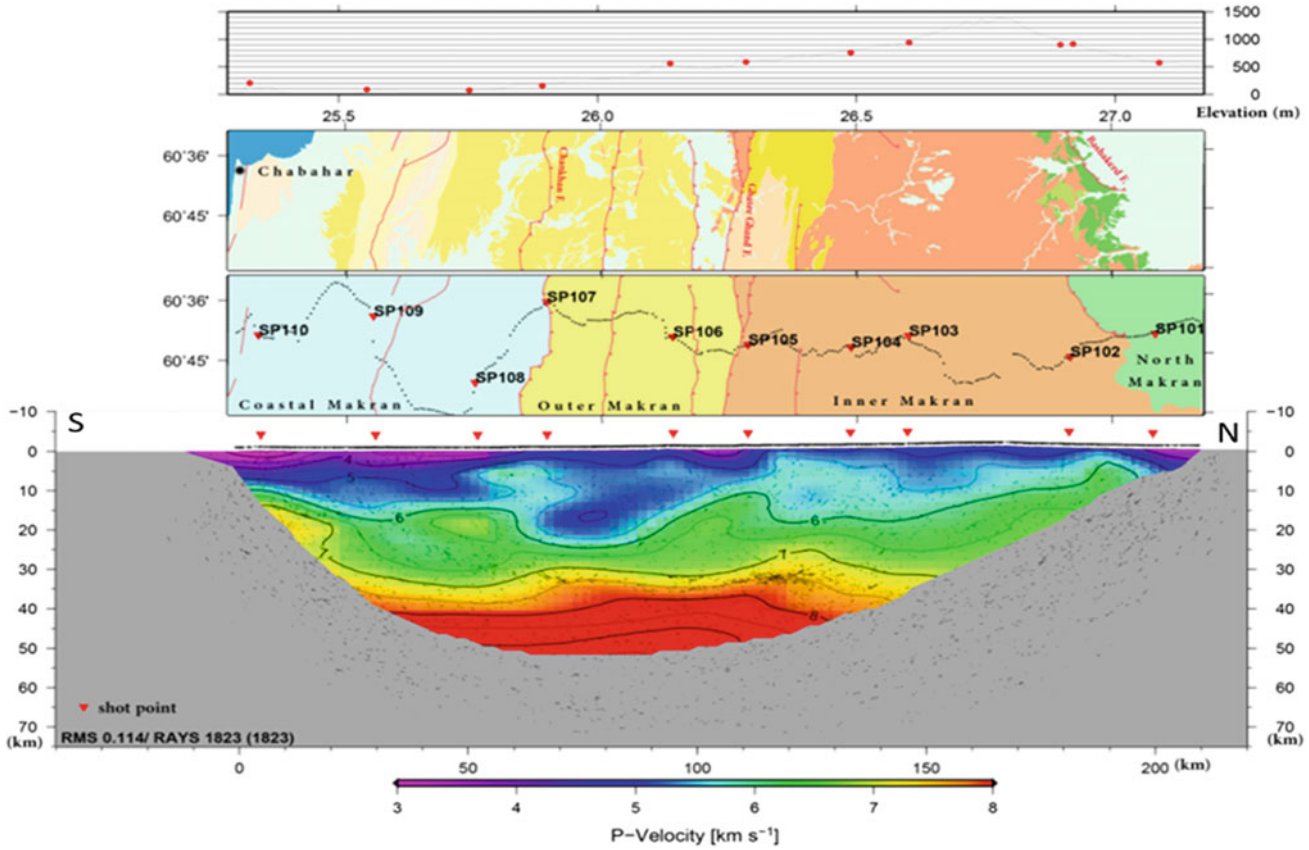

Fig. 3 The picked first arrivals have been tomographically inverted. The top of the figure is the shot point location and also elevation being plotted. The middle part shows the geological units and subdivision of Makran and the bottom part is the result of tomographic inversion. Red colors indicate mantle velocities, greenish colors crustal material. The yellow colors indicate the crust-mantle boundary

investigate the structure of the crust and upper mantle of the Makran using deep seismic refraction profiles. The active seismic data have provided a calibrated and well defined seismic interpretation with much higher resolution for a better definition of the structural elements and a well-defined velocity model in the region. The first result of the experiment so far has confirmed a better definition of the main velocity structure both within the crust and the upper mantle. This information combined with future offshore seismic and other geophysical data could be utilized for a better understanding of the main fault parameters that will be used for more accurate definition of the tsunami source modeling and simulation of the run-up and tsunami wave arrivals to the coastal region of Makran in general and Iran and Oman coastal regions in particular. The main out-come will be focussed at tsunami early warring and risk reduction.

5 Conclusion

- Successful acquisition of three crustal-scale seismic refraction profiles crossing the on-shore part of the Western Makran accretionary wedge.
- From tomographic and reflection seismic images the Moho can be inferred at a depth of 25 km beneath the coast, gently dipping toward the north.

- Next steps include the analysis of the data and the integration of geological, seismological and off-shore data.

References

1. Heidarzadeh, M., Pirooz, M.D., Zaker, N.H., Yalciner, A.C., Mokhtari, M., Esmaeily, A.: Historical tsunami in the Makran subduction zone off the southern coasts of Iran and Pakistan and results of numerical modeling. Ocean Eng. **35**(8 & 9), 774–786 (2008)
2. Mokhtari, M.: Seismicity, major structural elements and required Tsunami early warning system for Makran (Sea of Oman) region. Gulf Seismic Forum, Muscat, Oman, 19–22.2 (2006)
3. Ryberg, T., Haberland, C.H.: Bayesian inversion of refraction seismic travel time data. Geophys. J. Int. **212**(3), 1645–1656 (2018). https://doi.org/10.1093/gji/ggx500
4. Zarifi, Z.: Unusual subduction zones: case studies in Colombia and Iran. Unpublished Ph.D. Thesis, University of Bergen, Norway (2006)

Interaction Faults in the North-West of the Mitidja Basin: Chenoua–Tipasa–Ain Benian Earthquakes (1989–1996)

Ghania Dabouz and Hamoud Beldjoudi

Abstract

Several studies have shown that, in a given region, the previous seismicity has a strong influence on the location, and probably also on the date of subsequent seismicity. This works included the observation of "stress shadows" and the Coulomb stress triggering. From these studies, it was deduced that in the time receding an earthquake, stress is accumulated not only on the fault, but also in a large region surrounding this fault. In this work, we were interested in earthquakes that occurred in the western Algiers, the Mont Chenoua (Mw 6.0), Tipasa (Mw 4.7) and Ain Benian (Mw 5.7). The results obtained show a good correlation between the regions where the variation of the Coulomb failure function is positive ($\Delta CFF > 0$) and the distribution of the events of magnitude $M \geq 4.5$ occurred during 1989 to 1996. This means that there was a transfer of stress among these three faults. The Mont Chenoua earthquake has triggered the serial events which occurred in the region.

Keywords

ΔCFF • Fault interaction • Static stress change • Seismicity • Algeria

1 Introduction

Northern Algeria has been the site of numerous historical earthquakes, and was therefore subject to extensive damages and several thousand casualties in the past. On October 29th, 1989 an earthquake hit the Mont Chenoua locality in the Tipasa region, located ~70 km west of Algiers (capital of Algeria). The main shock with Mw = 6.0 [1], severely affected villages in the vicinity of the epicentral area. It was located at 36.66°N; 2.48°E [1]. The focal mechanism was a nearly pure reverse faulting along a plane striking 246°N and dipping 56° [1]. A large aftershock; Ms = 5.4, followed the main shock by about 10 min. On 9th February, 1990 a second earthquake hit the region again with Mw = 4.9, located at the east of the first shock (36.63°N; 2.51°E) [2]. The earthquake of 04th September 1996; Mw = 5.6, occured 20 km offshore area NW from Ain Benian village located ~65 km east of Tipasa.

G. Dabouz (✉) · H. Beldjoudi
Centre de Recherche En Astronomie Astrophysique et Géophysique (CRAAG), BP 63 Route de L'Observatoire Bouzaréah, Alger, Algérie
e-mail: g.dabouz@craag.dz

2 Static Stress Change Method (ΔCFF)

The stress state of a fault, or those faults around it, is a crucial indicator of the likelihood that further earthquakes will occur. The Coulomb failure function (CFF) is a quantitative description of stress state. To calculate static Coulomb stress parameters pertaining to the source fault (such as position, length, width, depth, strike, dip and slip vectors) and those pertaining to the receiver fault (such as strike, dip and rake) should be determined first.

In this study, we use the Coulomb 3.3 software [3], which implements the elastic half space of Okada [4]. The Coulomb stress change is defined as:

$$\Delta CFF = \Delta\tau + \mu'.\Delta\sigma$$

where $\Delta\tau$ is the shear stress change on the fault (positive in the inferred direction of slip), $\Delta\sigma$ is the normal stress change (positive for fault unclamping), and μ' is the effective fault friction coefficient numerically equal to 0.4 in this study as an average value. The location and geometry of the source rupture, as well as the slip distribution over the source plane, play an important role in calculating the Coulomb stress change. Based on earthquake magnitude, we modeled the source geometry with the empirical relations of Wells and Coppersmith [5], for reverse faults, which were built into the Coulomb 3.3 software.

N. Sundararajan et al. (eds.), *On Significant Applications of Geophysical Methods*,
Advances in Science, Technology & Innovation, https://doi.org/10.1007/978-3-030-01656-2_59

3 Results and Discussion

In order to examine the relationship between aftershocks and stress changes we calculated the Coulomb stress change caused by Mont Chenoua earthquake on the surroundings area. The map shows two main positive lobes in the fault extremities NE, and SW (see Fig. 1). Most aftershocks occurred in raised stress regions, other aftershocks were located where the stress dropped. Two cross-sections, of 10 km wide and orthogonal to the general trend of the fault and aftershocks were presented (see Fig. 1b, c), both cross sections, show the distribution of aftershocks on depth, which are located between 2 and 10 km, most of them are located on positive area where Coulomb stress change is raised.

Therefore, to figure out the fault plane ambiguity, we computed the co-seismic Coulomb stress changes on both nodal planes for the 55 available focal mechanisms (aftershocks). The coulomb stress change is positive for at least one nodal plane in 37 cases (67%). 19 focal mechanisms (35%) present a positive Coulomb stress change for both nodal planes, while the shear stress change is positive for at least one plane (43%).

Coulomb stress changes do not only predict aftershock distributions. The Mont Chenoua earthquake rupture occurred within a narrow zone where a series of pre-seismic and post-seismic events occurred. In order to see if the Mont Chenoua earthquake has disrupted the state of stress of the Tipasa earthquake, we computed coulomb stress change in the aim to understand this link if it exists (see Fig. 2a).

The faults of Mont Chenoua and Tipaza earthquakes are two reverse faults which plunge to the NW direction. According to Lin [7], the rupture of receiver thrust fault is favored when the source thrust fault dip plunges toward the same direction as the receiver. In the map (see Fig. 2a), we can see that the Tipasa fault is located in the region where the Coulomb stress change raised. This is well demonstrated by the cross section (see Fig. 2b). This may be little less reliable than the case of the Ain Benian earthquake. This is due to the effect of the distance between these two faults and also the moderate size of the Mont Chenoua earthquake.

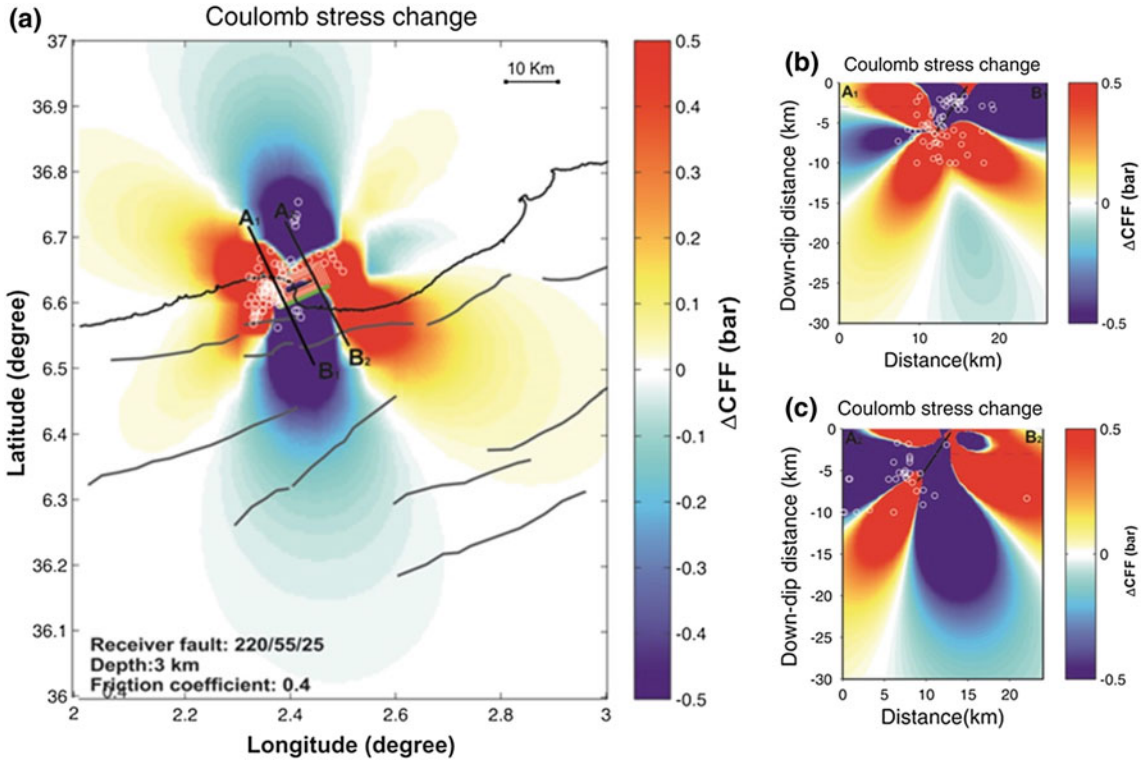

Fig. 1 **a** Coulomb stress change at 3 km caused by the 1989, Mont Chenoua (Mw = 6) rupture onto aftershocks distribution (Receiver fault: Strike 220°, Dip 55°, Rake 25°). **b** Coulomb stress changes along a cross section (A_1B_1), with aftershocks along a wide band of 10 km. **c** Same as **b** but for cross section (A_2B_2). Gray lines show active faults in the study area [6]. Coefficient of friction is taken equal 0.4 as in [7, 8]

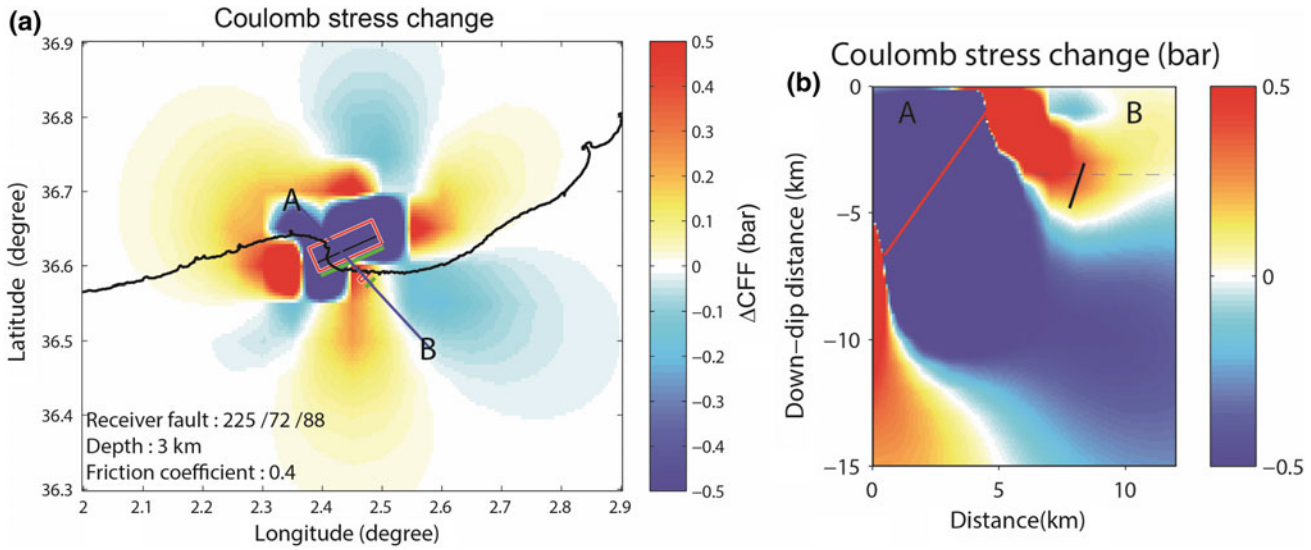

Fig. 2 **a** Stress changes caused by 1989 Mont Chenoua (M_w = 6) source faults resolved onto the plane of the subsequent 1990, Tipasa rupture (M_w = 4.7) (Receiver fault: Strike 225°, Dip 72°, Rake 88°). **b** Coulomb stress changes along a cross section

4 Conclusion

In this example of stress triggering among moderate sized earthquakes, we showed that if the faults (source and receiver) are in the vicinity, the source fault can load the receiver; if the last has certain conditions of optimal orientation. In our case we confirmed that the Tipasa fault was loaded by the Mont Chenoua earthquake.

References

1. Bounif, A.: Seismic source study of the 1989, October, Chenoua (Algeria) earthquake from aftershocks, broad-band and strong ground motion records. Ann. Geophys. **46**(4), 625–646 (2003)
2. Sebai, A.: Analyse sismologique des séismes récents du sahel d'Alger. Thèse de Magister, USTHB, Alger, 178 p. (1997)
3. Toda, S., Stein, R.S., Sevilgen, V., Lin, J.: Coulomb 3.3 graphic-rich deformation and stress-change software for earthquake, tectonic, and volcano research and teaching—user guide. U.S. Geological Survey Open-File Report 2011–1060 (2011b)
4. Okada, Y.: Internal deformation due to shear and tensile faults in a half-space. Bull. Seismol. Soc. Am. **82**(2), 1018–1040 (1992)
5. Wells, D.L., Coppersmith, K.J.: New empirical relationships among magnitude rupture length, rupture area, and surface displacement. Bull. Seismol. Soc. Am. **84**, 974–1002 (1994)
6. Meghraoui, M.: Géologie des zones sismiques du nord de l'Algérie Paléosismologie, Tectonique active et synthèse sismotectonique. Ph. D. Thesis, Université de Paris XI, Centre d'Ossay (France), 356 pp. (in French) (1988)
7. Lin, J., Stein, R.S., Meghraoui, M., Toda, S., Ayadi, A., Dorbath, C., Belabbes, S.: Stress transfer among en echelon and opposing thrusts and tear faults: triggering caused by the 2003 M_6:9 Zemmouri, Algeria, earthquake. J. Geophys. Res. **116**, no. B03305 (2011). https://doi.org/10.1029/2010jb007654
8. Kariche, J., Meghraoui, M., Ayadi, A., Boughacha, M.S.: Stress change and fault interaction from a two century-long earthquake sequence in the central Tell Atlas (Algeria). Bull. Seism. Soc. Amer. **107**(6), 2624–2635 (2017). https://doi.org/10.1785/0120170041